Government of **Western Australia**
Department of **Mines and Petroleum**

RECORD 2010/26

CONTROLS ON GIANT MINERAL SYSTEMS IN THE YILGARN CRATON — A FIELD GUIDE

compiled by
TC McCuaig, JM Miller and S Beresford

2010 Perth 5iaS Geo conferences (WA) Inc.

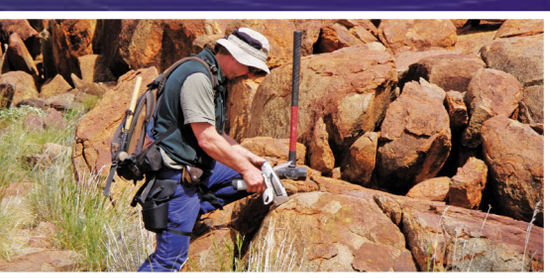
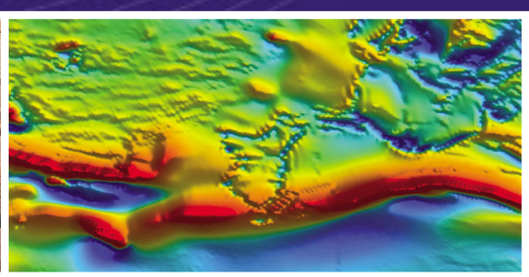


Geological Survey of Western Australia

CONTROLS ON GIANT MINERAL SYSTEMS IN YILGARN CRATON

FIELD GUIDE

30 AUGUST - 4 SEPTEMBER 2010

Professor T. Campbell McCuaig,
Research Professor John Miller &
Dr Steve Beresford

THE UNIVERSITY OF WESTERN AUSTRALIA
Curtin University

Government of Western Australia
Department of Mines and Petroleum

Record 2010/26

CONTROLS ON GIANT MINERAL SYSTEMS IN THE YILGARN CRATON — A FIELD GUIDE

compiled by
TC McCuaig, J Miller and S Beresford

Perth 2010

Geological Survey of
Western Australia

MINISTER FOR MINES AND PETROLEUM
Hon. Norman Moore MLC

DIRECTOR GENERAL, DEPARTMENT OF MINES AND PETROLEUM
Richard Sellers

EXECUTIVE DIRECTOR, GEOLOGICAL SURVEY OF WESTERN AUSTRALIA
Rick Rogerson

REFERENCE
The recommended reference for this publication is:
McCuaig, TC, Miller, J and Beresford, S (compilers) 2010, Controls on giant minerals systems in the Yilgarn Craton – a field guide: Geological Survey of Western Australia, Record 2010/26, 164p.

National Library of Australia Card Number and ISBN 978-1-74168-344-8

Grid references in this publication refer to the Geocentric Datum of Australia 1994 (GDA94). Locations mentioned in the text are referenced using Map Grid Australia (MGA) coordinates, Zones 50 and 51. All locations are quoted to at least the nearest 100 m.

Published 2010 by Geological Survey of Western Australia
This Record is published in digital format (PDF) and is available online at <http://www.dmp.wa.gov.au/GSWApublications>.

Further details of geological publications and maps produced by the Geological Survey of Western Australia are available from:

Information Centre
Department of Mines and Petroleum
100 Plain Street
EAST PERTH WA 6004
Telephone: +61 8 9222 3459 Facsimile: +61 8 9222 3444
<http://www.dmp.wa.gov.au/GSWApublications>

Contents

Acknowledgements

The authors acknowledge the support of The Australian Research Council though Linkage projects LP0776780 and LP 100100647, as well as partner organisations St. Barbara Mining, BHP Billiton, and Norilsk. This field excursion could not be possible without the enthusiastic support of the following companies for site visits: Anglogold Ashanti (Sunrise Dam), Independence Group (Long–Victor), Gold Fields Australia (St. Ives), Western Areas Ltd (Forrestania), St. Barbara Mining (Sons of Gwalia, Marvel Loch), and Focus Minerals (Coolgardie). In particular, we acknowledge the help and support of Jocelyn Thomson, Somealy Sheppard, Paull Parker, Terry Gillings, John Haywood, Michael Nugus, Garry Adams, Travis Craig, Jason Beccaria, Damien Keys, Matt Briggs, Kezia Duncan, Michael Doublier, Wayne Hitchcock, Askok Doorgapershad, Tim Canam and Wendy Carter. In addition, we would like to thank researchers from the GSWA and the staff from all sites visited for their logistical support and assistance in planning this trip. We have also greatly benefitted from discussions with many collegues, in particular Steve Beresford and Steve Barnes.

Chapter 1 — Controls on giant mineral systems in the Yilgarn

TC McCuaig, JM Miller, ML Fiorentini, N Thébaud, D Mole

Centre for Exploration Targeting, School of Earth and Environment, The University of Western Australia

Introduction and background

The past decade has seen remarkable advances in understanding the architecture and assembly of the Yilgarn Craton, as well as advances in understanding the absolute timing, genesis and structural modification of nickel-sulphide (NiS), orogenic gold, intrusion-related gold, iron-oxide (Fe) and volcanogenic massive sulphide (VMS) systems within the context of the tectonic evolution of the craton. This field trip focuses on the major mineral systems of the Neoarchean Eastern Goldfields Superterrane, particularly the Au, NiS and VMS systems, and contrasts them with Au and NiS systems of the Meso-Neoarchean Youanmi Terrane of the central Yilgarn. Major deposits/camps to be visited will include: Kambalda (1.5 Mt Ni; >10 Moz Au); Kalgoorlie (100 Moz Au); Laverton (e.g. Sunrise >12.5Moz Au; Wallaby >7 Moz Au); Southern Cross (e.g. Marvel Loch >2 Moz Au); Forrestania (e.g. Flying Fox >100 kt Ni). This is the first ever field trip to cover the metallogeny of all of these terranes. This field guide is designed to provide context for the overall trip and specific mine sites visited.

Geology of the Yilgarn — advances in the past decade

The situation in 2000

At the turn of the century, the understanding of Yilgarn geology was relatively advanced. The craton was divided into a series of provinces and, in the Eastern Goldfields Province, further subdivided into a series of terranes and constituent domains based on detailed 1:100 000 scale mapping through the region by Geoscience Australia and GSWA in the 1980s and 1990s (Swager et al., 1992; Myers, 1993). Stratigraphic columns were well developed for type localities in the Eastern Goldfields, particularly through the Kambalda Domain of the Kalgoorlie Terrane, and around some mining centres. Stratigraphy in the central and western Yilgarn was much less well established. Geochronological studies were well advanced, helping to underpin the understanding of stratigraphy. These data had revealed an early c. 2.9 Ga stratigraphy in the central Yilgarn and a dominantly 2.72 – 2.65 Ga volcano-sedimentary package in the Eastern Goldfields. Furthermore, a series of intrusive events had been identified that punctuated the tectonic history of the Eastern Goldfields between 2.68 and 2.61 Ga, and these igneous and

metamorphic events were noted as broadly synchronous with a principle deformation event in the Southern Cross province.

Although intuitively understood by many that multiple thermal pulses had affected the craton, maps of metamorphic mineral assemblages were still presented as single images of greenschist to upper-amphibolite facies assemblages, generally increasing towards the margins of the belt and in the contact aureoles of granites intruding the belt. No spatial analysis of the timing of metamorphism was available — issue in Precambrian granite–greenstone terranes. Crustal imaging was in its infancy, with the first two lines of seismic acquired in 1991 (Kalgoorlie region) and 1999 (Leonora–Laverton region). These data changed radically our view of the structure of the Archean crust, showing some trans-crustal structures and consistent apparent detachment zones at ca. 5–8 km depth. It furthermore showed that many of the granite intrusions within belts were in the form of 'surfboards' or laccoliths, with thinner root or feeder zones (Drummond et al., 2000; Swager et al., 1997).

Advances since 2000

Several advances have been made in understanding the architecture and evolution of the Yilgarn and particularly the Eastern Goldfields since the turn of the century. Many of these have been driven by highly collaborative research projects involving combinations of funding from industry, Geoscience Australia, GSWA, MERIWA, AMIRA projects, and the Australian Research Council. Of particular impact was the work of the predictive mineral discovery Cooperative Research Centre (pmd*CRC), a 7-year research program co-funded by industry and federal government that united traditionally disparate geosciences subdisciplines (geology, geophysics, geochemistry, igneous petrology, geochronology, structural geology) and geographically dispersed research groups towards understanding the architecture, evolution, and gold mineral systems of the Eastern Yilgarn. Much of what is presented below are the outcomes of these studies.

Subdivisions of the Yilgarn Craton

TheYilgarn Craton has been divided by Cassidy et al. (2006) into six major terranes, from west to east the Narryer, Southwest, Youanmi, Kalgoorlie, Kurnalpi, and Burtville Terranes, with the three easternmost forming the Eastern Goldfields Superterrane (EGST, Figs 1, 2). The terranes are denoted based on major differences in stratigraphic ages and whole rock and isotopic geochemistry of volcanic and intrusive rocks. Major differences in age of oldest crust, greenstones, granitoid rocks and deformation and metamorphism between the terranes are summarised in Table 1 and Figure 2.

Internally the terranes are subdivided into domains with internally consistent stratigraphy and structural evolution. The terranes and domains are bounded by series of interconnected faults interpreted largely from potential field geophysical datasets.

The field trip will encompass the northern and southern Kalgoorlie Terrane and northern Kurnapli Terrane of the EGST, and the Southern Cross Domain of the Youanmi Terrane (Figs 1, 2). The geology of the EGST and Youanmi Terrane are discussed separately in the following sections.

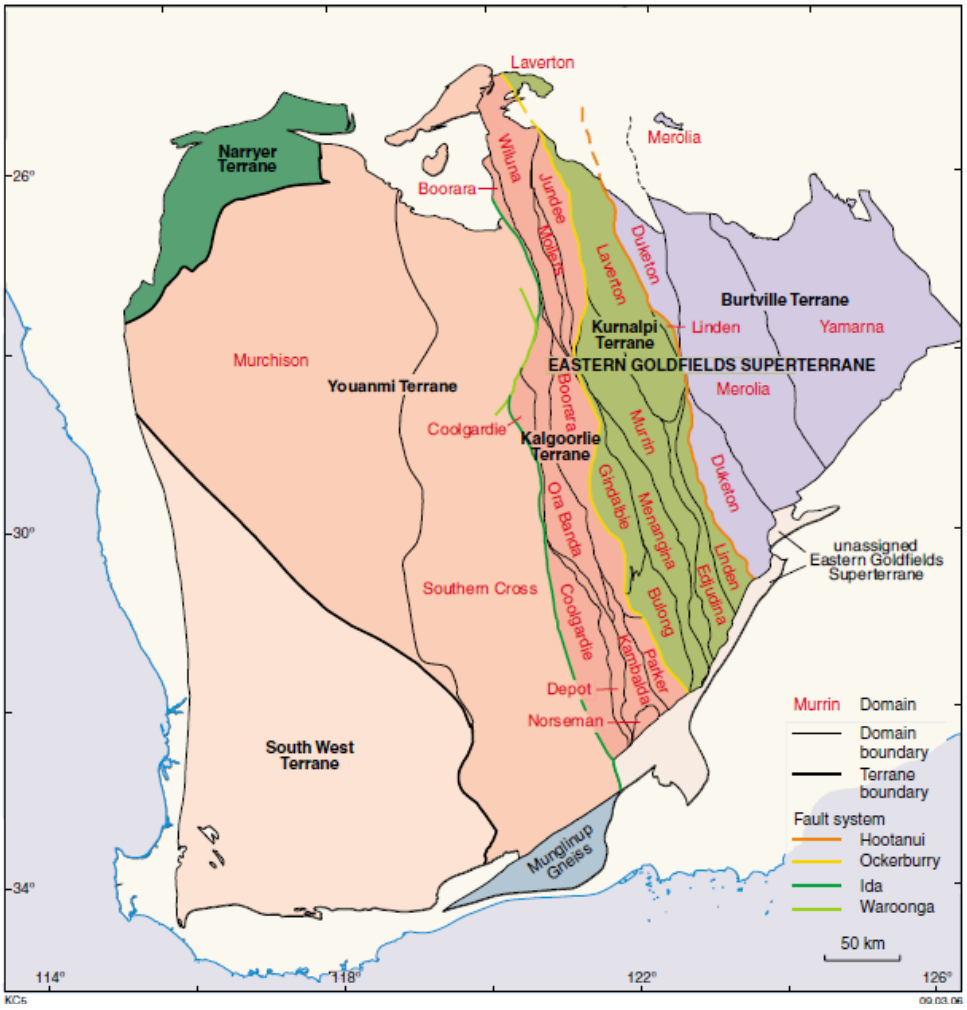

Figure 1. Map of the Yilgarn Craton showing major craton subdivisions (Cassidy et al., 2006)

Table 1. Summary of differences in ages of oldest crust, greenstone deposition, granitoid magmatism, and defomation–metamorphism for the terranes of the Yilgarn Craton (Cassidy et al., 2006)

Terrane	*Age of initial crust formation*	*Depositional ages of greenstones*	*Emplacement ages of granites and gneisses (Ga)*	*Age of deformation and metamorphism*
Narryer Terrane	3.8–3.4	?3.73	3.73–3.6, 3.48, 3.3 3.0, 2.75, 2.68–2.62	c. 3.3, ?2.75, 2.68–2.62
South West Terrane	?3.5–3.0	?3.0, ?2.8, 2.7	?3.2, 2.8, 2.68–2.62	?2.68–2.62
Youanmi Terrane	?3.4–2.9	3.01–2.92, 2.81, 2.76–2.72	3.01–2.92, 2.81, 2.76–2.68, 2.66–2.62	>2.74–2.68, 2.66–2.63
Eastern Goldfields Superterrane				
Kalgoorlie Terrane	?3.0–2.8	?2.94, ?2.81, 2.74–2.66	2.81, 2.75–2.74, 2.68–2.66, 2.65–2.63	2.67–2.63
Kurnalpi Terrane (western domains)	2.9–2.8	2.71–2.68	2.7, 2.68–2.66, 2.65–2.63	2.67–2.63
(eastern domains)	?3.1–2.9	>2.8, 2.72–2.68	?2.95, 2.71, 2.68–2.66, 2.65–2.63	2.67–2.63
Burtville Terrane	?3.0–2.8	2.81, 2.77–2.66	?2.95, 2.8–2.77, 2.69–2.63	?2.67–2.63

Eastern Goldfields Superterrane

The stratigraphic, intrusive, metamorphic, structural and mineralisation history of the EGST is summarised in Figure 2, with salient points noted below.

Stratigraphy

Key advances in the understanding of stratigraphy include the identification of three major greenstone deposition events: c. 2.9 Ga stratigraphy is identified in the eastern portion of the Norseman Domain, Kalgoorlie Terrane (Penneshaw Formation; Doepel, 1973; McGoldrick, 1993; not shown in Figure 2); a 2.81 – 2.79 Ga stratigraphy along the western margin of the EGST (e.g. Leonora), and within the Laverton Domain; and the dominant 2.72 – 2.65 Ga stratigraphy that constitutes the bulk of the surface exposures (Czarnota et al., 2010, and references therein).

The 2.8 Ga stratigraphy (Fig. 2) comprises mafic–ultramafic sequences, local coeval felsic volcanic centres, and an overlying siliciclastic sedimentary sequence. In the Kurnalpi Terrane these rocks are termed the Laverton Sequence.

Figure 2. (following page) Integrated tectonic framework for the Eastern Goldfields Superterrane showing the interrelationship between stratigraphy, granite history, tectonic mode, deformation history, metamorphism, and age of gold mineralisation (from Czarnota et al., 2009).

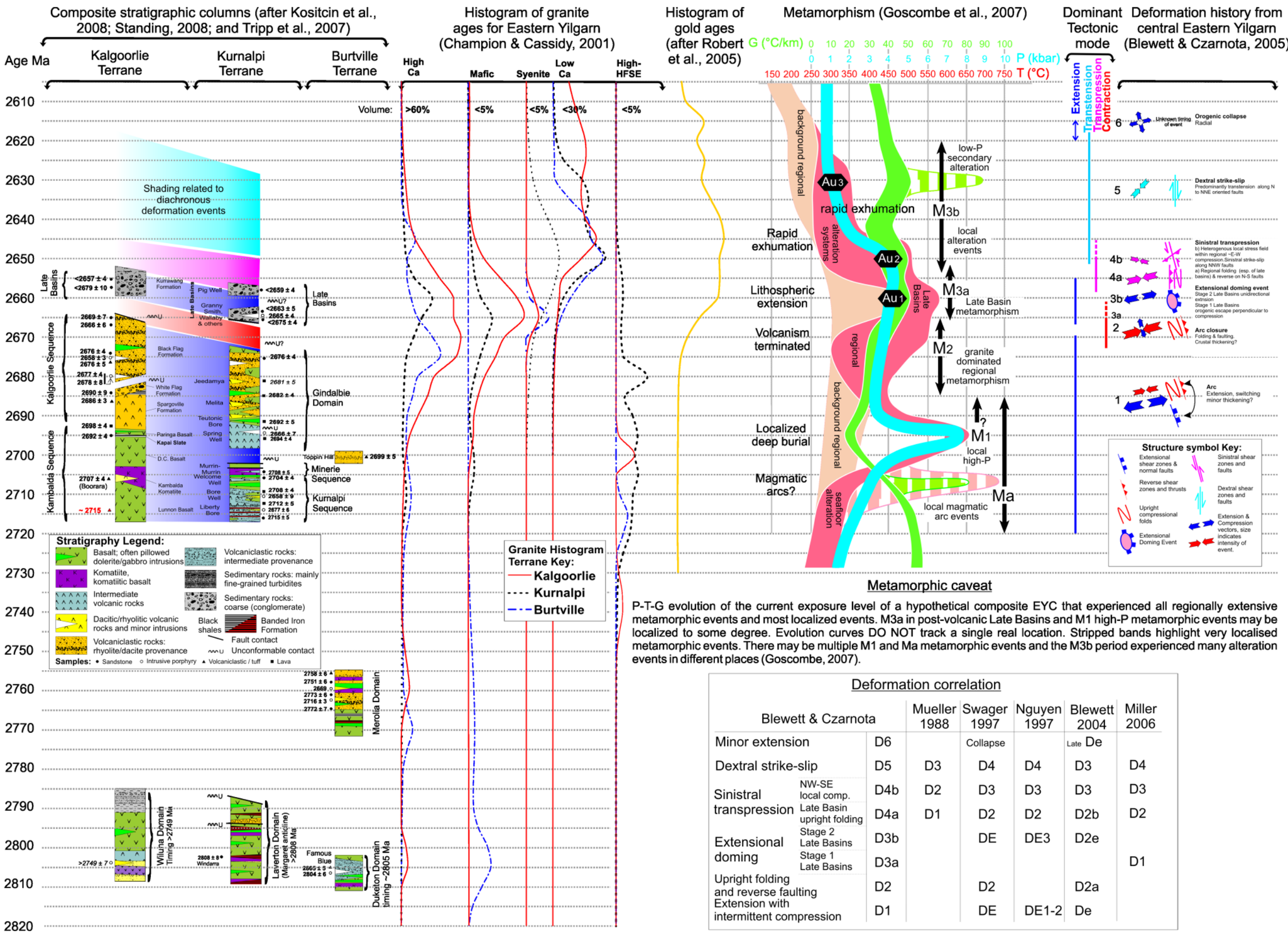

Metamorphic caveat

P-T-G evolution of the current exposure level of a hypothetical composite EYC that experienced all regionally extensive metamorphic events and most localized events. M3a in post-volcanic Late Basins and M1 high-P metamorphic events may be localized to some degree. Evolution curves DO NOT track a single real location. Stripped bands highlight very localised metamorphic events. There may be multiple M1 and Ma metamorphic events and the M3b period experienced many alteration events in different places (Goscombe, 2007).

Deformation correlation

Blewett & Czarnota		Mueller 1988	Swager 1997	Nguyen 1997	Blewett 2004	Miller 2006
Minor extension	D6		Collapse		Late De	
Dextral strike-slip	D5	D3	D4	D4	D3	D4
Sinistral transpression — NW-SE local comp.	D4b	D2	D3	D3	D3	D3
Sinistral transpression — Late Basin upright folding	D4a	D1	D2	D2	D2b	D2
Extensional doming — Stage 2 Late Basins	D3b		DE	DE3	D2e	
Extensional doming — Stage 1 Late Basins	D3a					D1
Upright folding and reverse faulting	D2		D2		D2a	
Extension with intermittent compression	D1		DE	DE1-2	De	

The 2.7 Ga stratigraphy varies between the Kalgoorlie and Kurnalpi Terranes (Fig. 2). In the Kalgoorlie Terrane, it is broadly subdivided into three sequences, each separated by a major unconformity: 1) the Kambalda Sequence, dominated by mafic–ultramafic rocks; 2) the Kalgoorlie Sequence, characterised by siliciclastic rocks, local felsic volcanic centres, and dolerite sills, and 3) late basins dominated by coarse clastic detritus. While variations in the Kambalda sequence are well understood, detailed stratigraphy of the Kalgoorlie sequence is less well understood, and the late basins have only recently been examined in detail (Krapež and Barley, 2008; Krapež et al., 2008a; Krapež et al., 2008b).

In the Kurnalpi Terrane, the 2.7 Ga stratigraphy can be subdivided into: the Kurnalpi Sequence, comprising a mixture of sedimentary and volcanic rocks; the Minerie Sequence, comprising mafic–ultramafic rocks and difficult to differentiate from 2.8 Ga Laverton Sequence mafic–ultramafic stratigraphy (Chapter 2); the Gindalbie Sequence, comprising coeval felsic and mafic volcanic (bimodal) or andesitic volcanic centres (Barley et al., 2008); and the late siliciclastic basins.

Intrusive history

A major step forward in understanding the Yilgarn Terrane emerged from a granite study undertaken by Geoscience Australia (Champion and Sheraton, 1997). Broad sampling of granitoid intrusive rocks from across the northern Yilgarn (Fig. 3) resulted in the identification of five geochemical groups: 1) high-Ca (granodiorite, trondhjemite, monzogranite); 2) low-Ca (granodiorite, monzogranite, syenogranite); 3) high-HFSE (granite); 4) mafic (diorite, tonalite, trondhjemite, granodiorite, granite); and 5) syenitic (syenite, quartz syenite, monzonite).

Granitoid petrogenesis is based on the trace element and isotope geochemistry of each of the geochemical groups. High-Ca granitoid units are similar to other tonalite–trondjhemite–granodiorite (TTG) systems derived from a mafic source with stable garnet (but not plagioclase) in the source area (Martin, 1994). Probable models involve partial melting of a thickened crust or melting of a subducted slab (Martin, 1994). The common presence of older inherited zircons (Hill et al., 1992; Nelson, 1997) supports the melting of a pre-existing thickened crust. Conversely, the low-Ca granitoid intrusions represent reworking of crust and partial melting of tonalitic rocks (Brown et al., 2001). Similarly, the high-HFSE granitoid intrusions are derived from crustal melting (Champion and Sheraton, 1997). The source for the mafic and syenitic groups is more ambiguous, with possible contributions from both crustal and mantle sources (Champion and Sheraton, 1997).

Thermal history

For at least two decades it has been realised that there are several intrusive events in the EGST, and therefore there should be multiple thermal pulses through the crust. Yet available maps of metamorphic assemblages, which had no depiction of time, treated these assemblages as

representative of one thermal event (Binns et al., 1976), although they are actually the sum of several overprinting events. Details of timing eluded us because of limitations in available techniques to date minerals (in situ analytical capability + larger-scale context of fabric development versus mineral growth) and the thermobarometric models on typical greenstone minerals with large solid solution ranges carried large uncertainties.

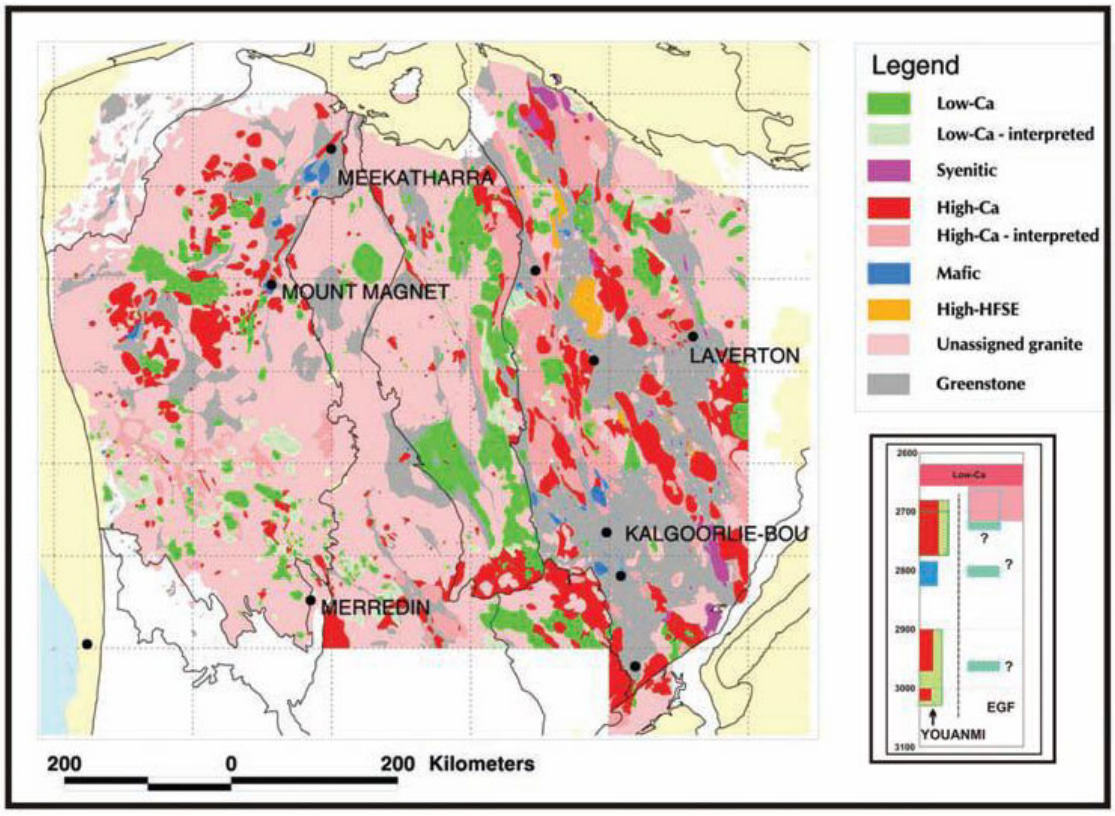

Figure 3. Distribution of granites groups within the Youanmi Terrane and Eastern Goldfields Superterrane of the Yilgarn Craton. Granite groups are as outlined in Table 1. Figure from Cassidy et al. (2002). Inset shows the relative age distributions of greenstone rocks and granites.

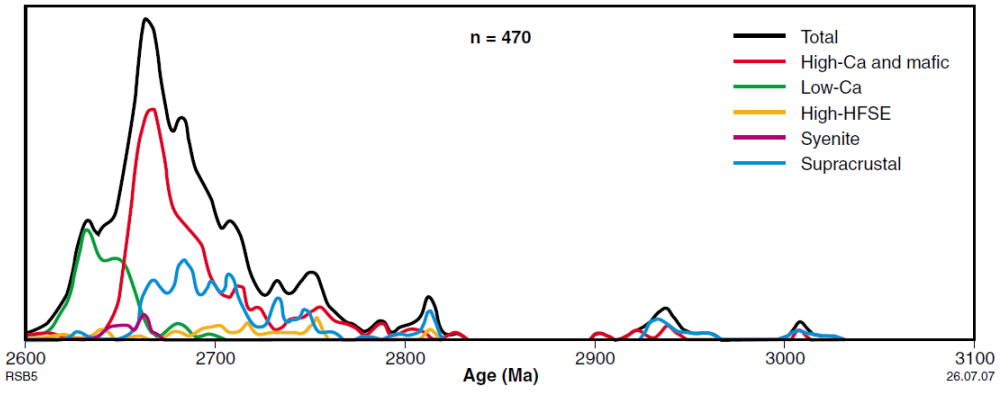

Figure 4. Histogram of granite and greenstone ages for the Yilgarn Craton (after Blewett et al., 2004). Note the peak in ages at around 2660 Ma, and the change from high-Ca magmatism to low-Ca magmatism (from Champion and Cassidy, 2007).

Goscombe et al. (2007) undertook a detailed study of mineral paragenesis, coupled with dating of metamorphic phases and thermobarometric calculations, over a wide area such that variations in metamorphism in space and time could be elucidated. This marks a fundamental dataset to advance our understanding of Archean tectonics. Results of the study are shown in Figure 5 and Figure 6.

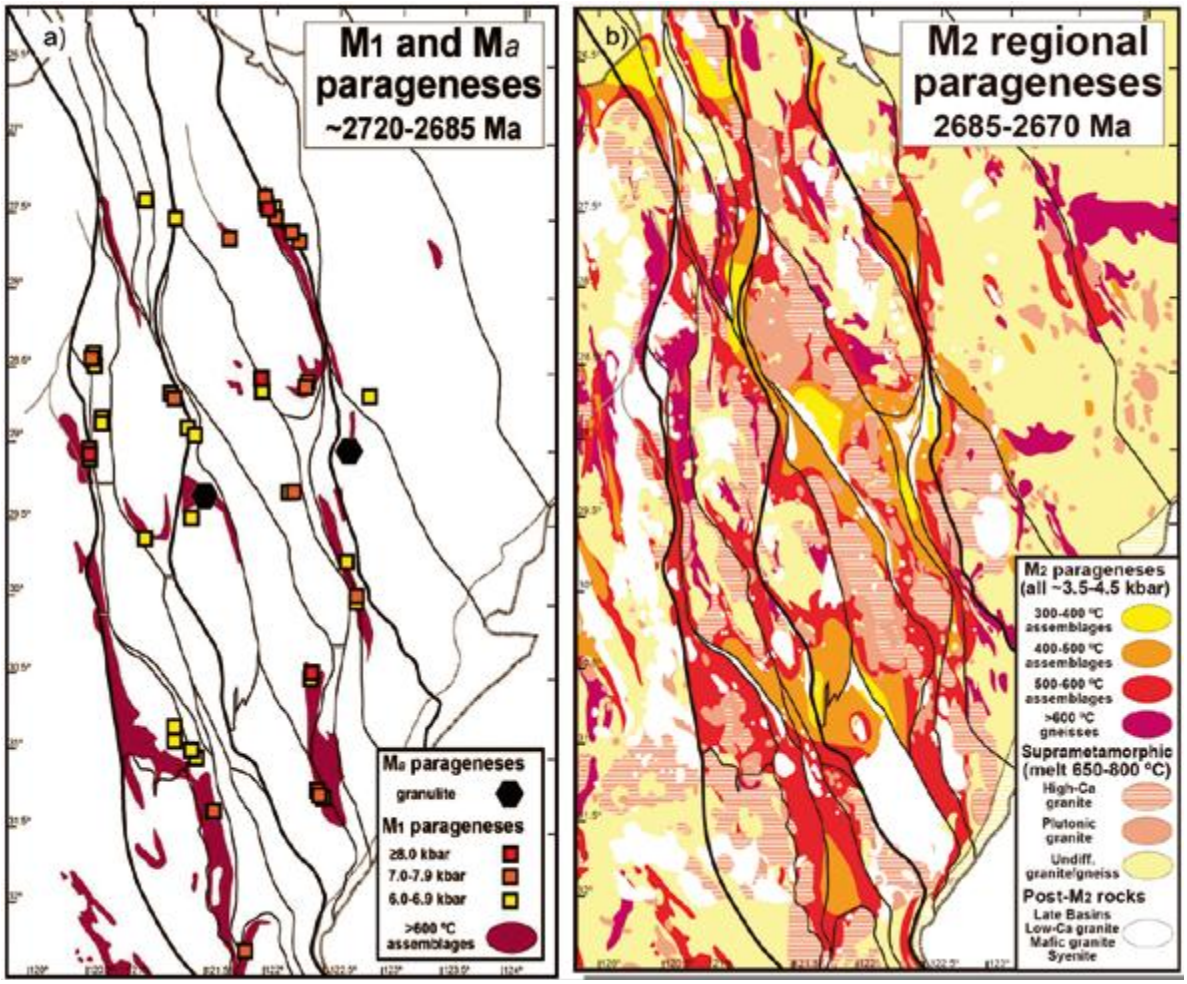

Figure 5. Distributions of metamorphic parageneses and effects during two metamorphic periods (from Goscombe et al., 2007): a) M1 and Ma parageneses highlighting the distribution of high pressure metamorphism; b) M2 metamorphic pattern — a composite including M3a parageneses, which cannot be isolated from M2 away from the late basins. Nevertheless, the widespread distribution of M2 effects is interpreted as generally correct, with temperature remaining elevated in parts, forming a continuum with M3a.

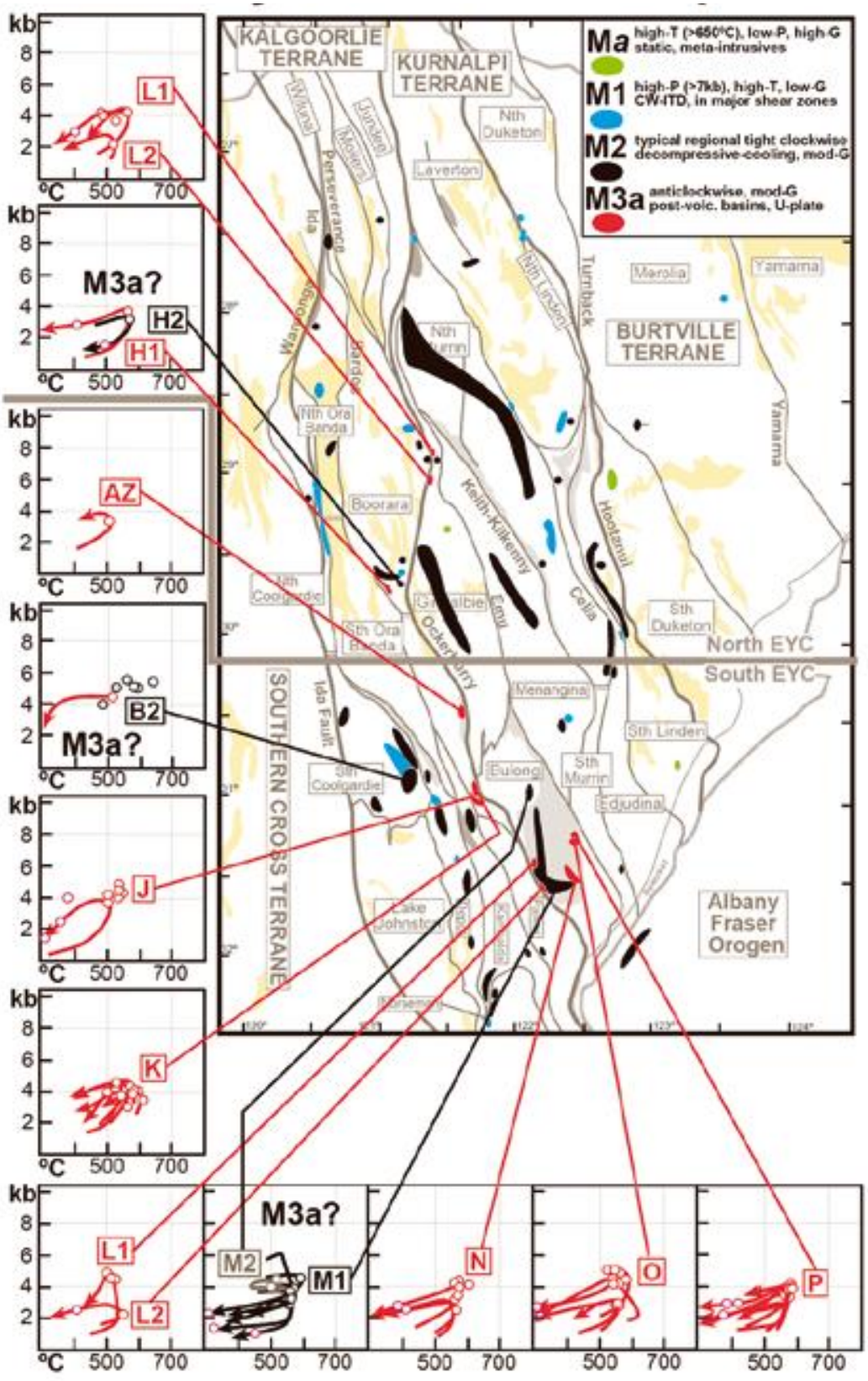

Figure 6. Summary of M3a metamorphism, highlighting anticlockwise P–T paths defining a corridor parallel with the Ockerburry Shear System (Czarnota et al., 2009).

Five metamorphic events have been distinguished: M*a*, M1, M2, M3a and M3b, as follows:

- M*a* = rare granulite facies rocks (high-T, high-geothermal gradient) metamorphism at c. 2720–2685 Ma synchronous with voluminous magmatic activity and deposition of volcanic sequences. Peak metamorphic conditions of c. 730 °C at low pressures between 2.5 – 5.0 kbar, indicating very high average thermal gradients between 45–80°C/km. Postulated as representing the roots of arcs**.**
- M1 = discrete, medium-P (P >6kbar, up to 8.7 kbar), high-T (>600°), low-geothermal gradient (≤20 °C /km) metamorphism, also at c. 2720–2685 Ma. It is not known whether the restriction of these M1 assemblages in long linear exposures (Fig. 5) reflects preferential exhumation of a more widespread metamorphic event (e.g. in the footwall plate of the M3a extensional event), or if they reflect the original distribution of these assemblages. If the distribution is original, they may reflect conditions attained in Archean subduction zones.M2 = regional metamorphism at c. 2685–2665 Ma characterised by tight clockwise P–T–t paths with low T (300–550°C), low P (3.5 – 5 kbar) and moderate-geothermal gradients (30–40°C/km), synchronous with widespread emplacement of high-Ca granitoid rocks. Metamorphic grades increase towards granitoid margins and reflect advection of heat into the crust by granitoid melts. This event forms the dominant regional metamorphic event, and predates the late basins.
- M3a = characterised by moderate-T (500–580°C), low-P (3–5 kbar) extension related, high-geothermal gradient metamorphism (40–50°C/km), characterised by anticlockwise P–T–t paths. This event is only recognised as spatially associated with late siliciclastic basins at 2665–2650 Ma, although regionally it would be difficult to distinguish from M2 assemblages. This metamorphic event is interpreted as related to extension, formation of late basins, and generation and emplacement of low-Ca granites into the crust.
- M3b = hydrothermal alteration assemblages representing multiple potential pulses of gold mineralisation c. 2650–2620 Ma. These assemblages form at temperatures generally between 250–500°C and pressure ranges of 3.0 – 3.5 kbar at moderately elevated thermal gradients of 30–50°C/km.

Structural evolution and architecture

Traditionally, deformation schemes had been developed over small portions of the Kalgoorlie and Kurnalpi Terranes, largely around mine sites, and in particular the Kambalda Domain of the Kalgoorlie Terrane. These schemes focussed on documenting overprinting compressional/transpressional events, which were the dominant fabrics preserved in the belt.

Recent integrated interpretation of stratigraphic variations, intrusive events and mechanisms of magma emplacement, isotopic datasets, crustal-scale seismic and potential field geophysics has revealed:

1. Structural event schemes are broadly comparable across the EGST, albeit with local variations in expression
2. Extensional events are critically important, and punctuate the tectonic history of the belt
3. A fundamental architecture to the belt was established early, and has likely been repeatedly reactivated on a number of scales.

Seismic transects across the EGST were available in 2000; however, it is only with integration of improved stratigraphic and structural understanding, and more detailed geochronology, that these images can be comprehensively interpreted. Furthermore, the geophysical data give us a snapshot of the crust now, not at the time of formation. Maps of radiogenic isotopic data, on the other hand, serve as a proxy to map the architecture of the crust at the time the EGST was formed, as discussed later in this section. Available regional seismic data are shown in Figures 7, 8 and 9.

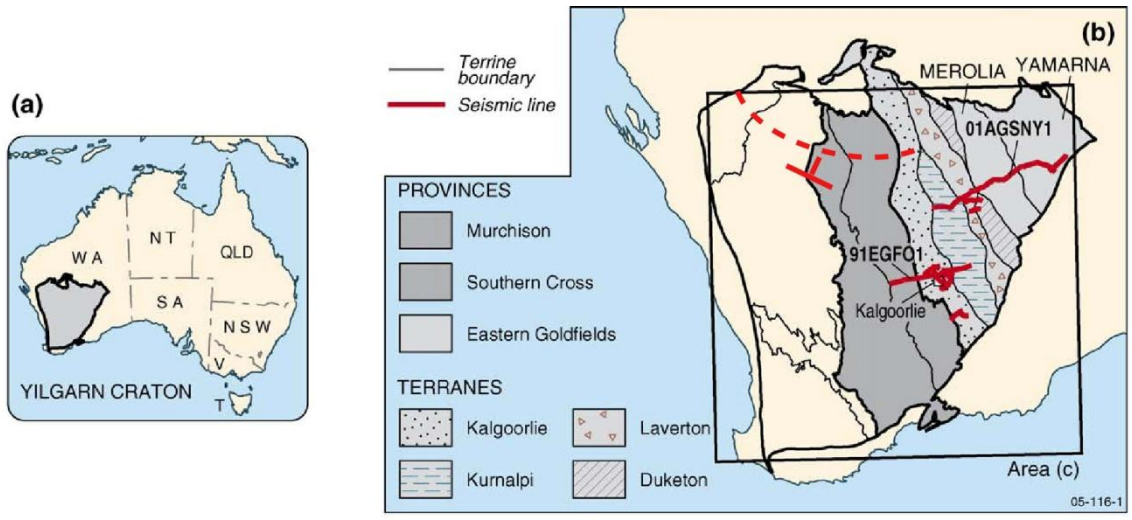

Figure 7. Yilgarn Craton and locations of seismic traverses: a) map of Australia showing location of the Yilgarn Craton; b) map of the Yilgarn Craton showing subdivision into different provinces, terranes, and domains, with locations of the deep seismic reflection traverses. Dashed red line is approximate location of recent seismic reflection survey, yet to be released (after Goleby et al., 2006).

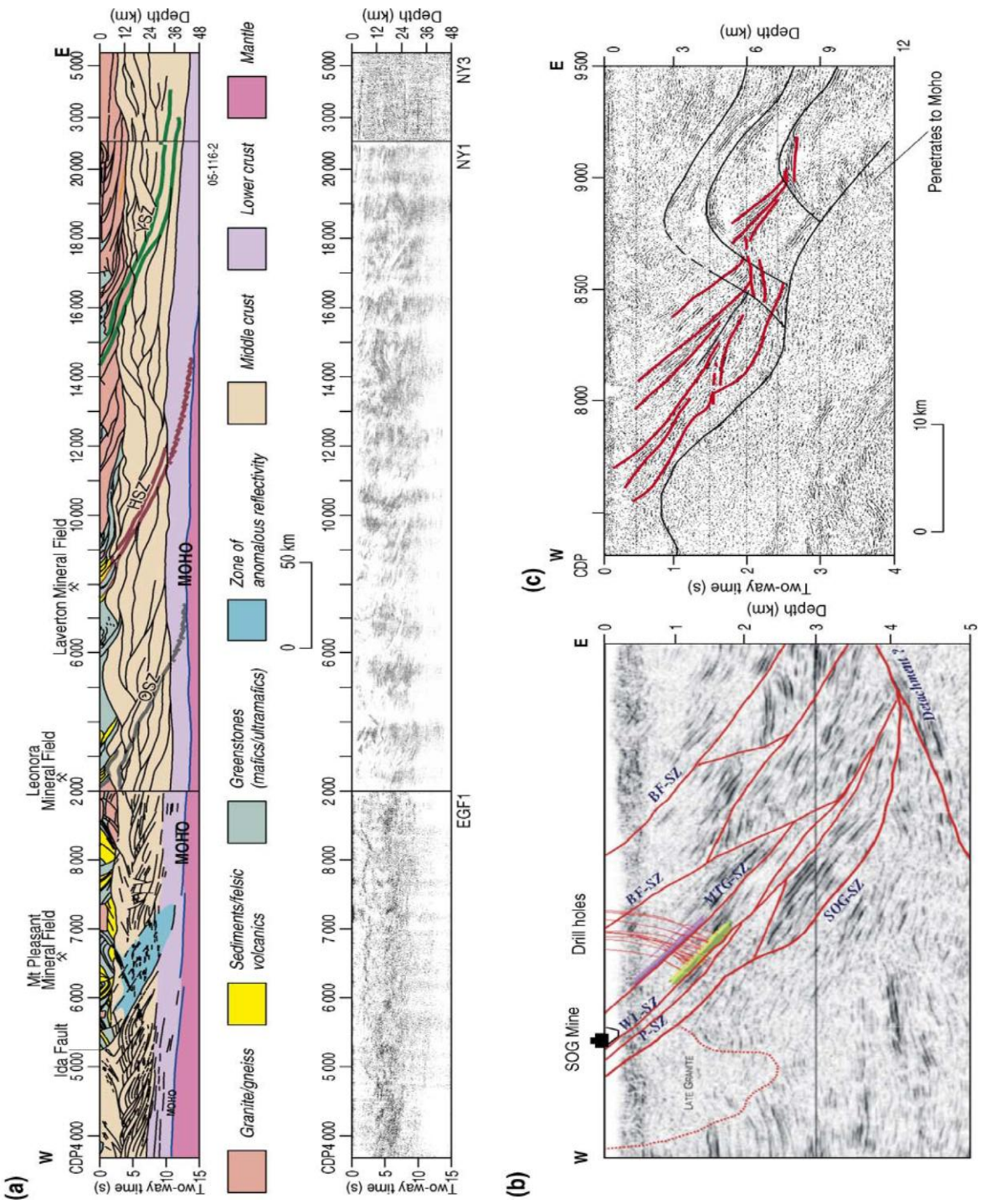

Figure 8. Interpretations of crustal-scale seismic traverses: a) composite image of the 1991 Eastern Goldfields seismic traverse and the 2001 northeastern Yilgarn Craton seismic traverse showing prominent crustal-scale features imaged by the deep seismic reflection studies. The raw seismic sections are displayed underneath. This composite section shows four sub-horizontal layers; the lowest is the mantle, above which are a thin non to poorly reflective lower-crustal layer, then a mid-crustal layer containing large scale lozenges and a more complex upper crustal granite–greenstone layer. The composite section is approximately 630 km long by 45 km deep; b) detailed view of the western most part of the 2001 northeastern Yilgarn Craton seismic traverse, across the Leonora Mineral Field, showing drill hole locations, seismic interpretation, and location of the SOG mine; c) Detailed view of the middle part of the 2001 northeastern Yilgarn Craton seismic traverse, across the Laverton Mineral Field, showing the seismic interpretation and possible fluid flow paths (Goleby et al., 2006). The preservation of older stratigraphy over younger stratigraphy on a reverse fault supports the interpretation of reactivation of earlier-formed basin-controlling faults.

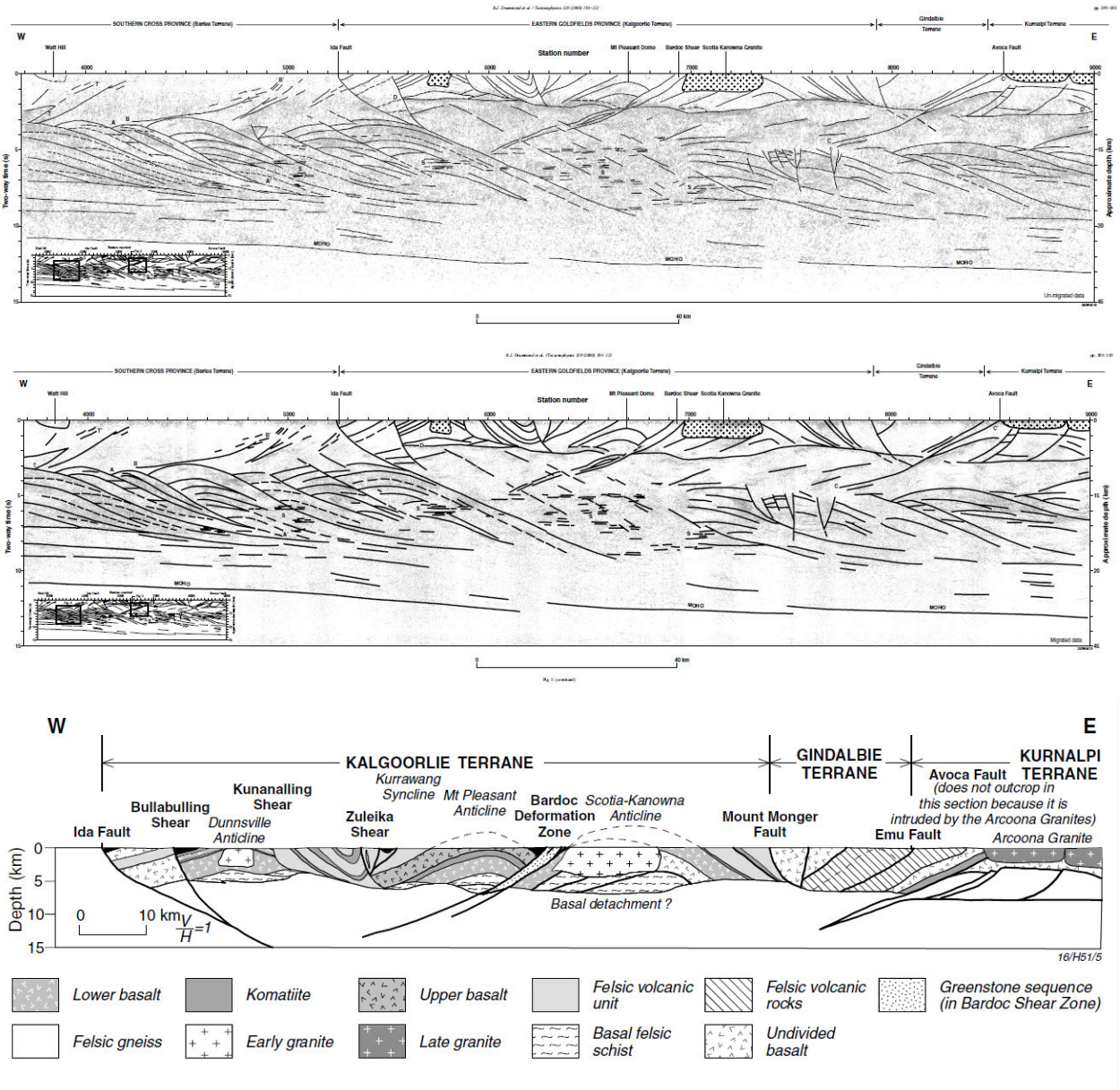

Figure 9. Top: Traverse EGF1 un-migrated seismic data with the interpreted structures superimposed. Terrane boundaries are marked at the top of the section. Bottom: Cross section through the greenstones of the Eastern Goldfields Province based on the interpretation of the EGF1 seismic traverse (Drummond et al., 2000).

The analysis of the isotopic character of intrusive and volcanic rocks has been instrumental in developing an understanding of the paleoarchitecture of the craton. Pioneered by Champion and Cassidy (2007), this mapping of paleocraton margins by isotopic proxy (initially whole-rock Nd model ages) and integration with other geophysical and geological datasets has significantly augmented our understanding of the tectonic history and assembly of the EGST in particular.

A map of whole-rock Nd model ages is shown in Figure 10, and highlights the distinct boundary between older crust of the Youanmi Terrane to the west and dominantly juvenile rocks of the EGST to the east. This boundary correlates well with the Ida Fault, the surface expression of the boundary between the two terranes. The isotopic map may serve as a proxy for mapping cratonic

architecture, with the boundary between the Youanmi and EGST is interpreted as imaging an Archean paleocraton margin.

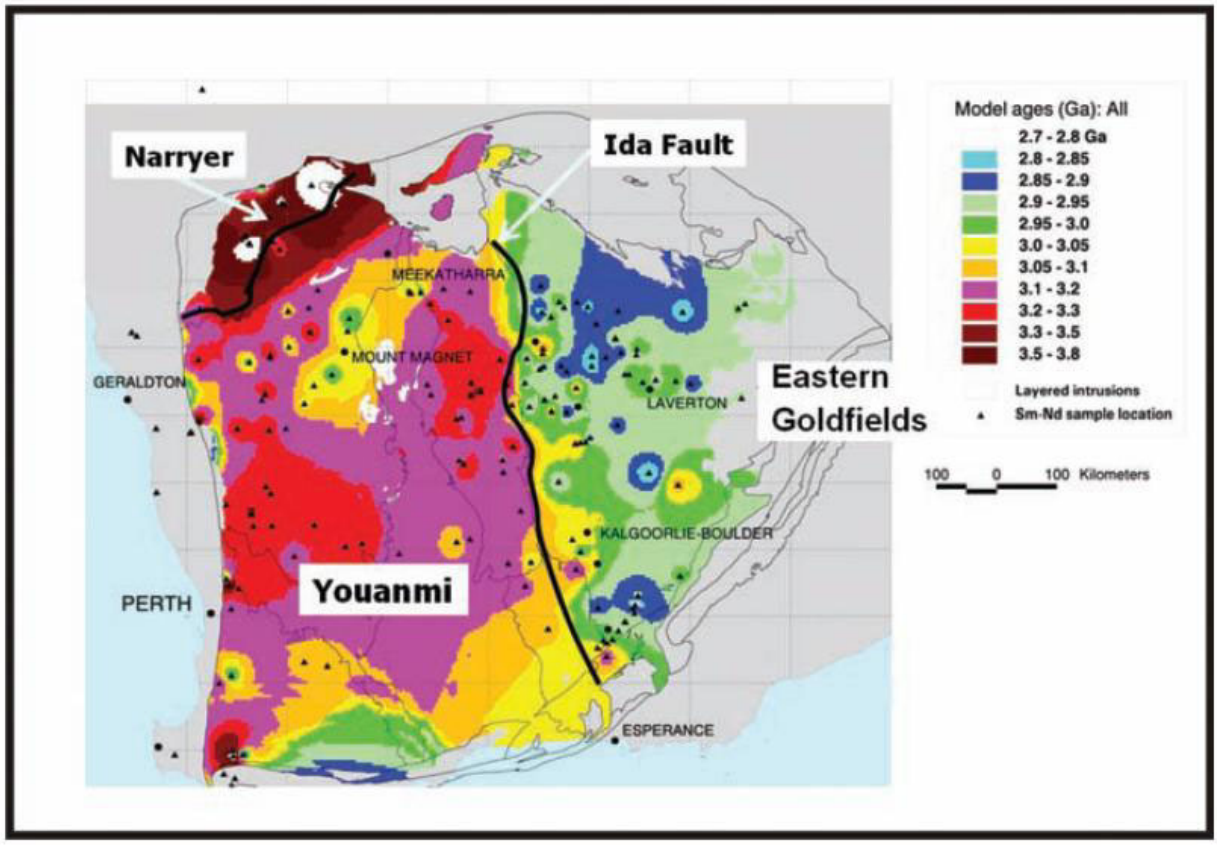

Figure 10. Nd depleted-mantle model age map of the Yilgarn Craton. Image produced by gridding Nd depleted-mantle model ages of low-Ca granitoids calculated from Sm–Nd point data (from Champion and Cassidy, 2007). Hot colours indicate granitoids that have melted older crust, cooler colours indicate granitoids that have melted juvenile crust.

Tectonic models

Several tectonic models for the Eastern Goldfield Superterrane have been proposed based on various lines of evidence. These models are simplistically grouped below with key supporting evidence:

- plume tectonics — based on need for hot jets of ascending lower mantle material to generate high volume komatiitic melts (Campbell et al., 1989)
- accretionary tectonics — based on linear patterns to greenstone belts, different stratigraphic assemblages between terranes, sequence stratigraphy in late basins, geochemistry of volcanic rocks showing arc (Kurnalpi) – backarc (Kalgoorlie) affinities (Barley et al., 2008; Krapež and Barley, 2008).

- intracontinental rifting — based on isotopic evidence for older substrate to greenstones, interpreted emplacement of granitic gneiss domes, metamorphic patterns increasing in temperature (± pressure) towards gneiss domes (Groves and Batt, 1984; Hammond and Nisbet, 1992), bimodal volcanism in the Kalgoorlie Sequence. Proponents of rifting models debate about early vs late or punctuated extension
- gravity-driven tectonics — based on patterns of high metamorphic grade granitoid gneiss domes rimmed by thin greenstone sequences of lower metamorphic grade facing away from domes and forming synclinal keels between domes.
- Each of these models is underpinned by a specific set of observations and datasets, and all of these models struggle to account for all of the features observed in the rock record. However, integration of all datasets is leading towards a convergence of models. The series of diagrams in Figure 11 represent a synthesis of several studies over the EGST as part of the pmd*CRC (Czarnota et al., 2009). This is the most comprehensive model attempting to explain all aspects of the rock record, from stratigraphy and structural histories through to intrusive rock geochemistry and geochronology, spatial and temporal distribution of rock sequences, and metamorphic patterns.

Southern Cross Domain, Youanmi Terrane

Early descriptions of the Southern Cross stratigraphy, structure and metamorphic patterns were presented by Gee (1982) and Ahmat (1986). The following presents an update by Thébaud and Miller (2009) of these early investigations, with the timing of events synthesised in Figure 12.

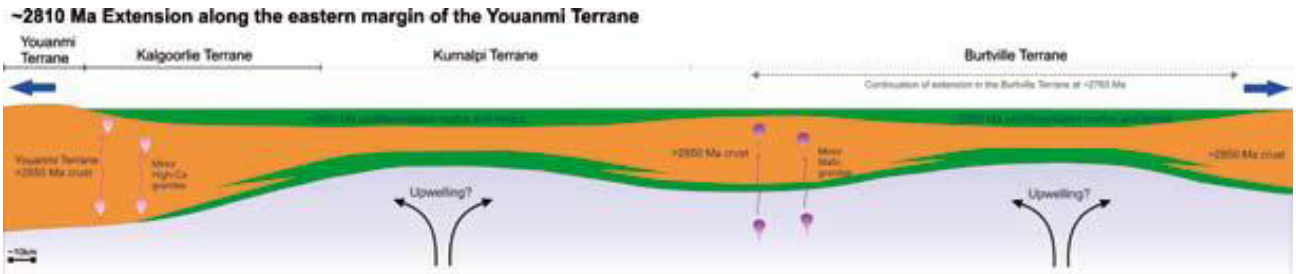

Figure 11. Series of schematic diagrams depicting a model for the evolution of the Eastern Goldfields Superterrane (from Czarnota et al., 2009) based on the outcomes of the 7-year predictive mineral discovery Cooperative Research Centre.

~2715-2690 Ma Initiation of west dipping subduction: arc and back-arc volcanism; *Ni mineralisation*

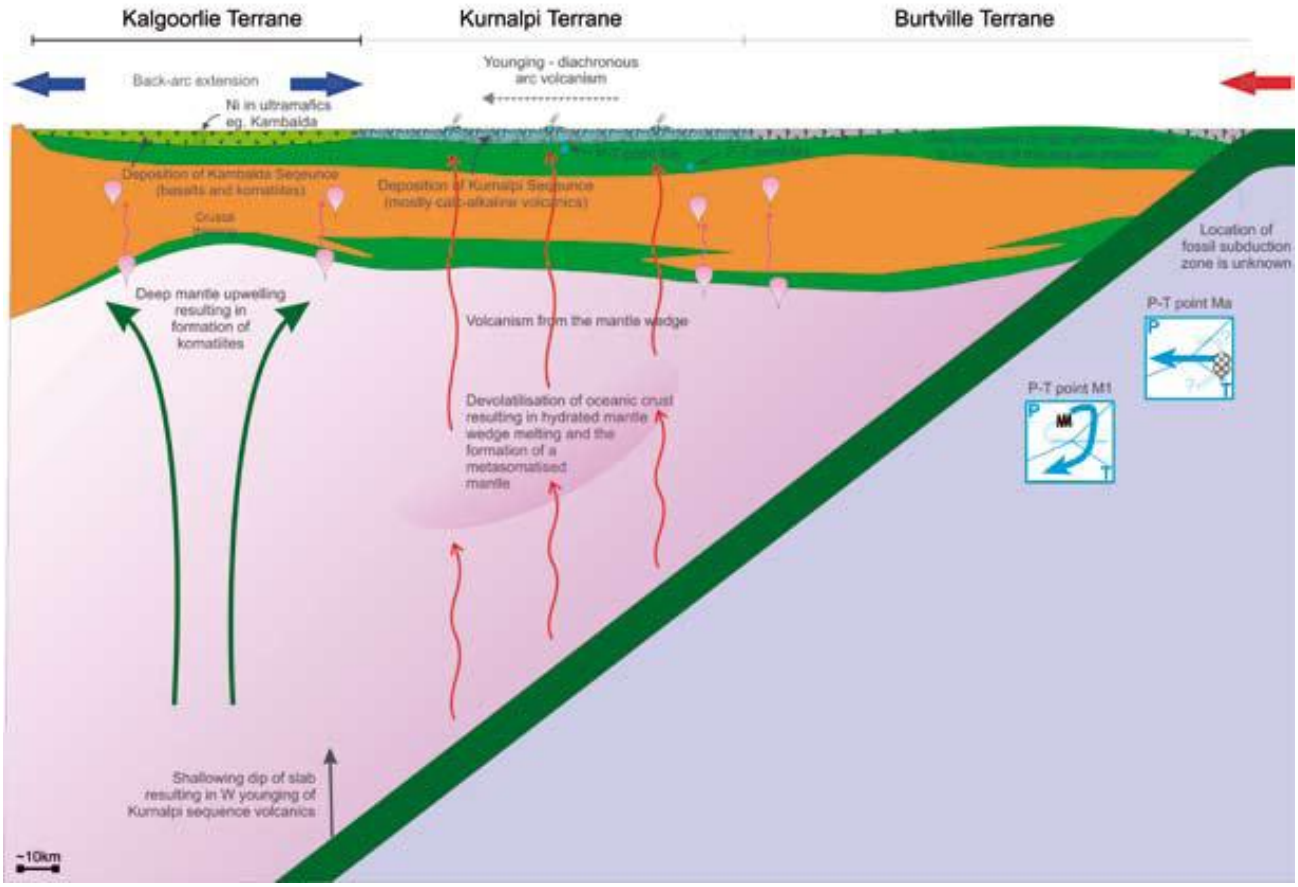

~2690-2670 Ma Shallowing of subduction slab: bimodal volcanism; voluminous High-Ca granite magmatism; *VHMS mineralisation*

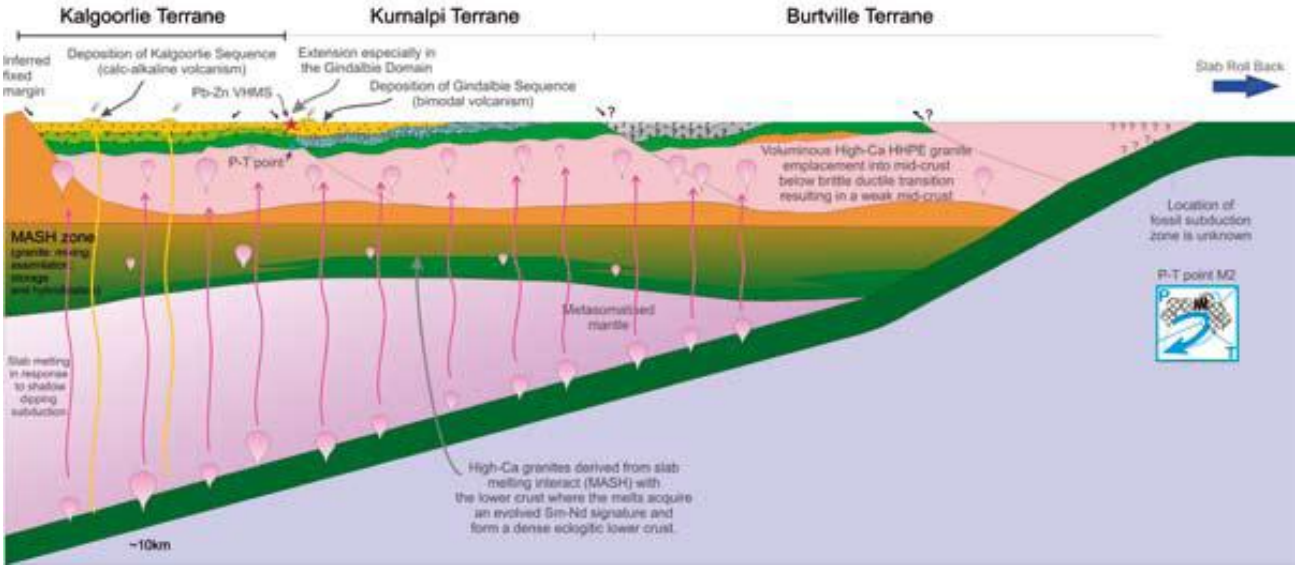

Figure 11. (continued)

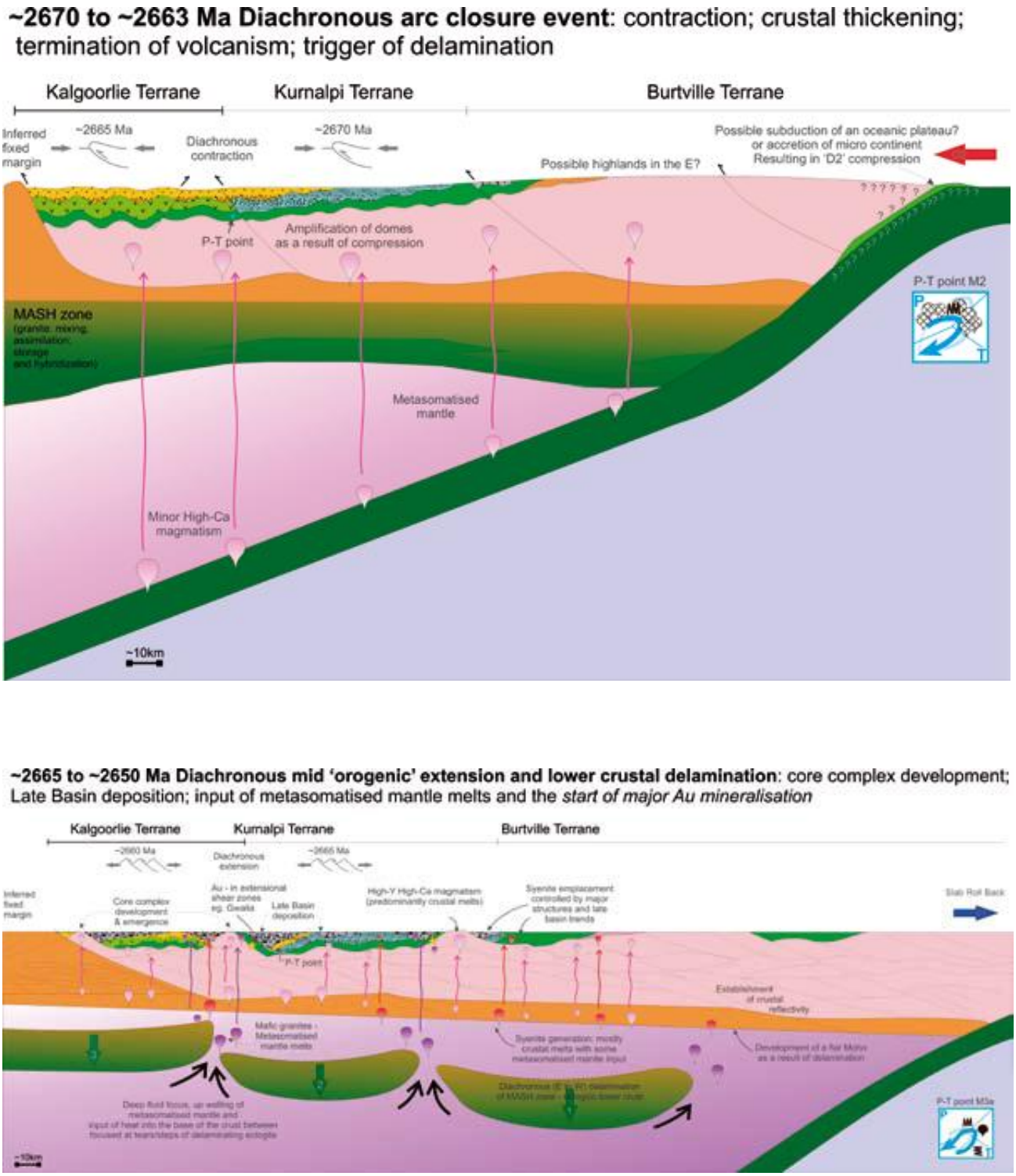

Figure 11. (continued)

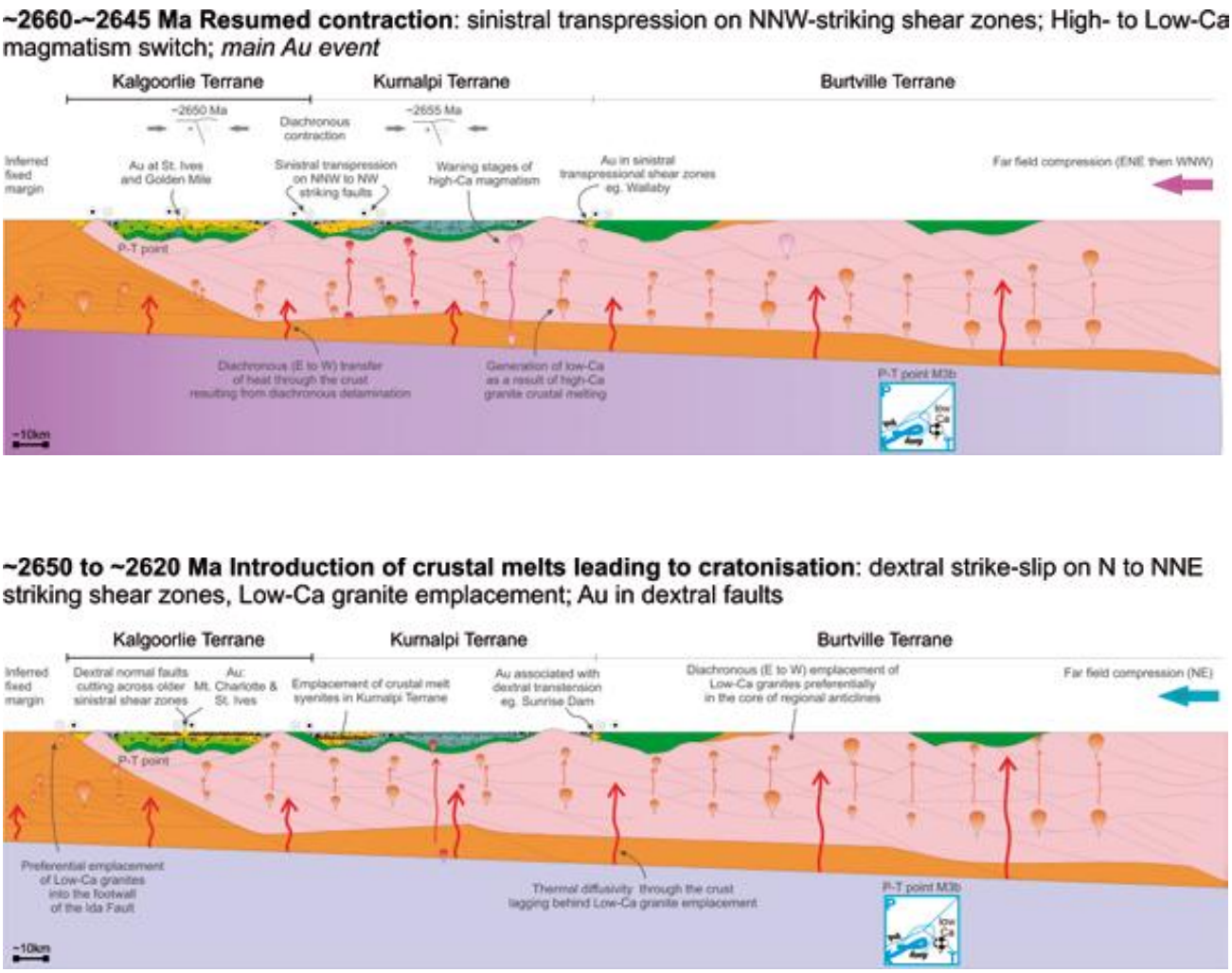

Figure 11. (continued)

Greenstone stratigraphy

The broad stratigraphic distribution observed in the Southern Cross greenstone belt is evident from the concentric distribution of the various rock types around the Parker and Ghooli granitoid domes (Fig. 13). All primary facing and dip orientations of sedimentary and volcanic layering points away from the granitoid, defining a syncline geometry to the belt.

At the lowest stratigraphic level is a thin layer of quartzite and muscovite schist in direct contact with the sheared margin of Ghooli dome. This lower level has been recognized as regionally forming the base of the central Yilgarn Craton greenstone belts (e.g. Marda Complex, Illaara greenstone belt, Maynard Hills greenstone belt) and may be the remanent of Mesoarchean proto-crust (Wyche et al., 2004). Undated in the Southern Cross greenstone belt, this basal layer preserved a minimum age of ca. 3130 Ma in the Marda Complex (Wyche et al., 2004).

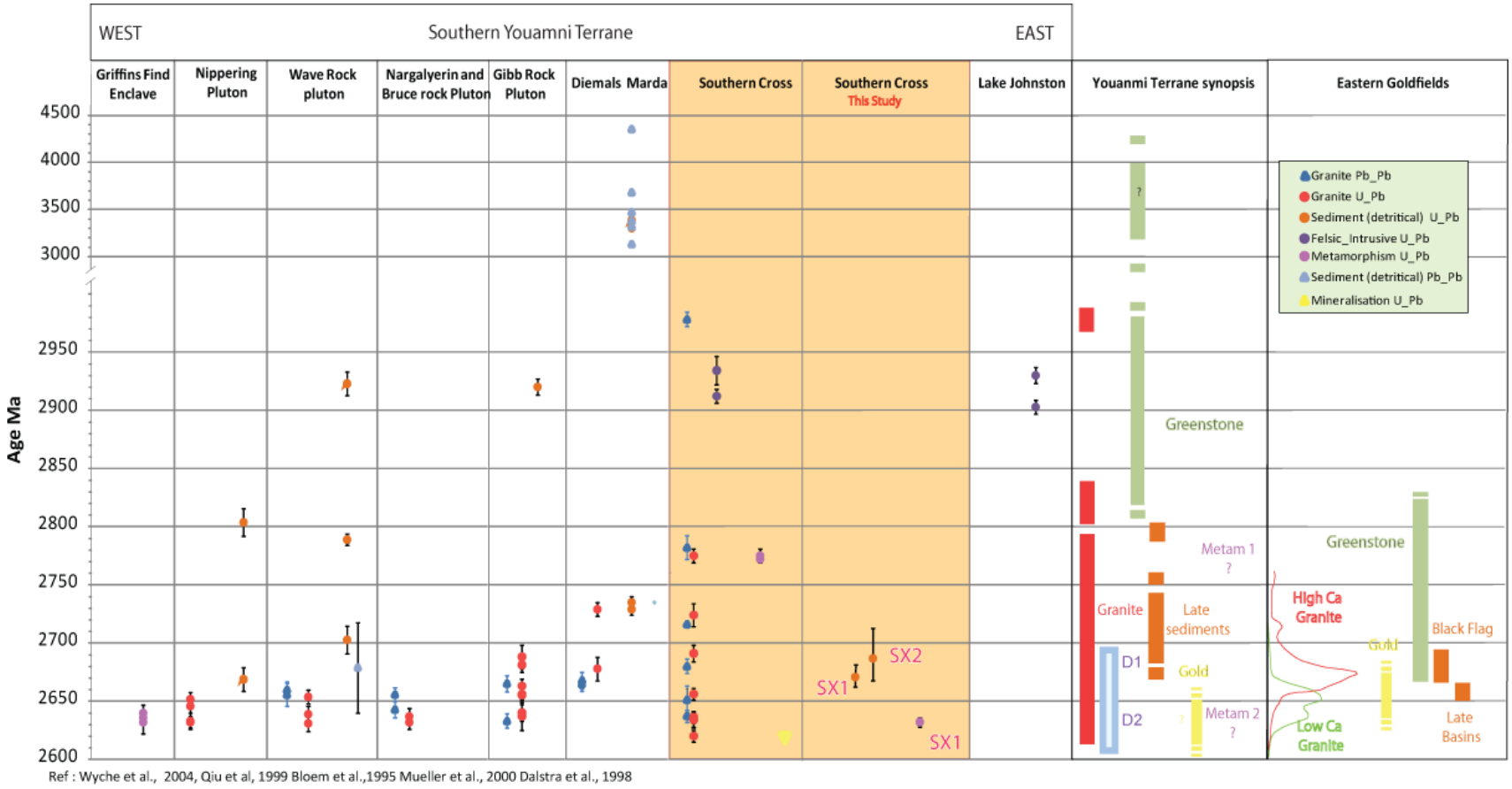

Figure 12. Space–time chart for the southern Youanmi Terrane showing available geochronology and the ages of supracrustal and intrusive events, metamorphism, and deformation. At right is a comparison to the evolution of the Eastern Goldfields Superterrane (Thébaud and Miller, 2009).

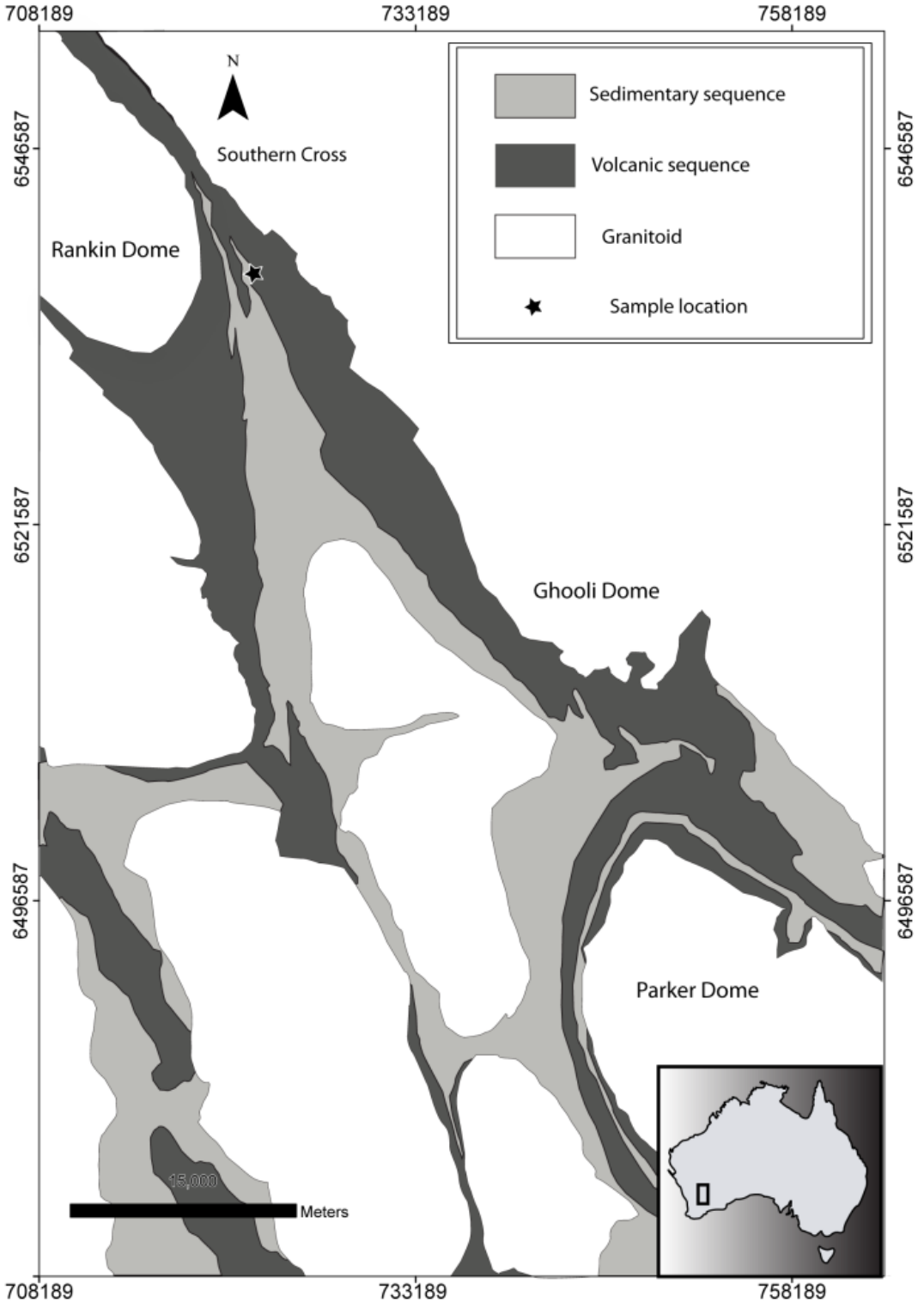

Figure 13. Simplified geological map of the main stratigraphic sequences of the Southern Cross district (Thébaud and Miller, 2009)

This basal layer is unconformably overlain by a 3–5 km thick interlayer of metamorphosed volcanic units comprising tholeiitic basalts, komatiitic basalts, komatiites, and minor banded iron-formation. The volcanic sequence age is constrained by one date obtained from quartz–feldspar porphyry associated with the Golconda iron-formation. Concordant U–Pb zircon ages of 2912 ± 5 Ma are recorded for this unit (Mueller and McNaughton, 2000).

Unconformably overlying this volcanic succession is a 3–5 km thick sediment pile. This sedimentary succession consists of metamorphosed sulphidic black shales, thick-bedded psammite, thin-bedded pellite, and minor quartz conglomerate. This metasedimentary succession has traditionally been attributed to the Mt Farmer (c. 2.8 Ga) greenstone successions, but is yet to be dated (Mueller et al., 2004).

Metamorphism

All lithologies are strongly metamorphosed with mineral assemblages indicative of amphibolite to granulite facies (Fig. 14). An early metamorphic event is interpreted to have developed in response to the granitoid emplacement and is associated with a concentric distribution of the metamorphic grades (Dalstra et al., 1998). Crystallisation pressure in the granitic domes in the order of 4.3 to 6.2 kbar is about 2 kbar higher than peak metamorphic pressure in the supracrustal greenstone succession (3.0 to 4.0 kbar). The higher-grade marginal zones of the granitoid domes are characterised by dynamic type metamorphism, while the lower grade dome cores present a more static-style metamorphism (Dalstra et al., 1998). A second retrograde metamorphism is documented in the Southern Cross greenstone belt and post-dates all deformation.

Structural evolution

The deformation history recorded in the greenstone succession of the Southern Cross district involved four main stages of deformations (Bloem et al., 1997). D1 is characterised by constriction folding forming large-scale upright folds and a penetrative axial planar foliation (S1). D2 is associated with the development of major strike-slip shear zones and foliation reorientation. D3 coincides with the formation of transcurent faulting with minor foliation reorientation. Finally, D4 is marked by the development of reverse brittle faults. It is argued that D1 to D3 represent a progressive brittle–ductile deformation process, broadly in an ENE–WSW compressional regime. Peak metamorphic conditions are believed to be broadly synchronous with D1 and D2.

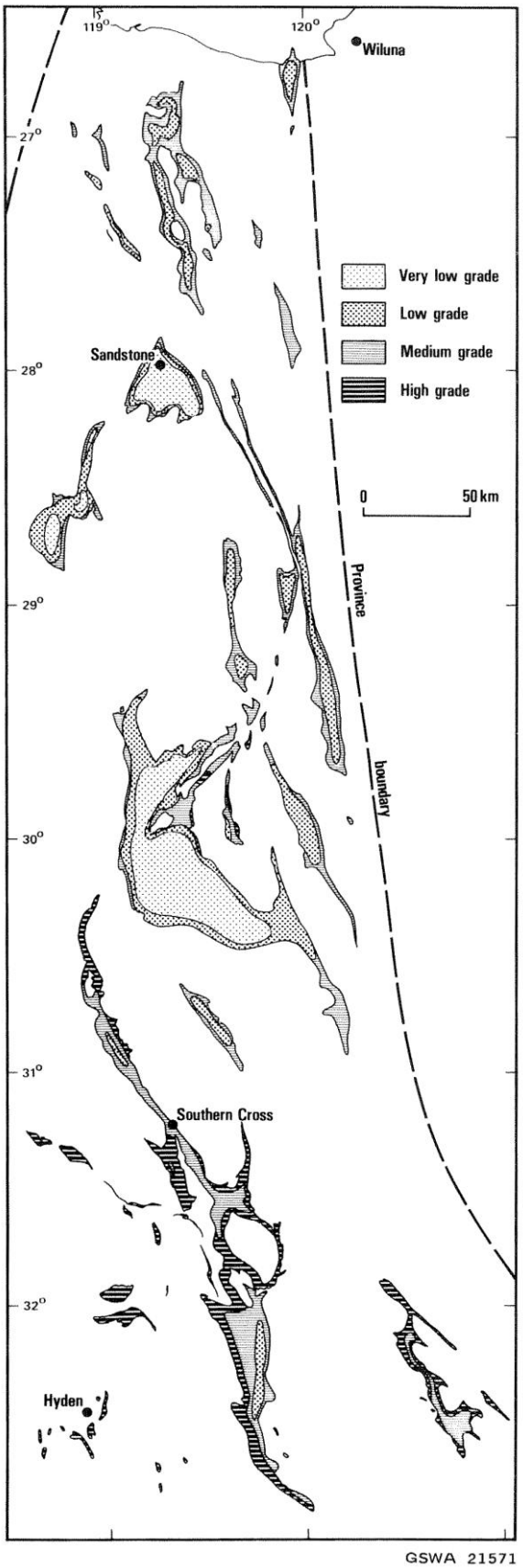

Figure 14. Distribution of metamorphic facies in the Southern Cross Domain, Youanmi Terrane (from Ahmat, 1986). Note preservation of lowest metamorphic grades in the centre of the Southern Cross Domain.

Dating of the deformation is loosely constrained between c. 2.77 Ga to 2.63 Ga (Bloem et al., 1997; Dalstra et al., 1998; Mueller and McNaughton, 2000; Mueller et al., 2004). The existing geochronological dataset for the Southern Cross district remains largely ambiguous with respect to the timing of the supracrustal cover deposition, the timing of the granitoid emplacement, and the timing of deformation and metamorphism. Recent reinvestigation of the Southern Cross has shed new light on this region (Thébaud and Miller, 2009).

The deposition of the supracrustal succession is interpreted to have occurred between c. 2.9 Ga and c. 2.8 Ga. Although the volcanic succession may have been emplaced at c. 2912 Ma (Mueller and McNaughton, 2000), the sedimentary succession preserves a minimum age of 2702 ± 17 Ma, considerably younger than initially expected. Deposition ages in the same range have been obtained for the sedimentary succession from the Marda Complex (2735 ± 2 Ma) and the Diemals Formation (2729 ± 9 Ma). The significance of these relatively late siliciclastic basins remains unclear for the tectonostratigraphic evolution of the Southern Cross greenstone belt and more generally for the Youanmi Terrane. The sediments forming the upper supracrustal succession in the Youanmi Terrane may have formed in response to the accretion of the Eastern Goldfields onto the Yilgarn Craton in a similar fashion as that of the late-stage basins in the Kalgoorlie, Gindalbie, and Kurnalpi Terranes (Krapež and Barley, 2008). Alternatively, these basins could be equivalent to the Black Flag sediments from the Kalgoorlie sequence (Krapež and Barley, 2008), and could have developed in response to the early deformation of the granite–greenstone belt. This recent work implies these younger basins had a much larger extent than previously envisioned, and the Southern Cross gold system may be located on an intracratonic rift.

Since the siliciclastic sediments of the upper supracrustal cover are strongly deformed and metamorphosed, most of the deformation and associated metamorphism must have had occurred after c. 2702 Ma. Previous studies argued that the main D1 and D2 gold-related deformation stage, which was coeval with peak metamorphism conditions, occurred between 2636 and 2620 Ma (Dalstra et al., 1998). The metamorphic zircon data presented by Thébaud and Miller (2009; 2633 ± 6 Ma) and recent dates for ductile deformation and peak metamorphism of c. 2634 ± 1 Ma to 2629 ± 1 Ma (Joly et al., 2010) support the timing of this main metamorphic event and associated deformation stage.

These early conclusions suggest that a major part of the tectonic evolution of the Southern Cross granite–greenstone terrane remains largely unconstrained. Further geochronology and tectonostratigraphic reconstruction in progress will hopefully help to further develop our understanding of the tectonostratigraphic evolution of the Southern Cross and, more generally, the geodynamic evolution and associated lode gold mineralisation of the Yilgarn Craton.

Evolution of crustal architecture in the southern Yilgarn

Recent integration of in situ analyses of Lu–Hf and U–Pb in zircons, combined with the available whole-rock Sm–Nd database (Fig. 10), has allowed creation of time slices showing the progressive

cratonisation of the EGST and southern Youanmi Terranes (Fig. 15; Mole et al., 2010). Stratigraphic variations across the southern Yilgarn are neatly explained within this time slice construct (Fig. 16).

Preliminary data support the presence of an old stable craton in the central Southern Cross Domain at the time of widespread greenstone deposition and komatiite volcanism at c. 2.9 Ga. The identification of an older cratonic block in this region explains a number of north–south variations noted in the rock record in this domain, which previously have been difficult to explain as they occur along strike of the dominant structural grain of the region.

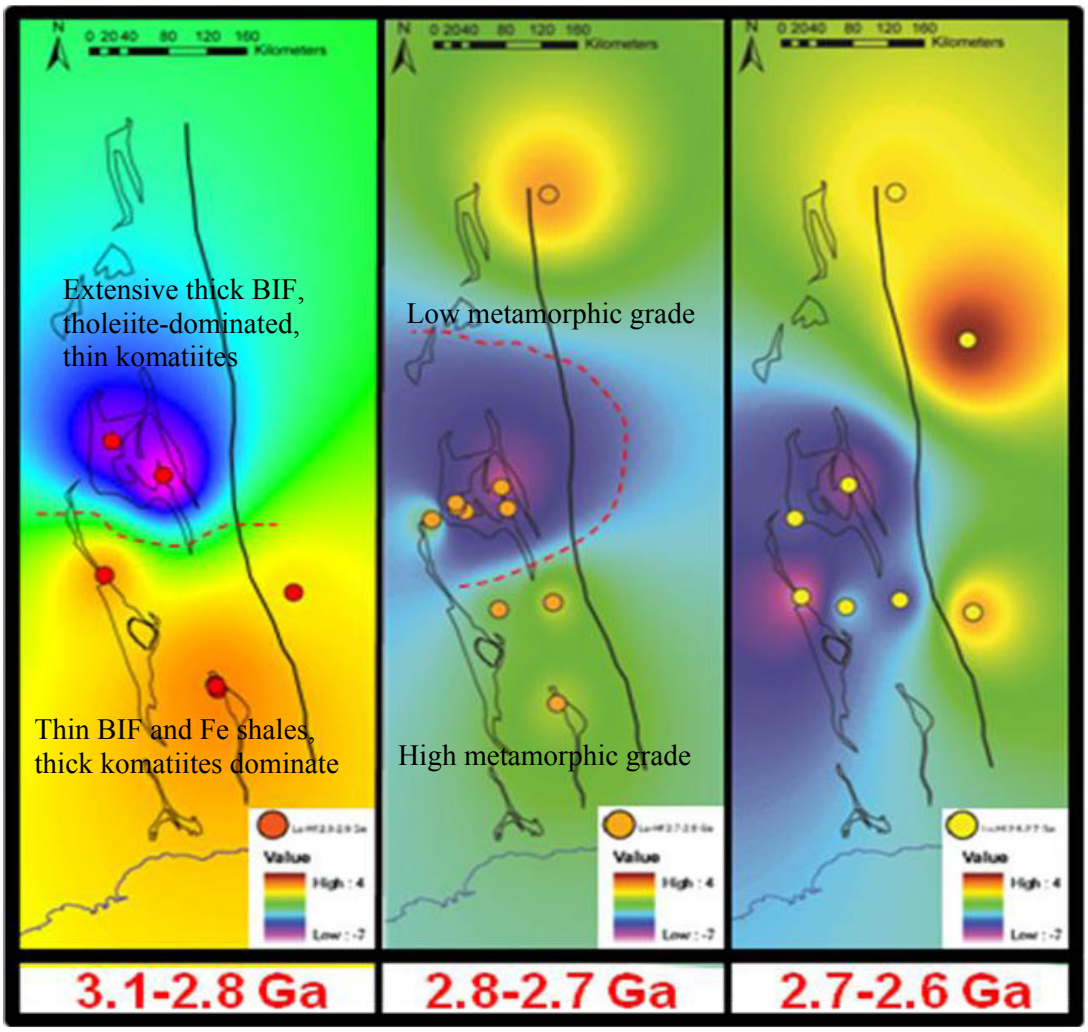

Figure 15. Time slices of ε_{Hf} data obtained from zircons in felsic volcanic and intrusive rocks from the southern Yilgarn. Outlines of greenstone belts and the position of the Ida Fault (boundary between EGST and Youanmi Terrane) are shown for reference. The images are interpreted as coarse representations of the growth of continental crust and progressive cratonisation of the Yilgarn (after Mole et al., 2010).

A fundamental control of the paleocraton on the distribution of rock types is noted. Rocks on the older paleocraton comprise extensive BIF sequences, abundant tholeiitic volcanic and intrusive rocks and thin komatiites with low Mg numbers. Komatiites are of both Al-depleted (deep mantle melting) and Al-undepleted (shallow mantle melting) types, and lack significant adcumulate

facies. Rocks to the south (Forrestania and Lake Johnston regions) comprise thicker ultramafic sequences with higher Mg numbers and more abundant adcumulate facies. BIF comprise Fe-rich shales and thin BIF–chert horizons with interlayered fine-grained siliciclastic layers. These variations are consistent with the transition from a stable continental shelf to a deeper-water, off-craton environment of deposition.

Furthermore, this early cratonic architecture plays a key role in the response of the crust to subsequent deformation events. Comparison of Figure 15 to Figure 14 shows that the lowest metamorphic grades and more arcuate greenstone sequences are preserved in the region of oldest lithosphere, whereas areas to the south (and north) comprise more linear greenstone belts that are more highly deformed and metamorphosed to higher grades. This distribution is interpreted as reflecting preferential preservation of supracrustal sequences on the old craton, which is assumed to have originally had a thicker lithosphere.

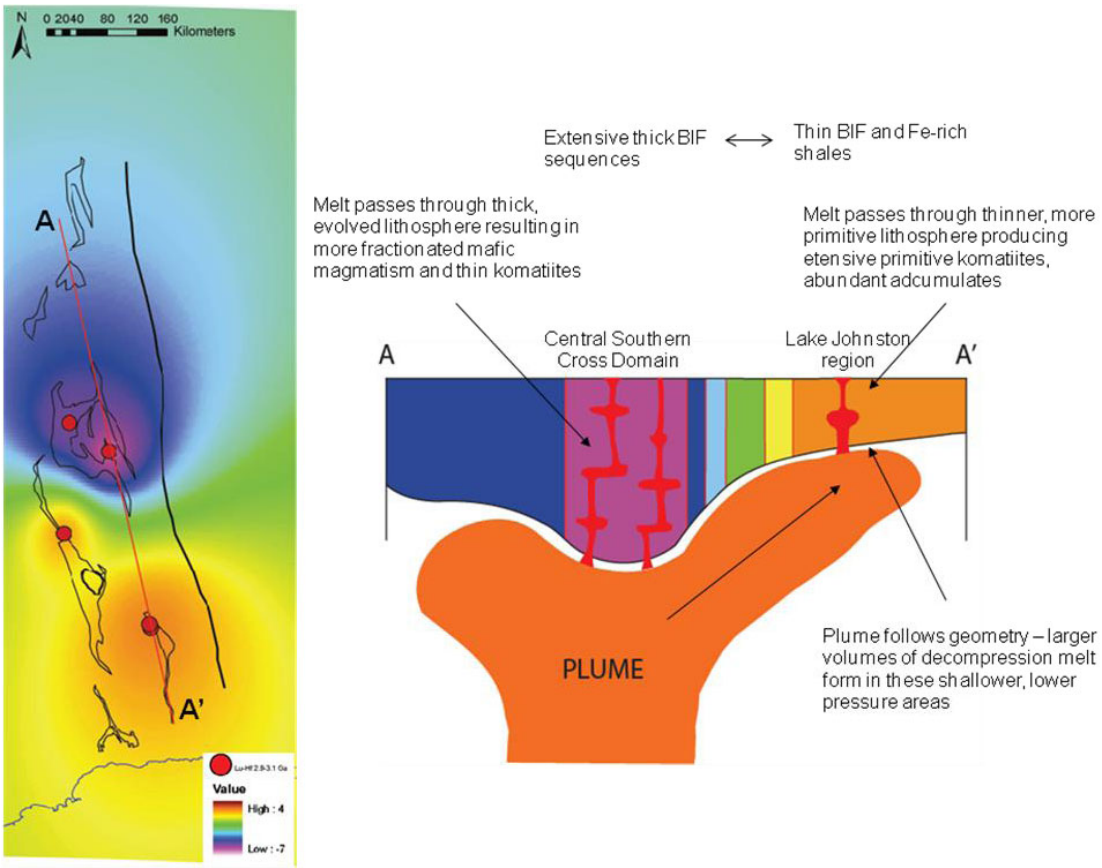

Figure 16. N–S cross section through 3.1 – 2.8 Ga timeslice of Figure 15. Colours of lithosphere on cross section correspond to colours on map view image at left. Interpreted control of older craton on character of BIF and mafic–ultramafic sequences is shown (after Mole et al., 2010).

Mineral systems of the Yilgarn — advances in the past decade

The Yilgarn Craton has long been recognised as having world class endowments of Au and komatiite-hosted NiS deposits, with appreciable high-grade Fe resources, and more modest

endowments of VHMS. Yet the endowment varies dramatically between terranes of the Yilgarn, and between constituent geological domains, showing a tendency to cluster in districts or 'camps'. What controls this spatial distribution of resources? Is it due to formational or preservational factors, or simply a lack of exploration?

Situation in 2000

At the turn of the century, academic studies of mineral systems in the Yilgarn had largely been focussed at the scale of the deposit — elucidating processes that have occurred in their formation, structural controls on ore geometry, and relative and absolute timing of mineralising events. The prevalent models of the time are listed below:

For gold in the Yilgarn, the prevailing model was a crustal continuum model (Groves, 1993) comprising craton wide 'orogenic Au' at ca. 2.64 – 2.63 Ga, syn- to post-peak metamorphism, with fluids considered dominantly deeply sourced metamorphic or orthomagmatic (Groves, 1993; Groves et al., 1998; Groves et al., 1995; McCuaig and Kerrich, 1998).

For nickel sulphide deposits (NiS), the prevailing model comprised formation of these deposits at the base of komatiitic extrusive flows. The komatiites were all considered to be extrusive rocks, which assimilated underlying sulphidic sediments triggering sulphur saturation upon emplacement. Nickel sulphides (NiS) accumulated at the base of flow channels due to gravitational settling or suspension within flow channels.

Iron deposits of the Yilgarn were viewed much like their Proterozoic (Hamersley) counterparts. Hematite deposits were interpreted as formed by supergene weathering of BIF causing an upgrade in Fe since the exposure of the craton in the Mesozoic. Where deposits were predominantly magnetite, these high grade Fe concentrations were interpreted as metamorphosed equivalents of ancient supergene enrichments. However, the genesis of the high-grade Fe deposits in the Yilgarn had not been extensively studied.

Volcanic-Hosted Massive Sulphide deposits (VHMS) in the Yilgarn were known to occur at two periods of history: c. 2.95 Ga (Golden Grove, Youanmi Terrane), and c. 2.7 Ga (Teutonic Bore, Gindalbie Domain, Kurnalpi Terrane). The model for these occurrences followed those developed in the Superior Province of Canada, with broadly syn-volcanic accumulations of sulphide on or near the seafloor (Barley, 1992; Yeats, 2007).

Advances since 2000

Although deposit models explained variations in mineralisation style and character between deposits, they still focussed on differences observed at the site of deposition, and did not explain why such large differences in metal endowment occurred in areas with similar apparent geology and geological history. Furthermore, the past decades of study had shown that at the deposit scale, the characteristics of small and large deposits were remarkably similar. In other words, the deposit models could not help us distinguish between a large and small concentration of metal. A key

reason for this deficiency of models of the time was that they were based on observations at the wrong scale to be predictive (Groves et al., 2009).

Throughout the last decade there has been a growing acceptance of a systems approach to understanding mineralisation (Wyborn et al., 1994), whereby the mineral deposits themselves are recognised as small expressions of much larger earth processes that control the flux of mass and energy through the lithosphere (Hronsky, 2004; Hronsky and Groves, 2008). In the Yilgarn, this approach had been embraced by several studies, most notably the predictive mineral discovery Cooperative Research Centre (pmd*CRC – gold focus), AMIRA P710, 710a (NiS–PGE focus) and P680 (dating gold mineralisation), and two ARC linkage projects (integrating NiS, Au and Fe mineralising systems in the context of lithospheric architecture).

Details of new knowledge from specific camps of mineralisation are detailed in subsequent chapters of this volume relating to specific field trip locations, but the major advances in understanding each mineral system are summarised below.

Gold systems

Key recent advances in understanding gold mineral systems have been summarised by Miller (2009). The three key advances are: 1) the recognition of multiple sources of fluid involved in the deposit genesis, sparking a resurgence of intrusion-related mineralisation models; 2) the recognition of multiple timings of mineralisation within single gold deposits or camps, and 3) the recognition of the influence of large-scale lithospheric architecture on the localisation of mineralisation. Other important advances include the recognition that (at least) some high temperature deposits have been metamorphosed, and the characterisation of large scale footprints of gold-related hydrothermal alteration that can be potentially be mapped by combinations of spectral and lithogeochemical means.

Work by the pmd*CRC, based on detailed paragenetic and analytical studies, has indicated the involvement of three fluids in gold deposits of the EGST (Fig. 17; Walshe et al., 2009): a reduced and acid fluid, interpreted to be derived from the upper crust; an oxidised fluid, interpreted as sourced from oxidised magmas; a hydric fluid interpreted as sourced from the mantle.

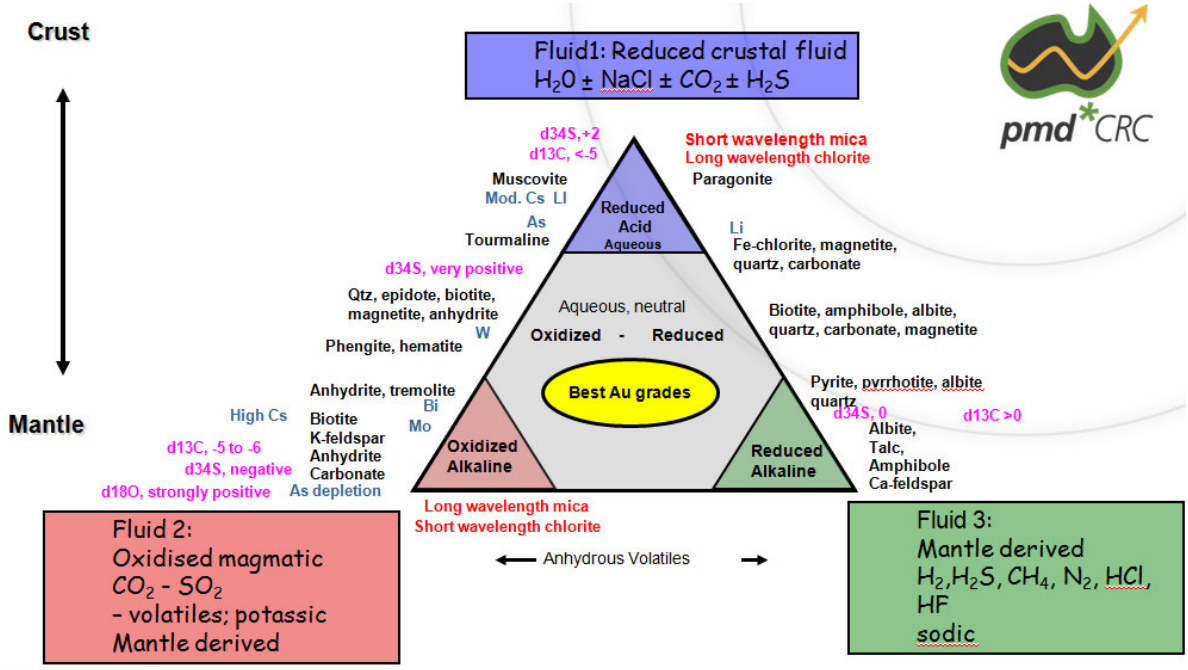

Figure 17. Diagram depicting end-member fluids detected in Yilgarn gold systems determined through pmd*CRC research. Also shown are the characteristic mineral assemblages (black lettering), chemistry (blue lettering), isotopic compositions (pink lettering) and spectral response (red lettering) associated with these fluids (after Walshe et al., 2009).

The presence of the oxidised fluid and the reduced acid fluid are acknowledged by several workers, although the mechanism of their generation (transient oxidation of a single ore fluid (Hodkiewicz et al., 2009) versus fluid mixing (Walshe et al., 2009)) is still hotly debated. Detailed paragenetic work has also indicated that there may be a sequencing to these alteration events in each camp, ruling out both transient oxidation and fluid mixing models (Miller and Henson, 2008; Miller et al., 2010). This issue of fluid mixing versus fluid overprinting is discussed further in subsequent deposit-scale chapters. Despite the debate in the timing and genesis of the fluids, there is a mounting body of evidence that these differing alteration signatures can be detected in regional datasets, including spectral and lithogeochemical data, when normalised to rock type. Preliminary work by the pmd*CRC indicates that gold is deposited at gradients in mineralogy and chemistry in these datasets, and therefore provides the potential to map alteration systems and potential sites of deposition (Neumayr et al., 2008).

A key development in understanding gold mineral systems in the Yilgarn has been the recognition of multiple mineralising events within deposits or camps (Bateman and Hagemann, 2004; Robert et al., 2005; Miller and Henson, 2008; Miller et al., 2010; see subsequent chapters). In the Laverton area in particular, Miller and Henson (2008) demonstrated four periods of Au introduction over a window of 11 to 25 Ma. This dramatically changes the question of gold deposit genesis from ‘Why is the gold in this specific depositional site, at this specfic time’, to ‘Why did this segment of the lithosphere get mineralised so many times?’ To answer this question requires working at a scale larger than the deposit itself.

The high-temperature end of the crustal continuum model for orogenic gold deposits has recently been called into question, with some authors arguing that these deposits represent metamorphosed equivalents of greenschist facies deposits (Tomkins and Grundy, 2009; Phillips and Powell, 2009). While evidence of melting of assemblages in granulite facies deposits has been demonstrated (Tomkins and Grundy, 2009), several deposits at lower amphibolite facies are still best explained by high temperature alteration and gold deposition, rather than metamorphism of pre-exisiting deposits (McCuaig and Kerrich, 1998; Mikucki, 1998).

Perhaps the most significant advance in understanding gold mineral systems has been the recognition of the role that early architecture of the greenstone belt plays on the clustering of gold mineralisation, or gold camps. Studies at St Ives have shown how an architecture established at the time of mafic–ultramafic volcanism at c. 2.71 Ga has been continually reactivated through approximately 70 Ma, controlling the subsequent greenstone depositional events, all subsequent responses of the crust to deformation, and the location of gold deposits (Chapter 5; Miller et al., 2010). Similar controls of early architecture on stratigraphy, deformation and gold mineral systems have recently been proposed for the Leonora district (Chapter 3).

Nickel systems

The most significant advances in understanding komatiite-hosted NiS deposits in the Yilgarn are the recognition of: 1) different modes of emplacement, sulphur assimilation, and the difference in resultant mineralisation styles, and 2) large-scale architectural control on the location of NiS deposit clusters.

It has recently been demonstrated that some komatiitic units in the Yilgarn are intrusive. Specifically, in the 2.7 Ga systems of the EGST, Rosengren et al. (2005, 2008) demonstrated an intrusive origin for the Mt Keith Dunite body, and in the 2.9 Ga systems of the Youanmi Terrane, Heggie et al. (2010) demonstrated an intrusive origin for the Maggie Hays host intrusion. Work by Fiorentini et al. (2007) postulated that intrusive emplacement of komatiite may be favoured by the presence of felsic volcanic rocks in the host stratigraphic pile, and that the emplacement style dictates the style of ore deposit formed: Type I massive sulphides at basal contacts can form in extrusive or intrusive komatiites, whereas Type II large tonnage, disseminated orebodies are restricted to zones of highest magma flux in intrusive systems (Fig. 18). Furthermore, Bekker et al. (2009) have definitively demonstrated, using mass-independent fractionation of sulphur isotopes, that komatiites assimilate sulphur from the sequences they are emplaced into, but moreover, that large deposits assimilate volcanogenic sulphur, whereas smaller deposits derive sulphur from sedimentary wallrocks or substrate. Degree of crustal contamination is a poor indicator of fertile versus infertile magmas (due to high recharge rates in large systems), but the type of crustal material assimilated (as indicated by mass-independent sulphur isotopes) may be a good indicator of ore potential (Fiorentini et al., 2010).

The second major advancement in understanding komatiite-hosted NiS deposits is the control of lithospheric architecture on the location of major deposit clusters. Although komatiites are distributed throughout the greenstone belts of the Yilgarn, large clusters of NiS mineralisation occur next to major paleocraton margins that can be imaged by isotopic means (Begg et al., 2010; Fig. 19). Begg et al. (2010) show that this craton margin control on NiS systems is present in all large NiS deposits worldwide, and is related to the higher degrees of partial melting of upwelling mantle plumes and higher magma flux rates that occur at these margins. Placed in the context of the progressive cratonisation of the southern Yilgarn through time (Mole et al., 2010; Figs 15, 16), the distribution of NiS deposits in both the 2.7 Ga and 2.9 Ga sequences of the Youanmi Terrane and EGST appear to favour zones of thinner lithosphere at the margins of older cratonic blocks.

Taken together, the advances in understanding craton scale control on deposit clusters, and emplacement controls on deposit style and mineralisation potential can be used as scale dependent proxies for exploration (McCuaig et al., 2010). The isotopic datasets can be used as proxies for identifying regions with high potential magma flux, whereas the felsic volcanics, mappable komatiite thickness, and presence of assimilated volcanogenic sulphur may mark the position of rifts within these belts, and therefore regions with the highest potential for ore concentrations.

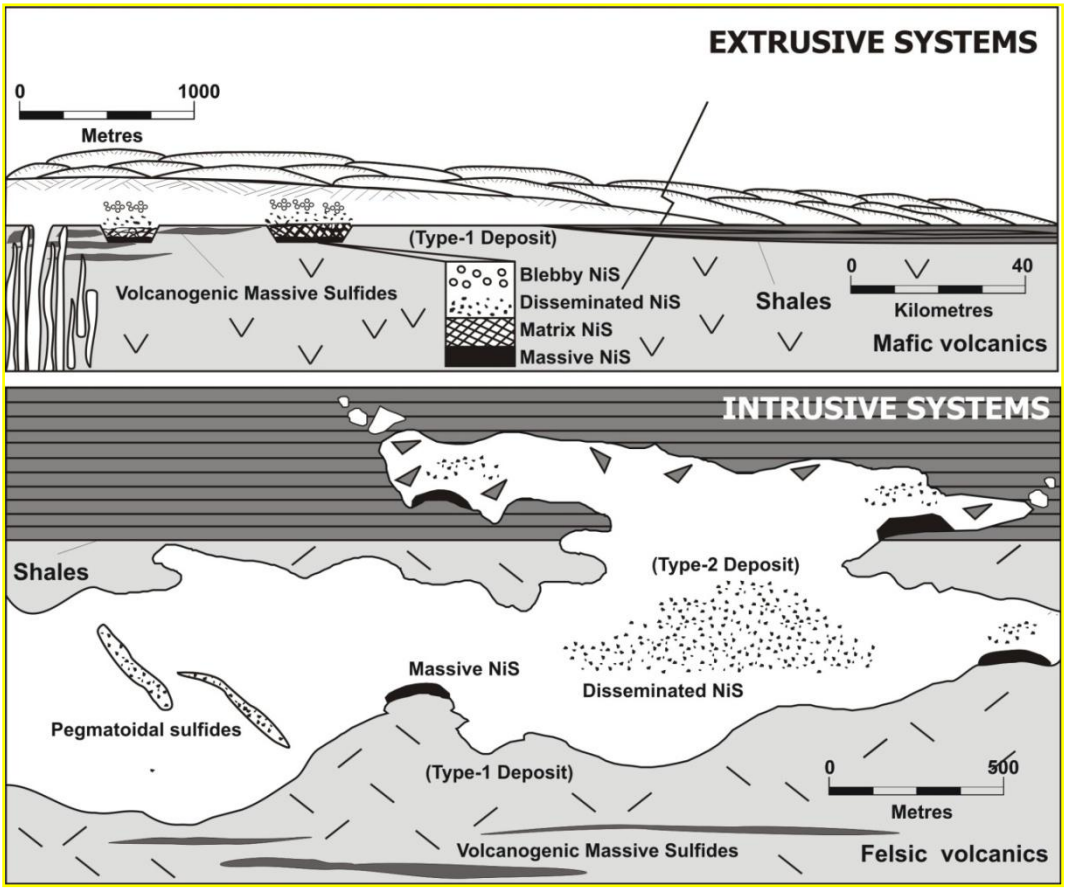

Figure 18. Schematic diagram showing the relationship of extrusive komatiites (top) to intrusive komatiites (bottom) and the respective mineralisation styles hosted in each (after Bekker et al., 2009).

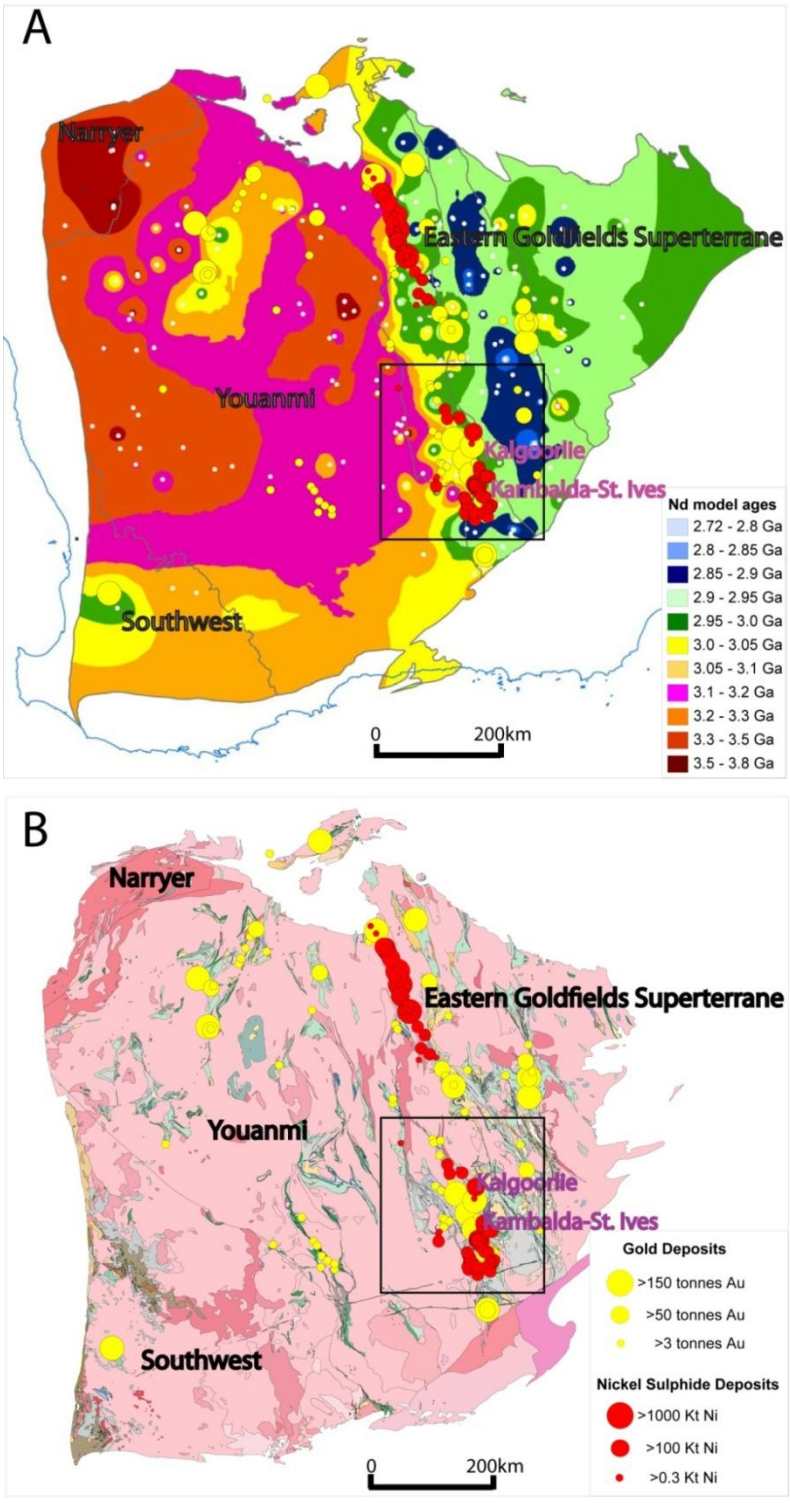

Figure 19. a) Map of neodymium model ages for low-calcium granites (emplaced at 2.66 – 2.63 Ga) of the Yilgarn Craton (Champion and Cassidy, 2007), also showing the location of low-calcium granite samples (white circles). The contoured data effectively map the age of the lithosphere from which the granitic melts were derived and, by proxy, the edges of the paleocraton at the time of granite emplacement. Superimposed are the locations of late Archean gold deposits (2.67 – 2.63 Ga; yellow circles; modified from Robert et al., 2005), and 2.7 Ga nickel–sulphide camps (red circles; Mamuse et al., 2010); b) simplified geology of the Yilgarn (scale 1:500 000, Geological Survey of Western Australia, 2008). Pink colours denote granitoid and granitoid gneiss, other colours represent supracrustal lithologies. Nickel sulphide and gold systems overlain as in a). Note the spatial correlation between transitional craton margins (green–yellow colours in a) and the location of mineral systems. Deposit size ranges are indicated by circle size. From McCuaig et al. (2010).

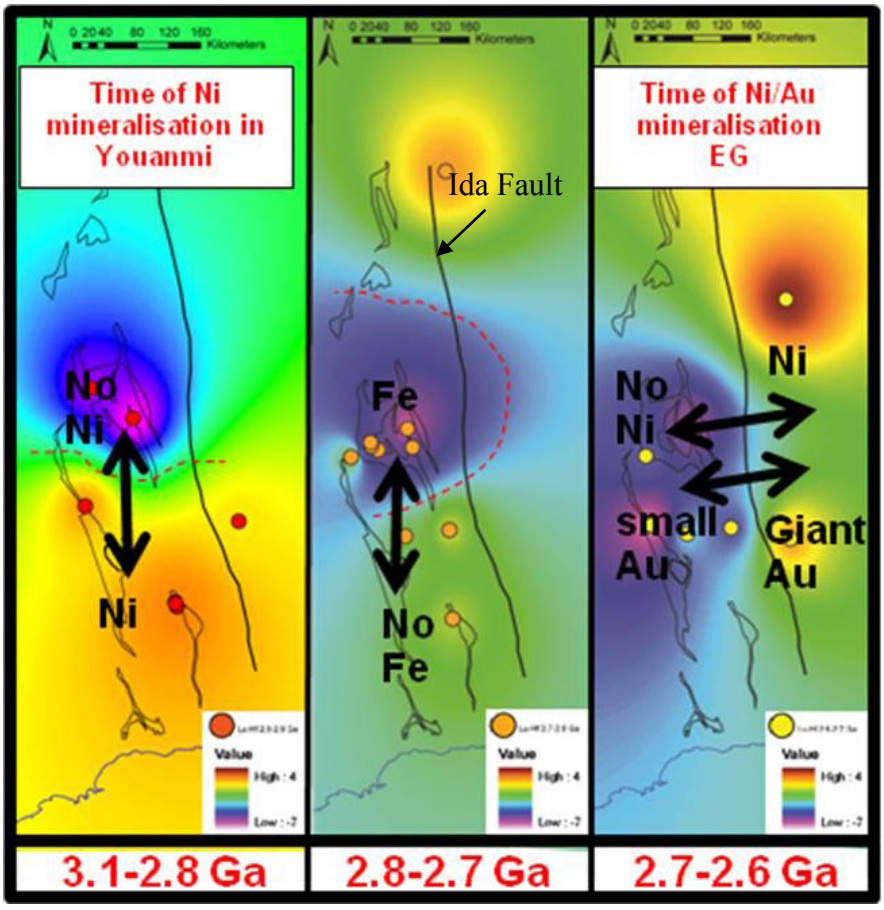

Figure 20. Time slices of ε_{Hf} data as shown in Figure 15, with the distribution of mineralisation in each time slice overlain. Note how 2.9 Ga Ni systems are limited to off-craton areas (hot colours), hypogene Fe upgrades only occur on the stable continental platform in thicker BIF sequences, and giant 2.7 Ga gold systems are restricted to the EGST east of the Ida Fault.

Iron systems

The distribution of major iron ore deposits and prospects over the Yilgarn Craton are shown in Figure 21. The iron deposits of the Yilgarn are associated with BIF sequences, which are common in the Youanmi Terrane of the Yilgarn, and locally in the Kurnalpi and Burtville Terranes of the EGST. Yet the known iron ore deposits are largely restricted to the central Southern Cross and Murchison Domains of the Youanmi Terrane, and the northern margin of the Yilgarn.

Exciting advances in understanding Archean BIF-hosted iron ore deposits have been the result of careful documentation of the paragenesis of deformation and hydrothermal alteration events that have affected the BIF (Angerer et al., 2010). This work has shown that the iron deposits are affected by several hydrothermal events that contribute to a hypogene upgrade of the iron ore prior to the supergene upgrade that has occurred since the Mezozoic. The sequence of hydrothermal upgrades has been summarised by Angerer et al. (2010), and shows remarkable similarity to the hypogene upgrade sequence of the iron ores of the Hammersley province (Hagemann et al., 2007; Taylor et al., 2001; Thorne et al., 2008). This sequence is shown in Figure 22.

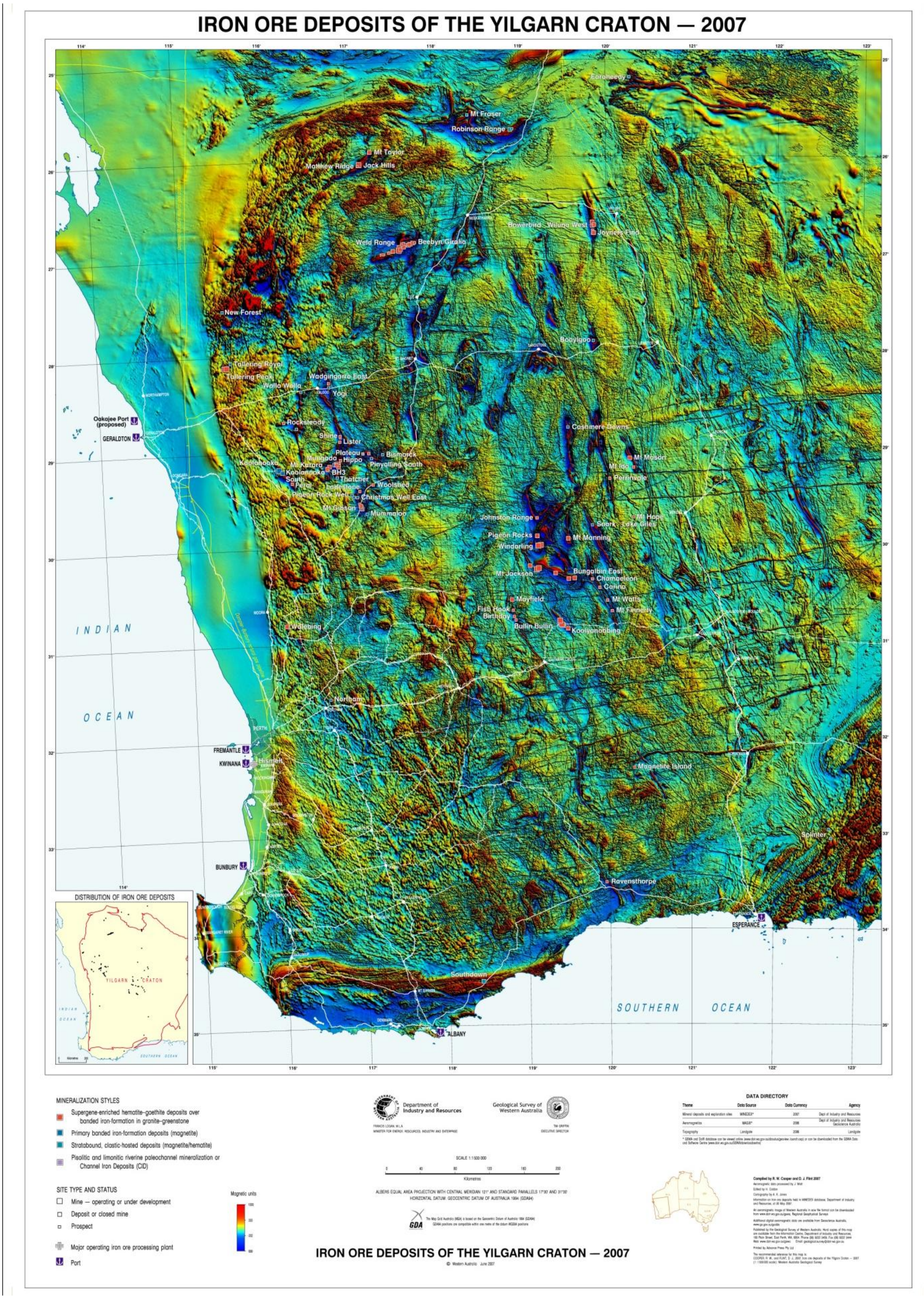

Figure 21. Distribution of iron ore deposits and prospects in the Yilgarn Craton overlain on an image of aeromagnetic data (Cooper and Flint, 2007).

Note that, although the BIF sequences occur throughout the Southern Cross Domain, they are best developed around the older protocraton of the Marda–Diemals area in the central Southern Cross Domain. Comparing Fe deposit distribution to the new understanding of lithospheric architecture through time that is emerging in the southern Yilgarn (Mole et al., 2010; Fig. 20), the iron deposits look to be best developed on what may have been shelf regions of a cratonic margin at c. 3.05 – 2.95 Ga.

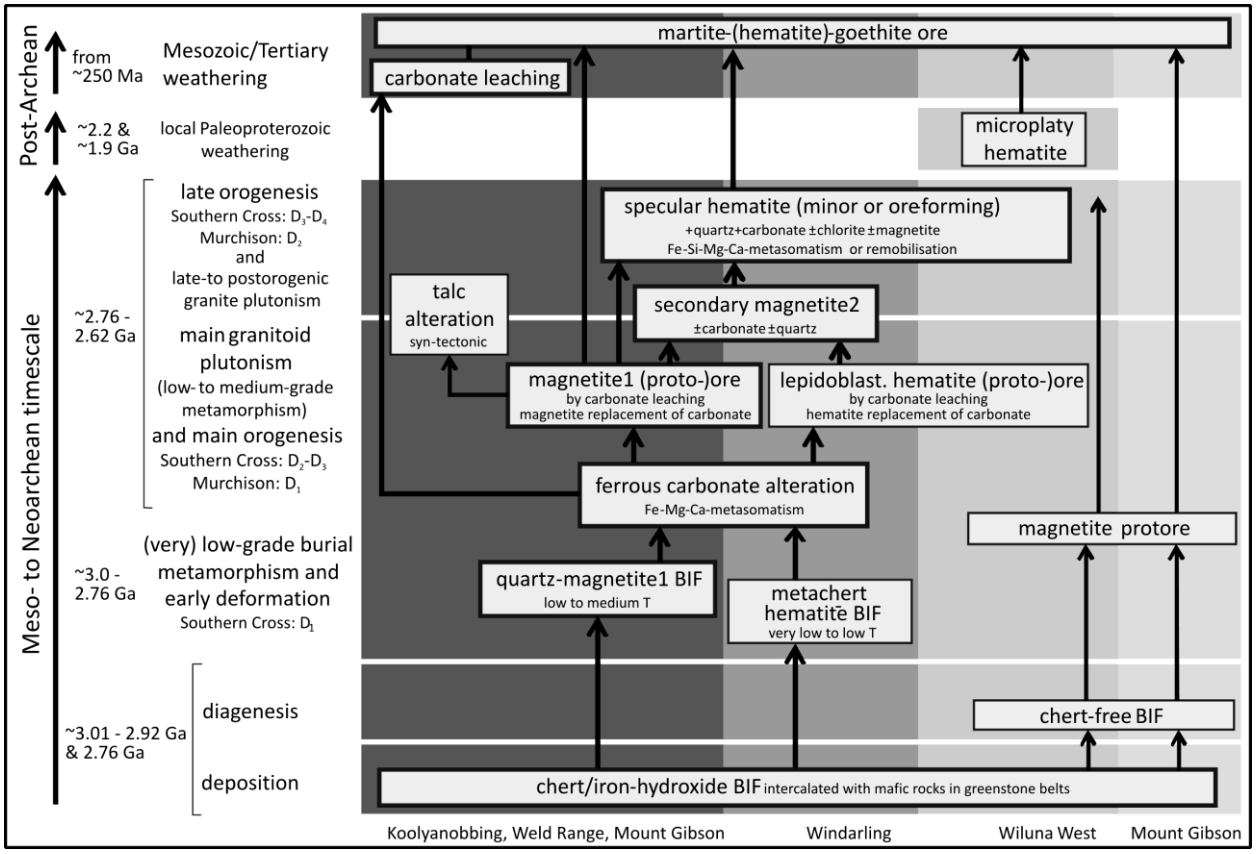

Figure 22. Paragenesis and approximate timing of hydrothermal events affecting iron ore deposits of the Yilgarn (Angerer et al., 2010).

Volcanic-Hosted Massive Sulphide (VHMS) systems

The exploration history and styles of VHMS mineralisation in the Yilgarn were reviewed by Barley (1992) and more recently by Yeats (2007). Most discoveries were made in the 1960s and 1970s, and exploration was hampered by generally poor outcrop of preferred host sequences (felsic volcaniclastics and sedimentary sequences) and deeply weathered regolith. Only two economic camps have been delineated to date: the Golden Grove – Scuddles deposits (Murchison Domain, Youanmi Terrane) and the Teutonic Bore – Jaguar deposits (Gindalbie Domain, Kurnalpi Terrane) (Fig. 23). The deposits are similar to Mattabi-type deposits in the Superior Province of Canada (Barley, 1992).

The paucity of VHMS deposits in the Yilgarn compared to the Superior Province of Canada has been ascribed to either formational reasons (tectonic setting) or exploration difficulty (depth of

weathering). Recently, Huston et al. (2005) used combined Pb and Nd isotopic data to show that the Teutonic Bore and Jaguar deposits are located in a narrow zone of the Eastern Goldfields that contains juvenile crust. This juvenile crust also corresponds with the Gindalbie Domain, which is unique in terms of its intermediate volcanic rock complexes and coeval bimodal basalt–rhyolite complexes at 2694 ± 4 to 2676 ± 5 Ma. These are interpreted as representing marginal arc and arc–rift sequences, respectively (Barley et al., 2008).

Based on these isotopic proxies for lithospheric architecture, and comparison to the relatively juvenile crust of the well endowed Abitibi subprovince of Canada, Huston et al. (2005) argued that the Yilgarn lacks significant VHMS in the EGST due to the presence of older crust, which inhibited heat flow and the occurrence of large VHMS systems.

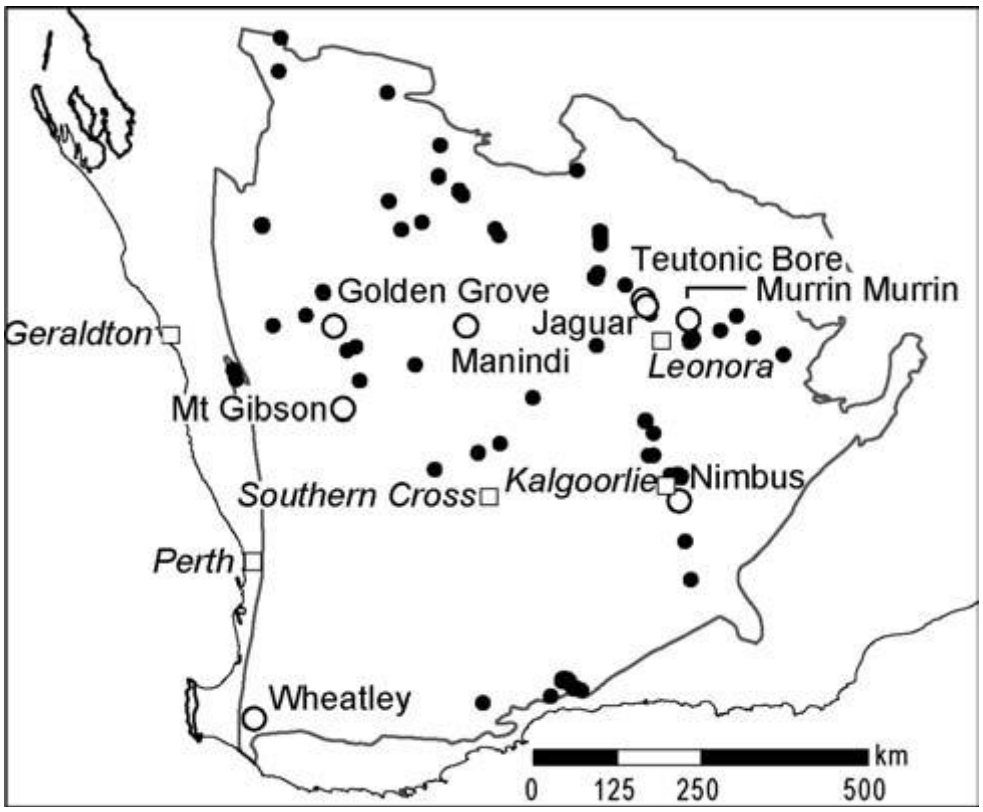

Figure 23. Distribution of base metal occurrences, excluding nickel, in the Yilgarn Craton (Yeats, 2007).

Summary

Advances in the past decade have clarified the tectonic history of the Yilgarn Province, and in particular the Eastern Goldfields Superterrane. Key developments have been: 1) the recognition of large scale lithospheric architecture reactivated through time; 2) the control of this architecture on the distribution and preservation of supracrustal sequences; 3) clarification of the intrusive and metamorphic histories of the region; 4) the integration of these multiple geoscience disciplines to resolve the tectonic history of the region.

In terms of mineralisation, the key advances have been: 1) the recognition of multiple timings of gold mineralisation, often in the same locations; 2) the treatment of mineral deposits as small-scale expressions of earth processes acting on a much larger scale to focus mass and energy flux through the lithosphere; 3) the control of lithospheric architecture on the clustering of mineral systems of various types, representing a fundamental relationship of lithosphere architecture, stratigraphy, and the evolution of the mineral systems through time in Yilgarn.

References

Ahmat, AL 1986, Metamorphic patterns in the greenstone belts of the Southern Cross province, Western Australia: Geological Survey of Western Australia, Professional Papers, v. 19, p. 1–21.

Angerer, T, Duuring, P, Lascelles, DF and Hagemann, SG 2010, BIF-related iron ore in the Yilgarn craton, Western Australia: geological setting and ore forming processes, 5th International Archean Symposium Abstracts *edited by* IM Tyler and CM Knox-Robinson: Geological Survey of Western Australia, Record 2010/18, p. 277–280.

Barley, ME 1992, A review of volcanic-hosted massive sulphide and sulphate mineralisation in Western Australia: Economic Geology v. 87, p. 855–872.

Barley, ME, Brown, SJA, Krapež, B and Kositcin, N 2008, Physical volcanology and geochemistry of a Late Archean volcanic arc: Kurnalpi and Gindalbie Terranes, Eastern Goldfields Superterrane, Western Australia: Precambrian Research, v. 161, p. 53–76.

Bateman, R and Hagemann, S 2004, Gold mineralisation throughout about 45 Ma of Archaean orogenesis: protracted flux of gold in the Golden Mile, Yilgarn Craton, Western Australia: Mineralium Deposita, v. 39, p. 536–559.

Begg, GC, Hronsky, JMA, Arndt, NT, Griffin, WL, O'Reilly, SY and Hayward, N in press, Lithospheric, cratonic and geodynamic setting of Ni–Cu–PGE sulphide deposits: Economic Geology.

Bekker, A, Barley, ME, Fiorentini, M, Rouxel, OJ, Rumble, D and Beresford, SW 2009, Atmospheric sulfur in Archaean komatiite-hosted nickel deposits: Science, v. 326, p. 1086–1089.

Binns, RA, Gunthorpe, RJ and Groves, DI 1976, Metamorphic patterns and development of greenstone belts in the Yilgarn Block, Western Australia, *in* The Early History of the Earth *edited by* BF Windley: Wiley, New York, USA, p. 303–313.

Blewett, RS, Cassidy, KE, Champion, DC, Henson, PA, Goleby, BS, Jones, L and Groenewald, PB 2004, The Wangkathaa Orogeny: an example of episodic regional 'd-2' in the Late Archaean Eastern Goldfields Province, Western Australia: Precambrian Research, v. 130, p. 139–159.

Bloem, EJM, Dalstra, HJ, Ridley, JR and Groves, DI 1997, Granitoid diapirism during protracted tectonism in an Archaean granitoid –greenstone belt, Yilgarn Block, Western Australia: Precambrian Research, v. 85, p. 147–171.

Brown, SJA, Krapež, B, Beresford, SW, Cassidy, KF, Champion, DC, Barley, ME and Cas, RAF 2001, Archean volcanic and sedientary environments of the Eastern Goldfields Province, Western Australia — a field guide: Geological Survey of Western Australia, Record 2001/13, p. 66.

Campbell, IH, Griffiths, RW and Hill, RI 1989, Melting in an Archaean mantle plume: heads it's basalts, tails it's komatiites: Nature, v. 339, p. 697–699.

Cassidy, KF, Champion, DC, McNaughton, NJ, Fletcher, IR, Whitaker, A, Bastrakova, I and Budd, AR 2002, Granitoid of the southeastern Yilgarn Craton; distribution, geochronology, geochemistry, petrogenesis and relationship to mineralisation.

Cassidy, KF, Champion, DC, Krapež, BB, ME, Brown, SJA, Blewett, RS, Groenewald, PB and Tyler, IM 2006, A revised geological framework for the Yilgarn Craton, Western Australia: Geological Survey of Western Australia, Record 2006/8, 8p.

Champion, DC and Cassidy, KF 2007, An overview of the Yilgarn Craton and its crustal evolution, *in* Proceedings of Geoconferences (WA) Inc. Kalgoorlie ’07 Conference, Kalgoorlie, Western Australia *edited by* FP Bierlein and CM Knox-Robinson: Geoscience Australia Record, 2007/14, p. 8–12.

Champion, DC and Sheraton, JW 1997, Geochemistry and Nd isotope systematics of Archaean granites of the Eastern Goldfields, Yilgarn Craton, Australia: Implications for crustal growth processes: Precambrian Research, v. 83, p. 109–132.

Cooper, RW and Flint, DJ 2007, Iron ore deposits of the Yilgarn Craton (1:500 000 scale): Geological Survey of Western Australia.

Czarnota, K, Champion, DC, Goscombe, B, Blewett, RS, Cassidy, KF, Henson, PA and Groenewald, PB 2010, Geodynamics of the Eastern Goldfields Superterrane: Precambrian Research.

Czarnota, K, Champion, DC, Goscombe, B, Blewett, RS, Henson, PB, Cassidy, KF and Groenewald, B 2009, Question 1: Geodynamics of the Eastern Goldfields Superterrane *in* Concepts to targets: a scale-integrated mineral systems study of the Eastern Yilgarn Craton: pmd*CRC, Project Y4, Final Report, Part III, p. 10-52.

Dalstra, HJ, Bloem, EJM, Ridley, JR and Groves, DI 1998, Diapirism synchronous with regional deformation and gold mineralisation: a new concept for granitoid emplacement in the Southern Cross Province, Western Australia: Geologie En Mijnbouw, v. 76, p. 321–338.

Doepel, JJG (compiler) 1973, Norseman, Western Australia: Geological Survey of Western Australia, 1:250 000 Explanatory Notes, 40p.

Drummond, BJ, Goleby, BR and Swager, CP 2000, Crustal signature of Late Archaean tectonic episodes in the Yilgarn Craton, Western Australia: evidence from deep seismic sounding: Tectonophysics, v. 329, p. 193– 221.

Fiorentini, M, Rosengren, N, Beresford, S, Grguric, B and Barley, M 2007, Controls on the emplacement and genesis of the MKD5 and Sarah's Find Ni–Cu–PGE deposits, Mount Keith, Agnew–Wiluna Greenstone Belt, Western Australia: Mineralium Deposita, v. 42, p. 847–877.

Fiorentini, ML, Beresford, SW, Rosengren, N, Barley, ME and McCuaig, TC 2010, Contrasting komatiite belts, associated Ni–Cu–(PGE) deposit styles and assimilation histories: Australian Journal of Earth Sciences, v. 57, p. 543–566.

Gee, RD (compiler) 1982, Southern Cross, Western Australia: Geological Survey of Western Australia, 1: 250 000 Geological Series Explanatory Notes, 25p.

Goleby, BR, Blewett, RS, Fomin, T, Fishwick, S, Reading, AM, Henson, PA, Kennett, BLN, Champion, DC, Jones, L, Drummond, BJ and Nicoll, M 2006, An integrated multi-scale 3D seismic model of the Archaean Yilgarn Craton, Australia: Tectonophysics, v. 420, p. 75–90.

Goscombe, B, Blewett, R, Czarnota, K, Maas, R and Groenewald, B 2007, Broad thermo-barometric evolution of the Eastern Goldfields Superterrane: Integrated Terrane Analysis Research, viewed 30 December 2010, <www.terraneanalysis.com.au/projects/yilgarn>.

Groves, DI 1993, The crustal continuum model for late-Archaean lode-gold deposits of the Yilgarn Block, Western Australia: Mineralium Deposita, v. 28, p. 366–374.

Groves, DI and Batt, WD 1984, Spatial and temporal variations of Archaean metallogenic associations in terms of evolution of granitoid–greenstone terrains with particular emphasis on the Western Australian Shield, *in* Archean Geochemistry: the origin and evolution of the Archean continental crust *edited by* A Kroner, GN Hanson and AM Goodwin: Springer-Verlag, Berlin, Germany, p. 73–98.

Groves, DI, Bierlein, FP and Goldfarb, RJ 2009, Some Irks with IRGS and Snags with TAGs, *in* Smart science for exploration and mining *edited by* PJ Williams: The Society for Geology Applied to Mineral Deposits,10th Biennial Meeting, Townsville, Queensland, 17–20 August 2009, Proceedings, p. 356–358.

Groves, DI, Goldfarb, RJ, Gebre, MM, Hagemann, SG and Robert, F 1998, Orogenic gold deposits: a proposed classification in the context of their crustal distribution and relationship to other gold deposit types, *in* Mesothermal gold mineralization in space and time *edited by* WRH Ramsay, FP Bierlein and DC Arne: Ore Geology Reviews, v. 13, p. 7–27.

Groves, DI, Ridley, JR, Bloem, EMJ, Gebre-Mariam, G, Hagemann, SG, Hronsky, JMA, Knight, JT, McNaughton, NJ, Ojala, J, Vielreicher, RM, McCuaig, TC and Holyland, PW 1995, Lode-gold deposits of the Yilgarn Block; products of late Archaean crustal-scale overpressured hydrothermal systems: Geological Society Special Publications, v. 95, p. 155–172.

Hagemann, S, Dalstra, HI, Hodkiewicz, P, Flis, M, Thorne, W and McCuaig, C 2007, Recent advances in BIF-related iron ore models and exploration strategies: Exploration in the New Millenium, 5th Decennial International Conference on Mineral Exploration, Toronto, Canada, 9–12 September 2007, Proceedings; p. 10

Hammond, RL and Nisbet, BW 1992, Archaean crustal processes as indicated by structural geology, Eastern Goldfields Province of Western Australia, *in* An international conference on crustal evolution, metallogeny and exploration of the Eastern Goldfields *edited by* PR Williams and JA Haldane:Australian Geological Survey Organisation, Extended Abstracts 1993/54, p. 105–113.

Heggie, GJ, Fiorentini, ML, Barnes, SJ and Barley, ME in press, Maggie Hays nickel deposit: Part 1. Stratigraphic control on the style of komatiite emplacement in the 2.9 Ga Lake Johnston Greenstone Belt, Yilgarn Craton, Western Australia: Economic Geology.

Hill, RI, Chappell, BW and Campbell, IH 1992, Late Archaean granites of the southeastern Yilgarn Block, Western Australia: age, geochemistry, and origin: Earth and Environmental Science Transactions of the Royal Society of Edinburgh v. 83, p. 211–226.

Hodkiewicz, P, Groves, D, Davidson, G, Weinberg, R and Hagemann, S 2009, Influence of structural setting on sulphur isotopes in Archean orogenic gold deposits, Eastern Goldfields Province, Yilgarn, Western Australia: Mineralium Deposita, v. 44, p. 129.

Hronsky, JMA 2004, The science of exploration targeting, *in* Predictive Mineral Discovery Under Cover — Extended abstracts, v. 33 *edited by* J Muhling: Centre for Global Metallogeny, The University of Western Australia, Perth, p. 129–133.

Hronsky, JMA and Groves, DI 2008, Science of targeting: definition, strategies, targeting and performance measurement: Australian Journal of Earth Sciences, v. 55, p. 3–12.

Huston, DL, Champion, DC and Cassidy, KF 2005, Tectonic controls on the endowment of Archean cratons in VHMS deposits: evidence from Pb and Nd isotopes, *in* Mineral Deposit Research: Meeting the Global Challenge *edited by* J Mao and FP Beierlein: 8th Biennial Meeting of the Society for Geology Applied to Mineral Deposits, Beijing, China, 18–21 August 2005, Proceedings; p. 15–18.

Joly, A, Miller, J and McCuaig, TC 2010, Archaean polyphase deformation in the Lake Johnston Greenstone Belt area: implications for the understanding of ore systems of the Yilgarn Craton: Precambrian Research, v. 177, p. 181–198.

Krapež, B and Barley, ME 2008, Late Archaean synorogenic basins of the Eastern Goldfields Superterrane, Yilgarn Craton, Western Australia: Part III. Signatures of tectonic escape in an arc–continent collision zone: Precambrian Research, v. 161, p. 183–199.

Krapež, B, Barley, ME and Brown, SJA 2008a, Late Archaean synorogenic basins of the Eastern Goldfields Superterrane, Yilgarn Craton, Western Australia: Part I. Kalgoorlie and Gindalbie Terranes: Precambrian Research, v. 161, p. 135–153.

Krapež, B, Standing, JG, Brown, SJA and Barley, ME 2008b, Late Archaean synorogenic basins of the Eastern Goldfields Superterrane, Yilgarn Craton, Western Australia: Part II. Kurnalpi Terrane: Precambrian Research, v. 161, p. 154–182.

Mamuse, A, Porwal, A, Kreuzer, O and Beresford, S 2010, Spatial statisical analysis of the distribution of komatiite-hosted nickel sulfide deposits in the Kalgoorlie Terrane, Western Australia: clustered or not?: Economic Geology, v. 105, p. 229–242.

Martin, F 1994, Archaean grey gneisses and genesis of continental crust, *in* Crustal Evolution *edited by* KC Condie: Elsevier, Amsterdam, The Netherlands, p. 205–259.

McCuaig, TC 1996, The genesis and evolution of lode gold mineralization and mafic host lithologies in the late-Archean Norseman Terrane, Yilgarn Block, Western Australia: University of Saskatchewan, Saskatchewan, Canada, PhD thesis (unpublished).

McCuaig, TC, Beresford, SW and Hronsky, J in press, Translating the mineral systems approach into an effective exploration targeting system: Ore Geology Reviews.

McCuaig, TC and Kerrich, R 1998, P–T–t–deformation–fluid characteristics of lode gold deposits: evidence from alteration systematics: Ore Geology Reviews, v. 12, p. 381–454.

McGoldrick, PJ 1993, Norseman WA, Sheet 3233: Geological Survey of Western Australia Australia, 1:100 000 Geological Series.

Mikucki, EJ 1998, Hydrothermal transport and depositional processes in Archean lode-gold systems — a review: Ore Geology Reviews, v. 13, p. 307– 321.

Miller, J, Blewett, R, Tunjic, J and Connors, K in press, The role of early formed structures on the development of the world class St Ives Goldfield, Yilgarn, WA: Precambrian Research.

Miller, J and Henson, P 2008, Multiple gold events at Laverton, Eastern Goldfields Superterrane, WA: Geological Society of Australia, Australian Earth Science Convention, 20–24 July 2008, Perth, Western Australia.

Miller, JM 2009, Recent advances in understanding orogenic gold systems: CET Quarterly News, p. 12–17.

Mole, DR, Fiorentini, M, Thébaud, N, McCuaig, C, Cassidy, KF, Barnes, SJ, Belousova, EA, Mudrovska, I and Doublier, M 2010, Lithospheric controls on the localization of komatiite-hosted nickel-sulphide deposits, *in* 5th International Archaean Symposium, Perth Western, Australia, Abstracts *edited by* IM Tyler and CM Knox-Robinson: Geological Survey of Western Australia, Record 2010/18, p. 101–103.

Mueller, AG and McNaughton, NJ 2000, U–Pb ages constraining batholith emplacement, contact metamorphism, and the formation of gold and W–Mo skarns in the Southern Cross area, Yilgarn craton, Western Australia: Economic Geology and the Bulletin of the Society of Economic Geologists, v. 95, p. 1231– 1257.

Mueller, AG, Nemchin, AA and Frei, R 2004, The Nevoria gold skarn deposit, Southern Cross greenstone belt, Western Australia: II. Pressure–temperature–time path and relationship to postorogenic granites: Economic Geology, v. 99, p. 453–478.

Myers, JS 1993, Precambrian history of the West Australian Craton and adjacent orogens: Annual Review of Earth and Planetary Sciences, v. 21, p. 453–485.

Nelson, DR 1997, Evolution of the Archaean granite–greenstone terranes of the Eastern Goldfields, Western Australia: SHRIMP U–Pb zircon constraints: Precambrian Research, v. 83, p. 57–81.

Neumayr, P, Walshe, J, Hagemann, S, Petersen, K, Roache, A, Frikken, P, Horn, L and Halley, S 2008, Oxidized and reduced mineral assemblages in greenstone belt rocks of the St Ives gold camp, Western Australia: vectors to high-grade ore bodies in Archaean gold deposits?: Mineralium Deposita, v. 43, p. 363.

Phillips, GN and Powell, R 2009, Formation of gold deposits: Review and evaluation of the continuum model: Earth Science Reviews, v. 94, p. 1–21.

Robert, F, Poulsen, KH, Cassidy, KF and Hodgson, CJ 2005, Gold metallogeny of the Superior and Yilgarn cratons, *in* Economic Geology, 100th Anniversary Volume 1905–2005 *edited by* JW Hedenquist, JFH Thompson, RJ Goldfarb and JP Richards: Society of Economic Geologists, Littleton, Colorado, USA, p. 1001–1034.

Rosengren, NM, Beresford, SW, Grguric, BA and Cas, RAF 2005, An intrusive origin for the komatiitic–dunite hosted Mount Keith disseminated nickel sulphide deposit, Western Australia: Economic Geology, v. 100, p. 149–156.

Rosengren, NM, Cas, RAF, Beresford, SW and Palich, BM 2008, Reconstruction of an extensive Archaean dacitic submarine volcanic complex associated with the komatiite-hosted Mt Keith nickel deposit, Agnew–Wiluna Greenstone Belt, Yilgarn Craton, Western Australia: Precambrian Research, v. 161, p. 34–52.

Swager, CP, Goleby, BR, Drummond, BJ, Rattenbury, MS and Williams, PR 1997, Crustal structure of granite–greenstone terranes in the Eastern Goldfields, Yilgarn Craton, as revealed by seismic reflection profiling: Precambrian Research, v. 83, p. 43–56.

Swager, CP, Witt, WK, Griffin, TJ, Ahmat, AL, Hunter, WM, McGoldrick, PJ and Wyche, S 1992, Late Archaean granite–greenstones of the Kalgoorlie Terrane, Yilgarn Craton, Western Australia, *in* JE Glover and SE Ho: Geology Deptartment (Key Centre) and University Extension, The University of Western Australia, Perth, Western Australia, p. 107–122.

Taylor, D, Dalstra, HJ, Harding, AE, Broadbent, GC and Barley, ME 2001, Genesis of high-grade hematite orebodies of the Hamersley Province, Western Australia: Economic Geology, v. 96, p. 837–873.

Thébaud, N and Miller, JN 2009, U–Pb age constraints on the siliciclastic sediments from the upper supracrustal cover in the Southern Cross greenstone belt, Youanmi Terrane, Western Australia, *in* Smart Science for Exploration and Mining *edited by* PJ Williams: The Society for Geology Applied to Mineral Deposits,10th Biennial Meeting, Townsville, Queensland, 17–20 August 2009, Proceedings, p. 960–962.

Thorne, W, Hagemann, S, Webb, A and Clout, J 2008, Banded iron formation-related iron ore deposits of the Hamersley Province, Western Australia, *in* Banded Iron Formation-Related High-Grade Iron Ore *edited by* SG Hagemann, CA Rosièr, J Gutzmer, J and NJ Beukes: Society of Economic Geologists, v. 15, p. 197–222.

Tomkins, AG and Grundy, C 2009, Upper temperature limits of orogenic gold deposit formation: constraints from the granulite hosted Griffin's Find Deposit, Yilgarn Craton: Economic Geology, v. 104, p. 669–686.

Walshe, JL, Neumayr, P, Cleverley, J, Petersen, K, Andrew, A, Whitford, D, Carr, GR, Kendrick, M, Young, C and Halley, S 2009, Question 3: Multiple fluid reservoirs in Eastern Yilgarn gold systems, *in* Concepts to Targets: a scale-integrated mineral systems study of the Eastern Yilgarn Craton: pmd*CRC, Project Y4, Final Report, Part III, p. 113–152.

Wyborn, LAI, Heinrich, CA and Jaques, AL 1994, Australian Proterozoic mineral systems: essential ingredients and mappable criteria: Australasian Institute of Mining and Metallurgy Annual Conference, Melbourne, Victoria, 1994, p. 109–115.

Wyche, S, Nelson, DR and Riganti, A 2004, 4350–3130 Ma Detrital zircons in the Southern Cross granite–greenstone terrane, Western Australia: implications for the early evolution of the Yilgarn Craton: Australian Journal of Earth Sciences, v. 51, p. 31–45.

Yeats, CJ 2007, VHMS mineral systems in the Yilgarn — characteristics and exploration potential, *in* Proceedings of Geoconferences (WA) Inc. Kalgoorlie ’07 Conference, Kalgoorlie, Western Australia *edited by* FP Bierlein and CM Knox-Robinson: Geoscience Australia Record, 2007/14, p. 65–59.

Chapter 2 — Laverton Region

JM Miller

Centre for Exploration Targeting, School of Earth and Environment, The University of Western Australia

Introduction

The Laverton greenstone belt is located in the Eastern Goldfields Superterrane of the Archean Yilgarn Craton of Western Australia (Fig. 24). The area has a gold endowment in excess of 25 million ounces with two world class deposits, Sunrise Dam (10.2 moz Au; Sung et al., 2007) and Wallaby (7.5 million ounces; Salier et al., 2004), and also numerous gold deposits in excess of 1 million ounces (Mount Morgans, 1.79 million ounces; Lancefield, 1.9 million ounces; Granny Smith, 2.7 million ounces; Fig. 1; Coggon, 2003). Economic komatiite-associated nickel sulphide deposits also occur in the area (e.g. Windarra South; Fig. 25).

The Laverton greenstone belt is a complex region located on the boundary between two major tectonostratigraphic terranes of the Yilgarn Craton; the Kurnalpi and Burtville Terranes (Fig. 24; Cassidy et al., 2006). These are to the east of the Kalgoorlie Terrane that hosts the Norseman, St Ives, Kalgoorlie, Leonora, Agnew, and Wiluna gold camps within the Norseman–Wiluna greenstone belt (Fig. 24). The Kurnalpi and Burtville Terrane boundary is defined by major N- to NNW-trending shear zones (Far East Fault, Barnicoat West Fault, and Barnicoat East Fault; Fig. 25). The Laverton area also contains large-scale granitoid-cored domes (Mt Margaret Dome and Kirgella Domes) with regional faults along the flanks of these domes (e.g. the Celia Fault; Fig. 25). Between the Mt Margaret Dome and Kirgella Dome a series of N- to NE-trending shear zones also occur that host the largest gold deposits (Sunrise Dam and Wallaby; Fig. 25).

Stratigraphic description

Hallberg (1985) originally presented a stratigraphic framework for the Laverton region comprising two conformable stratigraphic associations based on distinct lithological groups. Association 1 was defined as a basal stratigraphic association, which comprised basalt with three ultramafic and banded iron-formation (BIF) units. These are intruded by gabbro and dolerite dykes and sills, overlain by conglomerates and turbiditic rocks. Association 2 conformably overlies Association 1, and is comprised of andesite and andesitic volcaniclastic sedimentary rocks overlain by basalt and ultramafic rocks. Subsequent structural and stratigraphic work (Standing, 2008), combined with geochronological work (see new results and summary by Kositcin et al., 2008), has now subdivided the area into seven distinct tectonostratigraphic domains, with the rocks broadly subdivided into the two terranes (Kurnalpi and Burtville Terranes), separated by the Barnicoat East Fault (Fig. 25).

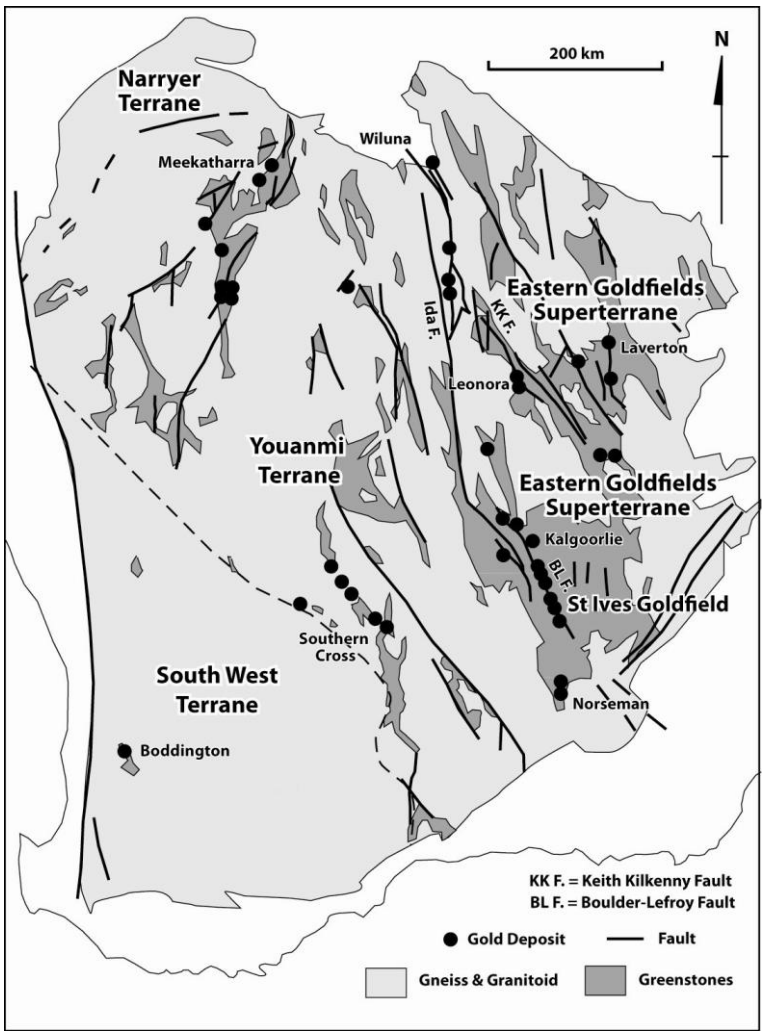

Figure 24. Major gold fields of the Yilgarn Craton. The township of Laverton is marked (Robert et al., 2005).

The Burtville Terrane (Figs 1, 25) comprises fault-bound successions that are made up of blocks of basalt, ultramafic schists, and quartzose sedimentary rocks (Standing, 2008). The age and stratigraphic evolution of the units within the Burtville Terrane are still poorly constrained.

Units within the Kurnalpi Terrane are divided into several rocks that can be correlated regionally (Kositcin et al., 2008; Standing, 2008). The oldest units in the Laverton region have been termed the Laverton Sequence (Kositcin et al., 2008), which is part of Association 1 of Hallberg (1985). Other rock units have been grouped into the Kurnalpi Sequence, the Minerie Sequence, and the Siliclastic Sequences (Kositcin et al., 2008), which previously had been grouped by Hallberg (1985) into both rock associations. The key units that define the Kurnalpi Terrane are calc-alkalic mafic and intermediate volcanic rocks (the Kurnalpi Sequence), which are conformably overlain by mafic to ultramafic lavas (the Minerie Sequence; Kositcin et al., 2008).

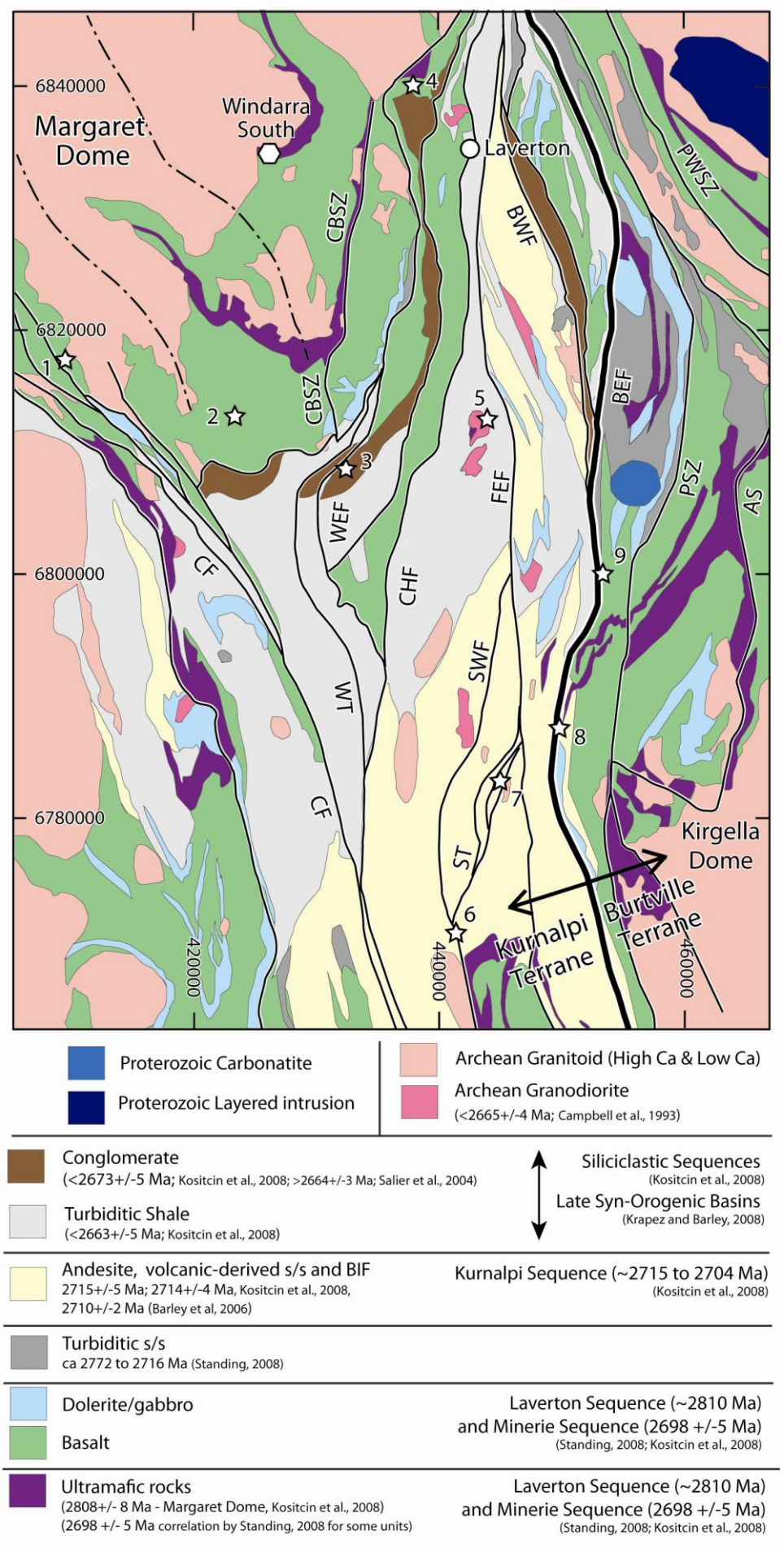
6840000
6820000
6800000
6780000
420000
440000
460000
Margaret Dome
Windarra South
Laverton
Kirgella Dome
Kurnalpi Terrane
Burtville Terrane
CBSZ
CBSZ
BWF
PWSZ
BEF
PSZ
AS
FEF
WEF
CHF
SWF
WT
CF
CF
ST
1
2
3
4
5
6
7
8
9
Proterozoic Carbonatite
Proterozoic Layered intrusion
Archean Granitoid (High Ca & Low Ca)
Archean Granodiorite
(<2665+/-4 Ma; Campbell et al., 1993)
Conglomerate
(<2673+/-5 Ma; Kositcin et al., 2008; >2664+/-3 Ma; Salier et al., 2004)
Turbiditic Shale
(<2663+/-5 Ma; Kositcin et al., 2008)
Siliciclastic Sequences
(Kositcin et al., 2008)
Late Syn-Orogenic Basins
(Krapez and Barley, 2008)
Andesite, volcanic-derived s/s and BIF
2715+/-5 Ma; 2714+/-4 Ma, Kositcin et al., 2008,
2710+/-2 Ma (Barley et al, 2006)
Kurnalpi Sequence (~2715 to 2704 Ma)
(Kositcin et al., 2008)
Turbiditic s/s
ca 2772 to 2716 Ma (Standing, 2008)
Dolerite/gabbro
Basalt
Laverton Sequence (~2810 Ma)
and Minerie Sequence (2698 +/-5 Ma)
(Standing, 2008; Kositcin et al., 2008)
Ultramafic rocks
(2808+/- 8 Ma - Margaret Dome, Kositcin et al., 2008)
(2698 +/- 5 Ma correlation by Standing, 2008 for some units)
Laverton Sequence (~2810 Ma)
and Minerie Sequence (2698 +/-5 Ma)
(Standing, 2008; Kositcin et al., 2008)

Figure 25. (Previous page) Geological map of the Laverton Greenstone Belt. Modified from Standing (2008) and Henson et al., (2008). Primary stratigraphic distribution and fault architecture was predominantly derived from Standing (2008). Abbreviations: CF – Celia Fault, CBSZ – Chatterbox Shear Zone, WT – Wallaby Thrust, WEF – Wallaby East Fault, CHF – Childe Harold Fault, SWT – Sunrise West Fault, ST – *Xyy* Thrust, FEF – Far East Fault, BWF – Barnicoat West Fault, BEF – Barnicoat East Fault, PSZ – Prendergast Shear Zone, AS – Apollo Shear, Fault, PWSZ – Probert Well Shear Zone. Gold deposits: 1 – Mt Morgans; 2 – Jupiter; 3 – Wallaby; 4 – Lancefield; 5 – Granny Smith; 6 – Red October; 7 – Sunrise Dam; 8 – Jubilee; 9 – Keringal. Windarra South is a komatiitehosted nickel sulphide deposit. Dashed lines mark major domal axis trends.

Regionally, the Kurnalpi Sequence ranges in age from 2715 ± 5 to 2704 ± 4 Ma (Kositcin et al., 2008). The calc-alkalic andesite-dominated Kurnalpi Sequence at Laverton is the same age as, or older than, the mafic–ultramafic Kambalda Sequence, which implies a different tectonic history for the Kurnalpi Terrane compared to the Kalgoorlie Terrane (Kositcin et al., 2008). The Minerie Sequence has units dated at 2698 ± 5 Ma (Kositcin et al., 2008).

The Laverton Sequence is a major component of the stratigraphy that now defines the Margaret Dome (Fig. 2). The base of the Laverton Sequence is defined by BIF and ultramafic sequences that host the Windarra and Windarra South nickel sulphide deposits (Standing, 2008; Fig. 25). These units are overlain by basalt that has been intruded by gabbro and dolerite dykes. Additional complex successions of BIF, basalt and sedimentary sequences overly these units (Standing, 2008). An interlayered volcaniclastic turbidite beneath the one of the ultramafic units at the Windarra South Mine (Fig. 25) has an age of 2808 ± 8 Ma (Kositcin et al., 2008). The Laverton Sequence is overlain by the Kurnalpi Sequence (Standing, 2008) which indicates the komatiite-hosted Ni-sulphide mineralisation within the Windarra ultramafic unit is older than 2715–2704 Ma. This Ni-sulfide mineralisation is therefore older than the komatiite-hosted Ni-sulphide mineralisation at Kambalda, which is located within the Kambalda Sequence, a component of which is time equivalent to the Kurnalpi Sequence (Kositcin et al., 2008).

The Laverton Sequence is unconformably overlain by the Kurnalpi Sequence, which comprises andesitic lavas and andesitic volcaniclastic sedimentary rocks that grade up into quartz-bearing sandy turbiditic rocks and conglomerate with clasts of dacite and andesite (Standing, 2008). At Sunrise Dam (Fig. 25) the sandy volcaniclastic turbiditic rocks grade up into magnetic shales (Standing, 2008), that within the mine stratigraphy have been termed banded iron-formation (BIF). The quartz-rich volcaniclastic turbiditic rocks have yielded U–Pb SHRIMP dates for detrital zircons of 2714 ± 4Ma and 2715 ± 5 Ma, which is inferred to be the depositional age (Kositcin et al., 2008).

Regionally, the Minerie Sequence conformably overlies the Kurnalpi sequence and comprises pillow basalt, dolerite and high-magnesian basalt (termed the Murrin Murrin komatiite) with minor sedimentary rocks (Kositcin et al., 2008). There is some uncertainty on regional maps (Fig. 25) as to the exact ages of the mapped mafic and ultramafic sequences (i.e. whether they are a fault bounded segments of the older Laverton Sequence or part of the younger Minerie Sequence). In

the Laverton region, a series of thin, laterally discontinuous flows of pillow basalt intruded by sills of peridotite–dunite, gabbro and dolerite (that are to the west of the Celia Fault) have been correlated with the Minerie Sequence (Standing, 2008). The ultramafic sills are inferred to have been subvolcanic feeders to the Murrin Murrin Komatiite higher in the sequence (Standing, 2008). In other areas, such as around the Sunrise Dam Mine, no known units that correlate with the Minerie Sequence have been identified (Standing, 2008).

The youngest Archean rocks are a sequence of siliciclastic sequences that have been deposited within late synorogenic basins (Krapež and Barley, 2008; Kositcin et al., 2008). In the Laverton area the sedimentary rocks are predominantly turbidites, but also include carbonaceous shale, sandstone, conglomerate, chert, and magnetic shales (termed BIFs; Standing, 2008). In the Wallaby gold deposit area (Fig. 25), the Wallaby Conglomerate is a polymictic, clast-supported cobble conglomerate that is overlain by sandy turbidites and carbonaceous shale (Standing, 2008).

Detrital zircon dating of the Wallaby conglomerate (Kositcin et al., 2008), and dating of a later crosscutting carbonatite intrusion (Salier et al., 2004), constrain the depositional age of the Wallaby Conglomerate to between 2673 ± 5 Ma and 2664 ± 3 Ma (Standing, 2008). Dating of detrital zircons from near the Granny Smith gold deposit (Fig. 25) indicates these units have a maximum depositional age of 2663 ± 5Ma (Kositcin et al., 2008). At this locality, the Wallaby Conglomerate is not recognised, with carbonaceous shale, sandstone, conglomerate and magnetic shale/chert dominating the stratigraphic sequence (Standing, 2008).

The Mount Margaret Dome is a large-scale, granite-cored batholith comprising high-Ca granitic gneiss, massive monzogranite and granodiorite, and low-Ca monzogranites (Cassidy et al., 2006). The only age constraint on this intrusion is from a high-Ca gneiss with a SHRIMP U–Pb date of 2672 ± 28 Ma (Black et al., 2002). Smaller granodiorites and synenite intrusives have ages ranging from 2664 ± 3 Ma for carbonatite dykes associated with syenite at the Wallaby deposit (Salier et al., 2004) to 2665 ± 4 Ma for mafic granodiorite intrusives at Granny Smith (Hill et al., 1992). These ages overlap with the detrital zircon age populations of the sediments they intrude and some of the ages on the intrusive rocks have been inferred to be related to inheritance and not crystallisation (Standing, 2008; Kositcin et al., 2008).

Structural models

Multiple structural models have been proposed for the Laverton Area. Unlike other areas of the Yilgarn Craton (Swager, 1997), an early phase of N–S related thrusting has not been recognised (Standing, 2008). Multiple event histories have been proposed for the region (Fig. 26), with the most recent proposing five major events encompassing the time of deposition of the stratigraphic units to the last major phase of gold mineralisation (Blewett et al., 2010).

There are major differences in the assignment of deformation numbers by different groups (Fig. 26), with structural models having variable event numbers, and in some cases different interpretations for the relative timing of the events. Key aspects of the different event histories that can be correlated are as follow:

- Two major phases of E–W shortening immediately pre- and post-deposition of the siliciclastic sequences have been identified (Fig. 26). These deformation events are inferred to have formed the dominant N-trending regional faults and large fold closures in the region (e.g. Standing, 2008). Standing (2008) relates his D1 event to the collision between the Kurnalpi and Burtville Terranes, and he has also mapped some pre-collision deformation events (Fig. 26). Blewett et al. (2004a) defined these two contractional events as D2a and D2b, with the formation of the late basins between the two events termed D2e and the entire D2 event labelled the Wangkathaa Orogeny.
- A major phase of dextral movement on the main fault systems in response to NE–SW shortening has been identified; however, the exact timing of this event has not been constrained to identical periods by different research groups. Standing (2008) termed this event D2 and placed it prior to the gold mineralisation within the Wallaby deposit. In contrast, Blewett et al. (2010) linked dextral shearing to a late stage D5 event, after the main phase of gold at the Wallaby deposit (Fig. 26).
- A number of research groups have argued that major gold systems have developed in regional restraining step-overs associated with sinistral transpression (Chen et al., 2001; Henson et al., 2008; Figs 26, 27, 28). During sinistral-slip on the N-trending regional faults, the Wallaby and Sunrise Dam gold deposits are interpreted to have been located in transpressional step-overs that are NE-trending (Figs 27, 28a,b).
- The formation of the late basins has been linked to a complex extensional history (NNW–SSE extension and ENE–WSW extension; Blewett and Czarnota, 2007). The formation of the Margaret Dome and the Kirgella Dome are interpreted to have been linked to the rapid deposition and burial of the Siliciclastic Sequences (e.g. Standing, 2008; Henson et al., 2008); that is, the D3 event as defined by Blewett and Czarnota (2007) and Blewett et al. (2010), which corresponds to the deposition of the Siliciclastic Sequences.
- The role of early-formed fault systems has been mapped by McIntyre and Martyn (2005), with the Wallaby deposit interpreted to be located on an early transfer fault related to extension. Standing (2008) related the location of the Wallaby deposit to an underlying shear that predated the deposition of the Wallaby conglomerate (the Chatterbox Shear Zone; Fig. 29).

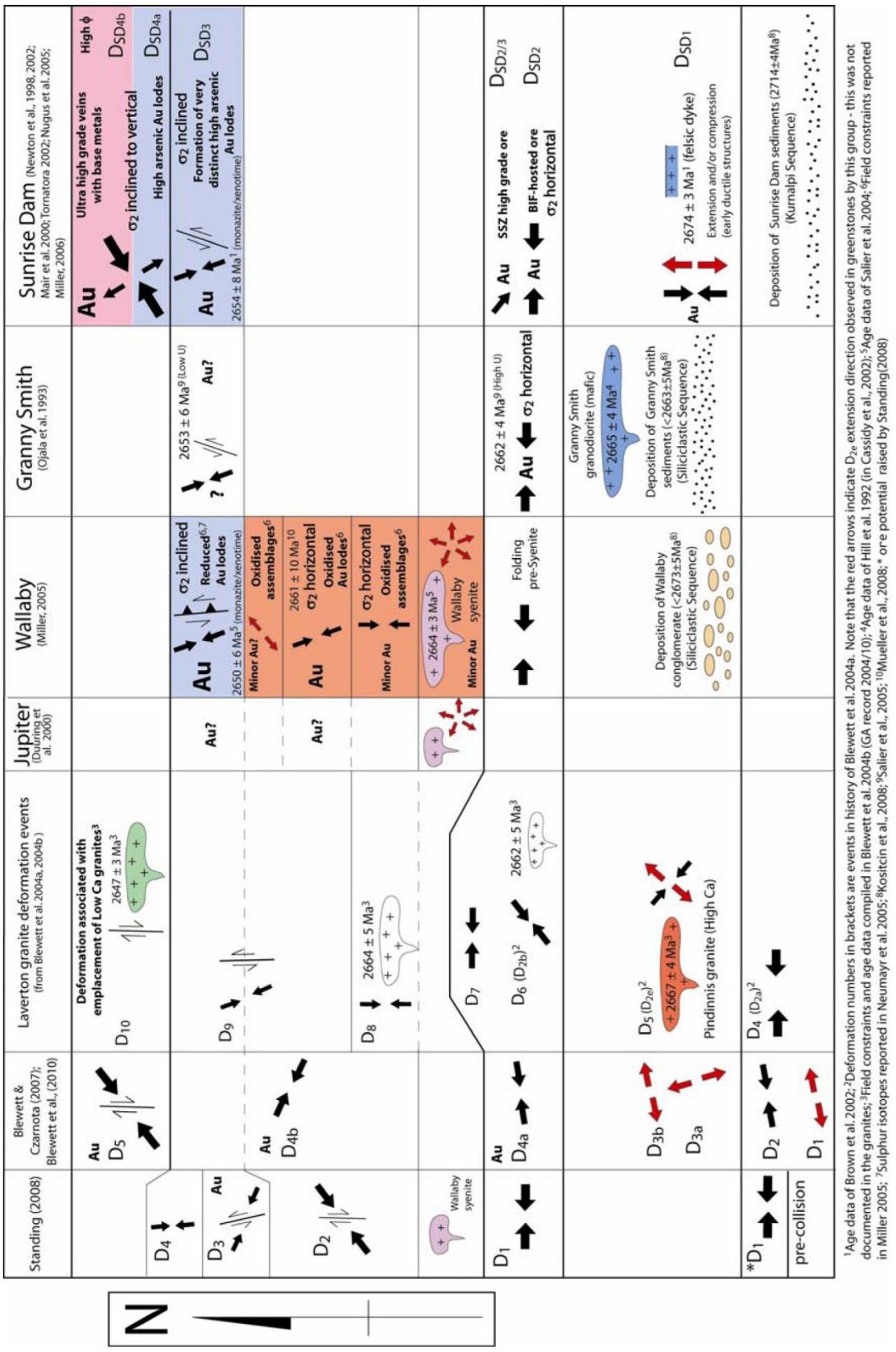

[1]Age data of Brown et al. 2002; [2]Deformation numbers in brackets are events in history of Blewett et al. 2004a. Note that the red arrows indicate D_{2e} extension direction observed in greenstones by this group - this was not documented in the granites; [3]Field constraints and age data compiled in Blewett et al. 2004b (GA record 2004/10); [4]Age data of Hill et al. 1992 (in Cassidy et al., 2002); [5]Age data of Salier et al. 2004; [6]Field constraints reported in Miller 2005; [7]Sulphur isotopes reported in Neumayr et al. 2005; [8]Kositcin et al., 2008; [9]Salier et al., 2005; [10]Mueller et al., 2008; * ore potential raised by Standing(2008)

Figure 26. Correlation diagram for the Laverton region. Modified from Miller et al. (2007).

- The age of deformation and mineralisation has been bracketed by U–Pb SHRIMP dating of: 1) intrusive rocks, which provide upper and lower age constraints on deformation, and 2) gold-related xenotime and monazite from alteration associated with the gold deposits. However, one issue is that the U–Pb dates on detrital zircon populations within the Siliciclastic Sequences are similar to the dates on younger intrusives units (e.g. compare the Granny Smith granodiorite and Granny Smith sediments; Fig. 26). This has been interpreted to mean that the U–Pb dates on the intrusive rocks may have an inherited component, making the U–Pb dates slightly too old (Kositcin et al., 2008; Standing, 2008).

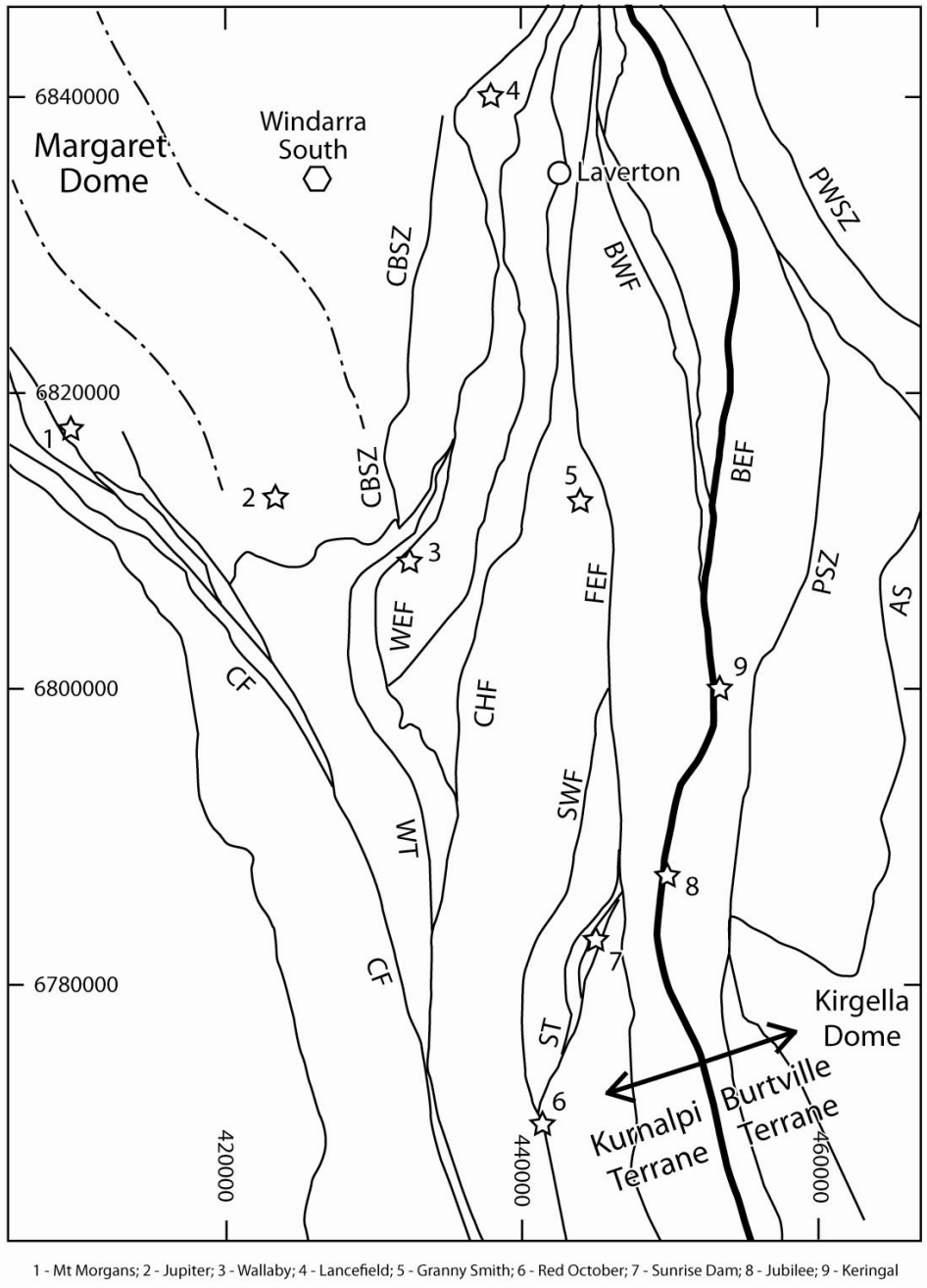

Figure 27. Map of main faults in the Laverton Greenstone Belt. Note that Wallaby and Sunrise Dam lie on NE-trending fault segments. Modified from Standing (2008) and Henson et al., (2008). Abbreviations as for Figure 25.

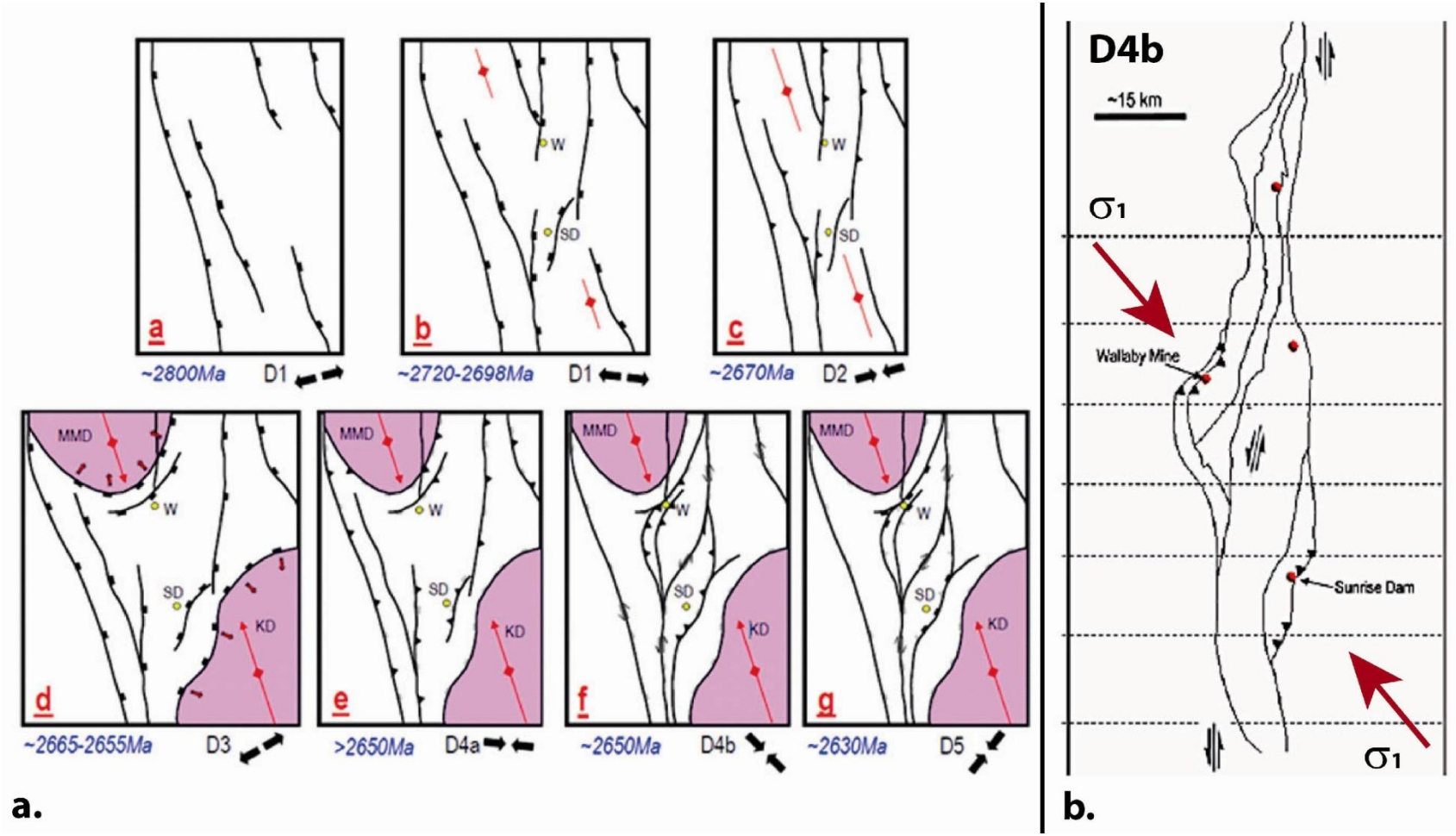

Figure 28. Examples of transpressional step-overs: a) regional model of Henson et al. (2008) for the Laverton region — this event history (D1 to D5) is also shown in Figure 26. This uses the deformation event history of Blewett and Czarnota (2007) and Blewett et al. (2010). The two world-class deposits are marked (W = Wallaby; SD = Sunrise Dam). D4b corresponds to the Wallaby and Sunrise Dam deposits being located on transpressional segments. D3 corresponds to the deposition of the Siliciclastic Sequences; b) mineralisation at Wallaby and Sunrise Dam is linked to contractional jogs during D4b NW–SE shortening at c. 2650 Ma.

Correlation of the major gold deposits

The Wallaby and Sunrise Dam gold deposits are located within 30 km of each other (Fig. 25) and key questions are:

- Can the deposits be correlated?
- Is there more than one gold event in the area?
- Can the syn-gold kinematics be linked back into a regional model to target new deposits on similar dilational or contractional fault segments?
- What is the role of the syenites — particularly for the Wallaby deposit?
- How does the alteration history fit with the structural evolution?

A revised correlation diagram (Fig. 26) has been made for the Wallaby, Granny Smith, and Sunrise Dam deposits (>18 Moz gold), with the integration of existing regional and granite event deformation histories (Swager, 1997; Blewett et al., 2004a,b; Blewett and Czarnota, 2007; Standing, 2008; Blewett et al., 2010).

Wallaby

The Wallaby 7.5 Moz gold deposit occurs within an actinolite–magnetite–epidote–calcite (AMEC) alteration pipe associated with a pipe-like 50° to 60° south-plunging syenite body that intruded a massive conglomerate unit (Salier et al., 2004) of the Siliciclastic Sequence. This pipe-like body is in the hanging wall of a series of ductile shears (termed Thet's and the Wedge Fault; Fig. 29). Low-angle gold lodes overprint the AMEC pipe with the assemblage dolomite, quartz, pyrite, calcite, sericite ± hematite (Salier et al., 2004). There has been controversy over whether the intrusions provided the auriferous fluids from which the deposit formed.

Salier et al. (2004) argued the Wallaby deposit is an orogenic overprint of the AMEC pipe with U–Pb SHRIMP ages indicating at least 5 m.y. between the intrusives (2664 ± 3 Ma) and gold (2650 ± 6 Ma). Furthermore, they argued the C and O isotopic composition of gold-bearing fluids was isotopically distinct from proximal magmatic fluids. Salier et al., (2004) inferred that Wallaby formed due to a competency contrast between unaltered and AMEC-altered conglomerate resulting in increased fracture permeability. Any fluid source was inferred to be distal (a fluid source from a deep seated intrusion was not discounted).

In contrast to Salier et al. (2004, 2005), other workers have argued for a pluton-related gold model (Hall et al., 2001). Gold deposition is related to wall rock interaction and mixing of oxidized magmatic fluids with fluid sourced from reduced sedimentary units. Geochronological evidence for this model is from a molybdenite Re–Os date (2661 ± 10 Ma) on the ore that suggests a genetic link to intrusive activity, but this is in apparent conflict with a monazite–xenotime U–Pb date (2651 ± 6 Ma; Mueller et al., 2008). Mueller et al. (2008) argue the relationships are inconsistent

with orogenic models. Instead, they argue mineralisation is related in space and time to late-orogenic, magnetite-series, monzodiorite–syenite intrusions of mantle origin.

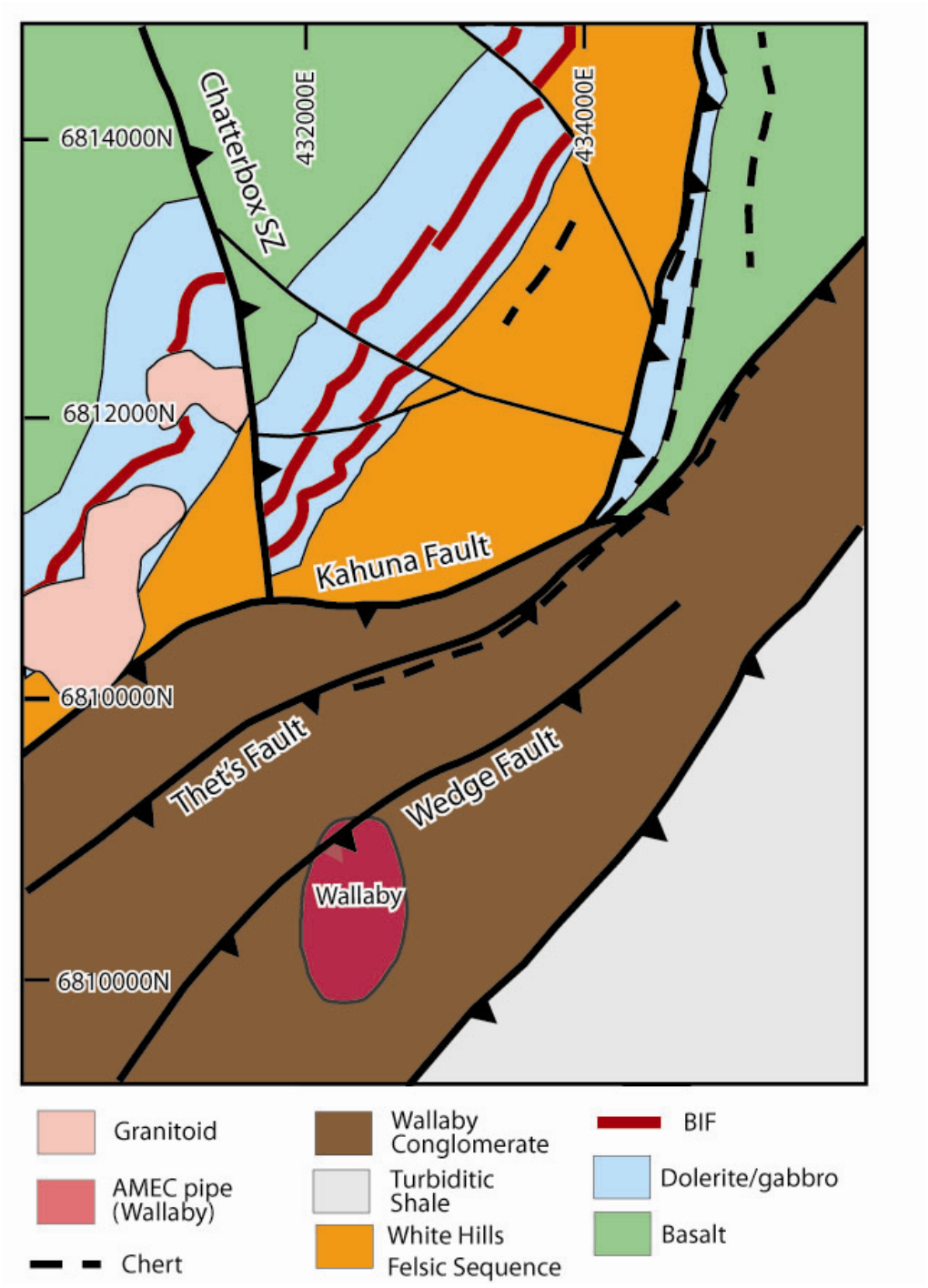

Figure 29. Geological map of the area surrounding the Wallaby Gold deposit. Modified from Standing (2008).

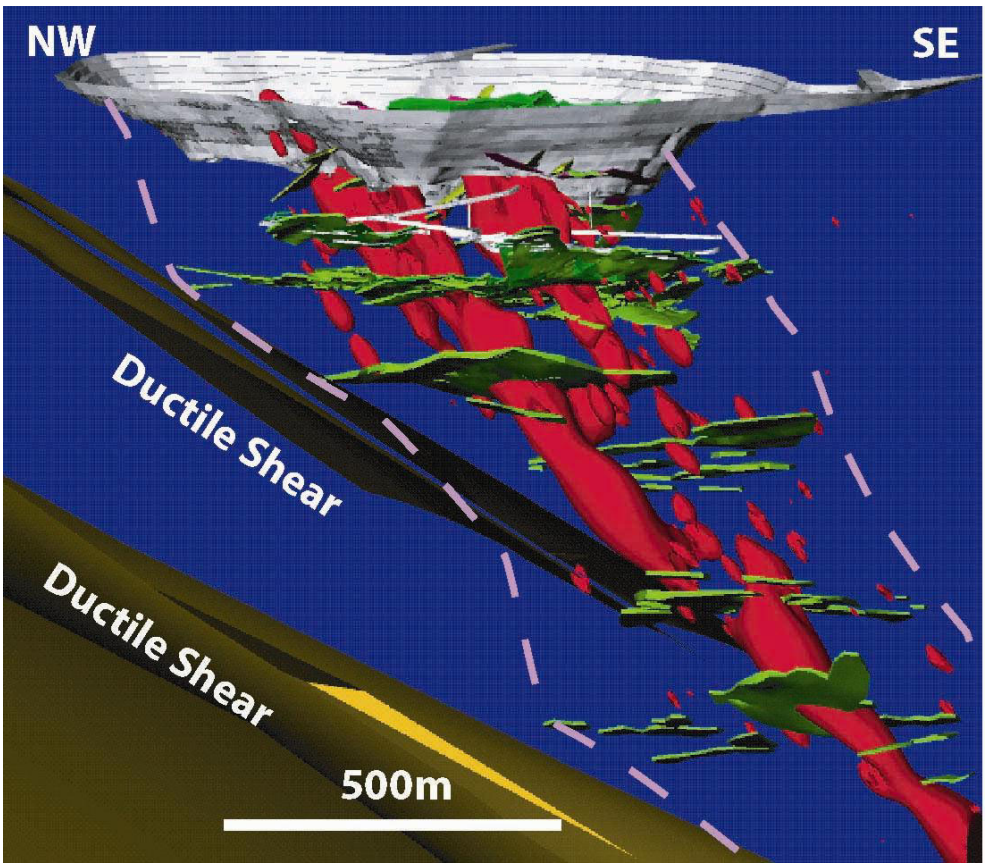

Figure 30. Screen capture of the Wallaby deposit. 3D model showing outline of open pit (grey). Red = syenite, green = gold lodes, dashed pink lines = AMEC pipe.

The Wallaby syenite intrudes through the SE-dipping eastern limb of a regional anticline and thus the gold lodes postdate the deformation that resulted in the current 50° to 70° SE dip of bedding. Syenite dykes within the deposit, and associated steep-dipping calcite veins (with pyrite, biotite, and some gold), have a radial distribution with an intersection direction that implies radial extension during magmatism (Fig. 26), where $\sigma_2 = \sigma_3$. Significantly the calcite veins, previously linked to the intrusion (Salier et al., 2004), have gold grades of up to 2.5 g/t.

The syenite dykes and calcite veins have been folded by a ductile top-to-the-N shearing event (N–S shortening in Fig. 26) linked to strong foliation development. This top-to-the-N ductile shearing marks the start of a phase of hematite-associated gold mineralisation (termed oxidized assemblages/lodes; Fig. 26). The ductile shears are overprinted by brittle deformation that marks the first phase of major gold lode development.

A series of brittle lodes associated with horizontal extension veins indicate these formed during NNW–SSE compression (Fig. 26; σ_1 horizontal to the NNW). The mineralisation is associated with quartz veins and extensive disseminated wall rock alteration, and major (up to 5 metres wide) flat-lying to low angle gold lodes with conjugate geometries. The end of the hematite-associated mineralisation is marked by an extensional overprint that produced steep-dipping hematite-bearing veins (Fig. 26).

The hematite-associated lodes are overprinted by a distinct phase of NE- to E-dipping sinistral oblique-slip faults (Fig. 26) that define the major gold event, with grades commonly >10g/t. The faults are low displacement and some mineralised faults have net offsets of less than a metre. These lodes have very distinct strong wall rock alteration (quartz, sericite, pyrite, dolomite, calcite ± fuchsite), lack hematite, and appear to be more reduced compared to earlier phases of alteration. The sinistral-slip faults were associated with σ_1 horizontal to the NNW but with an inclined σ_2, and reflects a rotation in the σ_2 direction from the stress field associated with the hematite-associated lodes.

The proposed model for Wallaby is one of multiple periods of mineralisation with at least two different fluid sources (Fig. 26). In the first stage, the observed radial extension for syenite emplacement records magma emplacement locally overwhelming a weak far-field stress field. Steep-dipping, low-grade calcite veins were emplaced, but the local extensional stress field was not ideal for major gold deposition. At the waning stage of magmatism, the far-field stress field was reimposed on the system resulting in an initial phase of ductile deformation. This change effectively sealed existing vertical fluid pathways, trapping the fluids, and led to supra-lithostatic fluid over pressure. Subsequent faulting resulted in the major hematite-associated lodes developing with an inferred genetic relationship to the syenite.

These lodes are interpreted to be analogous with the syenite-associated disseminated gold deposits documented by Robert (2001) in the Abitibi Belt in Canada. The sinistral-slip lodes are interpreted to be an orogenic-style lode overprint of the system linked to a deeper-level fluid and not a proximal fluid sourced from the intrusion (Salier et al., 2004).

Granny Smith

The 2.7 million ounce Granny Smith gold deposits (Fig. 225; Coggon, 2003) are located along a N–S striking fault that envelops the contact of a small granodiorite intrusion. Mineralisation is developed in the granitoid, and in the adjacent sedimentary sequence, with lower grades occurring inside the granitoid (Ojala et al., 1993). Conjugate carbonate–quartz vein arrays within the intrusion indicate the mineralisation was associated with E–W shortening (Ojala et al., 1993). However, variations in the conjugate vein orientations suggest that the local stress field was controlled by the shape of the granodiorite contact and was heterogeneous (Ojala et al., 1993). Fluid flow is inferred to have been focused into low mean-stress regions created by the shape of the intrusion (Ojala et al., 1993).

Sunrise Dam

The 10.2 Moz Sunrise Dam deposit (Fig. 25; Sung et al., 2007) is hosted by variable lithologies consisting of a coherent andesite volcanoclastic sequence that dips gently to the NW and is overlain by turbiditic sedimentary rocks that include magnetic shales that have been locally termed BIF (Fig. 31). These units are intruded by post-volcanic dolerites and felsic porphyries. The lithologies are folded, forming an open and upright anticline (the Spartan anticline) that plunges

shallowly north and displays thrust duplication of the units on limbs. The deposit has initial low gold grades associated with early ductile shearing (D_{SD1}) that is linked to a N–S trending mineral lineation and the development of low angle and now W-dipping ductile shear zones. These are termed the Cleo Upper Shear and the Sunrise Shear (Fig. 32). D_{SD1} is the first defined event at Sunrise Dam (e.g. Newton et al., 1998), but this equates to D_{3a} of Blewett and Czarnotta (2007; see Fig. 26).

This early event was also associated with the development of steep-dipping extensional shear veins, such as the Western Shear Zone and Watu (Fig. 32) that were reactivated during later deformation events (with high-grade gold) and also acted as pre-existing weaknesses that localised syn- to post-D_1 dykes (note Dolly Porphyry in Figure 32). Asymmetric pressure shadows on pyrite and associated 'C'-shear bands indicate D_{SD1} was associated with non coaxial shear (top-to-N). At the deposit-scale, the D_{SD1} event is associated with marked vertical flattening and may reflect larger-scale extension or be part of a contractional décollement. The D_{SD1} structures are overprinted by E–W to ENE–WSW shortening with associated BIF-style gold mineralisation and upright folding, cleavage development, and faulting (Fig. 26).

All of the D_{SD1} and D_{SD2} structures are overprinted by sinistral-slip deformation (σ_1 oriented NNW–SSE; termed local D_{SD3} of Nugus et al., 2005; Fig. 26) with the associated introduction of arsenic (blue infill in Fig. 26). Strongly mineralised, steep-dipping (60º to 90º) structures developed between the low angle ductile shear zones and are a combination of D_{SD1} and D_{SD2} structures that were reactivated during D_{SD3}. Reactivation of the low angle shears during D_{SD3} produced localised, but strongly developed, shallow-dipping crenulation cleavage (these commonly transect upright D_{SD2} folds).

The steeper dipping structures are also reactivated during ENE–WSW shortening as late-stage dextral faults with additional very high-grade (>100 g/t) gold mineralisation that, at the end-stage, is associated with base metals (local D_{SD4} of Nugus et al., 2005). During D_{SD4} there was a spatial and temporal variation in metal association from Au–As–Te initially to subsequent Au–Te – base metal sulphides and tellurides on shallow structures, which has been marked as a transition from D_{SD4a} to D_{SD4b} in Figure 26. These D_{SD4} stage structures contain both crustiform veins, and matrix-supported breccias with a combination of infill and alteration textures including epithermal-like textures with carbonate–pyrite-filled vugs, chalcedonic infill and replacement, and silica–carbonate zonation patterns.

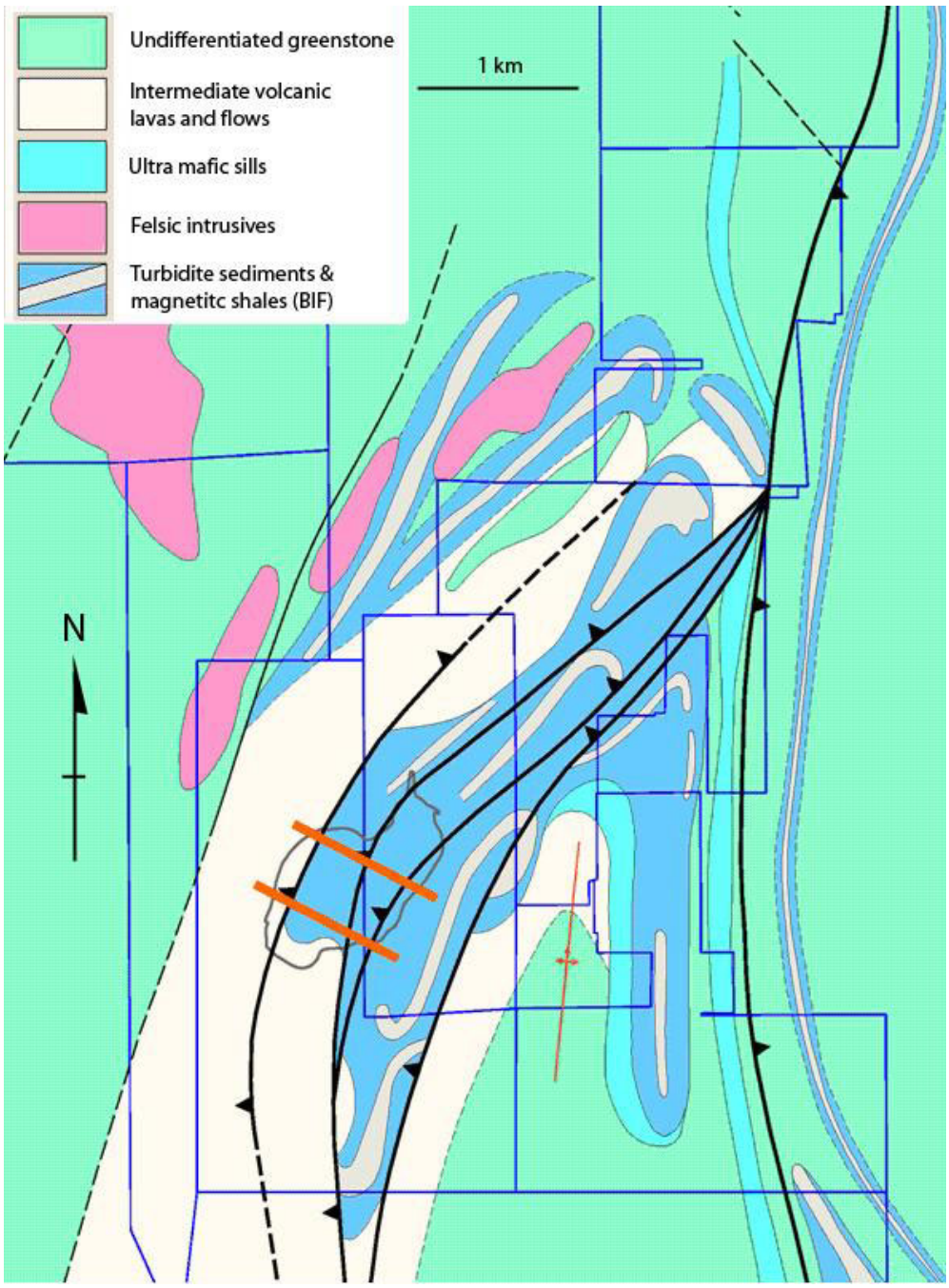

Figure 31. Geological map of Sunrise Dam. Map from Anglogold Ashanti (published in this form in the Y4 Sunrise Dam report; Miller and Nugus, 2006).

The D_{SD4} event has an unusually high stress shape ratio (ϕ), where σ_2 and σ_1 were close in magnitude. In such systems, the σ_3 direction controls the slip direction on a fault, rather than the orientation of σ_1. At Sunrise Dam, this high ϕ value produced unusual combinations of syn-gold extension on low angle shears (Newton et al., 2002) and synchronous dextral strike-slip kinematics on steeper dipping shears (Tornatora, 2002).

The entire system of steep dipping lodes is an anastamosing D_{SD3}/D_{SD4} fracture network that developed between major ductile shears due to preferential reactivation of particular fault trends.

The high-grade structures are located at strike-changes on the ductile shear zones and are inferred to be accommodation structures that developed in areas of the faults that were poorly oriented for slip within a given stress field. Gold mineralisation was associated with the Sunrise Dam deposit locality acting as alternately a dilational and a contractional jog throughout the deformation history (Fig. 33).

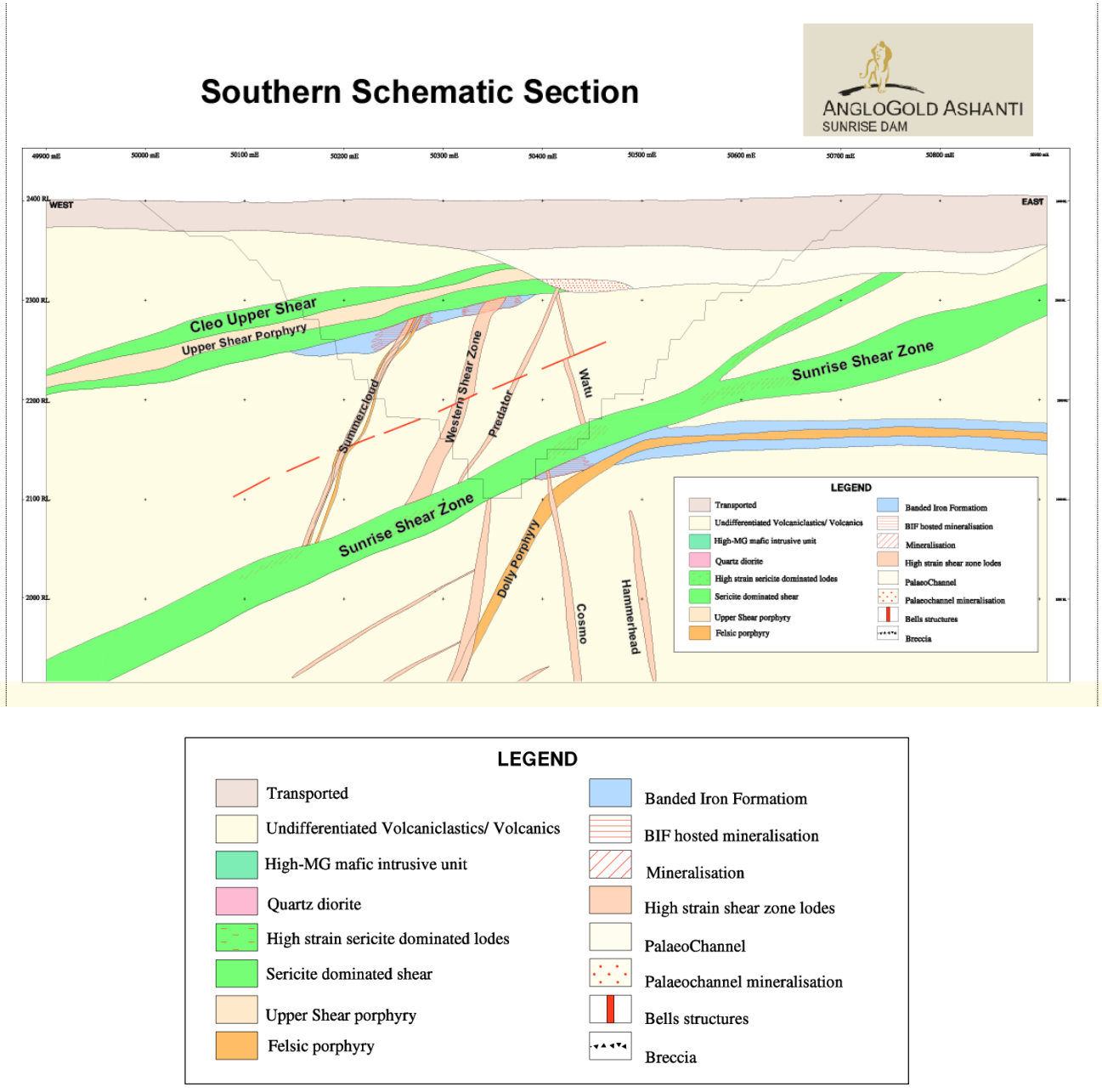

Figure 32. Southern section through the Sunrise Dam gold deposit (2002 interpretation). Anglogold Ashanti Australia Ltd.

Correlative evolution of the Wallaby, Granny Smith, and Sunrise Dam deposits

Multiple gold events occur at Wallaby and Sunrise Dam (Fig. 26), and nearly all phases of veining are associated with gold (although with major differences in the endowment associated with each event). One of the most striking observations for the Laverton region is that stress switches at both Sunrise Dam and Wallaby (marked by changes in fault kinematics and fault/extension vein geometries) are linked to changes in alteration assemblage. These changes are highlighted by the different shading in Figure 26, and marks an overall change from compression to strike-slip deformation.

These stress switches are inferred to have changed the fluid flow pathways, producing the sudden observed changes in alteration by: 1) accessing different fluid reservoirs and/or, 2) channelling fluid through and equilibrating with different rock types. Strike-slip systems can more efficiently tap deep-sourced fluids (which is inferred to have occurred during the sinistral-slip and dextral phases). Some of the observed stress switches from compression to extension could reflect a local stress field associated with emplacement of an intrusion overwhelming a weak far-field regional stress field.

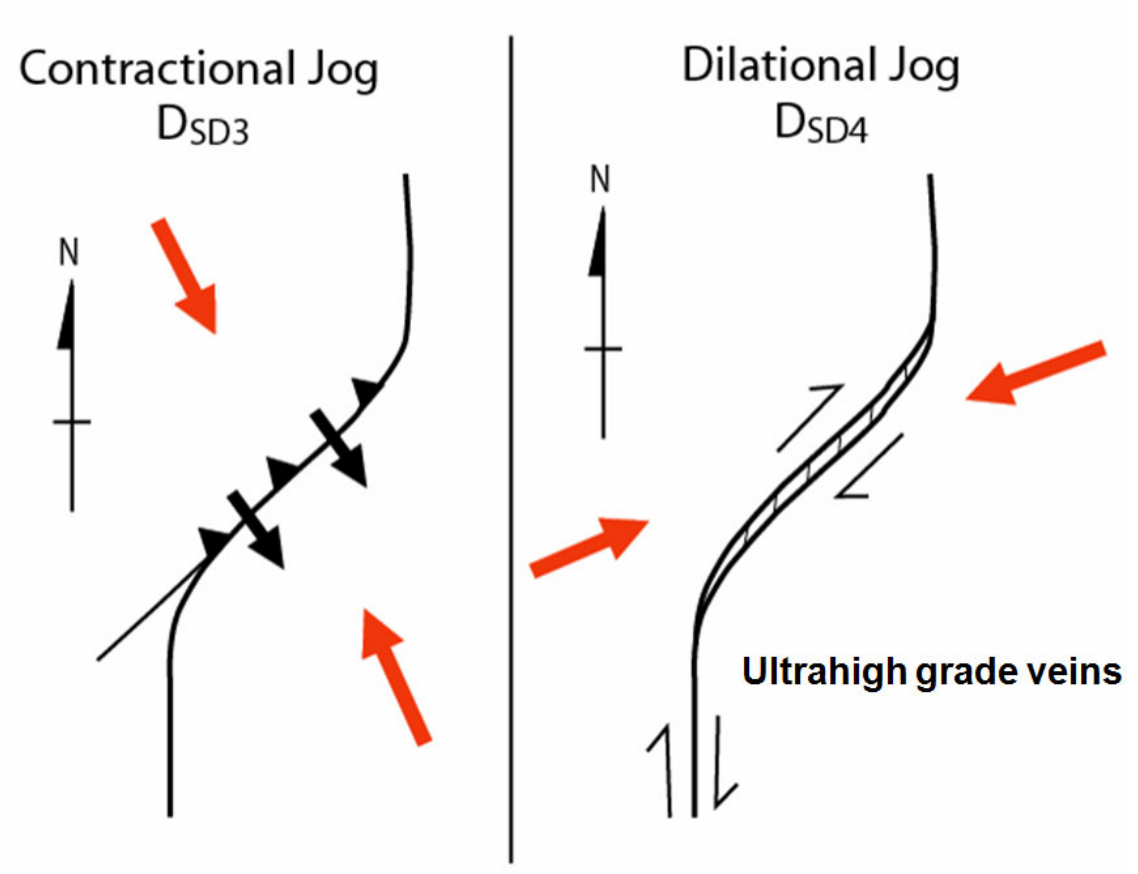

Figure 33. Gold at Sunrise Dam linked to a contractional jog (3rd deformation event at Sunrise Dam) and a dilational jog (4th deformation event at Sunrise Dam). See Figure 31 for regional context.

All three gold deposits have gold lodes linked to more than one stress field; however, some of the major periods of gold introduction at Wallaby and Sunrise Dam are not identical — i.e. no gold linked to E–W shortening at Wallaby (which is observed at Sunrise Dam and Granny Smith; Fig. 26), and no observed hematite-associated lodes linked to NNW–SSE shortening at Sunrise Dam (Fig. 26). The D_{SD4} dextral kinematics at Sunrise Dam are not observed at Wallaby (Miller, 2005), which may explain why Wallaby also does not have a base metal association. Wallaby also does not contain the very high grade D_{SD4} crustiform veins (with coarse visible gold) that occur at Sunrise Dam. This is a major difference between these two world-class ore bodies that are located within 30km of each other. The complex structural history indicates there were multiple ways to focus gold deposition to make a world-class deposit and this makes each major deposit unique.

The entire D_{SD2} to D_{SD4} deformation chronology at Sunrise Dam occurred during an interval of less than 20 million years. The gold event at Granny Smith (E–W shortening) overprints a granite dated at 2665 ± 4 Ma (reported in Cassidy et al., 2002) and two U–Pb age populations have been defined within the deposit, one at 2662 ± 4 Ma and the other at 2653 ± 6 Ma (Salier et al., 2005). U–Pb dates from the sinistral-slip lodes at Wallaby (2650 ± 6 Ma; Salier et al., 2004) and Sunrise Dam (2654 ± 8 Ma; Brown et al., 2002) are within 1σ error of each other. The timing of the dextral faulting linked to high-grade gold at Sunrise Dam is poorly constrained; however, Blewett et al. (2004b) linked the emplacement of low-Ca granites to the dextral event (D_{SD4}), providing an age constraint of 2647 ± 3 Ma (termed D_{10} in the granite event history of Blewett et al., 2004b; Fig. 26). The time period for the D_{SD3}–D_{SD4} events at Sunrise Dam are not discriminated by the existing geochronology, and most likely occurred over less than 5 million years at c. 2650 Ma.

The observed complexity within the deposits is inferred to reflect small total strain; i.e. the multiple gold events are not linked to major orogenic phases of deformation. It is inferred that the deformation was driven by fluid over pressure linked to gold mineralisation that preserved a weak far-field stress field with inconclusive evidence of the mineralisation-related stress fields left in the rock record any major distance from the deposits. Detailed studies of regional plutons (Blewett et al., 2004b) did produce similar structural results to the deposit-scale work (Fig. 25). However, the majority of Yilgarn-wide deformation histories (Swager, 1997; Blewett and Czarnotta, 2007; Standing, 2008; Blewett et al., 2010) have grouped multiple events observed at the deposits (and within the plutons) into single regional events. This implies deformation was progressive with local multiple events observed at a single field locality linked to one far-field stress field. That is, in detail more complex deformation histories can be documented (note the ten events documented in the granites by Blewett et al. (2004b) have been related to five major events by Blewett and Czarnota (2007) and Blewett et al. (2010).

Structural geology and reactive host rocks are critical aspects to the gold mineral system, particularly ore shoots. Mineralisation is to an extent independent of kinematics, with strike-slip and compressional stress fields both associated with gold mineralisation. A key question is: Why do multiple phases of gold occur in same location irrespective of structural kinematics and with

markedly different alteration types? Sunrise Dam was a transpressional and dilational jog at different points in the geological evolution with associated high grade mineralisation (Fig. 33). Furthermore, orogenic and magmatic-associated lodes have developed in the same locality (Wallaby). No matter what the genetic model, multiple pulses of fluids are evident in several deposits in the Laverton region, particularly for the world class systems. This suggests there is a fundamental architectural control on the focusing of gold-bearing fluids into the regions that develop world class gold deposits, which can act as a fluid pathway in more than one stress field.

Some implications for targeting in the Laverton region

- The same gold event linked to σ_1 oriented NNW–SSE has been documented at both Wallaby and Sunrise Dam. Within this stress field, both deposits are on contractional jogs (Fig. 28b) and are symmetrically opposed, supporting a model of the mineralisation forming within contractional jogs (Chen et al., 2001; Henson et al., 2008). Highlighting other similarly oriented contractional jogs within the regional 3D model has been used to generate targets regionally and it also identifies the existing Lancefield deposit (Henson et al., 2006).
- The right-stepping trend of the major shear zone associated with Sunrise Dam (Fig. 33) would have been a dilatant jog during dextral movement (D_{SD4}) and compressive in sinistral movement (D_{SD3}). These relationships indicate that both contractional and dilatant jogs are prospective, and the gold occurs at the strike change or inflexion point.
- The syenite intrusions at Wallaby are a key target for the hematite-associated gold style, which may be genetically linked to the intrusion, but the relationships at Wallaby suggest that it is lower grade than the later gold events, which have a more orogenic style of alteration.

References

Black, LP, Champion, DC and Cassidy, KF 2002, Compilation of SHRIMP U–Pb geochronology data, Yilgarn Craton, Western Australia, 1997–2000: Geoscience Australia, Record.

Blewett, RS, Cassidy, KF, Champion, DC, Henson, PA, Goleby, BR, Jones, L and Groenewald, PB 2004a, The Wangkathaa Orogeny: an example of episodic regional ‘D2’ in the late Archaean Eastern Goldfields Province, Western Australia. Precambrian Research, v. 130, 139–159.

Blewett, RS, Cassidy, KF, Champion, DC and Whitaker, AJ 2004b, The characterisation of granite deformation events in time across the Eastern Goldfields Province, Western Australia. Geoscience Australia, Record 2004/10, 10p.

Blewett, RS and Czarnota, K 2007, A new integrated tectonic framework of the Eastern Goldfields Superterrane *in* Proceedings of Geoconferences (WA) Inc. Kalgoorlie ’07 Conference, Kalgoorlie, Western Australia *edited by* FP Bierlein and CM Knox-Robinson: Geoscience Australia Record, 2007/14, p. 27–32.

Blewett, RS, Squire, R, Miller, JM, Henson, PA and Champion, DC 2010, Architecture and geodynamic evolution of the St Ives Goldfield, eastern Yilgarn Craton, Western Australia: Precambrian Research, v. 188, p. 275–291.

Brown, SM, Fletcher, IR, Stein, HJ, Snee, LW and Groves, DI 2002, Geochronological constraints on pre-, syn-, and postmineralization events at the world-class Cleo gold deposit, Eastern Goldfields Province, Western Australia. Economic Geology, v. 97, p. 541–559.

Cassidy, KF, Champion, DC, Fletcher, IR, Dunphy, JM, Black, LP and Claoué-Long, JC 2002, Geochronological constraints on the Leonora–Laverton transect area, northeastern Yilgarn Craton, *in* Geology, geochronology and geophysics of the north eastern Yilgarn Craton, with an emphasis on the Leonora-Laverton transect area *edited by* KF Cassidy: Geoscience Australia, Record 2002/18, p. 37–58.

Cassidy, KF, Champion, DC, Krapež, B, Barley, ME, Brown, SJA, Blewett, RS, Groenewald, PB and Tyler, IM 2006, A revised geological framework for the Yilgarn Craton, Western Australia: Geological Survey of Western Australia, Record 2006/8, 8p.

Chen, SF, Witt, WK and Liu, S 2001, Transpression and restraining jogs in the northeastern Yilgarn Craton, Western Australia. Precambrian Research. v. 106, p. 309–328.

Coggon, J 2003, Magnetism — key to the Wallaby gold deposit: Exploration Geophysics, v. 34, p. 125–130.

Duuring, P, Hagemann, SG and Groves, DI 2000, Structural setting, hydrothermal alteration, and gold mineralization at the Archaean syenite-hosted Jupiter deposit, Yilgarn Craton, Western Australia. Mineralium Deposita, v. 35, p. 402–421.

Goldfarb, RJ, Baker, T, Dubé, B, Groves, DI, Hart, CJR and Gosselin P 2005, Distribution, character, and genesis of gold deposits in metamorphic terranes *in* Economic Geology 100th Anniversary Volume , 1905–2005 *edited by* JW Hedenquist, JFH Thompson, RJ Goldfarb and JP Richards: Society of Economic Geologists, Littleton, Colorado, USA, p. 407–450.

Hall, GA, Wall, VJ and Massey 2001, Archaean pluton-related (thermal aureole) gold: the Kalgoorlie exploration model *in* A Hydrothermal Odyssey: new developments in metalliferous hydrothermal systems: James Cook University, Townsville, Queensland, Australia, p. 66–67.

Henson, PA, Blewett, RS, Champion, DC, Goleby, BR and Czarnota, K, 2006, Towards a unified architecture of the Laverton region, WA: Predictive Mineral Discovery Cooperative Research Centre, Extended Abstracts from the April 2006 Conference, Perth, Geoscience Australia, Record 2006/07, p. 47–51.

Henson, PA, Blewett, RS, Miller, JM, Roy, IG, Czarnota, K, Zhang, Y and Schaubs, PM 2008, The 4D architecture of the Laverton camp, Eastern Yilgarn Craton, *in* Concepts to targets: a scale-integrated mineral systems study of the Eastern Yilgarn Craton: pmd*CRC, Project Y4, Final Report, Part III, p. 325–349.

Hill, RI, Chappell, BW and Campbell, IH 1992, Late Archaean granites of the southeastern Yilgarn Block, Western Australia: age, geochemistry, and origin: Earth and Environmental Science Transactions of the Royal Society of Edinburgh v. 83, p. 211–226.

Kositcin, N, Brown, SJA, Barley, ME, Krapež, K, Cassidy, KF and Champion, DC 2008, SHRIMP U–Pb zircon age constraints on the Late Archaean tectonostratigraphic architecture of the Eastern Goldfields Superterrane, Yilgarn Craton, Western Australia: Precambrian Research, v. 161, p. 5–33.

Krapež, B and Barley, ME 2008, Late Archaean synorogenic basins of the Eastern Goldfields Superterrane, Yilgarn Craton, Western Australia: Part III. Signatures of tectonic escape in an arc–continent collision zone: Precambrian Research, v. 161, p. 183–199.

McIntyre, JR and Martyn, JE 2005, Early extension in the Late Archaean northeastern Eastern Goldfields Province, Yilgarn Craton, Western Australia: Australian Journal of Earth Sciences, v. 52, p. 975–992.

Mair, JL, Ojala VJ, Salier, BP, Groves, DI and Brown, SM 2000, Application of stress mapping in cross-section to understanding ore geometry, predicting ore zones and development of drilling strategies: Australian Journal of Earth Sciences, v. 47, p. 895–912.

Miller, JM 2005, The structural evolution of the Wallaby Gold Deposit, Laverton, WA: pmd*CRC, Project Y4 report, July 2004 (unpublished).

Miller, J McL and Nugus, M 2006, The structural evolution of the Sunrise Shear Zone and overlying Watu and Western Shear Zones, Laverton, WA: pmd*CRC, Project Y4 report, p. 90 (unpublished).

Miller, JM 2006, Linking structure and alteration in Laverton with specific reference to Sunrise Dam and Wallaby: pmd*CRC, Extended Abstracts, April 2006 Conference, Perth, Western Australia: Geoscience Australia, Record 2006/07, p. 62–67.

Miller, J, Nugus, M and Henson, P 2007, Importance of structural targeting: case studies from the eastern goldfields superterrane, *in* Proceedings of Geoconferences (WA) Inc. Kalgoorlie ’07 Conference, Kalgoorlie, Western Australia *edited by* FP Bierlein and CM Knox-Robinson: Geoscience Australia Record, 2007/14, p. 209–213.

Nelson, DR 1997a, Compilation of SHRIMP U–Pb zircon geochronology data, 1996, Western Australia: Geological Survey of Western Australia, Record 1997/2, 189p.

Nelson, DR 1997b, Evolution of the Archaean granite–greenstone terrane of the Eastern Goldfields, Western Australia: SHRIMP zircon constraints: Precambrian Research, v. 83, p. 57–81.

Newton, PG, Gibbs, D, Grove, A, Jones, CM and Ryall, AW 1998, The Sunrise–Cleo gold deposit, *in* Geology of Australian and Papua New Guinea Mineral Deposits *edited by* DA Berkman and DH McKenzie, Australasian Institute of Mining and Metallurgy, Monograph 22, p. 179–186.

Newton, PG, Tornatora, PMA, Smith, R and Clifford, M 2002, The Cleo–Sunrise Au deposit: contrasting structural styles within a thrust-duplex, *in* Applied structural geology for mineral exploration and mining, International Symposium, 23 to 25 September, 2002, Kalgoorlie, Western Australia *edited by* S Vearncombe: AIG, Bulletin 36, p. 1152–1155.

Nugus, M, Blenkinsop, T, Biggam, J and Doyle, M 2005, The role of early formed structures in lode gold mineralization: The Sunrise Dam Gold Mine, Yilgarn Craton, WA, *in* Structure, Tectonics and Ore Mineralisation Processes (STOMP), 29 August – 2 September 2005, Abstracts *edited by* Hancock: James Cook University, Townsville, Queensland, p. 99.

Ojala, VJ, Ridley, JR, Groves, DI and Hall, GC 1993, The Granny Smith gold deposit: the role of heterogenous stress distribution at an irregular granitoid contact in a greenschist facies terrane: Mineralium Deposita, v. 28, p. 409–419.

Robert, F 2001, Syenite-associated disseminated gold deposits in the Abitibi greenstone belt, Canada: Mineralium Deposita, v. 36, p. 503–516.

Robert, F, Poulsen, KH, Cassidy, KF and Hodgson, CJ 2005, Gold metallogeny of the Superior and Yilgarn cratons, *in in* Economic Geology, 100th Anniversary Volume 1905–2005 *edited by* JW Hedenquist, JFH Thompson, RJ Goldfarb and JP Richards: Society of Economic Geologists, Littleton, Colorado, USA, p. 1001–1034.

Salier, BP, Groves, DI, McNaughton, NJ, Fletcher, IR 2004, The world-class Wallaby gold deposit, Laverton, Western Australia: An orogenic-style overprint on a magmatic–hydrothermal magnetite–calcite alteration pipe?: Mineralium Deposita, v. 39, p. 473–393.

Salier, BP, Groves DI, McNaughton, NJ and Fletcher, IR 2005, Geochronological and stable isotope evidence for widespread orogenic gold mineralization from a deep-seated fluid source at c. 2.65 Ga in the Laverton Gold Province, Western Australia: Economic Geology, v. 100, p. 1363–1388.

Standing, JG 2008, Terrane amalgamation in the Eastern Goldfields Superterrane, Yilgarn Craton: evidence from tectonostratigraphic studies of the Laverton Greenstone Belt: Precambrian Research, v. 161, p. 114–134.

Sung, Y-H, Ciobanu, CL, Pring, A, Brügger, J, Skinner, W, Cook, NJ and Nugus, M 2007, Tellurides from Sunrise Dam gold deposit, Yilgarn Craton, Western Australia: a new occurrence of nagyágite: Mineralogy and Petrology, v. 91, p. 249–270.

Swager, CP 1997, Tectono-stratigraphy of late Archaean greenstone terranes in the southern Eastern Goldfields, Western Australia: Precambrian Research, v. 83, p. 11–42.

Tornatora, PM 2002, Structure and mineralization of the Western Shear Zone, Cleo–Sunrise gold deposit, Western Australia: University of Tasmania, Hobart, Tasmania, MSc thesis (unpublished).

Chapter 3 — Leonora Camp

N Thébaud, JM Miller, TC McCuaig

Centre for Exploration Targeting, School of Earth and Environment, The University of Western Australia

Regional geology

The Leonora district is located about 250 km north of Kalgoorlie in the Eastern Goldfield Superterrane, the eastern division of the Archean Yilgarn Craton of Western Australia. The Leonora district covers an area approximately 100 km long by 80 km wide and is well endowed with orogenic gold deposits (Fig. 34).

Despite many years of mining history, the geological and structural history documented in the area remain controversial due to poor outcrop exposure and the protracted structural history that has affected the terrain. The Leonora geology has been the focus of numerous studies and is summarized below (Skwarnecki, 1988; Williams et al., 1989; Passchier, 1990; Vearncombe, 1992; Williams and Curie, 1993; Passchier, 1994; Witt, 2001; Baggott, 2006; Blewett and Czarnota, 2007; Thébaud et al., 2010).

The Leonora district consists of Archean mafic and ultramafic rocks, interbedded sedimentary units, felsic volcanics, and late sedimentary basins that are intruded by the Raeside pluton to the west and the Bundarra pluton to the northeast. Based on contrasting lithostratigraphic content existing on either side of the northwest-trending Mt George discontinuity, the greenstone sequence can be divided into two domains, namely the Leonora Western Domain (LWD) and the Leonora Eastern Domain (LED).

In the LWD, the lithostratigraphy consists of tholeiitic basalts and komatiitic basalts, with minor interbedded sedimentary units. These rocks are metamorphosed to amphibolite and upper greenschist facies, with metamorphic grades increasing towards the contact with the Raeside pluton. The Mt George discontinuity unconformably caps the western greenstone succession and consists of deformed quartzite, chlorite schist, and quartz–sericite slate. The lithostratigraphy of the LED consists of tholeiitic basalt, minor komatiite, calc-alkaline volcanic rocks, and sedimentary rocks (Barley et al., 1989; Williams and Curie, 1993; Passchier, 1994). The calc-alkaline volcanic sequences are mainly andesitic and rhyolitic and were erupted from subaerial volcanic centres (Halberg and Giles, 1986).

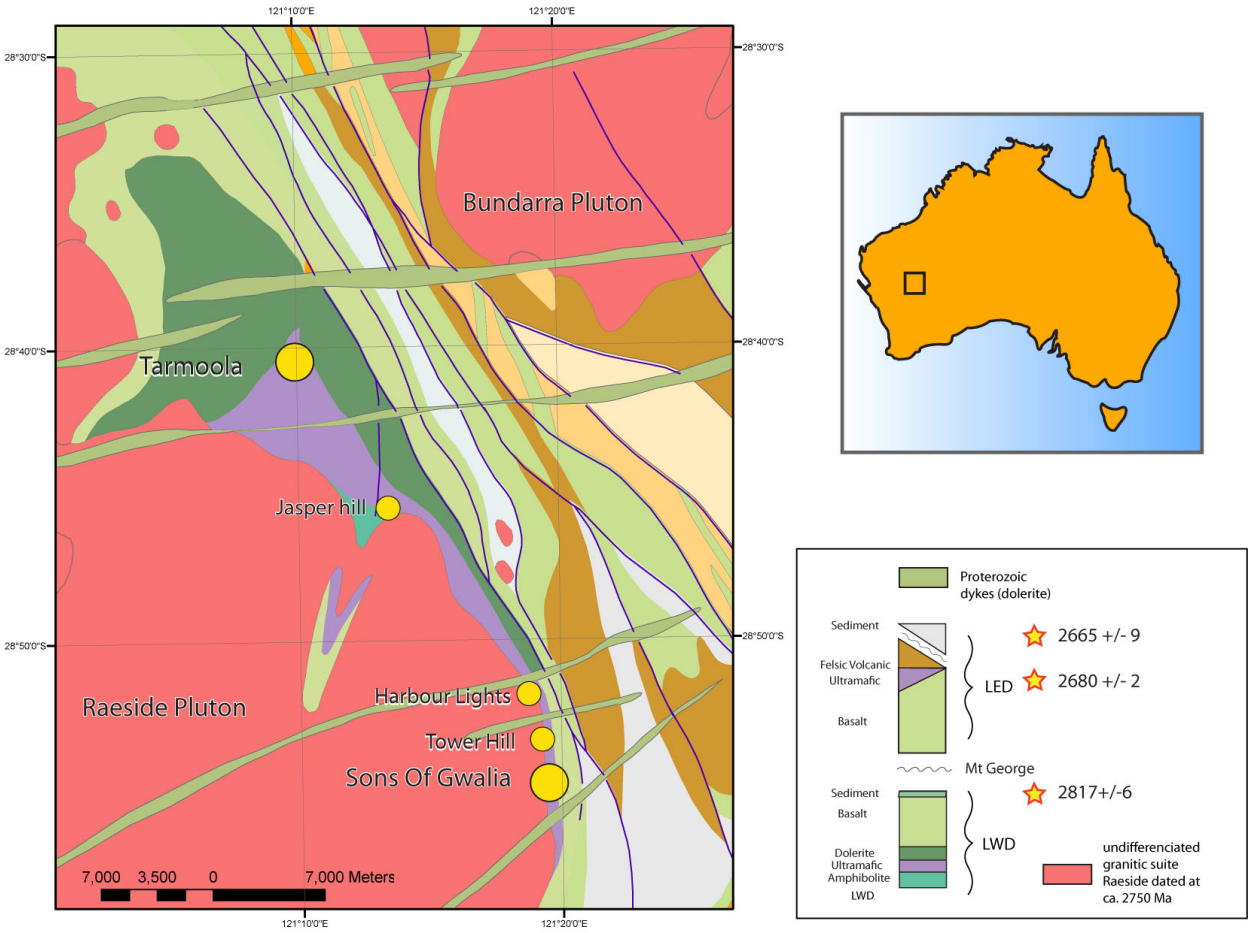

Figure 34. Geological map of the Leonora Gold Camp (modified after Thébaud et al., 2010).

Geochronology

The age for each of the domains is constrained by precise SHRIMP U–Pb zircon dates (Fig. 35). A minimum age for the LWD is 2750 ± 8 Ma, which is the age of a granodiorite intruding the lithostratigraphy in the Jasper Hill locality (Baggott, 2006). A similar minimum age constraint is provided by a crosscutting leucogranite in Jasper Hill dated at 2741 ± 5 Ma (Baggot, 2006). A banded greywacke from the Mt George discontinuity returned a robust age of 2817 ± 6 Ma (Baggott, 2006). This age is interpreted as a maximum age for deposition of the sedimentary unit forming the Mt George discontinuity. We therefore interpret these ages to indicate that deposition of the western domain occurred prior to 2750 Ma, and is possibly as old as the adjacent Youamni Terrane (c. 2.9 Ga).

The age of the LED is constrained by one precise SHRIMP U–Pb zircon date. Felsic volcanic rocks representing the northern extension of the Jeedamya Rhyolite from the Rifle Range locality in the hanging wall of the Mt George discontinuity were dated at 2680 ± 2 Ma (Baggott, 2006). A felsic volcanic rock from the Teutonic Bore locality to the north of the Leonora district returned a date of 2694 ± 4 Ma. These dates are similar to ages of Kalgoorlie Sequence and Kambalda

Sequence, respectively (Krapež et al., 2008). Both ages suggest the onset of the felsic volcanism from c. 2690 Ma. It is thus suggested that the mafic and ultramafic rocks to the east of the Mt George shear zone were deposited before 2690 Ma and likely c. 2720–2690, coeval with the Kambalda Sequence of the Southern Kalgoorlie Terrane (Baggott, 2006; Thébaud et al., 2010).

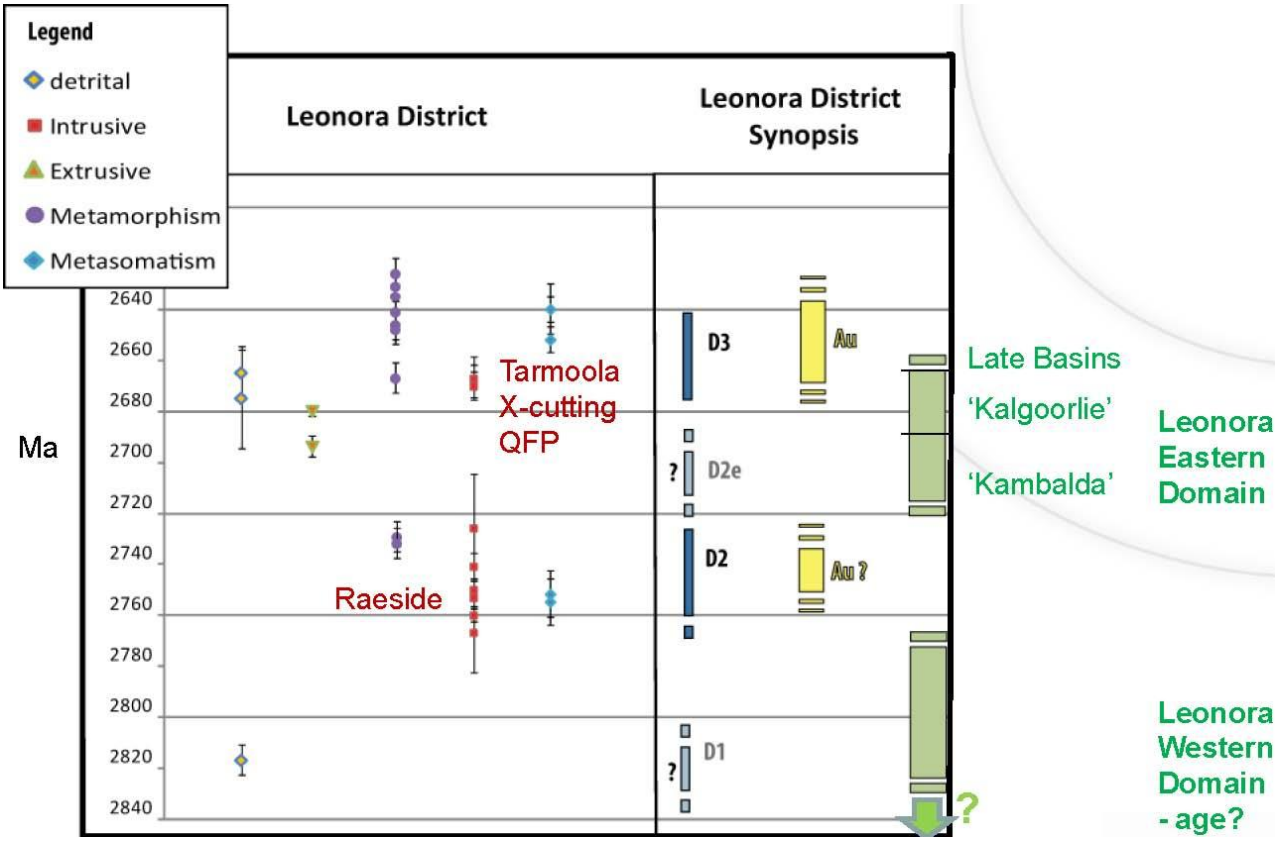

Figure 35. Chart established for the Leonora area from the available geochronological data (Witt, 2001; Fletcher et al., 2001; Dunphy et al., 2003; Black, 2004; Baggott, 2006; Thébaud et al., 2010).

Structural evolution

The structural evolution that affected the Leonora camp has been documented by numerous workers (Skwarnecki, 1988; Williams et al., 1989; Passchier, 1990; Vearncombe, 1992; Williams and Curie, 1993; Passchier, 1994; Witt, 2001; Baggott, 2006; Blewett and Czarnota, 2007; Thébaud et al., 2010). The local structural evolution presented below is derived from these previous studies but also relies on the integration of recent field observation with available geochronological data (Fig. 35). The structural evolution can be synthesized as follows (Fig. 36):

- **Early basin architecture:** Deposition of mafic–ultramafic sequence prior to c. 2741 Ma and possibly >2817 ± 6 Ma. The dramatic decrease in stratigraphic thickness from northwest to southeast between the Mt George shear zone and along the Raeside Pluton can be interpreted either as the product of structural excision during D1 as suggested by Passchier (1994), or as a lateral thickness variation within an early basin (Thébaud et al., 2010). The coherent Leonora lithostratigraphic succession along strike further suggests that the thickness variation documented is essentially primary in nature and associated with early basin architecture. This basin architecture is interpreted to have been accommodated by a set of NW-striking normal and N-striking transfer faults possibly associated with a (?local) N–S extension setting. This recently recognised early architecture is suspected to form a series of fundamental flaws in the crust that has played a central role in the response of the crust to subsequent deformation events, focussing magmas and auriferous fluids throughout the tectonic evolution.
- **Doming:** Emplacement of the Raeside dome occurred between c.2750 Ma (crystallization age on intrusive granitoid in dome) and c. 2741 Ma, which is the age of the Jasper Hill Leucogranite that cuts across the S1 planar fabric in the supracrustal cover. The granitoid dome emplacement was the result of regional extension, gravitationally driven tectonics, or the combination of both (Weinberg and van der Borgh, 2008; Thébaud et al., 2010). Deformation is characterised by strong layer-parallel ductile fabric and an arcuate ductile shear zone at the margin of the Raeside dome. Mineralisation: Gold related molybdenite veins from Tower Hill were dated at c. 2750 Ma and indicate possible early mineralisation in the Sons of Gwalia shear zone.
- **Extension and deposition of the LED:** Renewed extension and deposition of the LED lithostratigraphic succession interpreted as dated c. 2720 Ma. Mafic units from the LED are interpreted as a Kambalda sequence equivalent (2720–2690 Ma; undated at Leonora), and felsic volcanic and sedimentary sequences dated c. 2694 Ma and c 2660 Ma respectively are interpreted as Kalgoorlie sequence equivalent.
- **E–W compression and basin inversion:** Deformation is characterized by folds, brittle–ductile N–S shear zones and thrusts. Mineralisation: Geochronology on hydrothermal monazite and xenotime at Harbour Lights, Tower Hill, and overprinting events at Sons of Gwalia, provide an age of mineralisation at c. 2640 Ma (Baggott, 2006).

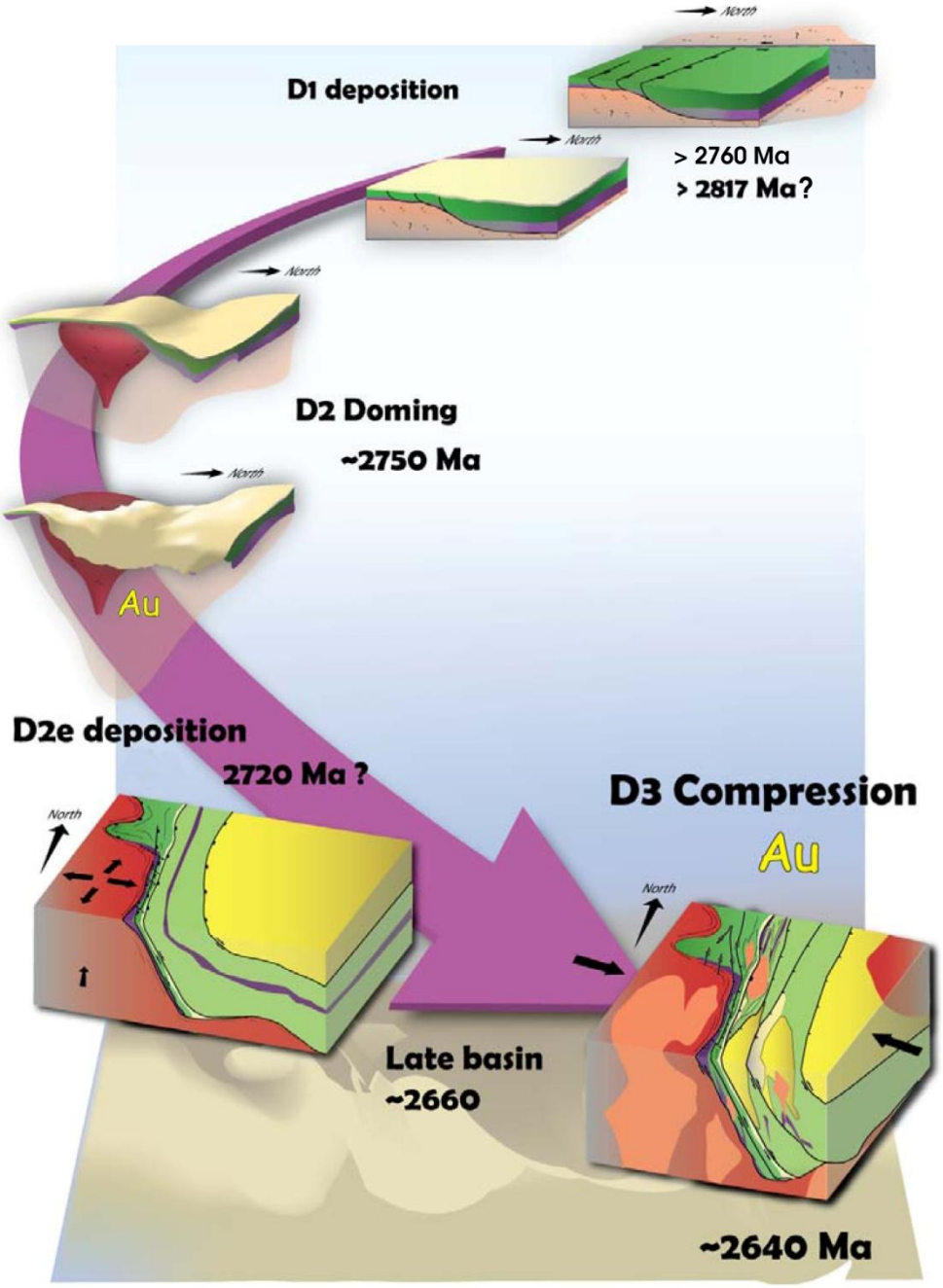

Figure 36. Summary of the tectonic evolution of the Leonora district (after Thébaud et al., 2010).

Mineralisation

In the Leonora area, the timing of mineralisation has been subject to controversy for a number of years. Early models based on field observations, structural relationships, and scarce geochronology traditionally supported a model whereby at least part of the mineralisation developed at an early stage (D2) of the deformation history (Witt, 2001; Weinberg and van der Borgh, 2008). However, this view has recently been challenged and the most recent model for mineralisation in the Leonora district is similar to that postulated for deposits in the southern Yilgarn Craton, with mineralisation occurring very late in the structural history of the belt. In the Leonora district, the mineralisation

has been interpreted to be synchronous with movement on NNE–SSW structures developed in response to a transpressive structural context (D3) (Baggott, 2006).

Mineralisation within the regional architectural framework of the Leonora area presented here is the product of the compilation of existing reports, regional field investigations, and discussions with SBM geologists. Gold mineralisation in the Leonora area can be broken into two main styles or settings. These styles of mineralisation are essentially separated on the basis of their structural context. Note that a similar division was originally proposed by Witt (2002).

Mineralisation style 1 (E1): 'Sons Of Gwalia'

The Sons of Gwalia deposit is located two kilometers south of Leonora and is hosted within the mafic portion of the stratigraphy between the Raeside granitoid and the Mt George lineament. At Sons of Gwalia, the ore body plunges 40° toward the ESE (Fig. 37). Between Main Lode and West Lode the underground exposure contains numerous, isoclinally boudinaged and folded mineralised veins. Ore shoots are parallel to the fold axis measured on small scale fold suggesting that the mineralisation is being controlled by deposit-scale isoclinal folds. As pointed out by Witt (2001), the deformation expression in the underground exposure is essentially a zone of intense pure shear rather than simple shear. The clear lineation than can be measured on the foliation planes plunges consistently to the SE parallel to the fold axes from folded veins. This lineation has been interpreted successively as an intersection or a mineral stretching lineation, but appears to be both and may represent sheath folding (McCuaig, 2004).

In Sons of Gwalia, the discontinuity of the lode within the overall fold structure is coherent with the development of transposition fold structure (Fig. 38). Transposition structures occur in foliated sequences of rocks with layers of slightly different competence (here mafic schist and auriferous quartz veins). During progressive folding, the more competent layers (Si) become progressively isoclinal so that the limbs of the folds become parallel to the axial planar foliation (S2). As deformation progresses S1 becomes coincident with the axial planar foliation (S2). Eventually, as the limbs become more attenuated, differential slip along the axial planar foliation may tear the folds closures apart along the stretched limbs. An alternative interpretation suggested that the mineralisation is associated with mylonitic zones that merge together forming the horseshoe appearance of the Sons of Gwalia ore body in plan view (Baggott, 2006). However, this model does not account for the different vergence noted from Western Lodes to Main Lodes.

E1 Mineralisation specifics

- This mineralisation style is represented by deposits such as Sons of Gwalia, Tower Hill and Harbour Lights.
- Mineralisation occurs in highly ductile strain zones which favored the development of a hydrothermal system and quartz veining controlled by competency contrast within the mine sequence producing a pipe-like ore body.

- Mineralisation presents clear evidence of syn- to post-mineralisation deformation such as isoclinal and possibly sheath folding and boudinage.
- Ore shoots are commonly developed along the plunge of transposed fold hinges and defined by mineralised quartz+sulphide+carbonate+mica veins, or as pointed out by Witt (2002) by the plunge of boudins of competent rock units (such as quartz veins) within the sheared mine sequence.
- Proximal alteration is characterized by potassic mica (muscovite, biotite), ankerite and dolomite. The carbonate alteration may extend tens of meters to hundreds of meters beyond the ore zone. Note that the ankerite as an alteration by-product is generally associated with lower temperature alteration and as such may represent a late overprint.

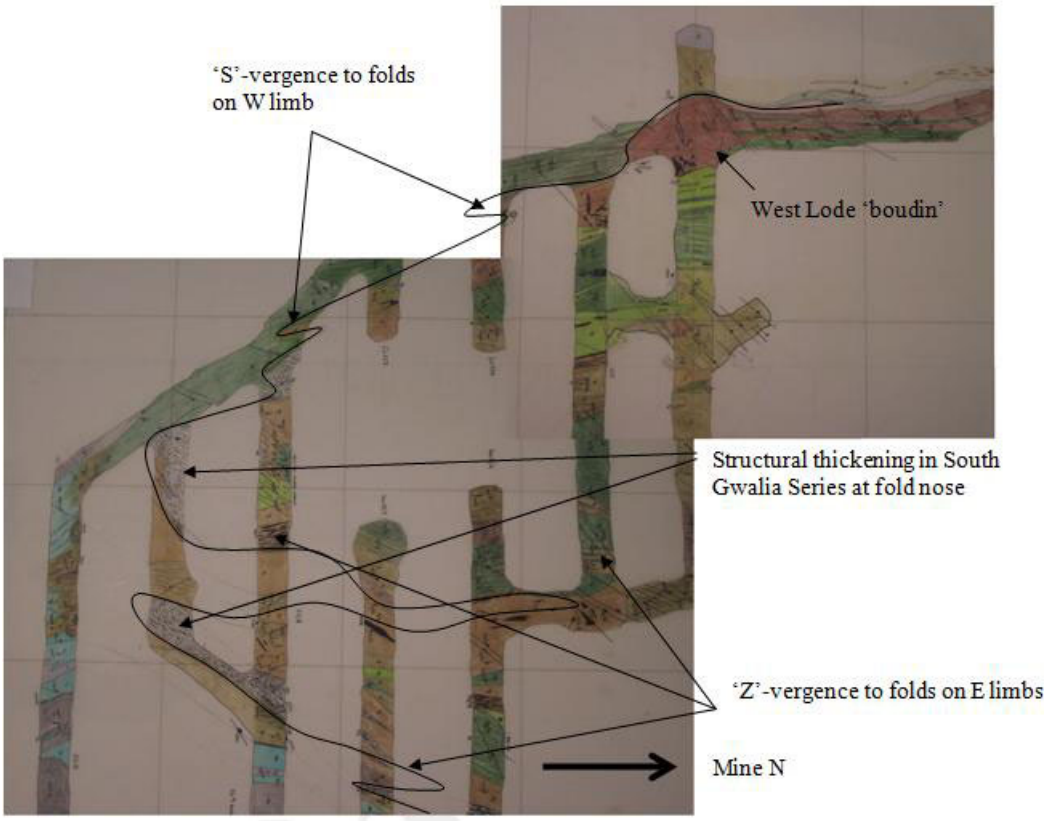

Figure 37. Photo of Sons of Gwalia geologists' mapping in the upper levels of the underground mine. Features indicating the folding of mineralisation are highlighted. Note the opposite sense of vergence on the fold limbs, structural thickening of ore in the fold noses, and the transposition of lodes sub-parallel to the axial planar cleavage (after McCuaig, 2004).

- According to Witt (2002) geochemical vectors include As and Sb (>500m dispersion), K, Rb and Cs (200 m dispersion), and Au, Bi, Mo, W (up to 150m dispersion).
- Relative timing of deformation in the Leonora Area implies that mineralisation took place prior to the brittle-ductile deformation (D2) dated at ~2640 Ma (see structural field relationships in Annex 1). Existing geochronology of early Mo-veins from the Harbour Lights deposit dated at ~2750 Ma (Re–Os; Witt, 2001) most likely represent an early stage of hydrothermal mineralisation (D1).

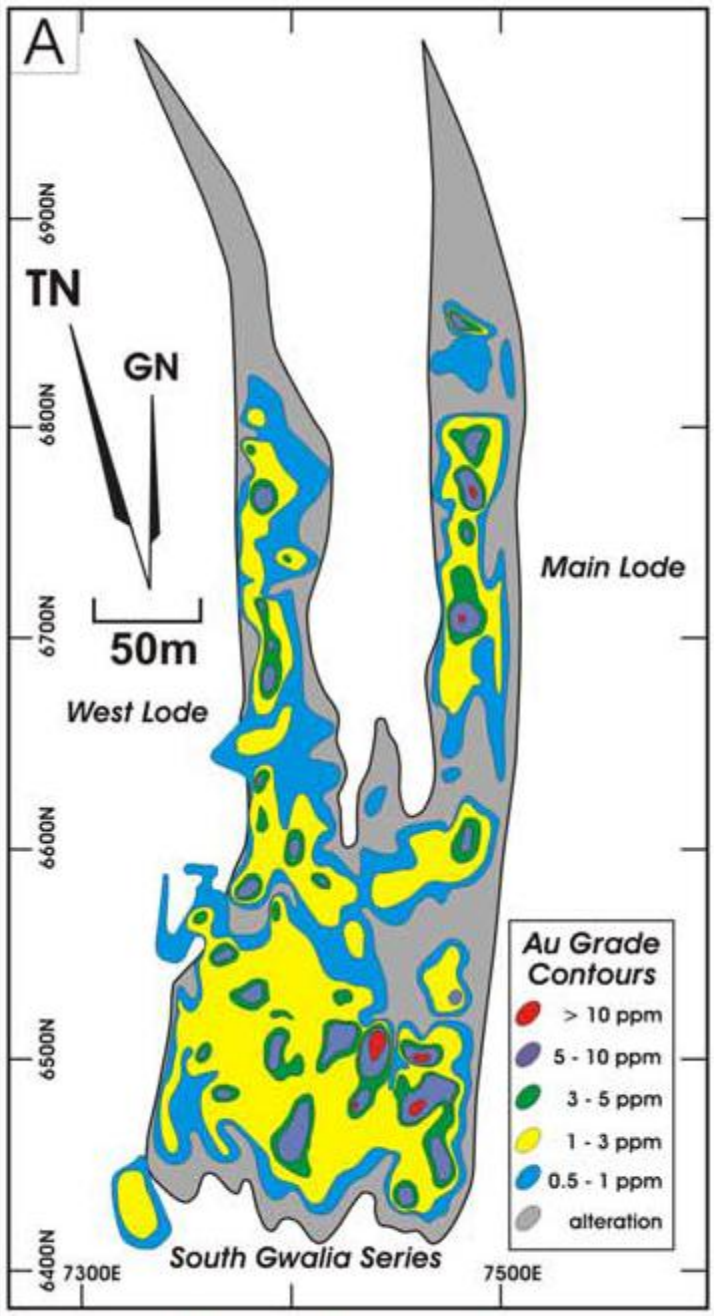

Figure 38. Grade contour level map of the Sons Of Gwalia mine showing the horse-shoe geometry (St Barbara Mines, unpublished data).

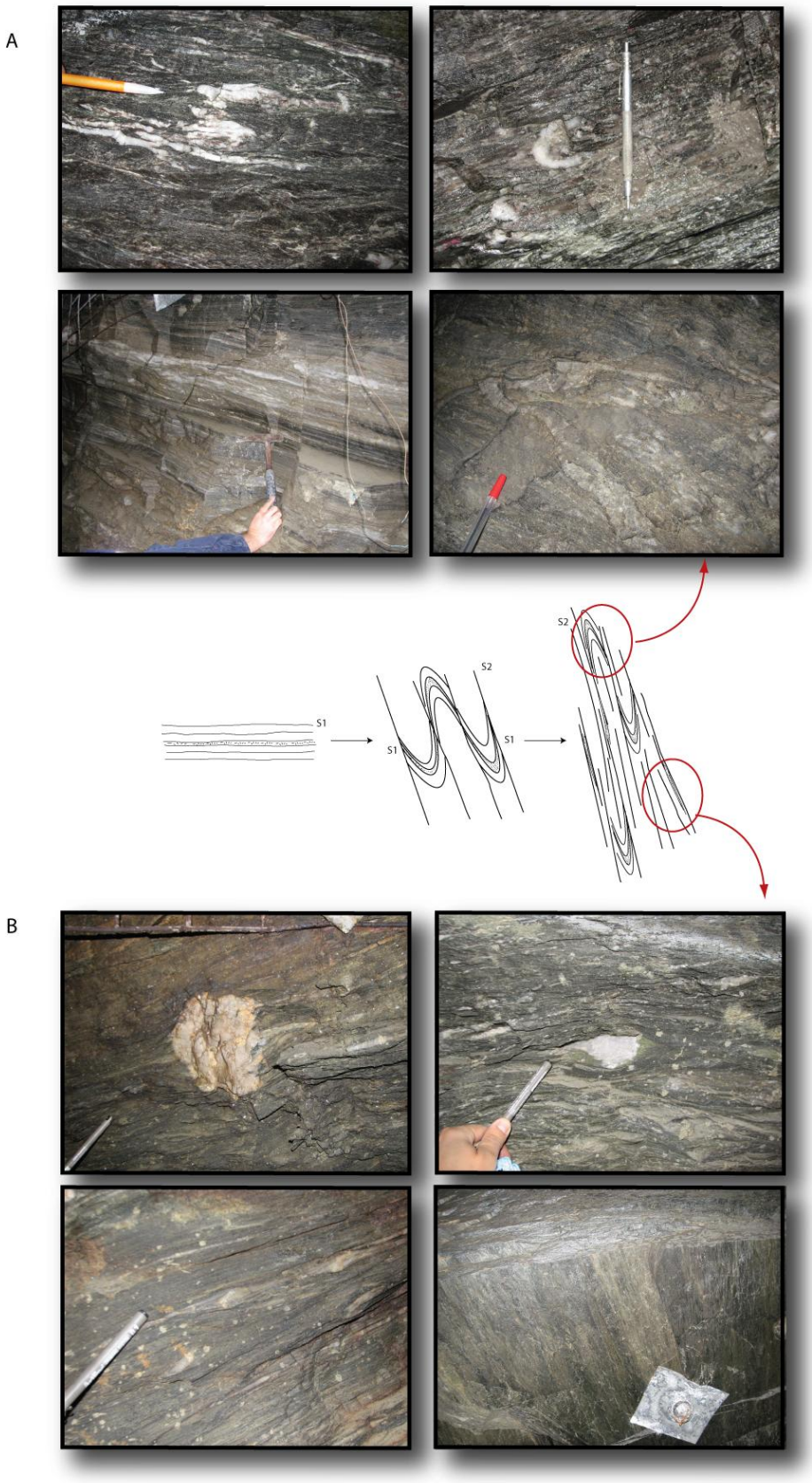

Figure 39. Underground exposures of Sons of Gwalia ore body with a schematic explanation of the development of fold transposition structure: a) photographs of (rootless) fold closure taken in the nose of the fold; b) stretched and boudinaged auriferous veins taken from the transposed fold limbs.

Mineralisation style 2 (E2): 'Tarmoola deposit'

The Tarmoola ore body is located about 45 kilometres northwest of the Sons Of Gwalia deposit. Lithologies at Tarmoola comprise a trondhjemite pluton that has intruded a northwest-striking and shallowly dipping mafic–ultramafic supracrustal sequence. Mineralisation at Tarmoola occurs on either side, and in the carapace, of the trondhjemite/supracrustal contact cover in the form of complex quartz vein networks within the trondhjemite or silicified and carbonatised ultramafic rock that envelops the pluton.

Structurally, the mineralisation is best explained by a thrust and ramp model in which the Tarmoola pluton acted as a solid body and its overall geometry controled the localisation of low mean stress domains favourable for fluid circulation (Fig. 40). In the NW corner of the Tarmoola pit, mineralisation is associated with a thrust on the shallow-dipping contact of the Tamoola pluton with north over south displacement. In the centre of the pit, steep S-dipping inflections in the carapace of the trondhjemite intrusion produce local extensional sites and en echelon veins with normal displacement. Mineralisation in the southern end of the pit is associated with en echelon vein array coherent with a oblique dextral strike slip motion (Duuring et al., 2001; Fig. 40).

In the original interpretation by Duuring et al. (2001), the various vein sets are interpreted to have developed in response to a two stage process (see D2 and D3 in Duuring et al., 2001). However, in the absence of clear overprinting relationship, the complex structural setting documented for Tarmoola may be interpreted as the result of a single deformation event. The presence of the trondhjemite pluton within an ultramafic host may have produced a large perturbation of the stress field, thus explaining some of the angular relationship between the various vein sets within the deposit (Fig. 40).

E2 Mineralisation specifics

- Mineralisation occurs as quartz + carbonate + sulphides in brittle–ductile faults related to the late compression (D2) that overprints the early ductile fabric. Mineralisation tends to develop in domains dominated by N–S faults and shear-zones, but the intersection with other sets of structures (WNW-trending cross-structures) may be important sites for mineralisation.
- Rheological contrasts within the lithological pile appears to be important in localising sites of gold mineralisation. For example, the occurrence of small granitic intrusions in ultramafic schists (e.g. Tarmoola) is a favorable setting for this style of mineralisation.
- The proximal alteration zone is characterized by potassic micas (muscovite, biotite) + ankerite + dolomite. Low mean stress areas such as dilatation jogs along faults and shears, and pressure shadows around plutons are important sites for gold mineralisation.

- Relative chronology suggests a rather late tectonic mineralisation stage. Existing geochronology suggest that mineralisation postdates the emplacement of felsic porphyry dated at 2667 ± 8 Ma.

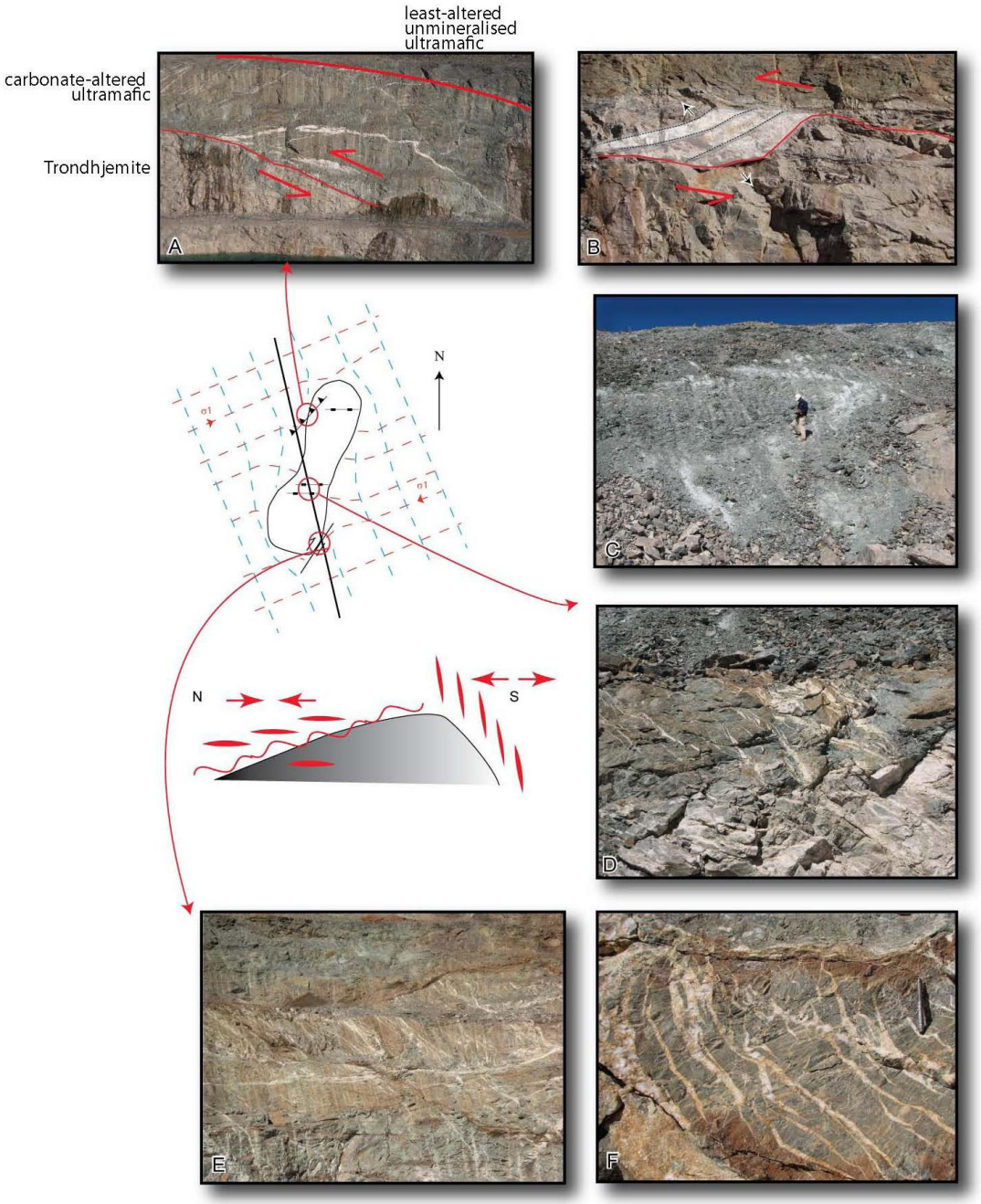

Figure 40. Field photographs from the Tarmoola pit exposure and diagram showing the thrust and ramp model: a) photograph to the W of the northern pit showing thrust structure at the contact between the trondhjemite and the ultramafic; b) local normal structure (ramp) associated with the inflection of the trondhjemite/ultramafic contact; c) foliated ultramafic above the trondhjemite contact, note that the veins arrays do not propagate in the foliated ultramafic unless previously silicified and/or carbonated (rheological contrast); d) en echelon vein set developed in the altered ultramafic at the contact with the trondhjemite pluton; e) and f) photographs of the dextral shear and normal en echelon vein set in the southeastern corner of the pit.

References

Baggottt, M 2006, A refined model for the magmatic, tectonometamorphic and hydrothermal evolution of Leonora District, Eastern Goldfields Province, Yilgarn Craton, Western Australia: The University of Western Australia, Perth, Western Australia, PhD thesis, 406 p (unpublished).

Black, LP, Champion, DC and Cassidy, KF 2006, Compilation of SHRIMP U–Pb geochronology data, Yilgarn Craton, Western Australia, 1996–2000: Geoscience Australia Record, ##/#, #p.

Blewett, R and Czarnota, K 2007, A new integrated tectonic framework of the Eastern Goldfields superterrane *in* Proceedings of Geoconferences (WA) Inc. Kalgoorlie '07 Conference, Kalgoorlie, Western Australia *edited by* FP Bierlein and CM Knox-Robinson: Geoscience Australia Record, 2007/14, p. 33–38.

Dunphy, JM, Fletcher, IR, Cassidy, KF and Champion, DC 2003, Compilation of SHRIMP U–Pb geochronology data, Yilgarn Craton, Western Australia, 2001–2002: Geoscience Australia Record, 2003/15, 139p.

Duuring, P, Hageman and Love, RJ 2001, A thrust ramp model for gold mineralisation at the Archean trondhjemite-hosted Tarmoola deposit: the importance of heterogeneous stress distributions around granitoid contacts: Economic Geology v. 96, p. 1379–1396.

Fletcher, IR, Dunphy, JM, Cassidy, KF and Champion, DC 2001, Compilation of SHRIMP U–Pb geochronology data, Yilgarn Craton, Western Australia, 2000–2001: Geosciences Australia Record, 2001/47, 111p.

Hallberg, JA 1985, Geology and mineral deposits of the Leonora–Laverton area, northeast Yilgarn Block, Western Australia: Hesperian Press, Perth, Western Australia, 140p.

Hall, GC 2007, Exploration success in the Yilgarn Craton: insights from the placer dome experience — the need for integrated research *in* Proceedings of Geoconferences (WA) Inc. Kalgoorlie '07 Conference, Kalgoorlie, Western Australia *edited by* FP Bierlein and CM Knox-Robinson: Geoscience Australia Record, 2007/14, p. 199–202.

Krapež, B, Barley, ME and Brown, SJA 2008, Late Archaean synorogenic basins of the Eastern Goldfields Superterrane, Yilgarn Craton, Western Australia, Part I. Kalgoorlie and Gindalbie Terranes: Precambrian Research, v. 161, p. 135–153.

McCuaig, C 2004, Gwalia Deeps Scoping Study Review. SRK Consulting, Project report, 71p (unpublished).

Passchier, CW 1990, Report on the geology of the Leonora area, Western Australia: Bureau of Mineral Resources, Geology and Geophysics, Record 1990/59, 14p.

Passchier, CW 1994, Structural geology across a proposed Archaean terrane boundary in the eastern Yilgarn Craton, Western Australia: Precambrian Research, v. 68, p. 43–64.

Skwarnecki, MS 1988, Alteration and deformation in a shear zone hosting gold mineralisation at Harbour Lights, Leonora, Western Australia, *in* Advances in Understanding Precambrian Gold Deposits, Volume II *edited by* DI Groves: The Geology Department (Key Centre) and University Extension, The University of Western Australia, Publication 12, p. 111–129.

Thébaud, N, Miller, J and McCuaig, C 2010, Review of controls on gold mineralisation in the Leonora gold field using 3D modelling techniques: The University of Western Australia, CET report for St Barbara. 67p (unpublished).

Vearncombe, JR 1992, Archaean gold mineralisation in a normal-motion shear zone at Harbour Lights, Leonora, Western Australia: Mineralium Deposita, v. 27, p. 182–191.

Weinberg, RF and van der Borgh, P 2008, Extension and gold mineralisation in the Archean Kalgoorlie Terrane, Yilgarn Craton: Precambrian Research. v. 161, 77–88.

Williams, PR and Currie, KL 1993, Character and regional implications of the sheared Archaean granite–greenstone contact near Leonora, Western Australia: Precambrian Research, v. 62, p. 343–365.

Williams, PR, Nisbet, BW and Etheridge, MA 1989, Shear zones, gold mineralisation and structural history in the Leonora District, Eastern Goldfields Province, Western Australia: Australian Journal of Earth Sciences, v. 36, p. 383–403.

Witt, WK 2001, Tower Hill gold deposit, Western Australia: an atypical, multiply deformed Archaean gold–quartz vein deposit: Australian Journal of Earth Sciences, v. 48, p. 81–99.

Witt, WK 2002, Leonora Exploration Models: St Barbara Limited, internal report (unpublished).

Chapter 4 — The Kambalda Nickel Camp

ML Fiorentini

Centre for Exploration Targeting, School of Earth and Environment, The University of Western Australia

Introduction

Nickel sulphide mineralisation was first discovered in the Kambalda Dome in 1966, approximately 70 years after gold was identified. The Kambalda Dome is a doubly plunging anticline cored by granitic intrusions post-dating nickel sulphide mineralisation. Nickel sulphide mineralisation is primarily hosted within the volcanic stratigraphy exposed along the flanks of the intrusions, and occurs as discontinuous to semi-continuous lenticular bodies of mineralisation termed ‘ore shoots’ (Gresham and Loftus-Hills, 1981).

The Kambalda Dome is hosted within the Kambalda Domain of the Kalgoorlie Terrane, which represents one of the fault-bounded tectonostratigraphic units into which the Eastern Goldfields Superterrane is subdivided (Swager et al., 2002, 2007; Cassidy et al. 2006; Kositcin et al., 2008; Figs 1, 41).

The three main lithostratigraphic sequences of the Kalgoorlie Terrane are: 1) the Kambalda Sequence, 2) the Kalgoorlie Sequence and 3) the Kurrawang and Merougil Sequences (Krapež et al., 2000). Figure 42 schematically illustrates the volcano-sedimentary sequence preserved in the Kambalda and Kalgoorlie Sequences at Kambalda: nickel sulfide mineralisation is mostly localised at the contact between the Lunnon Basalt and Silver Lake Member of the Kambalda Komatiite Formation.

The Kambalda Sequence comprises the Lunnon Basalt, Kambalda Komatiite (Silver Lake Member and Tripod Hill Member), Devon Consols Basalt, Kapai Slate, and Paringa Basalt. The eruption age of the Kambalda Komatiite in the Kambalda Sequence is constrained by contemporaneous komatiite and dacite volcanic activity in the Boorara Domain (Trofimovs et al., 2004) and in the Agnew–Wiluna greenstone belt (Fiorentini et al., 2005). Zircon U–Pb age determinations from the dacite volcanic rocks contain an average age of 2707 ± 4 Ma (Kositcin et al., 2008; Claoue-Long et al., 1988; Nelson, 1995, 1997, 1998). Direct Re–Os isotopic age determinations on nickel sulphide mineralisation from Mount Keith generated a comparable isochron age of 2706 ± 36 Ma (Foster et al., 1996). A detrital zircon age of 2692 ± 4 Ma was obtained from the Kapai Slate, which represents an upper age limit for the Paringa Basalt of the Kambalda Sequence (Claoue-Long et al., 1988).

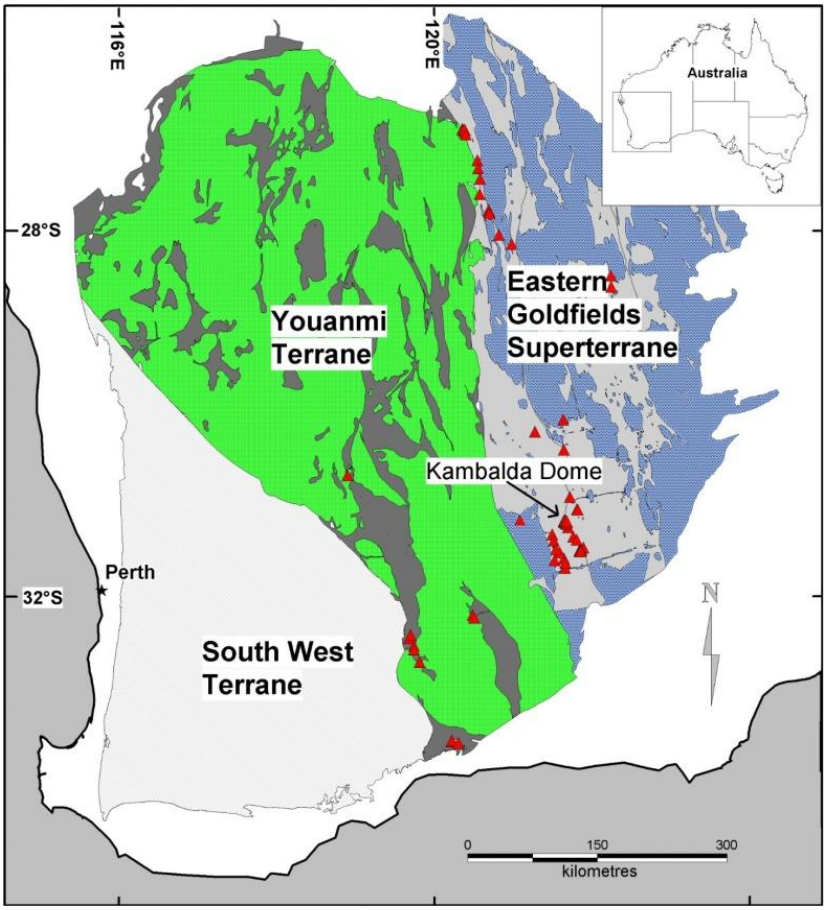

Figure 41. Regional map of the Yilgarn Craton modified from Cassidy et al. (2006). Nickel deposits are shown as red triangles and the Kambalda Dome is outlined.

The Kambalda Sequence is unconformably overlain by the Kalgoorlie Sequence (Black Flag and White Flag Formations), which comprises four unconformably bound sequences, characterised by andesite, dacite, and rhyolite volcaniclastic and epiclastic rocks with minor mafic lavas and sedimentary rocks (Woodall, 1965; Travis et al., 1971; Hunter, 1993; Hand, 1998; Krapež et al., 2000). Age determinations constrain the deposition of the Kalgoorlie Sequence to between 2686 ± 3 Ma and 2658 ± 3 Ma (Krapež et al., 2000). The Kalgoorlie Sequence has been interpreted to represent deposition in a series of deep-marine intra-arc basins within an extensional to transtensional tectonic environment (Hand, 1998; Brown et al., 2001; Krapež and Hand, 2008).

The Kurrawang and Merougil sequences unconformably overlie the Kalgoorlie Sequence (Krapež et al., 2000). The Kurrawang Sequence comprises an upwards-fining succession of conglomerate, sandstone, and mudstone, interpreted to represent high-density, coarse-grained to low-density, fine-grained turbidites (Krapež et al., 2000). The Merougil Sequence also consists of upward-fining successions of conglomerates and sandstones, but is interpreted to represent fluvial bar and channel systems (Krapež et al., 2000).

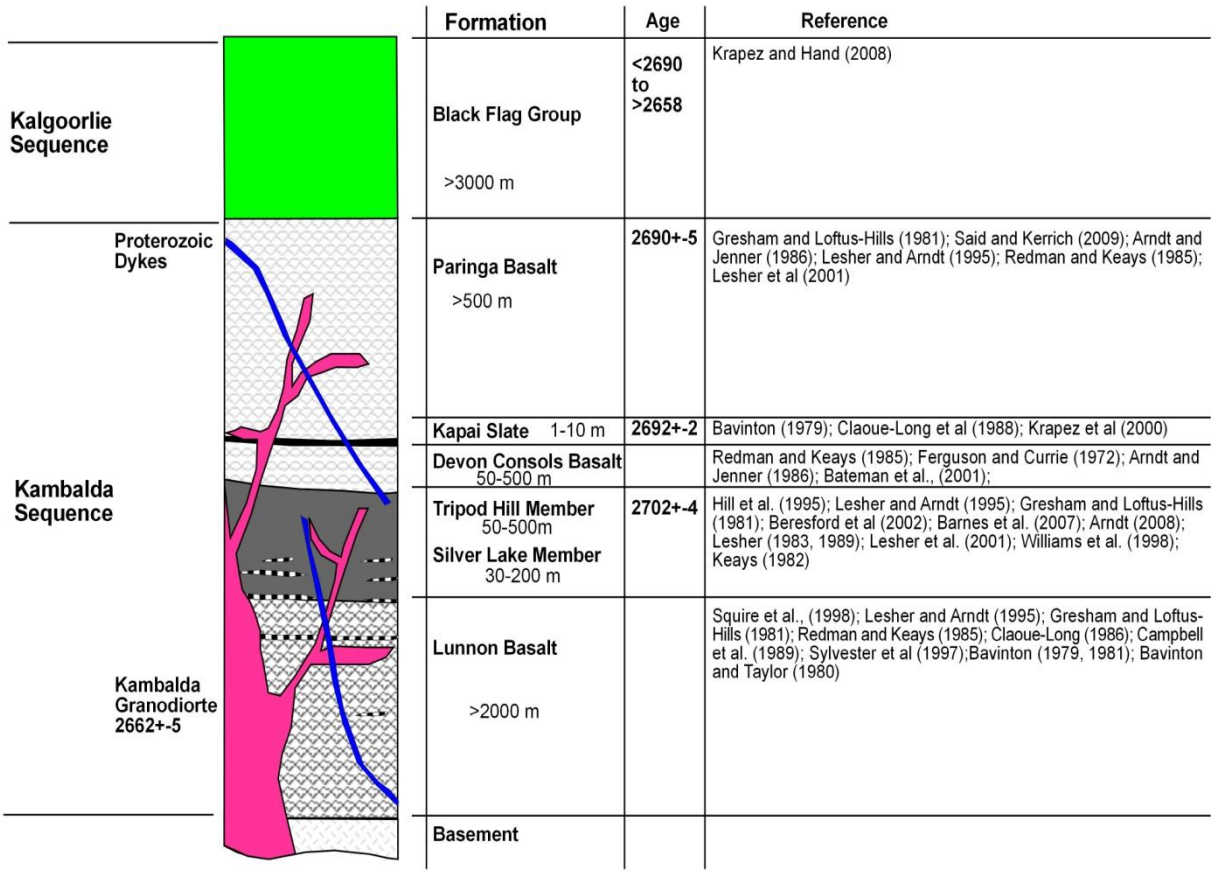

Figure 42. Stratigraphic sequence of the Kambalda and Kalgoorlie Sequences. Modified from Lesher and Arndt (1995) Beresford et al. (2002), Krapež and Hand (2008). Stratigraphy adapted from Gresham and Loftus-Hills (1981), Cowden and Roberts (1990), Swager et al. (1992), Krapež (1997). Ages based on U–Pb SHRIMP data from Claoue-Long et al. (1988), Krapez et al. (2000), Kositcin et al. (2008).

Kambalda Sequence stratigraphy

As the focus of this discussion is primarily concerned with the setting of nickel sulphide mineralisation in the Kambalda Dome, the following detailed stratigraphic summary is limited to those units contained within the Kambalda Sequence and underlying basement, and will not discuss the overlying Kalgoorlie, Kurrawang, and Merougil Sequences.

Basement

Over the years, various studies have speculated on the nature of the basement underlying the Kambalda Dome stratigraphy. A number of lines of indirect evidence support the presence of an older basement. Ages >3.4 Ga are identified within the cores of xenocrystic zircons from samples of the Lunnon Basalt, Devon Consuls, and Paringa Basalts (Compston et al., 1986), with subsequent metamorphic overgrowths occurring between 3.2 to 3.1 Ga, and final overgrowths dated at 2.7 Ga (Compston et al., 1986). Trace element and isotopic data support the hypothesis that magmas from the Kambalda Sequence (i.e. Lunnon Basalt – Kambalda Komatiite – Devon Consols – Paringa Basalt) may have been generated through varying degrees of crustal

contamination (Arndt and Jenner, 1986) and mixing of a depleted mantle source with an enriched subcontinental lithospheric mantle (Said and Kerrich, 2009).

Lunnon Basalt

The Lunnon Basalt forms the footwall to the Kambalda Komatiite Formation and is at least 2000 m thick, dominated by thin, 2–30 m flows, with a minimum lateral extent of 500 km^2 (Kambalda to Tramways, extending to Bluebush in the south; Squire et al., 1998). Stratigraphically equivalent basalts are observed throughout the Eastern Goldfields Terrane, and potentially represent 1.5 million km^3 of erupted basalt (Lesher and Arndt, 1995).

Four lithological facies are identified within the Lunnon Basalt and consist of: pillowed basalts, massive basalt, basalt breccia, and sulphidic metasediments (Squire et al., 1998). Pillowed flows contribute c. 45% of Lunnon Basalt stratigraphy and commonly exhibit well defined rims with radial and sub-concentric perlitic fractures, and associated periodic flow-top breccia (Gresham and Loftus-Hills, 1981; Squire et al., 1998). Massive basalts comprise c. 45% of the sequence and are dominated by fine- to medium-grained basalt flows ranging in thickness from 10–140 m. It is thought that the Lunnon Basalt erupted in an aqueous environment with at least 700 m of water depth (Squire et al., 1998), and that eruption was generally passive with magma transport through lava tubes on an average slope of <10° with paleo-flow towards the west, ranging from southwest to north-northwest (Squire et al., 1998).

The Lunnon Basalt tholeiites are characterised by moderately high MgO contents, high Ni and Cr abundances, low incompatible element concentrations, and minor LREE depletion (La/Sm_n = 0.76 to 0.85; Redman and Keays, 1985). The basalts have been subdivided into an upper and lower sequence, separated by interflow sediments. The lower basalts (high-Mg series basalts; HMSB) are slightly less evolved (0.69% TiO_2, 8.3% MgO) and contain olivine phenocrysts, whereas the upper basalts (low-Mg series basalt; LMSB) are more evolved (0.91% TiO_2, 7.8% MgO) and do not contain olivine phenocrysts (Redman and Keays, 1985). Vesicles and amygdales are observed in the lower sequence but absent from the upper sequence (Squire et al., 1998).

The Lunnon Basalts are interpreted to have formed during decompression melting of a mantle plume in the subcontinental lithospheric mantle, which was depleted in LREE by a previous small-degree partial melt extraction (Redman and Keays, 1985; Campbell et al., 1989). Geochemistry and isotope work indicates a possible mixed source for their generation, with a combination of both depleted and primitive mantle sources (Lesher and Arndt, 1995; Said and Kerrich, 2009).

Sediments

Metasedimentary units occur throughout the Kambalda Sequence, but are predominantly intercalated within the Silver Lake Member of the Kambalda Komatiite, rather than within the Lunnon Basalt, where sediments are commonly thin and discontinuous. Rare sedimentary structures (e.g. low-angle cross lamination, small scale scours, and scour truncations) are locally

observed and indicate a very-low energy depositional environment, in either deep or quiet shallow conditions (Squire et al., 1998). A thin sedimentary horizon is documented in a number of drill intersections approximately 100–200 m below the contact between the Lunnon Basalt and the overlying Kambalda Komatiite Formation. This horizon represents a rather continuous stratigraphic marker, which divides the geochemically less evolved from the slightly more evolved basalts in the Lunnon Basalt Sequence (Gresham and Loftus-Hills, 1981; Redman and Keays, 1985). Sediment abundance increases towards the top of Lunnon Basalt, with the unconformity between mafic and ultramafic units marked by a thin (≤ 5 m) stratigraphic sedimentary horizon (contact sediments of Bavinton, 1981).

Within the Silver Lake Member of the Kambalda Komatiite Formation, interflow sediments (internal sediments of Bavinton, 1981) are intercalated with komatiite flows, defining the boundary between successive flow lobes. Xenocrystic zircon age determinations of 2702 ± 4 Ma were derived from the sediments (Claoue-Long et al., 1988). In the Silver Lake Member there is a general (with very few exceptions; cf. Bavinton, 1979, 1981) antithetic spatial relationship between the localisation of nickel sulphide mineralisation, which is generally hosted within channelised/trough-like environments, and the sediments, which are dominantly restricted to the flanking environments, and are ubiquitously absent from the ore prism/channel facies and a 100–300 m wide zone flanking the channel (Bavinton, 1981).

Interflow sedimentary units have limited lateral continuity and are only continuous over 200–500 m, with highly variable thickness (Bavinton, 1981). The sediments are interpreted to attain a cumulative maximum thickness at a distance of c. 500 m from the channel facies, thinning towards the channel (Bavinton, 1981). Stratigraphically above the Silver Lake Member, interflow sediments progressively disappear, with only a few thin discontinuous intervals reported in the Tripod Hill Member (Bavinton, 1979; Gresham and Loftus-Hills, 1981).

Three main types of sediments have been documented within the Kambalda Dome area and described in detail by Bavinton (1979, 1981). In decreasing abundance they consist of: 1) light grey to white siliceous cherts, 2) dark grey to black carbon-bearing slates, and 3) dark-green chlorite and amphibolite-rich non-siliceous units. Sediment samples typically contain 20–25 wt% iron sulphide in the form of pyrrhotite in thin 5–15 mm layers, and periodically as small trains of spherical sulphide nodules parallel to the apparent layering. Total sulphide content increases up through the stratigraphy.

Sediment–ore association

Sediments are not commonly found associated with ore zones (Fig. 43). This has led to the interpretation that thermo-mechanical assimilation of sediments occurred within the channel environment, where turbulent magma effectively scoured the sediments upon emplacement of the komatiite units (Lesher, 1983; Lesher et al., 1984). Consequently, the assimilation of sulphur led the komatiites to sulphide saturation. Most ore zones are characterised by a trough-like feature

hosting mineralisation, with an abrupt transition to a barren contact, commonly containing a 5–30 cm thick chlorite zone. The basal chlorite zone grades laterally into planar metasediments, which are dominantly cherty in appearance (Bavinton, 1979). Sediment distribution in the Kambalda Dome is best summarised by Gresham and Loftus-Hills (1981), where 'approximately 60–70% of the ultramafic–basalt contact at the Kambalda Dome is sediment-bearing, and the majority of sediment-free contact areas contain ore'.

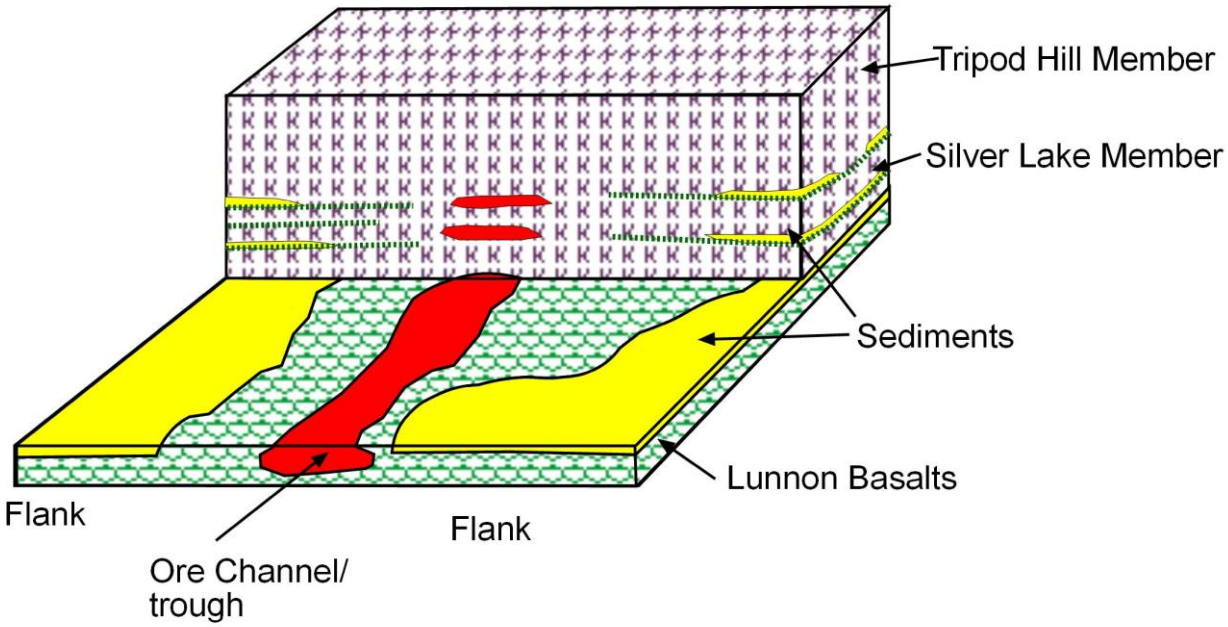

Figure 43. Block model showing distribution of contact sediments within the channel and flank facies. Modified from Gresham and Loftus-Hills (1981), and Stone and Masterman (1998).

Kambalda Komatiite Formation

Stratigraphy and volcanology

Silver Lake Member

The Silver Lake Member comprises approximately one-third of the Kambalda Komatiite Formation and varies in thickness from 50–200 m. The Silver Lake Member consists of one or more laterally continuous flow units, characterised by thick ortho-mesocumulate channels, and thinner flanking environments (Hill et al., 1995; Lesher and Arndt, 1995; Beresford et al., 2002). Nickel sulphide mineralisation is associated with thickened (>30 m) channels, whereas flanking facies environments are commonly barren. The basal flow channel is interpreted to reside in a shallow (5–30 m deep), pre-existing linear topographic feature, which was further modified by thermo-mechanical erosion and/or deformation (Gemuts and Theron, 1975; Lesher et al., 1984;

Groves et al., 1986; Lesher, 1983, 1989; Stone and Archibald, 2004; Stone et al., 2005; Williams et al., 1998).

Channel facies environments attain thicknesses of up to 100 m and are generally characterised by olivine ortho-mesocumulates. Thickened olivine cumulates are the product of sustained lava flow and continuous olivine accumulation with variable abundance of chromite (Hill et al., 1995). Consequently, channel environments are interpreted to be highly dynamic systems, and contain complex cooling histories within B-zone cumulates. B-zone cumulates commonly represent multiple composite cooling units, with the formation of spinifex (<1–10 m thick) at the flow top forming only once flow velocity has decreased, post-dating a portion of the lower B-zone olivine accumulation (Hill et al., 1995; Lesher and Arndt, 1995). We refer to Arndt et al. (2008) and Barnes (2006) for a comprehensive discussion of komatiitic textures and volcanological features.

Flanking environments of the Silver Lake Member commonly have a constant thickness of 15–35 m. Flanks exhibit a well-differentiated sequence of A-zone spinifex and B-zone cumulates dominated by orthocumulates. Thin interflow metasedimentary units are common in the flanking environment, ranging in thickness from <1–10 m. The relationship between channel and flanking facies is addressed in detail by Beresford et al. (2002).

Tripod Hill Member

The Tripod Hill Member comprises approximately the upper two-thirds of the Kambalda Komatiite Formation observed in the Kambalda Dome. The Tripod Hill Member ranges in thickness from 100–1000 m, and is thickest on the northern and western flanks of the Kambalda Dome, and thinner on the eastern flank and in the St Ives, Tramways, and Bluebush areas to the south (Lesher and Arndt, 1995; Beresford et al., 2002). The Tripod Hill Member is characterised by thin (1–10 m) well-differentiated komatiite flow units. Flows exhibit well-developed flow top breccia, thick spinifex zones, and well-developed B-zone cumulates (Gresham and Loftus-Hills, 1981).

Spinifex-textured samples from the Tripod Hill Member range from 15–32 wt% MgO, 0.4 – 0.5 wt% TiO2, 440–920 ppm Ni, and 2500–4020 ppm Cr (Lesher and Arndt, 1995). Overall, komatiite flows are characterised by a lower MgO content than in the underlying Silver Lake Member, the result of a lower overall proportion of cumulus olivine. Within the Tripod Hill Member, a trend of decreasing MgO content up-sequence is observed (Gresham and Loftus-Hills, 1981). Metasediments are generally absent from the Tripod Hill Member. The Tripod Hill Member displays LREE enrichment relative to the Silver Lake Member, the result of minor (c. 5%) crustal contamination (Lesher and Arndt, 1995). In terms of chalcophile element concentrations, the Tripod Hill Member displays normal background values (i.e. not enriched or depleted; cf. Lesher et al., 2001). Accordingly, it is likely that these komatiites did not equilibrate with any sulphide liquid during crystallisation and fractionation.

Devon Consuls Basalt and Paringa Basalt

Overlying the Kambalda Komatiite Formation is a sequence of mafic volcanic and intrusive bodies. In the Kambalda Dome, the transition from the underlying ultramafic units (Kambalda Komatiite) to the mafic volcanic units is generally sharp, with the exception of St Ives and Tramways, where the mafic and ultramafic units display interfingering relationships (Gresham and Loftus-Hills, 1981). The mafic units are siliceous high magnesium series basalts (SHMSB) comprising two members: the Devon Consuls Basalt (lower member) and the Paringa Basalt (upper member; Redman and Keays, 1985). Both members contain abundant (up to 30%) phenocryst phases of olivine, pyroxene, and feldspar (Redman and Keays, 1985). The Kapai Slate, which is a thin (1–10 m) sedimentary unit, separates the two members.

The Devon Consuls Basalt has a total thickness of 60–100 m and is characterised by two lithologies: 1) pillowed flows with felsic ocelli, and 2) massive komatiitic basalt with minor pillowed phases (Ferguson and Currie, 1972). The basalts are further classified into two geochemical groups: 1) high-Si, low-Mg basalt characterised by 52–60 wt% SiO_2, 4–6 wt% MgO, 6.7 – 7.4 wt% FeO_{tot}, 0.71 – 0.83 wt% TiO_2, 742–896 ppm Cr, 231–278 ppm Ni; and 2) low-Si, high-Mg basalt characterised by 47–52 wt% SiO_2, 9–16 wt% MgO, 9.8 – 12 wt% FeO_{tot}, 0.64 – 0.77 wt% TiO_2, 576–1173 ppm Cr, 152–393 ppm Ni (Redman and Keays, 1985; Arndt and Jenner, 1986). Trace element data of the Devon Consuls Basalt exhibit flat HREE primitive mantle normalised patterns with moderate LREE enrichment and no apparent Nb depletion (Arndt and Jenner, 1986; Bateman et al., 2001). Undepleted chalcophile element abundances within the unit indicate that the basalt lavas were emplaced sulphide undersaturated (Redman and Keays, 1985; Lesher et al., 2001). SHRIMP and U–Pb age determinations of xenocrystic zircon contained within the Devon Consuls Basalt exhibit a range of ages from 3450 ± 3 Ma to 2652 ± 12 Ma (Compston et al., 1986). Two geochrons are identified, where the oldest (3385 ± 10 Ma) represents crystallisation age of the basement, and a younger (2693 ± 50 Ma) is the age of basaltic volcanism (Compston et al., 1986).

The Kapai Slate is subdivided into two facies assemblages: a lower carbonaceous shale and an upper unit, which comprises incised turbidites and carbonaceous shales (Krapež et al., 2000). Lithologically, the Kapai slate is composed of carbonaceous shales, with minor, pale, cherty sediments and felsic volcaniclastic rocks (Bavinton, 1979; Bateman et al., 2001). Xenocrystic zircon age determinations from the Kapai Slate produced minimum ages of 2692 ± 4 Ma, with grains as old as 3441 ± 18 Ma (Claoue-Long et al., 1988).

The Paringa Basalt (upper member) exceeds 500 m in thickness and is dominated by massive or pillowed mafic flows. Massive units are interpreted as either massive sheet flows or intrusive units, and commonly contain medium- to coarse-grained differentiated portions in the central sections (Gresham and Loftus-Hills, 1981; Said and Kerrich, 2009). The Paringa Basalt rocks are characterised by c. 10.6 wt% MgO, 10.7 wt% FeO, 13.0 wt% Al_2O_3 1070–2020 ppm Cr, 280–470 ppm Ni with strong LREE-enrichment (Arndt and Jenner, 1986; Lesher and Arndt, 1995).

The Paringa Basalt is subdivided based on geochemistry into a lower enriched basalt, characterised as komatiitic basalt to high-magnesium tholeiitic basalt (HMTB), and an upper depleted basalt, characterised as HMTB (Said and Kerrich, 2009). The upper depleted basalt exhibits a narrow compositional range (Mg# 61–75) and a flat primitive mantle normalised pattern with slight LREE depletion. The lower enriched basalt is characterised by Mg# from 53–76 with LREE-enriched primitive mantle normalised patterns (Bateman et al., 2001; Said and Kerrich, 2009).

The enriched Paringa Basalt (lower unit), characterised by LREE enrichment with negative anomalies at Nb and Ti, was initially interpreted by Barley (1986) as a crustally contaminated ultramafic unit. However, Said and Kerrich (2009) indicated that the disparity in geochemistry between the two Paringa Basalt geochemical subunits can be attributed to a mantle plume interacting with the asthenospheric mantle that had a component of older crust recycled back into it (Said and Kerrich, 2009). Despite displaying a complex petrogenetic history, the Paringa Basalt lavas were emplaced sulphide-undersaturated and preserve normal chalcophile element concentrations (Redman and Keays, 1985; Lesher et al., 2001).

Intrusions

A complex sequence of intrusions post-dates and crosscuts the mafic and ultramafic units of the Kambalda Sequence stratigraphy. Geochronology indicates that the majority of these granitoid intrusions were emplaced between 2.70 to 2.63 Ga, both coeval with and post-dating felsic volcanism of the Kalgoorlie Sequence (Brown et al., 2001). Intrusion lithologies vary from biotite monzogranites, granodiorites to trondhjemites (Witt and Swager, 1989; Champion and Sheraton, 1993, 1997; Witt and Davy, 1997).

Geochemistry

The Silver Lake Member of the Kambalda Komatiite Formation comprises Munro-type komatiites with initial liquid compositions of up to 30 wt% MgO (Lesher et al., 1984; Lesher, 1989; Lesher and Arndt, 1995). Olivine in equilibrium with the initial liquid would be approximately Fo_{94}, similar to that observed within the channel facies olivine cumulate zones (Ross and Hopkins, 1979; Lesher, 1989). The Silver Lake Member komatiites exhibit major and trace element variations consistent with the fractionation and accumulation of olivine and minor chromite, akin to other Munro-type komatiite systems (Barnes et al., 2004, 2007). Accumulation of pyroxene is not observed in the channel facies. However, pyroxene (metamorphosed to amphibole) is prevalent in the more fractionated flanking facies of the Silver Lake Member and is interpreted to reflect the fractionated composition of magmas in this environment (Lesher and Arndt, 1995).

Channel facies are characterised by >40 wt% MgO and inferred olivine compositions ranging from $Fo_{90–94}$ (Ross and Hopkins, 1979; Lesher, 1989; Barnes et al., 2007). Channel facies spinifex ranges in composition from 16–31% MgO, 0.31 – 0.53 wt% TiO_2, 385–1610 ppm Ni, 1280–3670 ppm Cr; rare earth element abundances are characterised by La/Sm_n ratios from 0.4 – 0.7 with

slight LREE depletion over HREE (Lesher and Arndt, 1995). Conversely, flanking facies cumulates are characterised by lower MgO contents (35–40% MgO) and olivine compositions ranging from $Fo_{89–91}$. Spinifex-textured samples from the flanks are commonly characterised by 12–21 wt% MgO, 0.41 – 0.55 wt% TiO_2, 424–1810 ppm Cr, and 71–410 ppm Ni, with LREE enrichment relative to the channel spinifex (Lesher and Arndt, 1995).

Although thermo-mechanical assimilation of crustal material occurred upon komatiite emplacement (Groves et al., 1986; Williams et al., 1998; Bekker et al., 2009), channel environments from the Silver Lake Member do not generally exhibit evidence of crustal contamination, displaying LREE depletion (La/Sm_{cn} of 0.6 – 0.7) and chondritic ratios of MREE and HFSE ($Al_2O_3/TiO_2 \sim 20$, Ti/Zr = 97, $Gd/Yb_{cn} = 1$; Arndt and Jenner, 1986). However, evidence of crustal contamination is locally recorded in the flanking facies (Lesher and Arndt, 1995; Lesher et al. 2001), as observed with LREE enrichment. It is argued that geochemical evidence of crustal contamination is only preserved in the flanks and not in the channels because of the highly dynamic nature of komatiite systems. In fact, in the channels the assimilation and contamination process that occurred upon thermo-mechanical erosion of the substrate is generally followed by extensive magma recharge, effectively removing and diluting any geochemical signature of this interaction. Conversely, magma recharge in the flanks is less pronounced and preservation of a crustal contamination signature is permitted (Lesher and Arndt, 1995; Lesher et al., 2001). Throughout the Kambalda Dome komatiite system, there is very little physical evidence of contamination: locally, felsic ocelli, which may be derived from sediment assimilation, are identified along channel margins (Frost, 1985; McNaughton et al., 1988; Frost and Groves, 1989; Frost, 1992).

For a comprehensive review of PGE geochemistry of the Silver Lake Member of the Kambalda Komatiite Formation, we refer to Heggie (2010) and Fiorentini et al. (in press). The authors integrated a large body of high-precision PGE analyses from various locations, with a focus on the Long–Victor system on the eastern flank of the Kambalda Dome, and investigated the complex relationship between PGE variation and localisation of different styles of nickel sulphide mineralisation (Fig. 44). The authors concluded that the Silver Lake Member komatiites generally display background PGE concentrations typical of other 2.7 Ga Munro-type komatiites globally (Maier et al., 2009). Anomalously PGE depleted samples are rare and generally concentrated on the flanking environments of large channelised environments. Conversely, samples from the channels are either undepleted or display anomalous PGE enrichment.

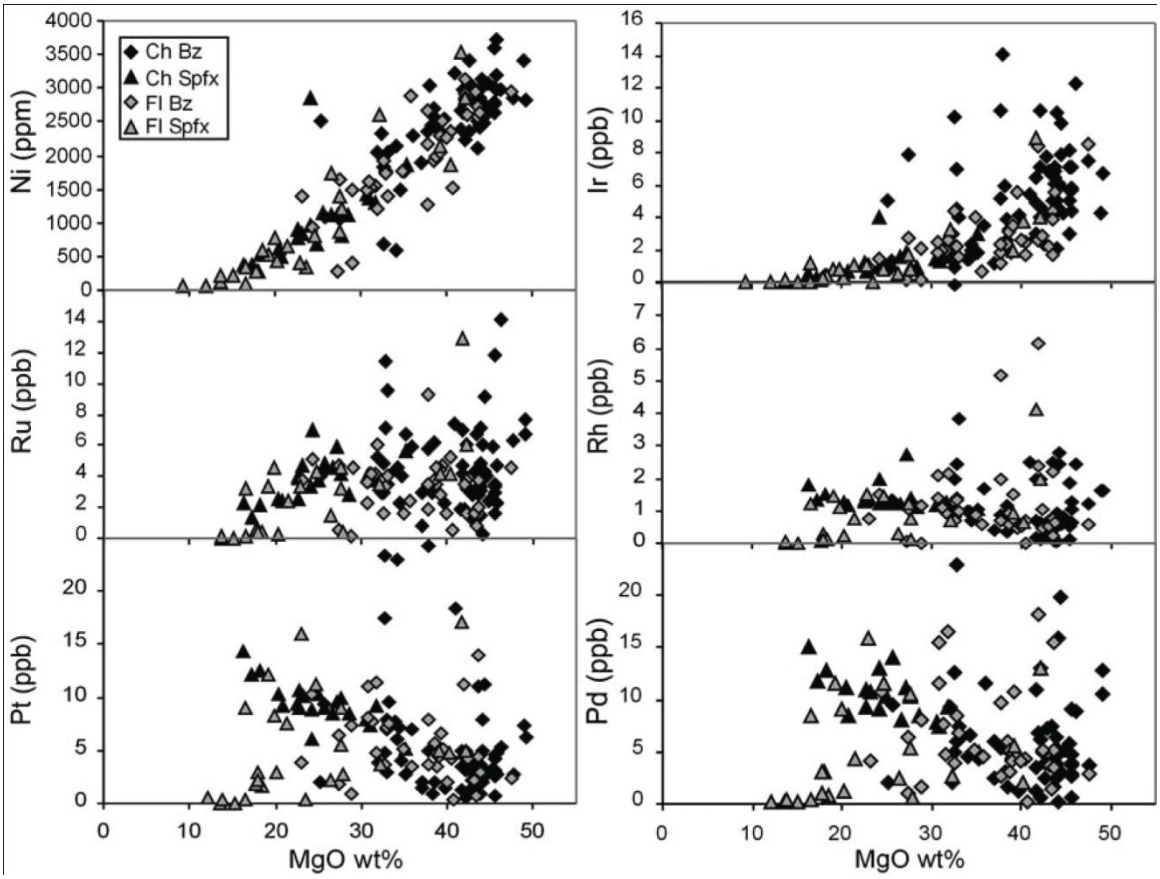

Figure 44. Relationship between MgO content and chalcophile element concentrations from samples collected at the Long–Victor deposit, located on the eastern flank of the Kambalda Dome (cf. Figure 45). All data are labelled according to volcanic facies where samples where collected: Ch Bz = B zone from channelised environments; Ch Spfx = A zone from channelised environments; Fl Bz = B zone from flanking environments; Fl Spfx = A zone from flanking environments. Data from Heggie (2010).

Nickel sulphide mineralisation

Mineralisation setting

Basal contact mineralisation occurs at the contact between the footwall basalts and the overlying ultramafic flows. Basal contact ore surfaces occur within embayments or depressions in the top of the footwall basalts, termed troughs or channels (Lesher, 1983). The formation of trough or embayment features is still contentious with two existing interpretations. The first interpretation states that thermal-mechanical erosion of flowing ultramafic lavas was responsible for the down-cutting and entrenchment of the ultramafic flows into the sediments overlying the pillowed basalts (Lesher, 1983, 1989; Beresford et al., 2005). The second interpretation suggests a strong structural control on the troughs, either through pre-existing faults with syn-eruption graben development, or during subsequent deformation of the greenstone belt (Stone and Archibald, 2004; Stone et al., 2005). Evidence for both interpretations is extensively documented, and a combination of both (pre-existing structures/topography and the erosive action of the ultramafic magma followed by regional deformation) is most likely responsible for the current ore surface configuration.

Troughs within the Kambalda Dome area vary in size, but are commonly narrow and elongate with lengths up to 2300 m and widths <300 m (Gresham and Loftus-Hills, 1981). Mineralisation within major troughs is dominantly continuous, yet occurs as small (20–130 m) elliptical ore bodies in minor troughs.

Hangingwall ore occurs stratigraphically higher but usually within 100 m of the komatiite–basalt contact (Gresham and Loftus-Hills, 1981). Hangingwall mineralisation within the Lunnon, Hunt, and McMahon ore shoots (Fig. 45) occurs at the contact of the basal ultramafic flow unit and the second flow unit, with nickel sulphides residing on the A-zone spinifex of the basal flow (Groves et al., 1986).

Finally, structurally mobilised ore is characterised by the mechanical transportation of sulphide into areas of dilation and lower tectonic pressure (e.g. fold hinges, fault dilation zones, shear zones) away from the primary accumulation site (Lesher and Keays, 2002). Mobilised ore is restricted to massive sulphides, because they are generally more ductile than disseminated sulphide (cf. McQueen, 1981, 1987).

Mineralisation style

Basal and strata-bound mineralisation zones are commonly 1–3 m thick, with intervals up to 10 m thick. Mineralisation consists of a massive sulphide layer, (<1m thick) overlain by a zone of matrix mineralisation. Massive sulphide ore is defined as >80% sulphide comprising pyrrhotite, pentlandite, pyrite, and chalcopyrite with minor spinels concentrated at some basal or top contacts (Groves et al., 1977). Massive ore is generally banded with alternating layers of pyrrhotite- and pentlandite-rich bands. These bands formed during recrystallisation under directed stress, and are generally parallel to the adjacent wallrock contacts (Ewers and Hudson, 1972).

Matrix mineralisation is defined as mineralisation with 40–80% sulphide abundance, with the remainder comprising serpentine or talc, pseudomorphs after original olivine, within a continuous matrix of sulphide. In the Kambalda Dome area, matrix mineralisation exhibits a gradation of sulphide abundance from 40–60% at the top, to 60–80% sulphide at the base of the unit, and ranges in thickness from 1–3 m (Gresham and Loftus-Hills, 1981; Keays et al., 1981). Matrix mineralisation exhibits a greater lateral continuity than the massive sulphide.

Finally, disseminated mineralisation is rarely observed within the Kambalda Dome area. However, disseminated mineralisation is observed in both basal contact and strata-bound settings. Disseminated mineralisation is characterised by <10–40%, commonly 5% interstitial sulphide within an ultramafic host.

Orthomagmatic mineralisation in the Kambalda Dome

The eastern flank of the Kambalda Dome contains the Gibb, Long, and Victor ore shoots. These ore shoots are characterised by dominant basal contact mineralisation with strong structural control on trough development or modification (for a review on the genesis and development of through-

like embayments see Beresford et al., 2002; Stone and Archibald, 2004). Sediments are generally absent from within the ore environment of the shoots. However, contact sediments are observed in the flanking positions to the troughs, and hanging-wall sediments are observed in the flanks, and can stratigraphically overlap the trough structures.

The Gibb ore shoot (Fig. 45), up-dip of the Long ore shoot, is 1300 m in length and attains a maximum width of 150 m. The Gibb shoot is arc-like, plunging shallowly to the north and south and terminated at the northern end by extensive felsic intrusions. Ni-sulphide mineralisation is hosted within the basal komatiite flow, which attains a maximum thickness of 50 m. The mineralisation resides in a complex trough structure dominated by basalt-basalt pinch-outs (Gresham and Loftus-Hills, 1981).

The Long ore shoot (Fig. 45) occurs down dip of the Gibb ore shoot and has a known plunge length of 2300 m, and remains open both up- and down-plunge (giving rise to the Long North and Long South targets of Independence Group and recent discoveries of the Moran and McLeay ore bodies; Fig. 45). The Long shoot attains a maximum width of 300 m and is characterised by steep to sub-vertical dips, but appears to shallow as it plunges to the south. Mineralisation is contained within a low-relief trough structure, within the basal komatiite flow which attains a thickness of c. 100 m.

The Victor ore shoot (Fig. 45), south of the Gibb shoot, represents its down-plunge extension, separated by extensive felsic intrusions. The basal flow unit attains thicknesses of >75 m within the trough, has a defined mineralised plunge length of 850 m, and another 700 m of unmineralised extension prior to the development of the McLeay ore body. Nickel sulphide mineralisation within the Victor shoot occurs in a well-defined trough structure c. 200 m in width, and is defined by high-angle normal faulting up dip and low angle reverse faulting down dip.

Alteration and metamorphism

Alteration and metamorphism studies on the Kambalda Dome have been conducted by Ross (1974), Barrett et al. (1977), Bavinton (1979), Marston and Kay (1980), Gresham and Loftus-Hills (1981), Arndt and Jenner (1986), Barley and Groves (1987), and summarised by Swager and Griffin (1990) and Lesher et al. (2001). Komatiite units in the Kambalda Dome have undergone seafloor hydrothermal alteration with alteration intensity (i.e. serpentinisation) increasing towards the top of the succession (Barley and Groves, 1987). Later regional metamorphism comprising further serpentine alteration and talc–carbonate alteration locally overprints the primary seafloor alteration assemblage.

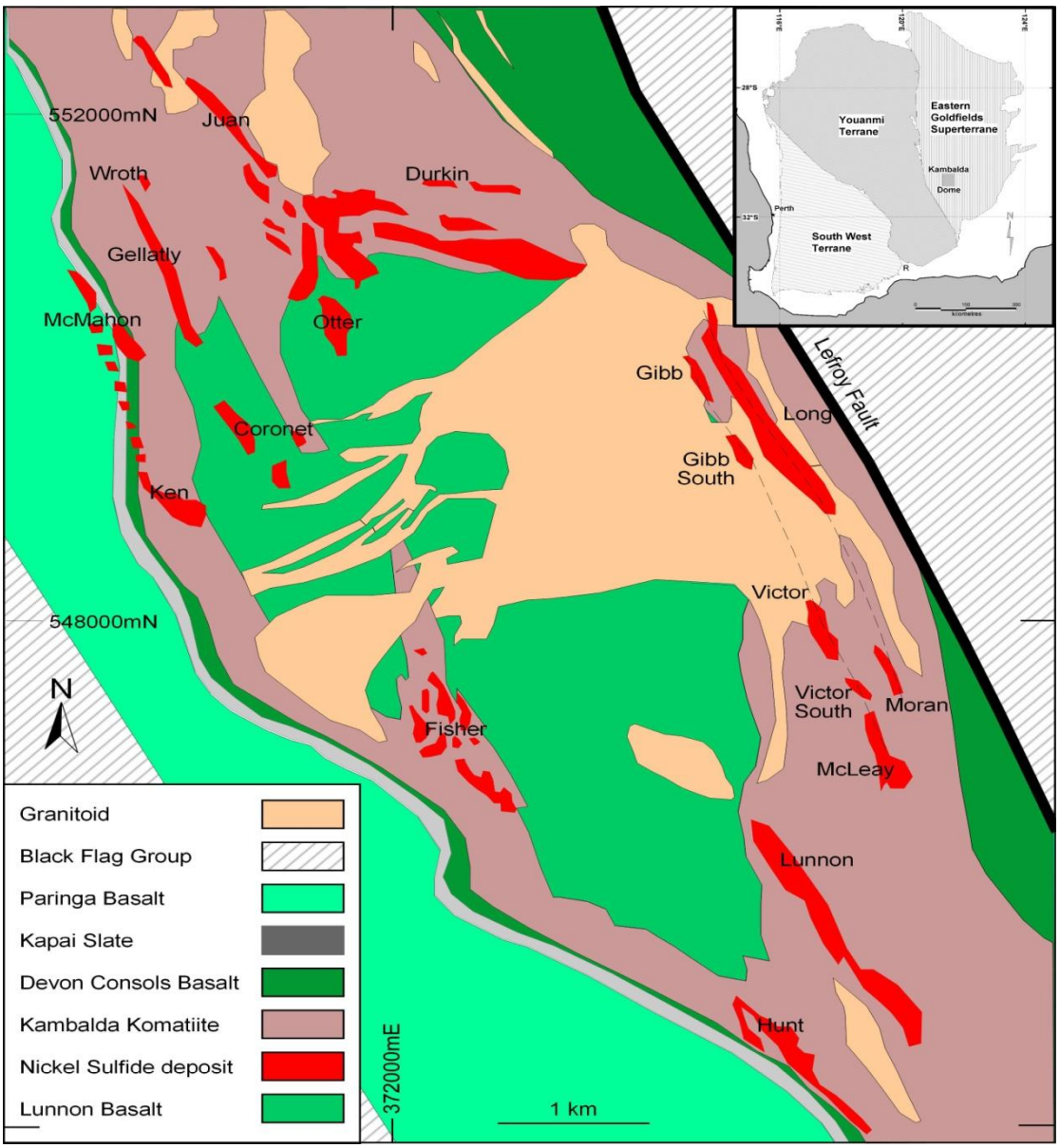

Figure 45. Geological map of the Kambalda Dome area with mineralised nickel sulphide ore shoots projected to surface. Major ore shoots are labelled. Map projection UTM zone 16 with WGS84 datum.

Regional metamorphism in the Kalgoorlie Terrane (e.g. Kambalda Dome) is dominantly upper greenschist facies, but exhibits variation from prehnite–pumpellyite to lower amphibolite facies. Metamorphism occurred at low to intermediate pressure (2.5 ± 1 kb to >4.5 kb) and temperatures of 500–600°C, with peak metamorphism occurring during late D2 to D3 (Binns et al., 1976; Bavinton, 1979; McQueen, 1981; Bickel and Archibald, 1984; Wong, 1986). Low-grade metamorphism is associated with the central cores of the greenstone belts, whereas higher grades are observed along the periphery (Brown et al., 2001).

Texturally, many primary igneous features are still visible within the lithological units around the Kambalda Dome, yet complete replacement by alteration assemblages has occurred locally. The limited development of penetrative deformation fabrics also aids in the preservation of primary

igneous textures. Progressive mineralogical changes through hydrothermal alteration were observed in the ultramafic lithologies (Gresham and Loftus-Hills, 1981; Cowden and Roberts, 1990). Glass and pyroxene were progressively hydrated to form tremolite and chlorite, whereas olivine is altered to serpentine. Antigorite was identified as the dominant serpentine mineral and either formed via direct serpentinisation of olivine at peak metamorphic conditions, or is a result of prograde metamorphism of a lizardite assemblage. Progressive carbonation of the serpentinites resulted in destruction of tremolite and antigorite and the formation of talc–dolomite and talc–magnesite assemblages. The only relict igneous minerals are chromite and rare portions of cumulate olivine within the Durkin and Victor shoots of the Kambalda Dome (Gresham and Loftus-Hills, 1981; Lesher, 1983).

Alteration effects on sulphide mineralisation are variable and highly dependent upon the metals involved, abundance of sulphide, and alteration conditions. Work on the Mt Keith disseminated ore body shows the progressive upgrading and Ni-enrichment of the sulphides with alteration (Donaldson, 1981; Grguric et al., 2006). However, recent work by Barnes et al. (2010) indicates that high tenor nickel sulphide assemblages may be primary and not require secondary enrichment. Furthermore, progressive alteration at the Black Swan deposit and selected ore shoots in the Kambalda Dome has shown limited effects on the composition of mineralisation (Lesher and Campbell, 1993; Barnes, 2004; Barnes et al., 2009).

Komatiite lithologies are especially susceptible to element redistribution due to the reactive nature of high-MgO rocks during low-grade metamorphism. Overall, most komatiite systems exhibit high loss on ignition values (during XRF whole rock analysis) attributed to the addition of volatiles to the system. More advanced alteration and metamorphism has variable effects on the geochemistry and mobility of elements within these systems (Arndt and Jenner, 1986; Lahaye et al., 1995; Lesher and Arndt, 1995; Kerrich and Wyman, 1996; Lesher and Stone, 1996). Large ion lithophile elements (LILE; Cs, Rb, K, Na, Ba, Sr, Ca, Eu^{+2}), with large ionic radii and low charge, have high susceptibility for mobilisation during alteration events (Xie et al., 1993; Lesher and Arndt, 1995; Lahaye et al., 1995). The mobility of LILE varies from local remobilization, complete removal or enrichment within the system during seafloor alteration, hydrothermal alteration, and regional metamorphism.

Rare earth element and high field strength element mobility is dependent upon fluid composition, with CO_2-rich fluids having a stronger influence on element mobility than H_2O-rich fluids (Lahaye et al., 1995). Light rare earth elements (LREE: La, Ce, P, Nd) are relatively immobile, yet may become mobile in CO_2-rich fluids. Limited mobility is observed at low fluid/rock ratios for the high field strength elements (U^{+4}, Th, Ta, Nb, Zr, Y, and HREE), aluminium, the first period transition elements (Sc, Ti, V, Cr; Mn, Co, Ni) and the highly siderophile elements (Fe and PGE).

Sulphur mobility within nickel sulphide systems of the Kambalda Dome was proposed by Marston and Kay (1980), Seccombe et al. (1981) and McQueen (1987). However, work by Keays et al. (1981) on ore tenors and chalcophile elements in the silicate host rocks did not show a strong

relationship between sulphur and the metal abundance in samples containing <0.2 wt% sulphur. The lack of correlation between the two was attributed to metamorphic and metasomatic redistribution of only S (± Au and Cu). Work by Seccombe et al. (1981) and Stone et al. (2004) identified sulphur loss through oxidation from prograde metamorphism, with disseminated sulphides being more susceptible to sulphur loss than net-textured and massive sulphides. Lesher and Campbell (1993) identified post crystallisation mobilisation of sulphur with no systematic correlation between degree of sulphur mobility and change in chalcophile element abundance.

Alteration effects on PGE abundances in whole-rock samples are perhaps the most difficult to identify, leading to the inference of limited PGE mobility during alteration. However, PGE-enriched hydrothermal ore deposits have been identified (Hanley, 2006; Wilde, 2005), and PGE mobility and fractionation during weathering is documented (Cameron and Hattori, 2005; Traoré et al., 2008) in aqueous solutions at very high salinities and oxidation states (Wood and Norman, 2008), thus supporting PGE mobility in sulphur poor rocks under certain conditions. However, PGE immobility is documented at the Black Swan deposit, which is characterised by pervasive talc–carbonate alteration (Barnes et al., 2004).

Geodynamic setting of the Kambalda Nickel Camp

The Kambalda Nickel Camp represents one of the largest komatiite-associated nickel sulphide systems in the world (Barnes, 2006). Refining our understanding of the ore forming process at the deposit scale may provide useful information in order to constrain the geometry and localisation of specific ore zones, but it does not provide insights into why the Kambalda Nickel Camp is where it is. Conversely, it is crucial to constrain the geodynamic environment that permitted the formation of such an endowed domain and the clustering of so many mineralised systems in a restricted area.

According to the mineral systems approach defined by McCuaig et al. (2010), in order to fully comprehend the salient features that control the clustering of mineralised systems it is necessary to investigate a wide range of data sets at multiple scales. Accordingly, it is necessary to also identify the lithospheric controls on the localisation of the Kambalda Nickel Camp. Figure 46a illustrates the Nd model age map of the Yilgarn Craton of Western Australia (Champion and Cassidy, 2007), whereas Figure 46b is a simplified geological map, which outlines the setting of the largest nickel sulphide systems. Figures 47a and b show a close up of the Kambalda domain of the Kalgoorlie Terrane.

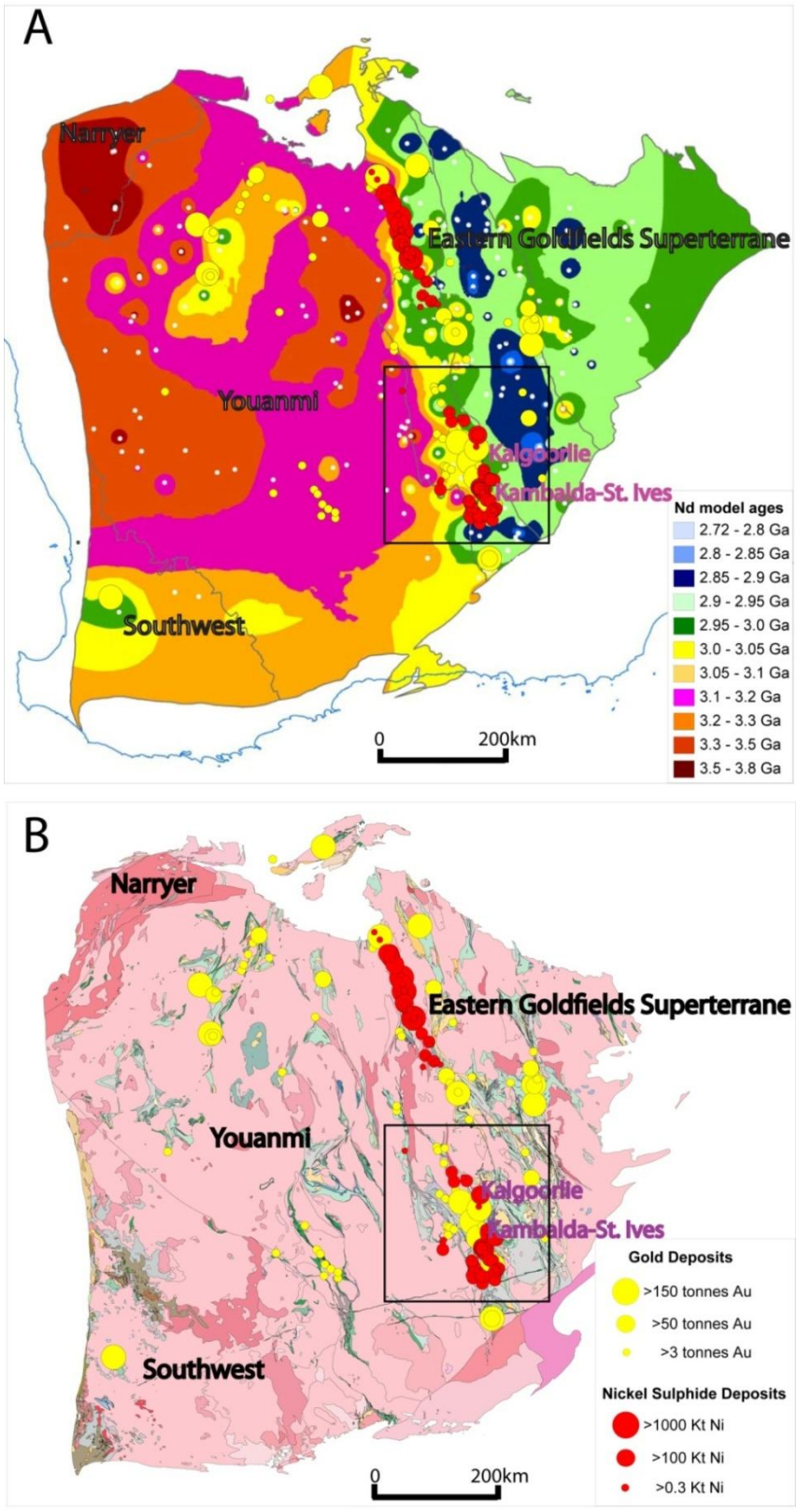

Figure 46 a) Nd model age map of the Yilgarn Craton (Champion and Cassidy, 2007); b) geological map of the Yilgarn Craton (GSWA 2008 1:500 000), showing the localisation of nickel sulphide deposits in the Eastern Goldfields Superterrane. Inset area outlined by square is shown in Figure 47. From McCuaig et al. (2010). See Chapter 1, Figure 19 for data sources.

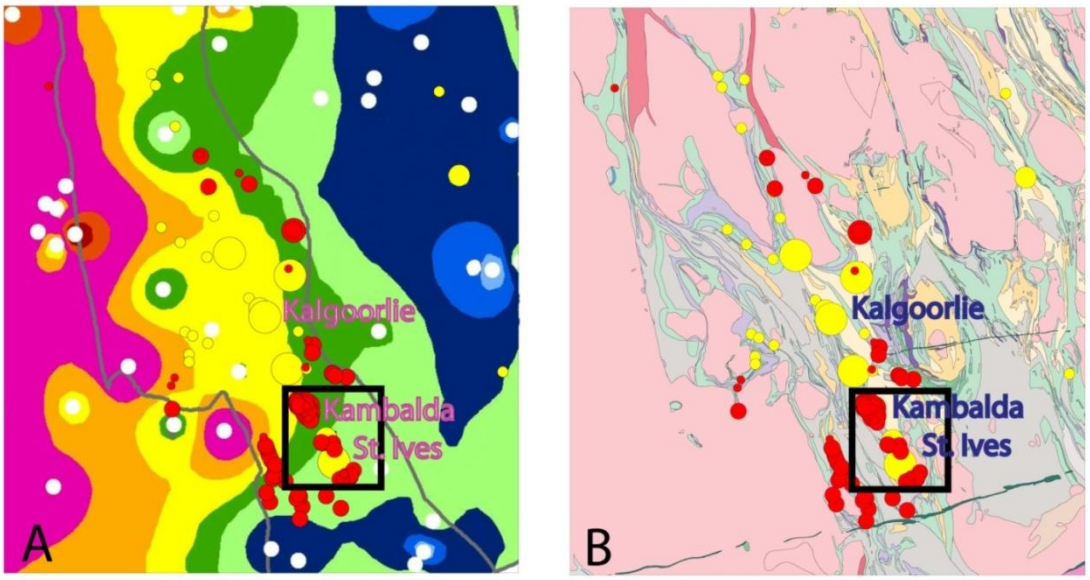

Figure 47. Inset from Figure 46: a) Nd model age map of the Kambalda domain in the Kalgoorlie Terrane (Champion and Cassidy, 2007); b) geological map of the Kambalda domain in the Kalgoorlie Terrane (GSWA 2008, 1:500 000), showing the localisation of nickel sulphide and gold deposits. The black box highlights the Kambalda Nickel Camp locations. From McCuaig et al. (2010).

The isotopic map is interpreted as providing a snapshot of the lithosphere architecture at c. 2.65 Ga. This map can be utilised as a proxy to image the major lithospheric discontinuities, which may have acted as active pathways for large volumes of hot mantle-derived melt to reach upper crustal levels without undergoing any significant differentiation. In other words, steep colour gradients (interpreted as lithosphere scale boundaries) in the isotopic map in Figure 46a show areas of where hot magmas were most likely emplaced.

All along the Kalgoorlie Terrane, from Wiluna in the north to south of the Kambalda Dome, highly mineralised komatiites (e.g. Mount Keith, Perseverance, Black Swan, Kambalda) are localised along the boundary between the isotopically juvenile Eastern Goldfields Superterrane and the older Youanmi Terrane. Arguably, this boundary may represent a significant lithospheric discontinuity at c. 2.7 Ga, along which high volumes of hot komatiites could be emplaced and interact with crustally derived sulphur (cf. Bekker et al., 2009) to generate giant nickel sulphide ore systems. Figure 47 shows how the spatial relationship between nickel sulphide mineralisation and the lithospheric boundary, as reflected by the different isotopic nature of the Youanmi and Eastern Goldfields Superterrane, holds down to the camp scale (Mole et al., 2009; Champion and Cassidy, 2007). On Figure 47 it is noted that the greenstone belts strike NNW, yet the camps of nickel sulphide mineralisation appear to follow the arc of the paleocraton margin imaged by the Nd model age map.

References

Arndt, NT and Jenner, GA 1986, Crustally contaminated komatiites and basalts from Kambalda, Western Australia: Chemical Geology, v. 56, p. 229–255

Arndt, NT, Lesher, CM and Barnes, SJ 2008, Komatiite: Cambridge University Press, Cambridge, UK, 467p.

Barley ME and Groves, DI 1987, Hydrothermal alteration of Archaean supracrustal sequences in the central Norseman–Wiluna belt, Western Australia, *in* Recent advances in understanding Precambrian Gold deposits *edited by* SE Ho and DI Groves: University of Western Australia, Geology Department and University Extension, Publication 11, p. 51–66.

Barnes, SJ, Fiorentini, ML, Godel, BM, Locmelis, M and Ryan, CG 2010, Origin of nickel-rich sulphide assemblages in the Betheno deposit, Yakabindie, WA: evidence from synchrotron X-ray fluorescence mapping *in* Earth Systems: change, sustainability, vulnerability: Geological Society of Australia, 20th Australian Earth Science Convention, Abstracts; Canberra, Australian Capital Territory, 4–8 July 2010, p.113–114

Barnes, SJ 2004, Komatiites and nickel sulfide ores of the Black Swan area, Yilgarn Block, Western Australia. 4: Platinum group element distribution in the ores, and genetic implications: Mineralium Deposita, v. 39, p. 752–765.

Barnes, SJ 2006, Komatiite-hosted nickel sulfide deposits: geology, geochemistry, and genesis, *in* Nickel Deposits of the Yilgarn Craton: Geology, Geochemistry, and Geophysics applied to Exploration *edited by* SJ Barnes: Society of Economic Geologists, Special Publication No. 13, p. 50–97.

Barnes, SJ, Gole, MJ and Hill, RET 1988, The Agnew nickel deposit, Western Australia: Part II: sulfide geochemistry, with emphasis on the platinum group elements: Economic Geology, v. 83, p. 537–550.

Barnes, SJ, Hill, RET and Evans, NJ 2004a, Komatiites and nickel sulfide ores of the Black Swan area, Yilgarn Craton, Western Australia. 3: komatiite geochemistry, and implications for ore forming processes: Mineralium Deposita, v. 39, p. 729–751.

Barnes, SJ, Hill, RET, Perring, CS and Dowling, SE 2004b, Lithogeochemical exploration for komatiite-associated Ni-sulfide deposits: strategies and limitations: Mineralogy and Petrology, v. 82, p. 259–293.

Barnes, SJ, Lesher, CM and Sproule, RA 2007, Geochemistry of komatiites in the Eastern Goldfields Superterrane, Western Australia and the Abitibi Greenstone Belt, Canada, and implications for the distribution of associated Ni–Cu–PGE deposits: Applied Earth Science, v. 116, p. 167–187.

Barnes, SJ, Wells, MA and Verrall, MR 2009, Effects of magmatic processes, serpentinization, and talc–carbonate alteration on sulfide mineralogy and ore textures in the Black Swan disseminated nickel sulfide deposit, Yilgarn Craton: Economic Geology, v. 104, p. 539–562.

Barrett, FM, Binns, RA, Groves, DI, Marston, RJ and McQueen, KG 1977, Structural history and metamorphic modification of Archean volcanic-type nickel deposits, Yilgarn Block, Western Australia: Economic Geology, v. 72, p. 1195–1223.

Batemann, R, Costa, S, Swe, T and Lambert, D 2001, Archaean mafic magmatism in the Kalgoorlie area of the Yilgarn Craton, Western Australia: a geochemical and Nd isotopic study of the petrogenetic and tectonic evolution of a greenstone belt: Precambrian Research. v. 108, p. 75–112.

Bavinton, OA 1979, Interflow sedimentary rocks from the Kambalda ultramafic sequence: Australia National University, Canberra, Australian Capital Territory, PhD thesis (unpublished).

Bavinton, OA 1981, The nature of sulfidic metasediments at Kambalda and their broad relationships with associated ultramafic rocks and nickel ore: Economic Geology, v. 78, p. 1606–1628.

Bavinton, OA and Keays, RR 1978, Precious metal values from interflow sedimentary rocks from the komatiite sequences at Kambalda, Western Australia: Geochimica et Cosmochimica Acta, v. 42, p. 1151–1163.

Bavinton, OA and Taylor, SR 1980, Rare earth element geochemistry of Archean metasedimentary rocks from Kambalda, Western Australia: Geochimica et Cosmochimica Acta, v. 44, p. 639–648.

Bekker, A, Barley, ME, Fiorentini, ML, Rouxel, OJ, Rumble, D and Beresford, SW 2009, Atmospheric sulfur in Archean komatiite-hosted nickel deposits: Science, v. 326, p. 1086–1089.

Beresford, S, Cas, R, Lahaye, Y and Jane, M 2002, Facies architecture of an Archean komatiite-hosted Ni-sulfide ore deposit, Victor, Kambalda, Western Australia: implications for komatiite lava emplacement: Journal of Volcanology and Geothermal Research, v. 118, p. 57–75.

Beresford, S, Stone, WE, Cas, R, Lahaye, Y and Jane, M 2005, Volcanological controls on the localization of the komatiite-hosted Ni–Cu–(PGE) Coronet Deposit, Kambalda, Western Australia: Economic Geology, v. 100, p. 1457–1467.

Bickel, MJ and Archibald, NJ 1984, Chloritoid and staurolite stability — implications for metamorphism in the Archaean Yilgarn Block in Western Australia: Journal of Metamorphic Petrology, v. 2, p. 179–203.

Binns, RA, Gunthorpe, RJ and Groves, DI 1976, Metamorphic patterns and development of greenstone belts in the eastern Yilgarn Block, *in* The Early History of the Earth *edited by* BF Windley: John Wiley and Sons, London, UK, p. 303–316.

Brown, SJA, Krapež, B, Beresford, SW, Cassidy, KF, Champion, DC, Barley, ME and Cas, RAF 2001, Archean volcanic and sedientary environments of the Eastern Goldfields Province Western Australia – a field guide: Geological Survey of Western Australia, Record 2001/13, 66p.

Campbell, IH and Hill, RI 1988, A two-stage model for the formation of the granite–greenstone terrains of the Kalgoorlie-Norseman area, Western Australia: Earth and Planetary Science Letters, v. 90, p. 11–25.

Campbell, IH, Griffiths, RW and Hill, RI 1989, Melting in an Archean mantle plume: heads it's basalts, tails it's komatiites: Nature, v. 339, p. 697–699.

Cameron, EM and Hattori, KH 2005, Platinum group elements in geochemical exploration, *in* Exploration for Platinum Group Element Deposits *edited by* JE Mungall: Mineralogical Association of Canada, Short Course, Volume 35, p. 287–303.

Cassidy, KF, Champion, DC, Krapež, B, Barley, ME, Brown, SJA, Blewett, RS, Groenewald, PB and Tyler, IM 2006, A revised geological framework for the Yilgarn Craton, Western Australia: Geological Survey of Western Australia, Record 2006/8, 8p.

Champion, DC and Sheraton, JW 1993, Geochemistry of granitoids in the Leonora–Laverton region, Eastern Goldfields Province, *in* Kalgoorlie '93. An International Conference on Crustal Evolution, Metallogeny and Exploration of the Eastern Goldfields, Extended Abstracts *edited by*PR Williams: Geoscience Australia, Record 1993/54, p. 39–54.

Champion, DC and Sheraton, JW 1997, Geochemistry and Nd isotope systematics of Archaean granites in the Eastern Goldfields, Yilgarn Craton, Australia: implications for crustal growth models: Precambrian Research, v. 83, p. 109–132.

Champion, DC and Smithies, RH 2004, Archean Granites, *in* The Ishihara Symposium: Granites and Associated Metallogenesis *edited by* P Blevin, M Jones, and B Chappell: Geoscience Australia, record 2003/14, p. 13–19.

Champion, DC, Cassidy, KF and Smithies, RH 2006, Sm–Nd isotope characteristics of the Pilbara and Yilgarn Cratons, Western Australia: Implications for crustal growth in the Archean *in* Geochemistry downunder: 16th Goldschmidt Conference, Melbourne, Victoria, 27 August – 1 September 2006, Abstracts; Geochimica et Cosmochimica Acta, v. 70, Suppl. 1, p. A95.

Champion, DC and Cassidy, KF 2007, An overview of the Yilgarn Craton and its crustal evolution *in* Proceedings of Geoconferences (WA) Inc. Kalgoorlie '07 Conference, Kalgoorlie, Western Australia *edited by* FP Bierlein and CM Knox-Robinson: Geoscience Australia Record, 2007/14, p. 8–12.

Chauvel, C, Dupré, B and Jenner, GA 1985, The Sm–Nd age of Kambalda volcanics is 500 Ma too old!: Earth and Planetary Science Letters, v. 74, p. 315–324.

Claoué-Long, JC, Thirlwall, MF and Nesbitt, RW 1984, Revised Sm–Nd systematics of Kambalda greenstones, Western Australia: Nature, v. 307, p. 697–701.

Claoué-Long, JC, Compston, W and Cowden, A 1988, The age of the Kambalda greenstones resolved by ion-microprobe: implications for Archean dating methods: Earth and Planetary Science Letters, v. 89, p. 239–259.

Compston, W, Williams, IS, Campbell, IH and Gresham, JJ 1986, Zircon xenocrysts from the Kambalda volcanics: age constraints and direct evidence for older continental crust below the Kambalda–Norseman greenstones: Earth and Planetary Science Letters, v. 76, p. 299–311.

Cowden, AC 1988, Emplacement of komatiite lava flows and associated nickel sulfides at Kambalda, Western Australia: Economic Geology, v. 83, p. 436–442.

Cowden, A and Archibald, NJ 1987, Massive-sulfide fabrics at Kambalda and their relevance to inferred stability of monosulfide solid-solution: Canadian Mineralogist, v. 25, p. 37–50.

Cowden, A and Roberts, DE 1990, Komatiite hosted nickel sulphide deposits, Kambalda, *in* Geology of Mineral Deposits of Australia and Papua New Guinea *edited by* FE Hughes: Australasian Institute of Mining and Metallurgy, Melbourne, Victoria, p. 567–581.

Doepel, JJG 1973, Norseman, Western Australia: Geological Survey of Western Australia,1:250 000 Geological Series Explanatory Notes, 40p.

Donaldson, MJ 1981, Redistribution of ore elements during serpentinization and talc–carbonate alteration of some Archean dunites, Western Australia: Economic Geology, v. 76, p. 1698–1713.

Ewers, WE and Hudson, DR 1972, An interpretative study of nickel-iron sulfide ore intersections. Lunnon Shoot, Kambalda, Western Australia: Economic Geology, v. 67, p. 1075–1092.

Ferguson, J and Currie, KL 1972, Silicate immiscibility in the ancient 'basalts' of the Barberton Mountain Land, Transvaal: Nature Physical Science, v. 235, p. 86–89.

Fiorentini, ML, Barley, ME, Pickard, A, Beresford, SW, Rosengren, NM, Cas, RAF and Duuring, P 2005, Age constraints of the structural and stratigraphic architecture of the Agnew–Wiluna greenstone belt: implications for the age of komatiite–felsic association and interaction in the Eastern Goldfields Province, Western Australia: MERIWA, Report 255, Project M356.

Fiorentini, ML, Barnes, SJ, Lesher, CM, Heggie, G, Keays, RR and Burnham, OM in press, Platinum-group element geochemistry of mineralized and non-mineralized komatiites and basalts: Economic Geology.

Foster, JG, Lambert, DD, Frick, LR and Maas, R 1996, Re–Os isotopic evidence for genesis of Archaean nickel ores from uncontaminated komatiites: Nature, v. 382, p. 703.

Frost, KM 1985, Ocellar komatiites at Kambalda, Western Australia: evidence of silicate liquid immiscibility and sediment assimilation: The University of Western Australia, Perth, Western Australia, BSc (Hons) thesis, 121p. (unpublished).

Frost, KM 1992, The role of ground melting in the genesis of komatiite-associated nickel sulfide deposits at Kambalda and Widgiemooltha, Western Australia: The University of Western Australia, Perth, Western Australia, PhD thesis, 239p. (unpublished).

Frost, KM and Groves, DI 1989, Ocellar units in the Kamabalda–Widgiemooltha komatiite sequence: evidence for sediment assimilation by komatiite lavas, *in* Magmatic Sulphides — The Zimbabwe Volume *edited by* MD Prendergast and MJ Jones: Institution of Mining and Metallurgy, London, UK p. 207–214.

Gemuts, I and Theron, A 1975, The Archean between Coolgardie and Norseman — stratigraphy and mineralization, *in* Economic Geology of Australia and Papua New Guinea, v.1, Metals *edited by* CL Knight: The Australasian Institute of Mining and Metallurgy, Parkville, Victoria, Monograph 5, p. 66–74.

Gresham, JJ and Loftus-Hill, GD 1981, The Geology of the Kambalda Nickel Field, Western Australia: Economic Geology, v. 76, p. 1373–1416.

Grguric, BA, Rosengren, NM, Fletcher, CM and Hronsky, JMA 2006, Type 2 Deposits: Geology, mineralogy, and processing of the Mount Keith and Yakabindie orebodies, Western Australia, *in* Nickel Deposits of the Yilgarn Craton: Geology, Geochemistry, and Geophysics applied to exploration *edited by* SJ Barnes: Society of Economic Geologists, Special Publication No. 13, p. 119–138.

Groves, DI, Barrett, FM, Binns, RA and McQueen, KG 1977, Spinel phases associated with metamorphosed volcanic-type iron-nickel sulfide ores from Western Australia: Economic Geology, v. 72, p. 1224–1244.

Groves, DI, Korkiakoski, EA, McNaughton, NJ, Lesher, CM and Cowden, A 1986, Thermal erosion by komatiites at Kambalda, Western Australia and the genesis of nickel ores: Nature, v. 319, p. 136–139.

Hand, JL 1998, The sedimentological and stratigraphic evolution of the Archaean Black Flag Beds, Kalgoorlie, Western Australia: implications for regional stratigraphy and basin setting of the Kalgoorlie Terrane: Monash University, Melbourne, Victoria, PhD thesis (unpublished).

Hall, HIE and Bekker, C 1965, Gold deposits of Norseman, *in* Geology of Australian Ore Deposits *edited by* J McAndrew: Australasian Institute of Mining and Metallurgy; 8th Commonwealth Mining and Metallurgical Congress, Melbourne, Victoria, p.101–107.

Hanley, JJ 2006, The aqueous geochemistry of the platinum-group elements (PGE) in surficial, low-T hydrothermal and high T-magmatic-hydrothermal environments, *in* Exploration for Platinum Group

Element Deposits *edited by* JE Mungall: Mineralogical Association of Canada, Short Course Volume 35, p. 35–50.

Heggie, G 2010, The spatial variation of PGE in barren and mineralised komatiite systems: The University of Western Australia, Perth, Western australia, PhD thesis (unpublished).

Hill, RI, Campbell, IH and Compston, W 1989, Age and origin of granitic rocks in the Kalgoorlie–Norseman region of Western Australia: Implications for the origin of Archaean crust: Geochimica et Cosmochimica Acta, v. 53, p. 1259–1275.

Hill, RI, Chappell, BW and Campbell, IH 1992, Late Archaean granites of the southeastern Yilgarn Block, Western Australia: age, geochemistry, and origin: Transactions of the Royal Society of Edinburgh, Earth Sciences, v. 83, p. 211–226.

Hill, RET, Barnes, SJ, Gole, MJ and Dowling, SE 1995, The volcanology of komatiites as deduced from field relationships in the Norseman–Wiluna greenstone belt, Western Australia: Lithos, v. 34, p. 159–188.

Hunter, WM 1993, Geology of the granite–greenstone terrane of the Kalgoorlie and Yilmia 1:100 000 sheets, Western Australia: Geological Survey of Western Australia, Report 35, 91p.

Keays, RR 1982, Palladium and iridium in komatiites and associated rocks: application to petrogentic problems, *in* Komatiites *edited by* NT Arndt and EG Nisbet: Allen and Unwin, London, UK, p. 435–457.

Keays, RR, Ross, JR and Woolrich, P 1981, Precious metals in volcanic peridotite-associated nickel sulfide deposits in Western Australia. II: Distribution within the ores and host rocks at Kambalda: Economic Geology, v. 76, p. 1645–1674.

Kerrich, R and Wyman, DA 1996, The trace element systematics of igneous rocks in mineral exploration: an overview *in* Trace Element Geochemistry of Volcanic Rocks: Applications for Massive Sulphide Exploration *edited by* DA Wyman: Geological Association of Canada, Short Course Notes, v. 12, p. 1–50.

Kositcin, N, Brown, AJA, Barley, ME, Krapez, B, Cassidy, KF and Champion, DC 2008, SHRIMP U–Pb zircon age constraints on the Late Archaean tectonostratigraphic architecture of the Eastern Goldfields Superterrane, Yilgarn Craton, Western Australia: Precambrian Research, v. 161, p. 5–33.

Krapež, B 1997, Sequence-stratigraphic concepts applied to the identification of depositional basins and global tectonic cycles: Australian Journal of Earth Sciences, v. 44, p. 1–36.

Krapež, B and Hand, JL 2008, Late Archaean deep-marine volcaniclastic sedimentation in an arc-related basin: the Kalgoorlie Sequence of the Eastern Goldfields Superterrane, Yilgarn Craton, Western Australia: Precambrian Research, v. 161, p. 89–113.

Krapež, B, Brown, SJA, Hand, J, Barley, ME and Cas, RAF 2000, Age constraints on recycled crustal and supracrustal sources of Archean metasedimentary sequences, Eastern Goldfields Province, Western Australia: evidence from SHRIMP zircon dating: Tectonophysics, v. 322, p. 89–133.

Lahaye, Y, Arndt, NT, Byerly, G, Chauvel, C, Fourcade, S and Gruau, G 1995, The influence of alteration on the trace-element and Nd isotopic compositions of komatiites: Chemical Geology, v. 126, p. 43–64.

Lesher, CM 1983, Localization and genesis of komatiite-associated Fe–Ni–Cu sulphide mineralization at Kambalda, Western Australia: The University of Western Australia, Perth, Western Australia, PhD thesis, 199p. (unpublished).

Lesher, CM 1989, Komatiite associated nickel sulfide deposits *in* Ore deposits associated with magmas: Reviews in Economic Geology, v. 4, p. 45–101.

Lesher, CM and Arndt, NT 1995, REE and Nd isotopic geochemistry, petrogenesis and volcanic evolution of contaminated komatiites at Kambalda, Western Australia: Lithos, v. 34, p. 127–157.

Lesher, CM and Campbell, IH 1993, Geochemical and fluid dynamic modeling of compositional variations in Archean Komatiite-hosted nickel sulfide ores in Western Australia: Economic Geology, v. 88, p. 804–816.

Lesher, CM and Stone, WE 1996, Exploration geochemistry of komatiites, *in* Igneous Trace Element Geochemistry Applications for Massive Sulphide Exploration *edited by* DA Wyman: Geological Association of Canada, Short Course Notes, v. 12, p. 153–204.

Lesher, CM and Keays, RR 2002, Komatiite-associated Ni–Cu–PGE deposits: geology, mineralogy, geochemistry, and genesis *in* The Geology, Geochemistry, Mineralogy, and Mineral Beneficiation of Platinum-Group Elements *edited by* LJ Cabri: Canadian Institute of Mining, Metallurgy and Petroleum, Special Volume 54, p. 579–618.

Lesher, CM, Arndt, NT and Groves, DI 1984, Genesis of komatiite-associated nickel sulphide deposits at Kambalda, West-Australia: A distal volcanic model, *in* Sulphide deposits in mafic and ultramafic rocks *edited by* DL Buchan and ML Jones: Institution of Mining and Metallurgy;Proceedings of International Geological Correlation Program, Projects 161 and 91, Third Nickel Sulphide Field Conference, Perth, Western Australia, p. 70–80.

Lesher, CM, Burnham, OM, Keays, RR, Barnes, SJ and Hulbert, L 2001, Trace-element geochemistry and petrogenesis of barren and ore-associated komatiites: Canadian Mineralogist, v. 39, p. 673–696.

Maier, WD, Barnes, SJ, Campbell, IH, Fiorentini, ML, Peltonen, P, Barnes, S-J and Smithies, H 2009, Mantle magmas reveal progressive mixing of meteoric veneer into the early Earth's deep mantle: Nature, v. 460, p. 620–623.

Marshall, B and Gilligan, LB 1987, An introduction to remobilization: information from ore-body geometry and experimental considerations: Ore Geology Reviews, v. 2, p. 87–131.

Marshall, B and Gilligan, LB 1993, Remobilization, syn-tectonic processes and massive sulphide deposits: Ore Geology Reviews, v. 8, p. 39–64.

Marshall, B, Vokes, FM and Larocque, ACL 2000, Regional metamorphic remobilization: upgrading and formation of ore deposits, *in* Metamorphosed and Metamorphogenic Ore Deposits *edited by* PG Spry, B Marshall and FM Vokes: Reviews in Economic Geology, v. 16, p. 19–38.

Martin, H 1994, The Archaean grey gneisses and genesis of continental crust, *in* Crustal Evolution *edited by* KC Condie: Elsevier, Amsterdam, The Netherlands, p. 205–259.

Marston, RJ and Kay, BD 1980, The distribution, petrology, and genesis of nickel ores at the Juan Complex, Kambalda, Western Australia: Economic Geology, v. 75, p. 546–565.

Marston, RJ, Groves, DI, Hudson, DR and Ross, JR 1981, Nickel sulfide deposits in Western Australia: a review: Economic Geology, v. 76, p. 1330–1363.

Mason, R, Hodkiewicz, P, Barrett, D and Buerger, R 2003, Structural geology of the Emily Ann nickel deposit and implications for the mining process: Australasian Institute of Mining and Metallurgy; 5th International Mining Geology Conference, Bengido, Voctoria, 17–19 November 2003, p. 155–170.

McCuaig, TC, Beresford, SW and Hronsky, J 2010, Translating the mineral systems approach into an effective exploration targeting system: Ore Geology Reviews, v. 38, p. 121–127 <doi:10.1016/j.oregeorev.2010.05.008>

McNaughton, NJ, Frost, KM and Groves, DI 1988, Ground melting and ocellar komatiites: a lead isotopic study at Kambalda, Western Australia: Geological Magazine, v. 125, p. 285–295.

McQueen, KG 1981, Volcanic-associated nickel deposits from around the Widgiemooltha Dome, Western Australia: Economic Geology, v. 76, p. 1417–1443.

McQueen, KG 1987, Deformation and remobilization in some Western Australian nickel ores: Ore Geology Reviews, v. 2, p. 269–286.

Mole, D, Fiorentini, ML, Thébaud, N, McCuaig, TC and Cassidy, K 2009, Using LA-ICP-MS Lu–Hf SHRIMP dating to investigate tectonostratigraphic controls on the localisation of Archaean komatiite-hosted nickel-sulphide deposits and camps in the Yilgarn craton, Western Australia: The Mineralogical

Society; Micro-analysis, Processes, Time (MAPT) Conference, Edinburgh, UK, 31 August –2 September 2009, Programme and abstracts, p. 143–144

Myers, JS 1997, Geology of granite: Journal of the Royal Society of Western Australia, v. 80, p. 87–100.

Nelson, DR 1995, Compilation of SHRIMP U–Pb zircon geochronology data, 1995: Geological Survey of Western Australia, Record 1996/5, 251p.

Nelson, DR 1997, Evolution of the Archaean granite–greenstone terranes of the Eastern Goldfields, Western Australia: SHRIMP zircon constraints: Precambrian Research, v. 83, p. 57–81.

Nelson, DR 1998, Compilation of SHRIMP U–Pb zircon geochronology data, 1997: Geological Survey of Western Australia, Record 1998/2, 196p.

Oversby, VM 1975, Lead isotope systematics and ages of Archean acid intrusives in the Kalgoorlie-Norseman area, Western Australia: Geochimica et Cosmochimica Acta, v. 39, p. 1107–1125.

Plimer, IR 1987, Remobilization in high-grade metamorphic environments: Ore Geology Reviews, v. 2, p. 231–245.

Redman, BA and Keays, RR 1985, Archean basic volcanism in the Eastern Goldfields Province, Yilgarn Block, Western Australia: Precambrian Research, v. 30, p. 113–152.

Ross, JRH 1974, Archaean nickel sulphide mineralization: Lunnon Shoot, Kambalda, Western Australia: University of California, Berkeley, PhD thesis, 283p. (unpublished).

Ross, JR and Hopkins, GMF 1979, Kambalda nickel sulfide deposits, *in* Economic Geology of Australia and Papua New Guinea I. Metals *edited by* CL Kight: Australasian Institute Mining and Metallurgy, Parkville, Victoria, p. 100–121.

Said, N and Kerrich, R 2009, Geochemistry of coexisting depleted and enriched Paringa Basalts, in the 2.7 Ga Kalgoorlie Terrane, Yilgarn Craton, Western Australia: Evidence for a heterogeneous mantle plume event: Precambrian Research, v. 174, p. 289–309.

Seat, Z, Stone, WE, Mapleson, DB and Daddow, BC 2004, Tenor variation within komatiite-associated nickel sulphide deposits: insights from the Wannaway Deposit, Widgiemooltha Dome, Western Australia: Mineralogy and Petrology, v. 82, p. 317–339.

Seccombe, PK, Groves, DI, Marston, RJ and Barrett, FM 1981, Sulfide paragenesis and sulfur mobility in Fe–Ni–Cu sulfide ores at Lunnon and Juan Main Shoots, Kambalda: textural and sulfur isotopic evidence: Economic Geology, v. 76, p. 1675–1685.

Squire, RJ, Cas, RAF, Clout, JMF and Behets, R 1998, Volcanology of the Archaean Lunnon Basalt and its relevance to nickel sulfide-bearing trough structures at Kambalda, Western Australia: Australian Journal of Earth Sciences, v. 45, p. 695–715.

Stone, WE and Archibald, NJ 2004, Structural controls on nickel sulfide ore shoots in Archean komatiite, Kambalda, WA: the volcanic trough controversy revisited: Journal of Structural Geology, v. 26, p. 1173–1194.

Stone, WE and Masterman, EE 1998, Kambalda nickel deposits, *in* Geology of Australian and Papua New Guinea Mineral Deposits *edited by* DA Berkman and DH Mackenzie: Australasian Institute of Mining and Metallurgy, Melbourne, Victoria, p. 347–356.

Stone, WE, Crocket, JH, Fleet, ME and Larson, MS 1996, PGE mineralization in Archean volcanic systems: geochemical evidence from thick, differentiated mafic–ultramafic flows, Abitibi greenstone belt, Ontario, and implications for exploration: Journal of Geochemical Exploration, v. 56, p. 237–263.

Stone, WE, Heydari, M and Seat, Z 2004, Nickel tenor variations between Archaean komatiite-associated nickel sulphide deposits, Kambalda ore field, Western Australia: the metamorphic modification model revisited: Mineralogy and Petrology, v. 82, p. 295–316.

Stone, WE, Beresford, SW and Archibald, NJ 2005, Structural setting and shape analysis of nickel sulfide shoots at the Kambalda Dome, Western Australia: implications for deformation and remobilization: Economic Geology v. 100, p. 1441–1455.

Swager, C 1989, Structure of Kalgoorlie Greenstones — Regional deformation history and implications for the structural setting of the Golden Mile gold deposits: Geological Survey of Western Australia, Report 25, p. 59–84.

Swager, CP and Griffin, TJ 1990, An early thrust duplex in the Kalgoorlie–Kambalda greenstone belt, Eastern Goldfields Province, Western Australia: Precambrian Research, v. 48, p. 63–73.

Swager, CP, Goleby, BR, Drummond, BJ, Rattenbury, MS and Williams, PR 1997, Crustal structure of granite–greenstone terranes in the Eastern Goldfields, Yilgarn Craton, as revealed by seismic reflection profiling: Precambrian Research, v. 83, p. 43–56.

Swager, CP, Witt, WK, Griffin, TJ, Ahmat, AL, Hunter, WM, McGoldrick, PJ and Wyche, S 1992, Late Archaean granite–greenstones of the Kalgoorlie Terrane, Yilgarn Craton, Western Australia, *in* JE Glover and SE Ho: Geology Deptartment (Key Centre) and University Extension, The University of Western Australia, Perth, Western Australia, p. 107–122.

Sylvester, PJ, Campbell, IH and Bowyer, DA 1997, Niobium/uranium evidence for early formation of the continental crust: Science, v. 275, p. 521–523.

Traore, D, Beauvais, A, Chabaux, F, Peiffert, C, Parisot, J-C, Ambrosi, J-P and Colin, F 2008, Chemical and physical transfers in an ultramafic rock weathering profile: Part 1. Supergene dissolution of Pt-bearing chromite: American Mineralogist, v. 93, p. 22–30.

Travis, GA, Woodhall, R and Bartram, GD 1971, The geology of the Kalgoorlie gold field: Geological Society of Australia, Special Publications, v. 3, p. 175–190.

Trofimovs, J, Davis, BK and Cas, RAF 2004, Contemporaneous ultramafic and felsic intrusive and extrusive magmatism in the Archaean Boorara Domain, Eastern Goldfields Superterrane, Western Australia, and its implications: Precambrian Research, v. 131, p. 283–304.

Weinberg, RF, Moresi, L and van der Borgh, P 2003, Timing of deformation in the Norseman–Wiluna Belt, Yilgarn Craton, Western Australia: Precambrian Research, v. 120, p. 219–239.

Wilde, A 2005, Descriptive ore deposit models: hydrothermal and supergene Pt and Pd deposits, *in* Exploration for platinum group element deposits *edited by* JE Mungall: Mineralogical Association of Canada Short Course 35, p. 145–162.

Williams, PR and Whitaker, AJ 1993, Gneiss domes and extensional deformation in the highly mineralised Archaean Eastern Goldfields Province, Western Australia: Ore Geology Reviews, v. 8, p. 141–162.

Williams, DA, Kerr, RC and Lesher, CM 1998, Emplacement and erosion by Archean komatiite lava flows at Kambalda: revisited: Journal of Geophysical Research, v. 103, p. 27533–27549.

Witt, WK 1994, Geology of the Melita 1:100 000 sheet: Geological Survey of Western Australia, Geological Series Explanatory Notes, 63 p.

Witt, WK and Davy, R 1997, Geology and geochemistry of Archaean granites in the Kalgoorlie region of the Eastern Goldfields, Western Australia: a syn-collisional tectonic setting?: Precambrian Research, v. 83, p. 133–183.

Witt, WK and Swager, CP 1989, Structural setting and geochemistry of Archaean I-type granites in the Bardoc-Coolgardie area of the Norseman–Wiluna Belt, Western Australia: Precambrian Research, v. 44, p. 323–351.

Wong, T 1986, Metamorphic patterns in the Kambalda area and their significance to Archaean greenstone belts of the Kambalda-Widgiemooltha area: The University of Western Australia, Perth, Western Australia, BSc (Hons) thesis (unpublished).

Wood, SA and Norman, C 2008, Mobility of palladium chloride complexes in mafic rocks: insight from a flow-through experiment at 25C using air-saturated, acidic and Cl-rich solutions: Mineralogy and Petrology, v. 92, p. 81–97.

Woodall, R 1965, Structure of the Kalgoorlie goldfield: 8th Commonwealth Mining and Metallurgy Congress, Melbourne, v. 1, p. 71–79.

Woodall, R and Travis, GA 1970, The Kambalda nickel deposits, Western Australia: 9th Commonwealth Mining Metallurgy Congress, London, 1969, Proceedings, v. 2, p. 517–533.

Xie, Q, Kerrich, R and Fan, J 1993, HFSE/REE fractionations recorded in three komatiite–basalt sequences, Archean Abitibi greenstone belt: implications for multiple plume sources and depths: Geochimica et Cosmochimica Acta, v. 57, p. 4111–4118.

Chapter 5 — The St Ives Goldfield

JM Miller

Centre for Exploration Targeting, School of Earth and Environment, The University of Western Australia

Introduction

The world class St Ives Goldfield occurs to the west of the regional Boulder–Lefroy Fault, within the Kalgoorlie Terrane of the Eastern Goldfields Superterrane (Figs 48, 49, 50, 51; Cassidy et al., 2006; Kositcin et al., 2008). Dilational and contractional jogs are a key control on the development of major gold systems along the Boulder–Lefroy Fault (e.g. Weinberg et al., 2004). At the world class 12 million ounce St Ives Goldfield, the largest gold deposits are located on major contractional jogs (e.g. Revenge and Repulse Faults; Nguyen et al., 1998; Cox and Ruming, 2004). Other world class deposits, such as the 70 million ounce Golden Mile at Kalgoorlie, are interpreted to lie on dilational jogs (Weinberg et al., 2004).

Extensive industry and academic research has focused on the control these structural jogs have on the formation of gold deposits along the Boulder–Lefroy Fault and associated second order structures. Recent research has focused on *why* these features developed, and why many also correlate with the location of key dolerite units with an inferred link to older syn volcanic architecture (Miller et al., 2010). Regionally, the link between early extensional architecture in the Yilgarn Craton, and the current map patterns, has been highlighted by several studies (e.g. Hammond and Nisbet, 1992; Williams and Whitaker, 1993; Williams and Currie, 1993; McIntyre and Martyn, 2005; Blewett et al., 2010a,b; Davis et al., 2010).

The field visit will look at a complex region with multiple lode orientations within the southern region of the Greater Revenge Area. This locality hosts a series of early WNW-trending structures that are inferred to have controlled the emplacement of the ultramafic and mafic stratigraphy and were also active during later main-stage gold mineralisation. The following descriptions are modified from Miller et al. (2010).

Geological setting

The St Ives Goldfield at Kambalda lies within the Norseman–Wiluna greenstone belt. This belt is dominated by c. 2.7 Ga volcanosedimentary assemblages consisting of predominantly mafic and ultramafic lavas and intrusive rocks, which have been metamorphosed to grades ranging from upper greenschist facies to lower amphibolite facies (Archibald et al., 1978; Wong, 1986; Clark et al., 1989; Barley and Groves, 1990; Stone et al., 2005).

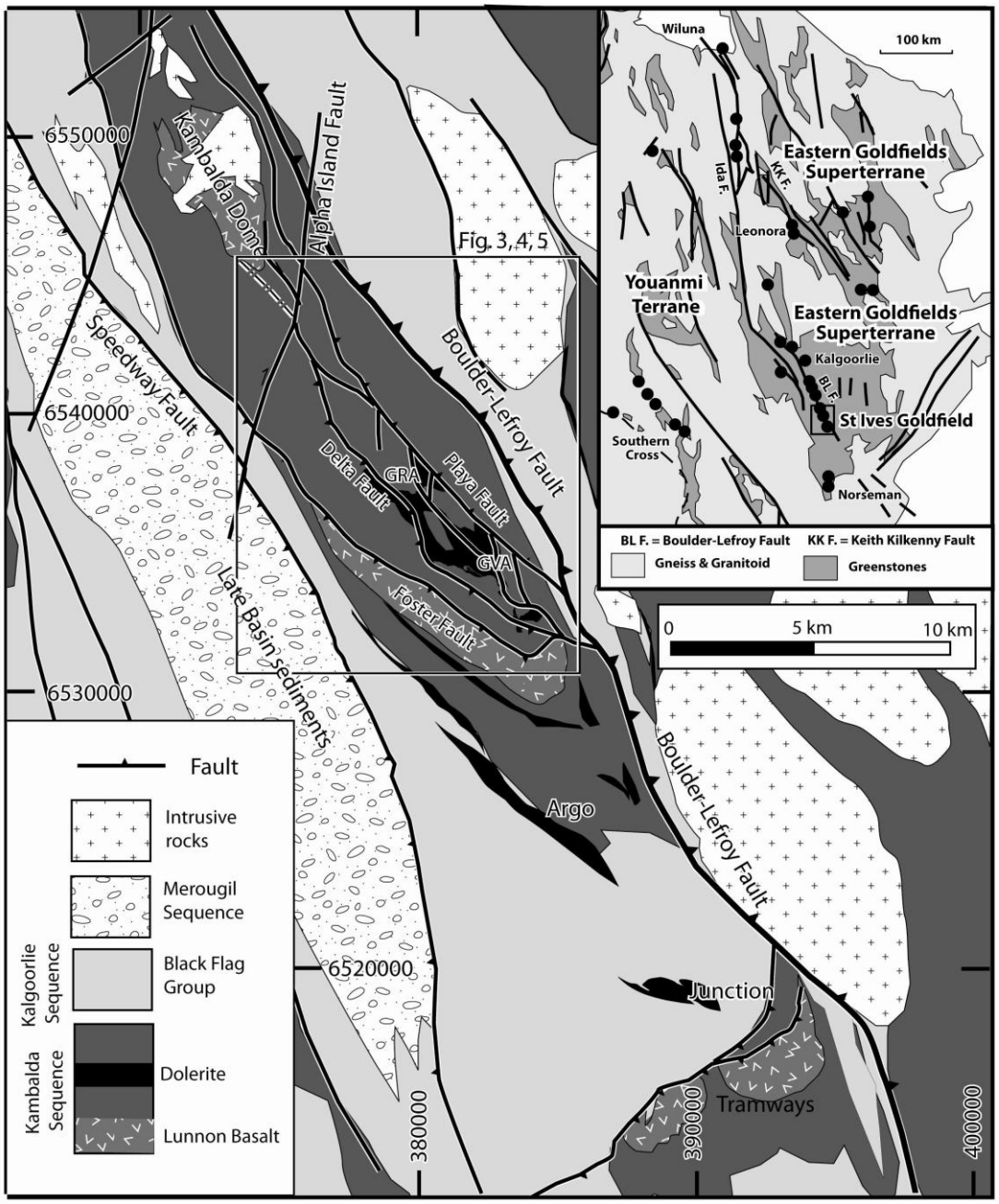

Figure 48. Regional geology map of the St Ives Goldfield. Inset figure at top right highlights the location of the St Ives Goldfield.

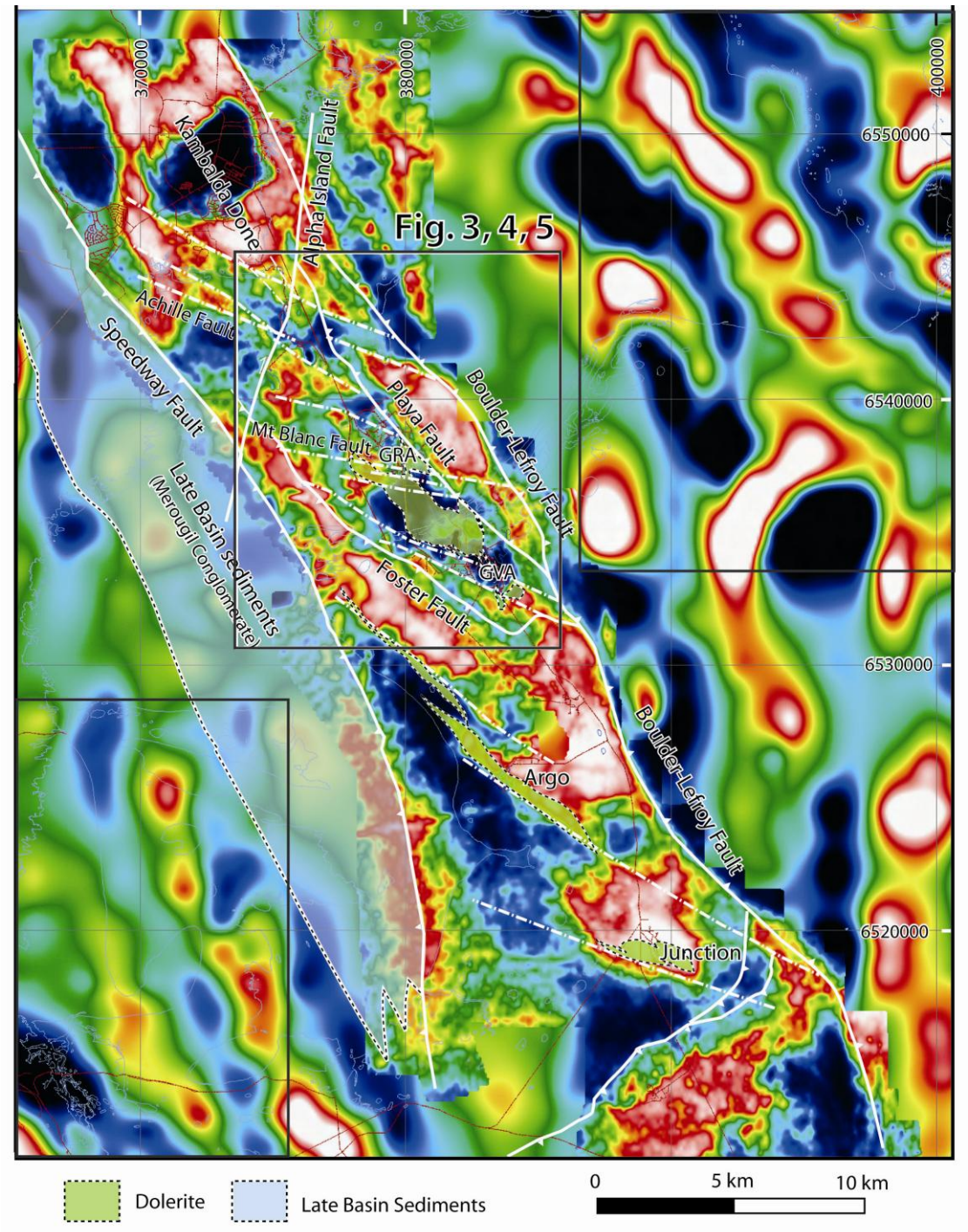

Figure 49. High-pass filtered gravity map of the St Ives Goldfield. Key gravity trends are annotated with dashed lines and major regional faults highlighted with solid white lines. This image depicts the same region as Figure 48. For reference the black rectangles at top right and bottom left of figure represent locations of key and inset in Fig. 48. The location of dolerite units and Late Basin sediments are shown; see text for explanation. Warm colours represent dense rocks such as the komatiite and basalts of the Kambalda Group. Cool colours represent less dense rocks such as the sediments, felsic volcanic rocks and granite plutons. Rectangle highlights the location of Figures 50, 51 and 52 (labelled here 3, 4 and 5, respectively). Image from Gold Fields Pty Ltd.

The stratigraphic succession at St Ives (Gresham and Loftus-Hills, 1981; Watchorn, 1998) is subdivided into the Kambalda Sequence, the Kalgoorlie Sequence, and the Merougil Sequence (terminology used in Kositcin et al., 2008; Fig. 52). In this area the Lunnon Basalt defines the base of the Kambalda Sequence and is overlain by the Kambalda Komatiite (composed of the Silver Lake Peridotite and Tripod Hill Komatiite). U–Pb dating of an interlayered dacitic layer within the Kambalda Komatiite yielded an age of 2708 ± 7 Ma; Nelson, 1997). These are in turn overlain by the Devon Consols Basalt, Kapai Slate (dated at 2691 ± 6 Ma; Claoué-Long et al., 1988), and Paringa Basalt (2691 ± 4 Ma; Nelson, 1997). Numerous mafic dolerites appear to be concordant with these volcanic rocks, and are similar in composition to the surrounding volcanic rocks (Prendergast, 2007). The granophyric zones within these dolerites are the best gold host rock type. World class komatiite-hosted massive nickel deposits occur at the contact between the Lunnon Basalt and Kambalda Komatiite formations (Chapter 4).

The mafic and ultramafic rocks are overlain by clastic sedimentary rocks and felsic volcanic–volcaniclastic sequences of the Black Flag Group (Gresham and Loftus-Hills, 1981; Watchorn, 1998), which in this area is defined as the Kalgoorlie Sequence (Krapež and Hand, 2008). In the St Ives Goldfield region, major variations in the age (c. 2689 Ma to younger than 2680 Ma) and provenance of the Black Flag Group occur (Squire et al., 2007). Regionally, sandstones within the Kalgoorlie Sequence have detrital zircons younger than 2690 Ma (Kositcin et al., 2008). The Merougil Conglomerate (or Merougil Beds; Watchorn, 1998) disconformably overlies the Black Flag Group (Fig. 52), is composed of conglomerate units and sandstones (Gresham and Loftus-Hills, 1981; Watchorn, 1998), and is now defined as part of the Merougil Sequence (Krapež and Barley, 2008). Detrital zircon dating and regional constraints indicate the Merougil Sequence was deposited after 2665–2660 Ma (Krapež et al., 2000; Kositcin et al., 2008).

The St Ives Goldfield has undergone multiple episodes of Archean deformation (Nguyen et al., 1998) and is bounded by the NNW-trending regional Boulder–Lefroy Fault to the east, and by the Speedway Fault to the west (Fig. 48). The Boulder–Lefroy Fault is a clearly defined gravity trend in potential field data sets (Fig. 49). At a camp-scale the structure of the goldfield is dominated by thrust repetitions of stratigraphy and broad anticlinal features, such as the Kambalda Dome.

Multiple structural models have been proposed for the St Ives Goldfield (Archibald, 1985; Swager, 1997; Nguyen et al., 1998; Watchorn, 1998; Weinberg et al., 2003, 2005; Blewett and Czarnota, 2007; Blewett et al., 2010b; Miller et al., 2010). There is currently some variation in the deformation numbers (i.e. D_1, D_2) applied to different events in the field. The most commonly used D_1 to D_4 event history of Swager (1997) only assigns deformation event numbers to compressional or strike-slip events with extensional events identified, but not assigned an event number. In contrast, Blewett and Czarnota (2007) have assigned deformation numbers to extensional events.

The repetition of the Lunnon Basalt stratigraphy via faults that have been folded by later deformation (e.g. Foster Fault; Fig. 48) has been linked to early D_1 N–S thrusting (Archibald et al.,

1978; Swager, 1997), whereas other workers define D_1 as an extensional event (Blewett and Czarnota, 2007). The major deformation event within the field was an ENE–WNW shortening that produced thrusts and upright, NNW-trending, gently plunging folds (Swager, 1997; Nguyen et al., 1998; Watchorn, 1998; Weinberg et al., 2003, 2005). The dominant anticlinal fold axis through the Kambalda Dome has been related to this event by previous workers (Fig. 48). This deformation was associated with marked flattening and the formation of a regional fabric, and is linked to peak regional metamorphism (Swager, 1997). Major crustal thickening was accommodated via ductile deformation along the regional first-order Boulder–Lefroy Fault (e.g. Weinberg et al., 2004, 2005), and also the Playa Fault which is inferred to be a second order splay fault (Fig. 48). Felsic to intermediate intrusive rocks were emplaced at a late stage in D_2 and also post D_2 (Watchorn, 1998; Nguyen et al., 1998).

D_2 was followed by phase of extension and plutonism regionally associated with the formation of the Late Basins (Krapež and Barley, 2008), and locally linked to the deposition of the Merougil Conglomerate. The regional setting and stratigraphic architecture of the Late Basins has been related to the development of basins within fault-bound compartments adjacent to strike-slip faults (Krapež and Barley, 2008). In contrast, regional kinematic studies have related these Late Basins to ENE–WSW extension (Blewett and Czarnota, 2007) — these workers have defined this extensional event as D_3.

The formation of the Late Basins was followed by the development of a brittle to ductile oblique-sinistral wrench fault system that was associated with the majority of gold mineralisation in the St Ives Goldfield (e.g. Nguyen et al., 1998; Cox and Ruming, 2004). This event was associated with WNW–ESE shortening with the NW- to NNW-trending D2 faults reactivated as sinistral-reverse faults (Nguyen et al., 1998; Cox and Ruming, 2004; Weinberg et al., 2005). During this main gold event, N-trending fault segments on reactivated D_2 faults behaved as contractional jogs (Nguyen, 1997; Nguyen et al., 1998; Cox and Ruming, 2004; Ruming, 2006). Newly formed N- to NNE-trending thrusts, some with conjugate fault geometries, were also formed, such as at Revenge (Nguyen et al., 1998). The majority of researchers have defined this sinistral wrenching event as D_3 (Swager, 1997; Nguyen et al., 1998; Cox and Ruming, 2004; Weinberg et al., 2005). Blewett and Czarnota (2007) and Blewett et al. (2010a,b) define the same gold event as D_4.

The last major deformation event in the St Ives Goldfield was related to the formation of NNE- to NE-trending dextral strike-slip faults (e.g. the Alpha Island Fault; Fig. 48). The majority of researchers have defined this dextral faulting event as D_4 (Swager, 1997; Nguyen et al., 1998; Cox and Ruming, 2004; Weinberg et al., 2005). Blewett and Czarnota (2007) and Blewett et al. (2010 a,b) define the same deformation event as D_5.

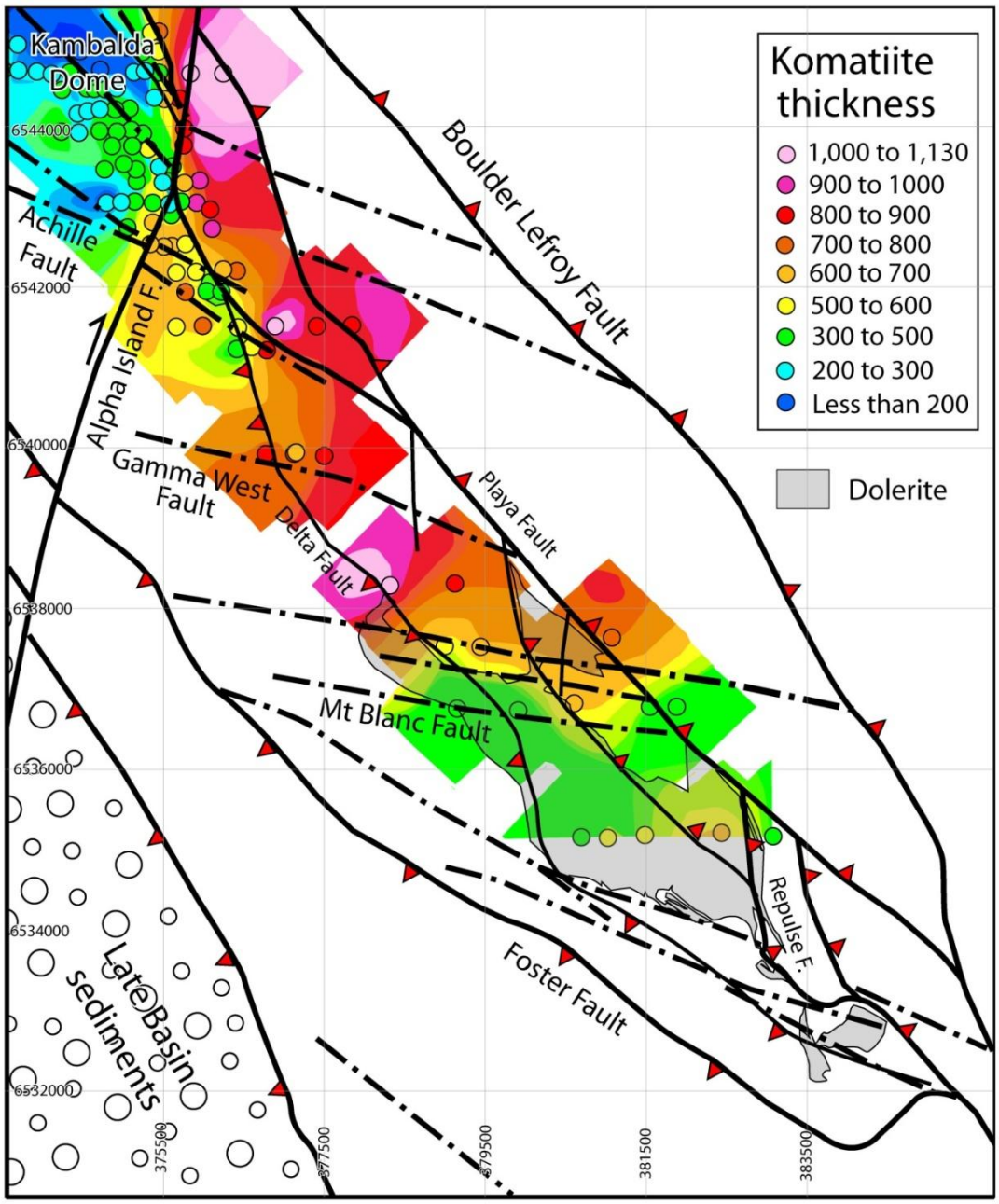

Figure 50. Isopach map of Kambalda Komatiite thickness (from Connors, 2002; Connors et al., 2002, 2005) and distribution of Defiance Dolerite at the top of basement (grey infill). These have been overlain with the key structural trends marked on the gravity image in Fig. 49. Key WNW-trending structures have been labeled (Achille, Gamma West and Mt Blanc Faults; Connors et al., 2002) and are marked with dashed lines; major regional faults are highlighted with solid white lines. See text for discussion.

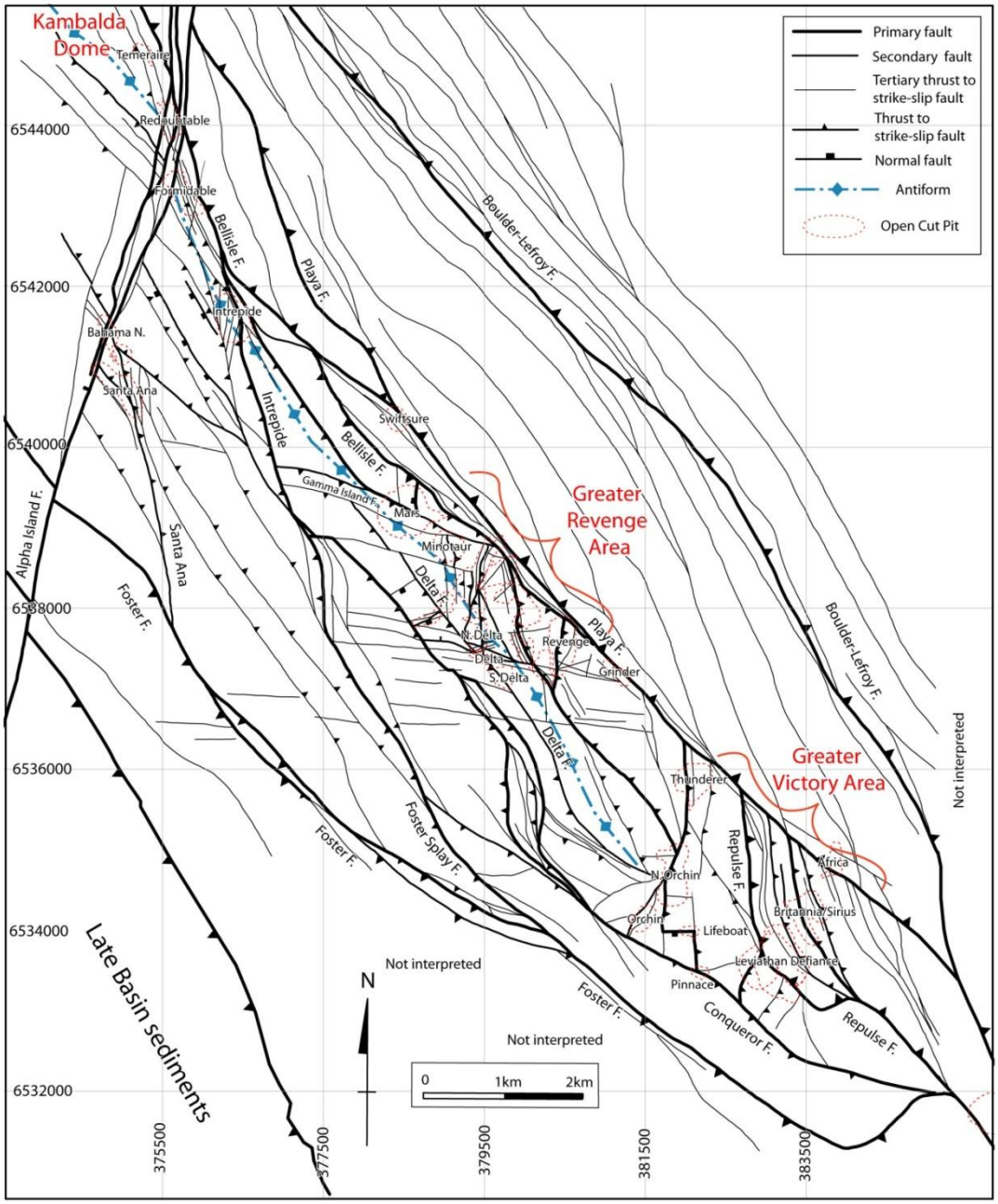

Figure 51. Revised structural interpretation for the St Ives Goldfield. Pits are dashed red lines. The Greater Revenge Area (GRA) is defined by the Mars–Agamemnon West–South Delta–Revenge pits. The Thunderer–Orchin–Leviathan/Defiance pits define the Greater Victory Area (GVA). Kambalda Dome is at top left. Note that many of the faults have low displacements and at this scale do not have marked offsets.

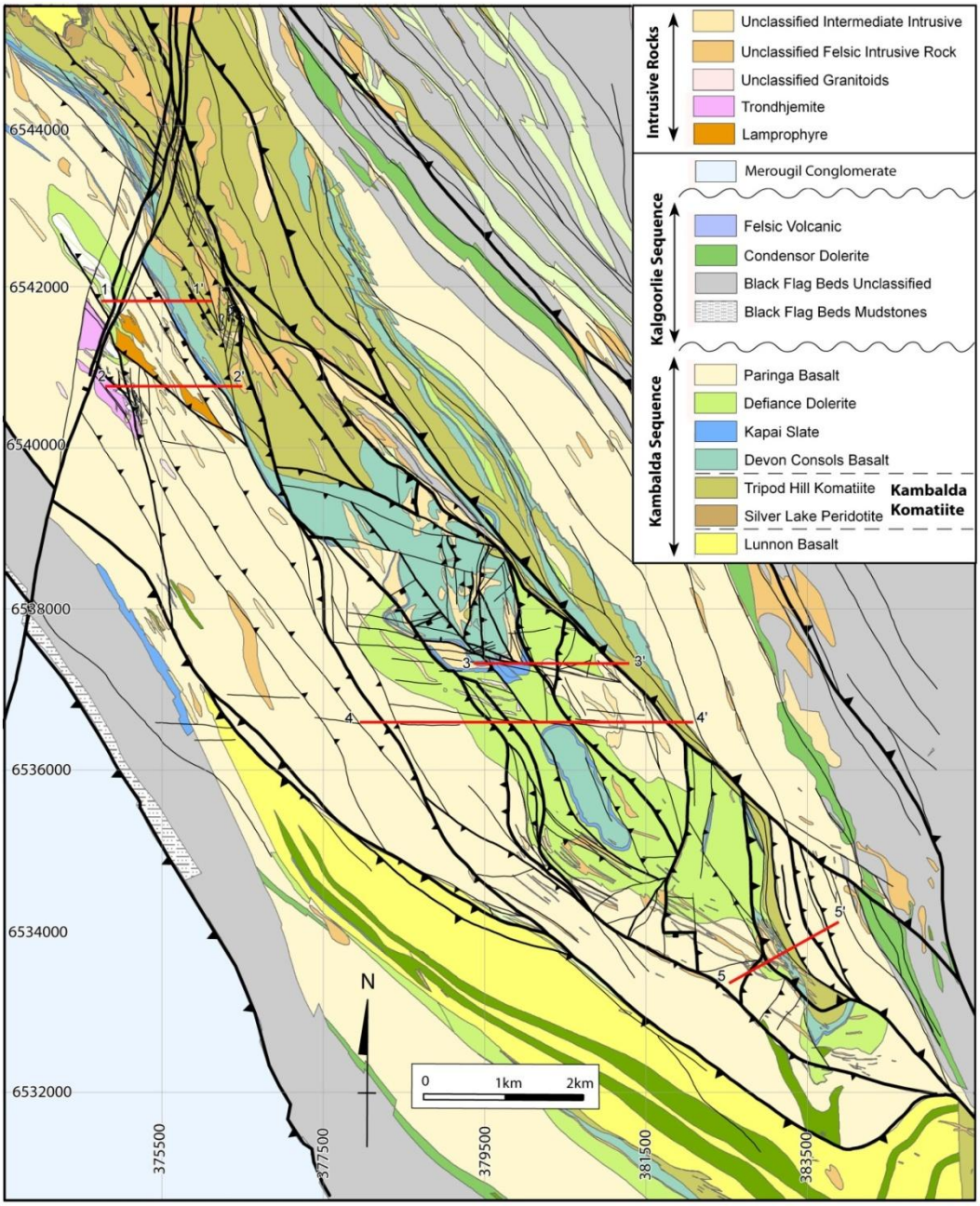

Figure 52. Solid Archean geology map with structural interpretation overlain. Section lines for Figure 53 are shown. Proterozoic dykes have been removed from this map. Note that many of the faults have low displacements and at this scale do not have marked offsets.

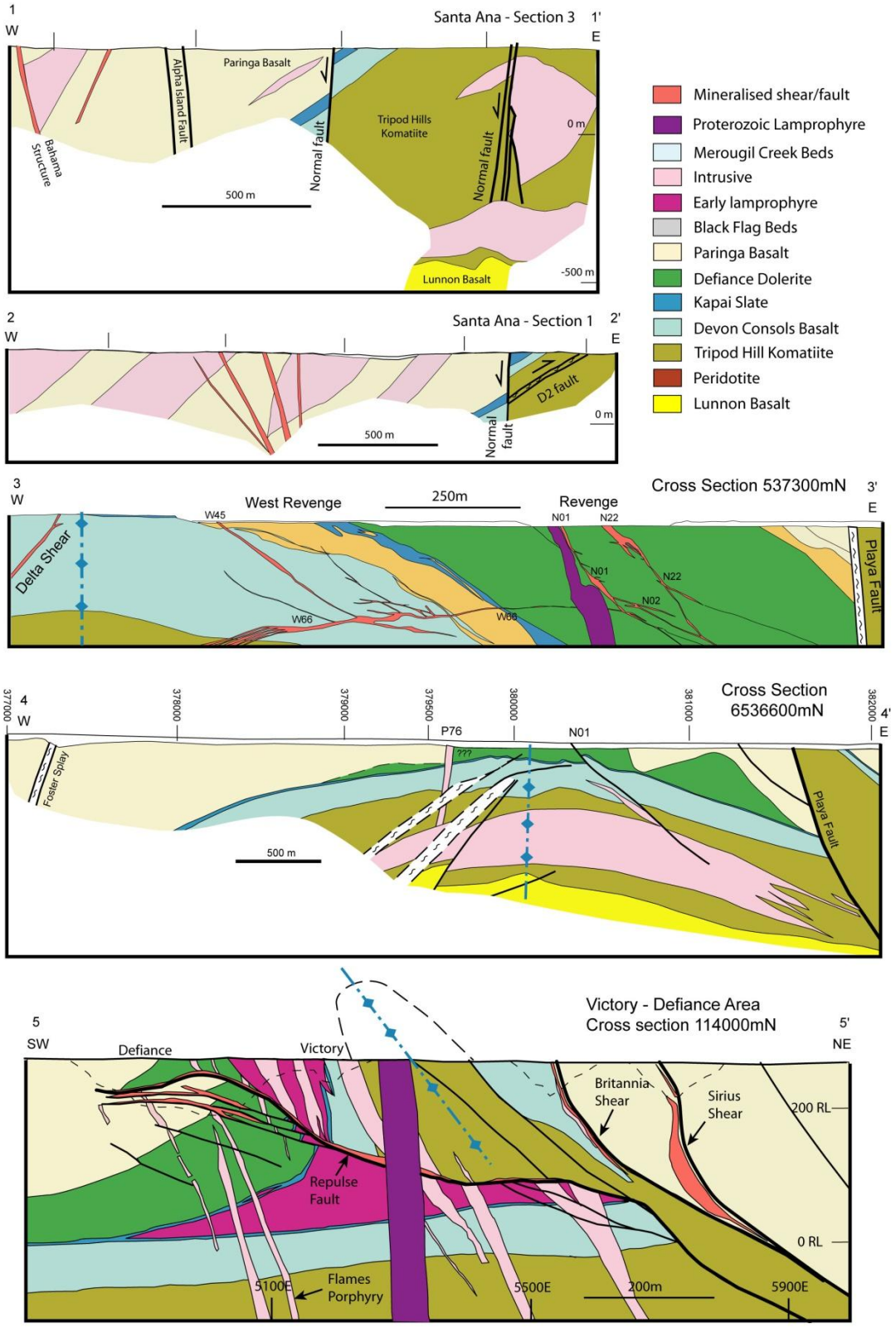

Figure 53. Selected section lines from the St Ives gold field. These sections are marked on Figure 52. Note that all intrusions have been coloured the same on the sections in contrast to the geological map (Fig. 52). Sections have been compiled from work undertaken by Western Mining and Gold Fields geologists. A version of section line 5 was published in Watchorn (1998) and Vanderhor and Groves (1998).

West-northwest trending lineaments substantially oblique to the main northwest- to north-trending structural elements

Within the goldfield a series of cryptic WNW- to W-trending lineaments substantially oblique to the main NW to NNW-trending structural grain have previously been identified, but there are no field structural constraints on the nature of these features. Published structural summary maps of the observed fault geometry associated with the gold deposits within the St Ives Gold Field have not depicted these WNW-trending features (e.g. Watchorn, 1998; Nguyen et al. 1998; Cox and Ruming, 2004; Weinberg et al.,2005). These WNW-trending features were termed by Connors et al. (2002) the Achille, Gamma West, and Mont Blanc Faults (Figs 49, 50) and were related to possible early rift architecture associated with deposition of the volcano-sedimentary succession. The WNW-trending features have been mapped or inferred via several different datasets:

1. Neumayr et al. (2008) inferred the location of WNW-trending to W-trending structures by the analysis of alteration footprints associated with gold mineralisation in the St Ives Gold Field
2. WNW-trending gravity lineaments can be defined on camp scale gravity data sets that diverge from the Boulder–Lefroy Fault (Fig. 49). Some of these correlate with the location of mafic dolerites that host major gold deposits in the camp (Junction, Argo, and Victory; Fig. 49)
3. Isopach mapping of the different rock types within the St Ives Goldfield has highlighted a major thickness variation within a key komatiite rock unit across the WNW-trending Mont Blanc Fault (Connors, 2002; Fig. 50). The isopachs indicate the komatiite unit becomes thicker by more than a hundred metres north of the Mont Blanc Fault (Fig. 50). Similar variations are not systematically documented across the Achille and Gamma West Faults (Fig. 50).
4. Stratigraphic work by Squire et al. (2007) linked WNW-trending structures, such as the Foster Fault, to variations in the Black Flag stratigraphy at a camp-scale.

Timing of deformation and gold mineralisation

The Kambalda Dome has traditionally been inferred to be a major D_2 antiformal fold that is crosscut by later granitoids (Fig. 48). U–Pb dating of the Kambalda Granodiorite (Compston et al., 1986), and also felsic–intermediate porphyry dykes at the Revenge deposit by Nguyen (1997), indicate they were emplaced at c. 2660 Ma providing a lower age limit on the timing of D_2 (Nguyen, 1997). However, there is a complex igneous paragenesis that has not been fully resolved. The potential input from primary volcanic architecture, or doming during magmatism, into the current shape of the dome has also not been addressed.

The timing of gold mineralisation within the St Ives Goldfield is problematic, but is younger than the Merougil Sequence, i.e. <2660 Ma. Nguyen (1997) presented U–Pb SHRIMP dates from

hydrothermal monazite from the Revenge deposit to suggest the main gold event occurred at c. 2630 Ma. However, recent U–Pb dating of hydrothermal xenotime from the Mt Charlotte gold deposit, along strike and to the north of the St Ives Goldfield, has produced ages of 2655 ± 13 Ma (Rasmussen et al., 2009) and 2644 ± 11 Ma (Vielreicher et al., 2010). The Mt Charlotte deposit is hosted within a late-stage dextral fault system (Mueller et al., 1988). This regional dextral faulting event post-dates the main-stage gold mineralisation at St Ives, suggesting the gold mineralisation could be older than c. 2640 Ma.

Structural interpretation of the Victory to Kambalda region

A structural interpretation of the Victory to Kambalda region of the St Ives Goldfield is presented in Figures 51 and 52 (from Miller et al., 2010).

The dominant structural features on the map are:

1. A series of major NNW-trending faults with long strike lengths, greater than several kilometres (such as the Playa, Boulder–Lefroy, Delta and Foster Faults). Some of these faults have marked strike changes in key regions with gold deposits (e.g. the Repulse Fault in the Greater Victory Area; Fig. 51).
2. A series of N-trending faults with short strike lengths. These have less than a kilometre in strike, with many having strike-lengths less than 500 m (e.g. at Minotaur in the Greater Revenge Area).
3. A series of WNW-trending shears and faults. In some areas these faults diverge from the NNW-trending faults but are also truncated by these structures. In many areas the short strike-length N-trending faults terminate against these.
4. A major antiformal hinge that runs through the major deposits (the axis of this is marked on Fig. 51).
5. A series of NNW-trending normal faults between the Santa Ana and Intrepide deposits (Fig. 52).
6. The late-stage NNE-trending Alpha Island Fault, which has a dextral offset.

A series of cross sections highlight the following key aspects;

1. There are major variations in the way shortening has been accommodated along strike in the gold field. The section line through the Victory-Defiance region (within the Greater Victory Area) shows a marked amount of shortening, with a tight to isoclinal hangingwall anticline above the Repulse Fault (section line 5–5’ in Figs 52 and 53). The Repulse Fault has approximately 400 m of displacement in this sectional view (as marked by the ultramafic Tripod Hills Komatiite contact with the Devon Consols Basalt). This section is in marked contrast to the Greater Revenge Area (Figs 52, 53), where extensive drilling has defined a broad open anticline (section line 4, Fig. 53). If no volume loss is assumed, the

open fold in the footwall of the Playa Fault reflects approximately 10% shortening via folding and faulting from the Playa Fault to the western-most defined edge of the fold (at easting 378000; Fig. 53).

2. Coupled with the low strain noted above, proprietary seismic data acquired by Goldfields show that the Boulder–Lefroy fault dips to the east, with a deep sedimentary basin of Kalgoorlie Sequence rocks overlying interpreted Kambalda Sequence at depth. This would point to the Boulder–Lefroy Fault existing as a very large syn-sedimentary fault, now partially inverted, and the Kambalda anticline as a footwall anticline formed during extension and deposition of the Kalgoorlie sequence.
3. A series of normal faults between the Santa Ana and Intrepide deposits have been identified that offset the Kapai Slate marker bed, and also D_2 faults (sections 1 and 2, Fig. 53). The associated normal faults are adjacent to a major late basin sequence (the Merougil Conglomerate sediments are located on Figs 48, 52), and the normal faults postdate D_2 thrusts (section line 2, Fig. 53). These normal faults (marked on Figs 51, 52) appear to have had a control on the geometry of some of the intrusive units, with one intrusive unit having a margin parallel to a normal fault (section line 1, Fig. 53).

Description of the southern Greater Revenge Area field trip site containing west-northwest trending faults (inferred early growth faults)

During the field excursion the southern Greater Revenge Area will be visited

Arrays of steeply N-dipping, WNW-trending faults occur in the southern Greater Revenge Area, with a prominent WNW-trending fault cutting through the Delta, Pluton, and Grinder Deposits (Fig. 54a). In some strike segments, this has been formally named the N01/N22 Transfer Fault, and will be referred to as the Transfer Fault in this paper. More than one WNW-trending fault occurs within the corridor that defines this fault (note the two sub-parallel faults near the Delta Pit in Figure 54a that merge into a single fault along strike to the ESE).

The Transfer Fault is parallel to, and just north of, the location of the Mont Blanc Fault as defined by Connors et al. (2002). The fault is also located close to the region where a thickness increase in the ultramafic rocks is defined in the isopach maps (Fig. 50). A major Archean porphyry dyke has intruded within the fault (Fig. 54b,c); this dyke is crosscut by NW- and N-trending faults (Fig. 54a) and the strike of this dyke is atypical for the study area.

The Transfer Fault also corresponds to a linear boundary between the Paringa Basalt and the Defiance Dolerite in the Revenge open pit area (line of arrows on the geological map in Fig. 54a). The Transfer Fault offsets the Kapai Slate with approximately 20 m vertical displacement at the Pluton Pit (south block down).

The WNW-trending Transfer Fault shows complex relationships with the other major N and NW structural trends containing gold deposits within the study area. Some segments of the Transfer Fault are strongly mineralised with high gold grades recorded on the fault plane and in adjacent wallrock (Fig. 55a). High-grade gold lodes occur in regions where the Transfer Fault intersects major NW-trending shears, such as the Delta Fault (Fig. 54a), and also the Playa Fault. The Grinder deposit is located at the intersection between the Playa Fault and the Transfer Fault (Figs 51, 54a). The Delta Fault also changes its strike where it intersects the Transfer Fault (Fig. 55a).

The Delta Fault (Fig. 56a,b) and Playa Fault both exhibit strong ductile fabric development. Low-angle striations, linked to sinistral-reverse movement, have been observed on the Playa Fault (Nguyen et al., 1998). Similar mineral lineations are also associated with sinistral-reverse movement on the Delta Fault (Fig. 56a). The Transfer Fault has an apparent dextral offset across the Delta Fault (Fig. 55a), which conflicts with the observed kinematics. The location of the Transfer Fault, across and to the east of the Playa Fault, is unknown. The Playa Fault has previously been interpreted as a D_2 fault, which was reactivated during syn-gold sinistral wrenching, with a total displacement possibly in the order of kilometres (e.g. Cox and Ruming; 2004).

The N-trending mineralised W43 structure terminates against the Transfer Fault zone (Fig. 55a). The W43 fault splays into two faults prior to terminating against the Transfer Fault with the upper splay (labeled W43_2 in Fig. 55a,b) terminating within the Transfer Fault, and the lower splay (labeled W43_1 in Fig. 55a,b) changing strike and merging into the Transfer Fault. The N22 structure is one of the major mineralised shears in the Revenge deposit (Section Line 3, Fig. 53). In contrast to the W43 Fault, the NNE-trending mineralised N22 structure clearly crosscuts the Transfer Fault in the south wall of the Revenge Pit (Fig. 56c). In the Pluton and Revenge pits, the NNW- to N-trending faults crosscut the Transfer Fault (Fig. 54a), and in the Pluton and Revenge deposits high grade gold does not occur parallel to the Transfer Fault. In many areas, late-stage S- to SSE-dipping thrusts also crosscut the Transfer Fault (Fig. 56d).

The Transfer Fault is not a discrete structure and it is commonly exposed as arrays of WNW-trending veins (Fig. 55b,c) with strong foliation development (predominantly defined by chlorite but also biotite). The veins within the Transfer Fault comprise early WNW-trending veins that are not mineralised (Fig. 57) and later distinctive WNW-trending veins that are mineralised (Figs 55c, 58).

The earliest set of veins within the Transfer Fault are associated with chlorite (± biotite) alteration and are clearly truncated by N- and NW-trending faults. These relationships are best observed adjacent to the W43 lode where the earlier WNW-trending quartz veins (with biotite wall rock alteration) are truncated and deformed by this structure (Fig. 57a–d). The N-trending lodes are notable for their intense quartz–carbonate–pyrite–albite alteration associated with mineralisation (Fig. 57).

The mineralised veins within the Transfer Fault have distinctive intense wall rock alteration that is mineralised (Fig. 58a). This alteration is dominantly quartz, carbonate, pyrite, and sericite (Fig. 58b,c). In some areas this distinctive alteration overprints earlier hematite alteration (Fig. 58c), but the distribution of this earlier hematite-associated assemblage is unconstrained. Ore-stage lineations have shallow plunges to the west with sinistral steps (Fig. 58c). The width of mineralisation along the Transfer Fault locally can reach 30 m (Fig. 55a). The true width of the fault is hard to estimate because earlier phases of deformation along the Transfer Fault are overprinted by later structures. The biotite-associated veins, shown in Figure 57, probably reflect deformation associated with the Transfer Fault and may indicate that the actual width of the structure originally extended further north.

One of the striking features of the WNW-trending Transfer Fault is that it has only developed high grade gold mineralisation in localized regions. This implies the structure may have only been locally active along its strike length at any one time. Under the inferred WNW–ESE shortening field associated with the main phase of gold mineralisation in the St Ives field (e.g. Nguyen et al., 1998; Cox and Ruming, 2004; Weinberg et al., 2005; Blewett et al., 2010b), the WNW-trending Transfer Fault was very poorly oriented to have been reactivated at this stage of the geological history. However, this fault is strongly mineralised where the W43 fault terminates against it (Fig. 55a).

Ore-stage stepped fibres suggest sinistral-slip occurred along the Transfer Fault during mineralisation (Fig. 58c), indicating that this fault was only mineralised in areas where it acted as a strike-slip fault syn-gold (Fig. 59). Previous studies have shown that during gold mineralisation in the Greater Revenge Area N-trending faults, such as the W43 fault, were active as thrusts (e.g. Nguyen et al., 1998). NW-trending faults, such as the Delta Fault, were active as sinistral-reverse faults (Nguyen et al., 1998; Cox and Ruming, 2004), consistent with the mapped lineations on the Delta Fault (Fig. 56a). In the case of the high-grade zone depicted in Figure 55a, the sinistral slip is inferred to reflect the transfer of shortening along the W43 across strike to the Delta Shear (Fig. 59). This steep-dipping WNW-trending fault transferred the strain by linking a complex combination of block-on-block movement associated with thrusting and strike-slip movement (Fig. 59).

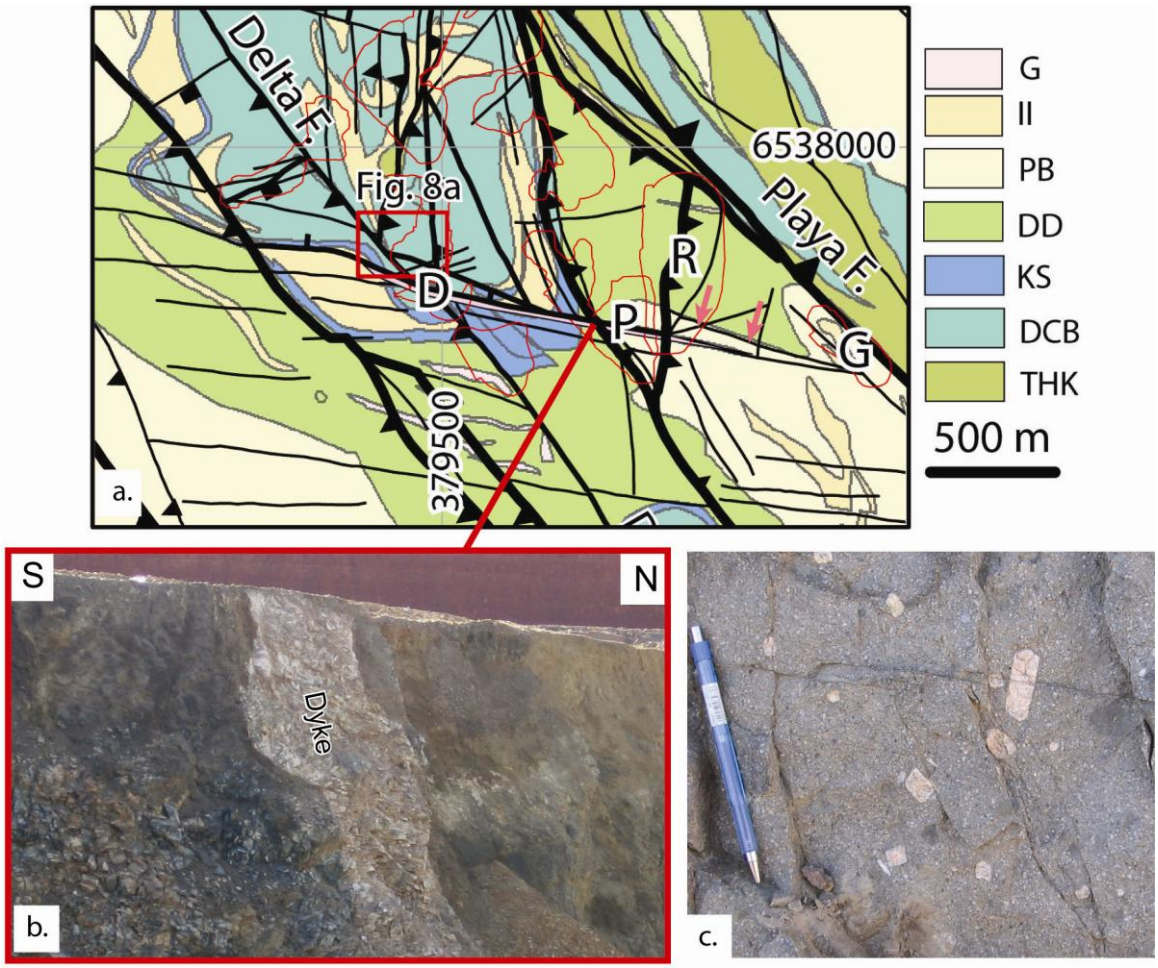

Figure 54. a) Location map highlighting a major WNW-trending fault that intersects the Delta (D), Pluton (P), and Grinder (G) deposits. This is termed the Transfer Fault and has been defined as the N01/N22 in some localities. Note the Paringa Basalt trend highlighted by the orange arrows that is parallel to the WNW-trending transfer faults (see coloured lithologies in Fig. 52). R is Revenge pit. Area labelled 'Fig. 8a' corresponds to Figure 55a; b) porphyry dyke intruding parallel to the Transfer Fault. The strike of the dyke is atypical for the region; c) detail of porphyry dyke highlighting feldspar phenocrysts that are common in Archean dykes within the goldfield.

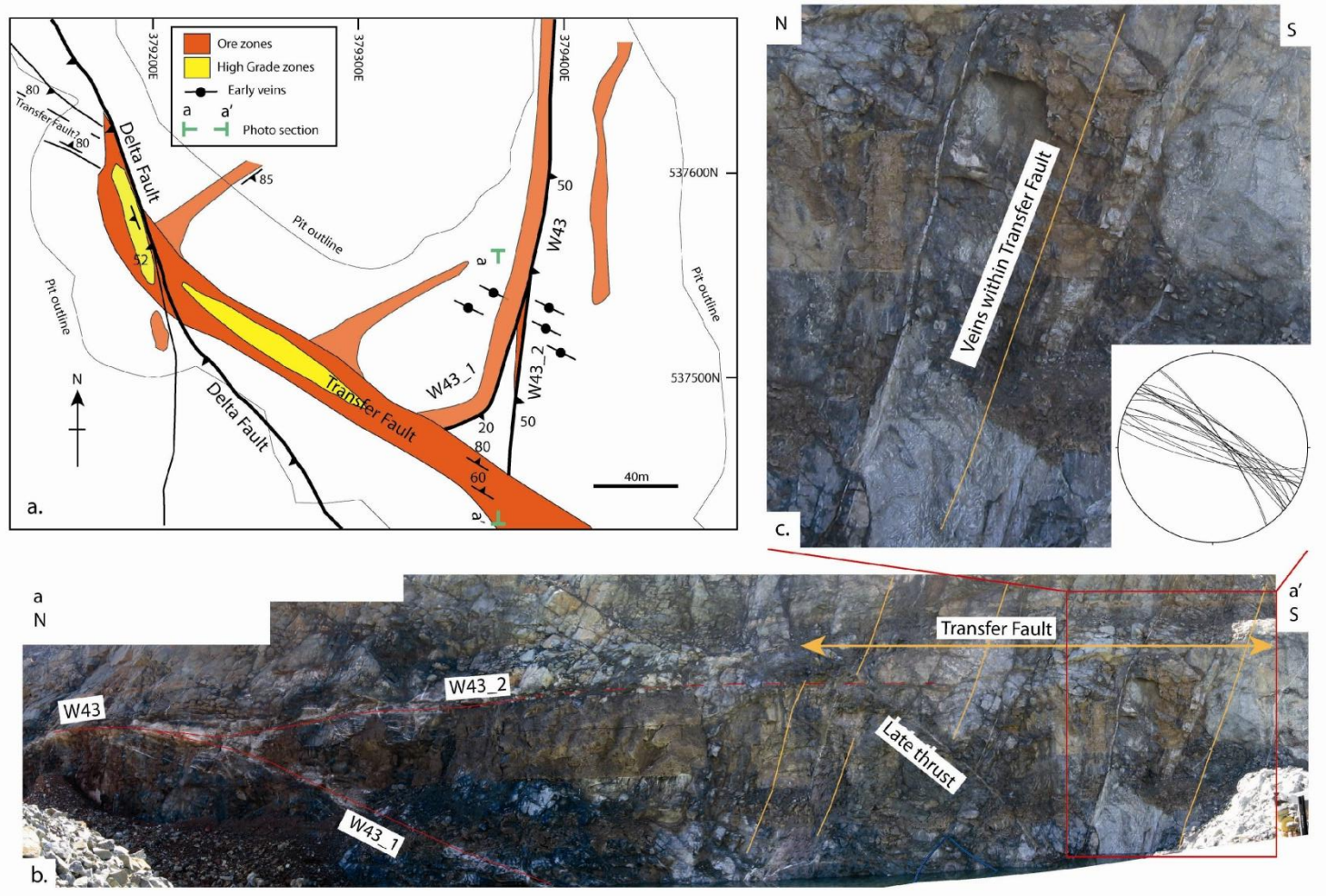

Figure 55. High-grade gold mineralisation along the Transfer Fault at the intersection with the Delta Fault. The location is marked on Figure 54: a) map of key structural elements and grade distribution. Note the strike change on the Delta Fault where the transfer intersects it — this area also corresponds with higher gold grade on the Delta Fault. The W43 fault terminates against the Transfer Fault with a splay geometry close to the fault; b) photo collage of W43 lode and the Transfer Fault. The W43 lode does not propagate through the transfer; c) detail of quartz veins within the Transfer Fault. Stereonet plot highlights vein orientations within the Transfer Fault.

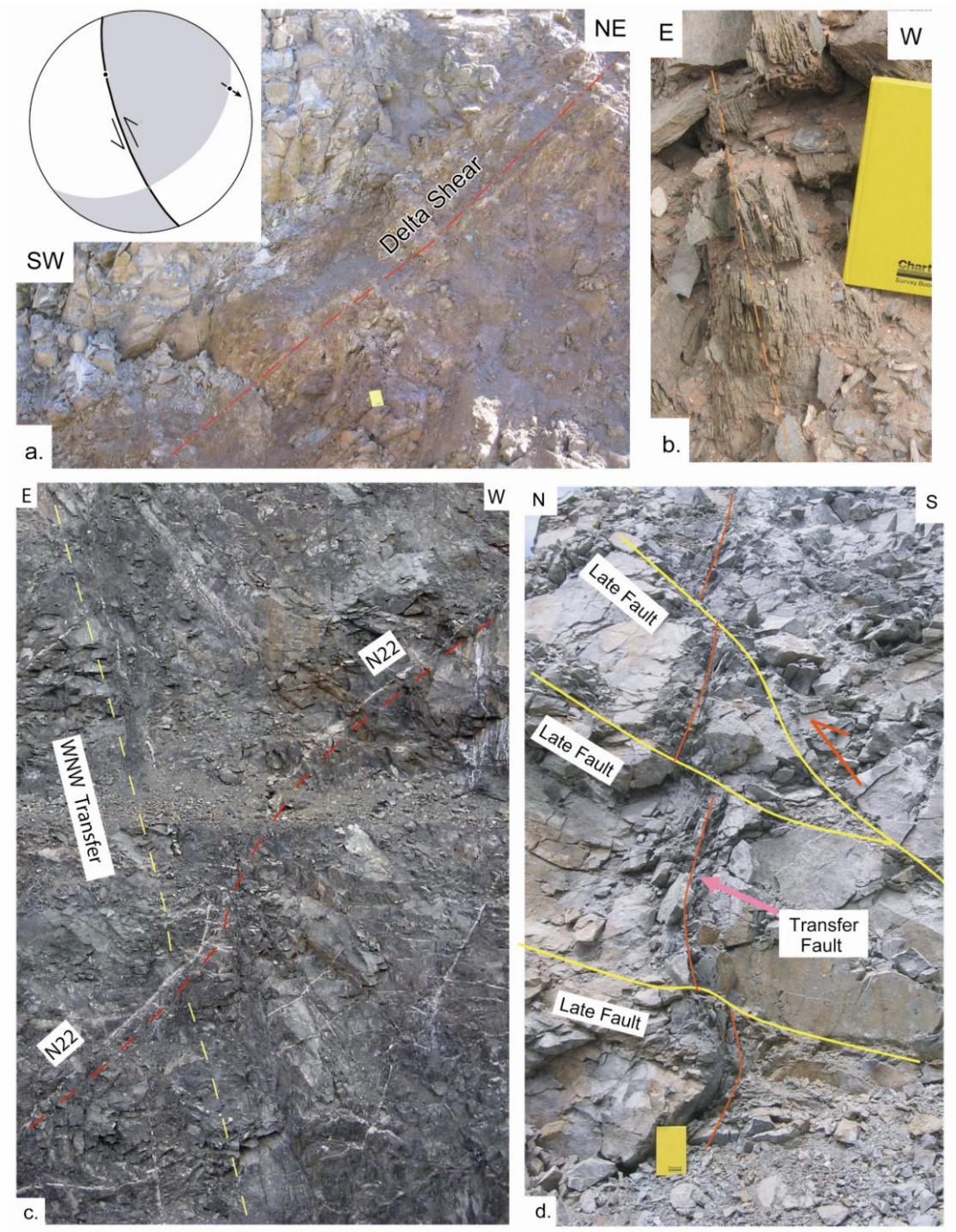

Figure 56. a) Delta Fault in the Delta pit (Delta pit location is marked with a P in Figure 54a). Stereonet plot highlights lineation within shear plane (sinistral-reverse kinematics are observed), P–T dihedra highlights fault kinematics, arrow plotted at the pole to the fault highlights hangingwall transport of lode; b) example of strong ductile fabric development within the Delta Fault; c) photocollage of the southern end of the Revenge Pit (the location of this pit is shown in Figures 51, 54). This highlights the mineralised N22 fault crosscutting the WNW-trending Transfer Fault. The N22 fault is depicted on section line 3 in Figure 53; d) late south dipping thrusts that offset a section of the Transfer Fault (photo locality is from the southern end of the Delta North pit).

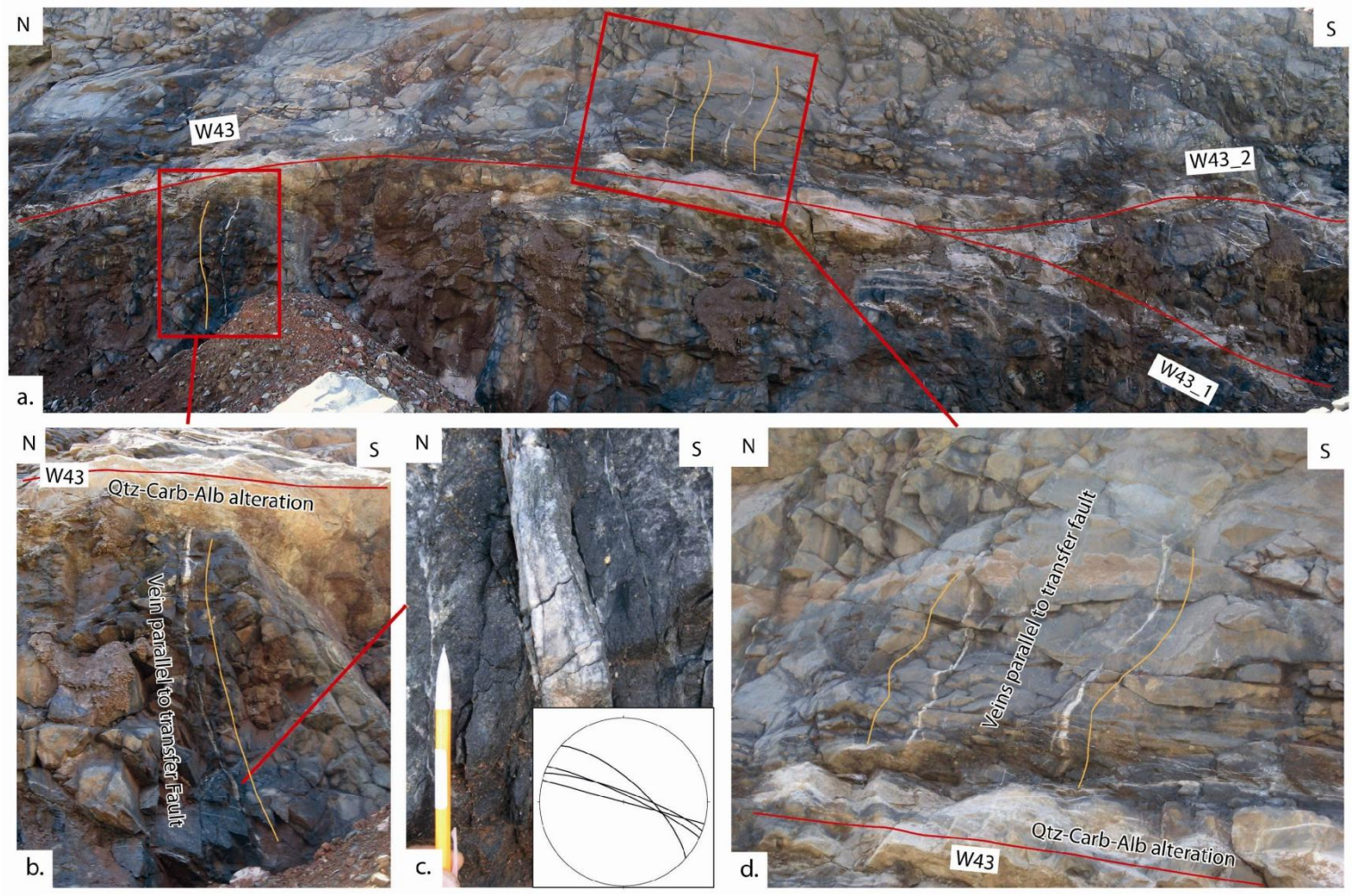

Figure 57. Photographic documentation of early vein arrays parallel to the Transfer Fault: a) W43 lode with earlier WNW-trending veins that have been truncated by the fault highlighted; b) early vein buckled and over printed by the W43 fault. Note the intense gold-related quartz, carbonate and albite alteration associated with the W43 fault; c) detail of early WNW-trending quartz vein from (b). The vein has with biotite alteration. Stereonet presents orientation of veins overprinted by the W43 fault; d) early vein arrays buckled and overprinted by the W43 fault. Note the intense gold-related quartz, carbonate, and albite alteration associated with the W43 fault.

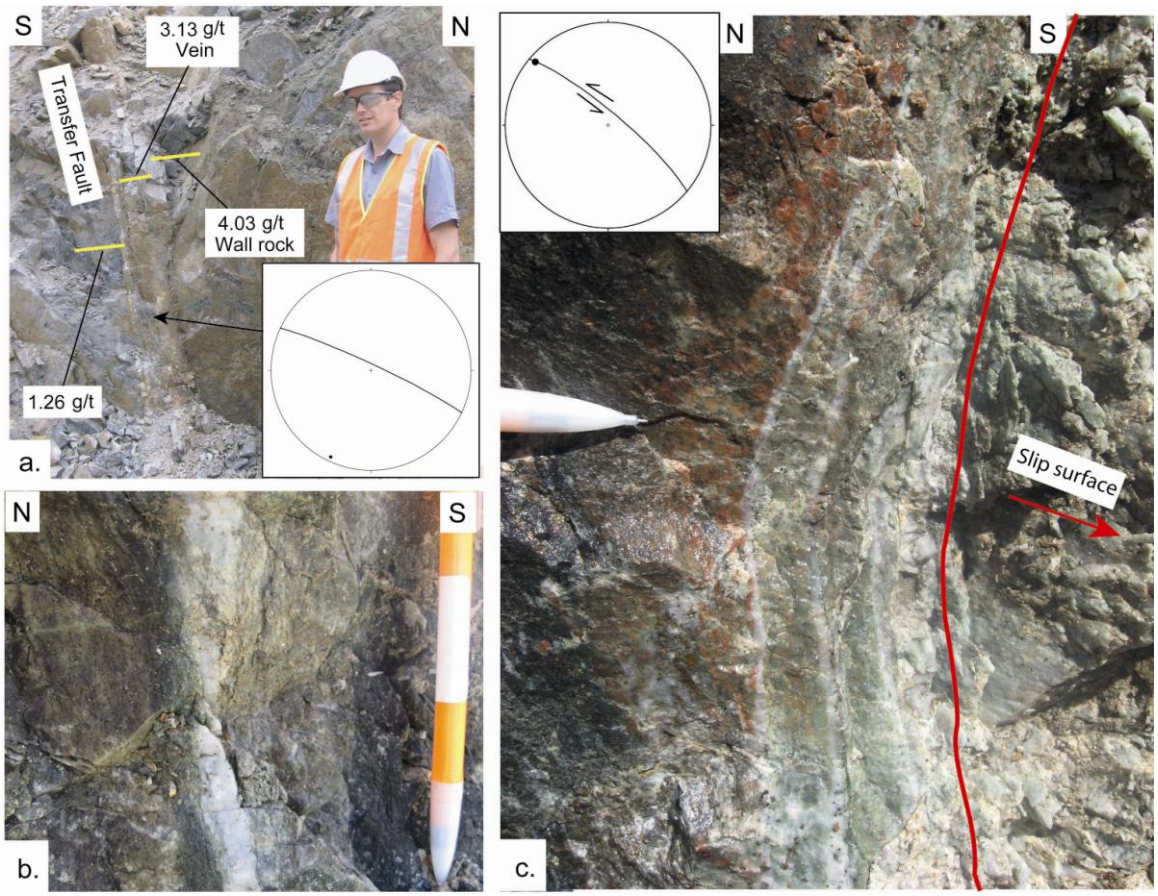

Figure 58. Mineralised veins within the Transfer Fault: a) assays highlighting mineralisation in the wall rock adjacent to the veins; b) intense gold-related carbonate, pyrite and, sericite alteration adjacent to WNW-trending Fault; c) intense gold-related carbonate, pyrite, and sericite alteration adjacent to WNW-trending fault that overprints earlier hematite alteration. The photograph is of a 3-dimensional surface that also shows the slip surface with a low angle gold-related mineral lineation and striations (highlighted by the red arrow). Stepped fibres indicate sinistral movement occurred during the growth of the ore-stage alteration minerals. Stereonet plots slip surface and gold-related mineral lineation.

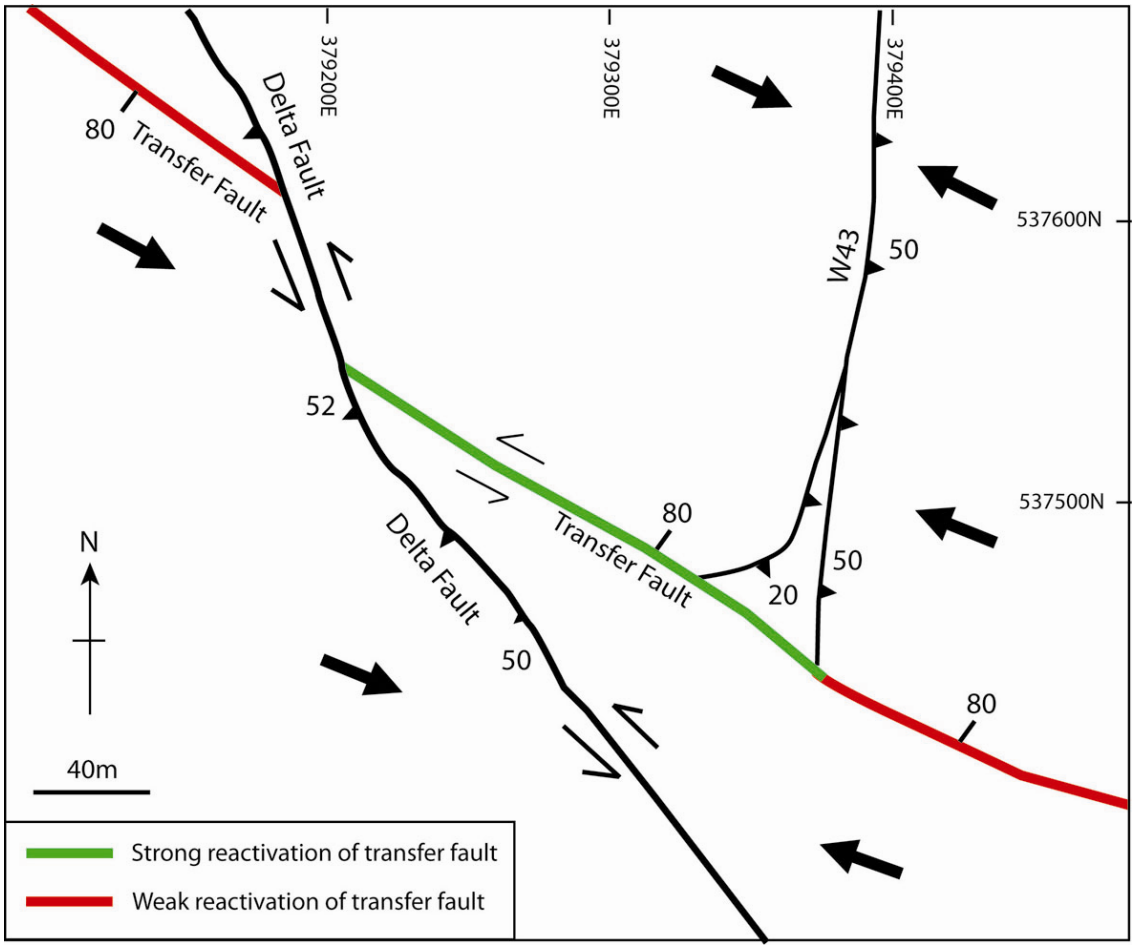

Figure 59. Summary diagram of kinematic relationships at the point the Transfer Fault intersects the Delta Fault and the W43 lode terminates against the Transfer Fault. Arrows reflect shortening associated with main stage gold in the St Ives Goldfield. See text for discussion.

Inferred evolution of west-northwest trending faults in the southern Greater Revenge Area observed during field visit

The following indicates the WNW-trending Transfer Fault predates the main gold event in the field:

1. It is intruded by an Archean dyke (Fig. 54). U–Pb dating of the Kambalda Granodiorite (Compston et al., 1986), and also felsic–intermediate porphyry dykes at the Revenge deposit by Nguyen (1997), indicate they were emplaced at c. 2660 Ma. The strike of this dyke is atypical for the study area and suggests it intruded along a pre-existing weakness defined by the Transfer Fault.
2. It has vein arrays associated with biotite that are clearly overprinted by syn-gold faults such as the W43 (Fig. 57).
3. The mineralised N22 fault clearly cross cuts this Transfer Fault (Fig. 56c).

The above relationships suggest the Transfer Fault existed at the time of late basin development, because U–Pb dating and regional constraints indicate the Merougil Conglomerate was deposited between 2660 and 2650 Ma (Krapež et al., 2000; Kositcin et al., 2008; Squire et al., this volume).

The Transfer Fault coincides with a marked thickness variation in the Kambalda Komatiite, with a greater thickness to the north of this steeply N-dipping feature (Fig. 50). It also corresponds to linear boundaries between basalt and the dolerite units. The stratigraphic thickness variations have been interpreted to reflect syn-volcanic growth faulting (Connors et al., 2002), and that these WNW-trending faults also controlled the distribution of mafic and ultramafic rocks at a camp-scale (Miller et al., 2010). One possible alternative interpretation is that the thickness variation in the ultramafic rocks across the Transfer Fault within the Greater Revenge Area (Fig. 50) reflects post-emplacement structural thickening, possibly via N–S thrusting. However, no strong field evidence in the Greater Revenge Area exists for extensive post-emplacement thickening (see Connors et al., 2002 for a discussion).

The lack of intense shortening via D_2 folding in the Greater Revenge Area (i.e. section line 4, Fig. 53) is the inferred reason that these old WNW-trending transfer faults can still be identified in this area. Other regions have undergone intense deformation (e.g. the contractional jog at Victory; Section Line 5, Fig. 53) making identification of such structures difficult in these areas. The Greater Revenge Area is a key to understanding the early fault architecture because of the lack of pervasive high-strain overprint. It is a type locality for defining the nature and timing of the WNW-trending structures.

The following summarises the long-lived event history for the WNW-trending Transfer Fault (Fig. 60). This fault is one example of an array of WNW-trending features in the goldfield (Gamma West and Achille Faults in Figure 50) and is inferred to be representative of the processes that have occurred along these structures. The description uses the recent deformation scheme and ages compiled by Blewett and Czarnota (2007) and Blewett et al. (2010a).

The initial phase of movement is inferred to have been associated with early growth faults, which allowed a greater infill of ultramafic volcanic rocks to the north of the fault (Fig. 60a). The fault is not inferred to have been linked to extensive rift-related topography, i.e. any accommodation space produced was rapidly infilled by volcanism. The Kapai Slate is a regional marker bed and during its deposition, only minor or no rift-related topography existed (Fig. 60b). There may have been an additional phase of extension associated with the emplacement of the dolerite units (Fig. 60c). Alternatively, the Transfer Fault may have acted as a feeder for the emplacement of the Defiance Dolerite. During D_2 inversion (associated with ENE–WSW shortening; e.g. Weinberg et al., 2005; Blewett et al., 2010b), the Transfer Fault would have been favourably oriented in the shortening field. The Transfer Fault underwent minor inversion (Fig. 60d), with the development of a biotite-defined flattening foliation as a record of this event. Minor thickening of the units in the hangingwall of the fault may have occurred, although no evidence for pervasive shortening exists more than 100 m from the fault. Offset of the Kapai Slate across the Transfer Fault in the Pluton

pit may have occurred at this time (Fig. 60d). The 20 m of offset of the Kapai Slate currently observed across the Transfer Fault (south block down) is substantially less than the large thickness increase in the thickness of the Kambalda Komatiite to the north across this fault corridor (Fig. 50). Some of the linear trends which currently define the Defiance Dolerite – Paringa Basalt contact (Fig. 54) also developed during this minor inversion event.

A period of minor extension along the structure is inferred to have been linked to the emplacement of early quartz vein arrays and dykes (termed D3 in Figure 60e), and was synchronous with the deposition of the late basin succession. During later sinistral wrenching associated with the main phase of gold, segments of the fault were crosscut by newly formed ore-related faults (e.g. the N22), with reactivation and associated gold deposition in areas where N-trending faults terminate against the Transfer Fault (e.g. the W43 in Fig. 60f).

Revised structural evolution of the Victory to Kambalda Region (Blewtt et al., 2010; Miller et al., 2010)

Role of D_1 thrusting

Previous workers have inferred an early N–S thrusting event within the Eastern Yilgarn Craton (termed D_1 by Swager, 1997). Faults that have been related to this event are folded by later D_2 folds, and commonly imbricate the Lunnon Basalt. In the study area, the Foster Fault is an example of one of these structures previously inferred to be a D_1 thrust fault (Figs 48, 51, 52). Apart from the repetition of the Lunnon Basalt, and the folded nature of the Foster Fault, there is a lack of meso-scale evidence from field mapping and drill core for N–S thrusting in the area of the St Ives Goldfield assessed in this study. Earlier D_1 thrusts were not been identified and alternative structural interpretations are plausible (see Blewett et al., 2010a). The Foster Fault could also be a D_2 thrust that imbricated the Lunnon Basalt, and was then folded during ongoing NE–SW D_2 contraction.

Early D_{1e} extensional architecture

The early fault architecture (Fig. 61a) has been inferred by integrating a large number of observations, and is a highly interpretative model. This has been defined as $D_{1e}$to prevent confusion with older D_1 terminology (Swager, 1997). In the Greater Revenge Area, the Mont Blanc Fault (Figs 49, 50, 61b) is interpreted to be an early structural feature that controlled the thickness variations in the Kambalda Komatiite, and is a clear trend in the gravity data. The fault is inferred to have defined by a broad zone of deformation, and we interpret that the northern extent of this zone has been mapped in the field as the Transfer Fault.

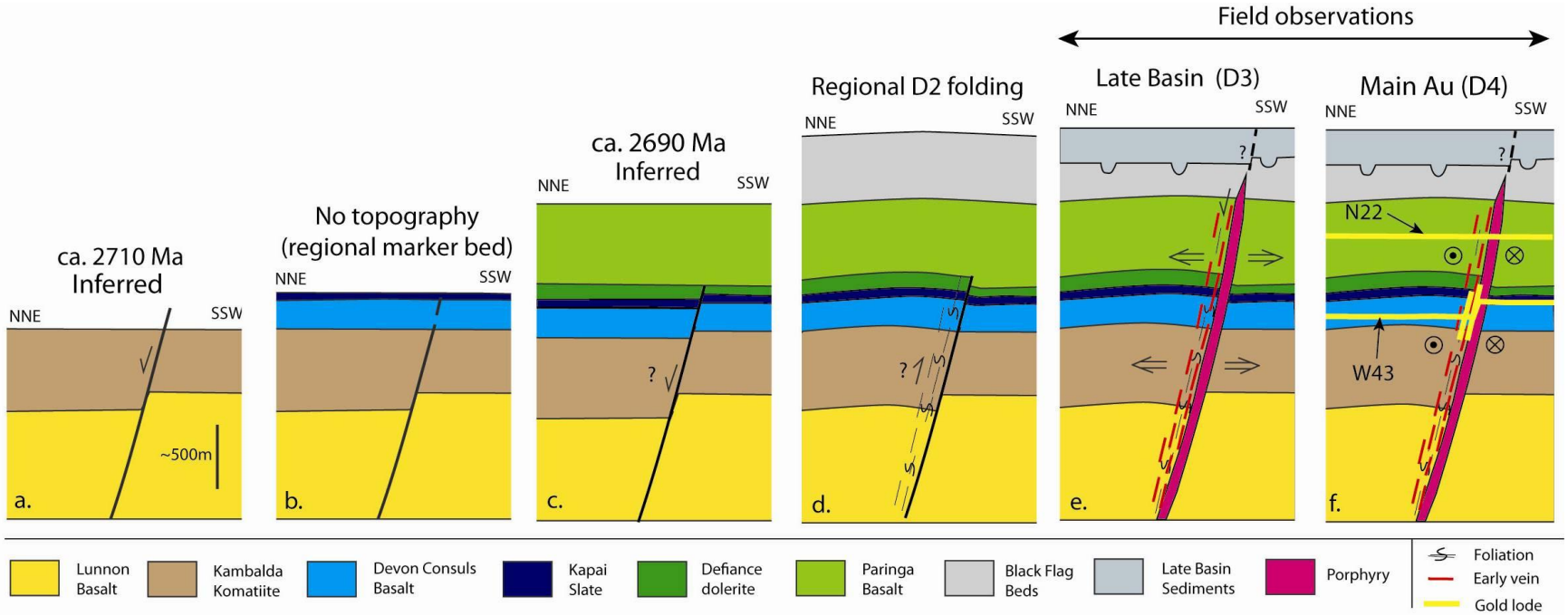

Figure 60. Inferred model for the development of the WNW-trending transfer faults in the southern Greater Revenge Area. See text for discussion. Note that the double headed arrow refers to the section of the evolution which can be clearly mapped in the surface outcrops. The earlier history is inferred from other relationships such as the isopach data in Fig. 3.

In many areas, the early WNW-trending transfer faults are transposed or overprinted by later high-strain zones. With the exception of the Gamma West Fault, which correlates with the location of the Gamma Island Shear, other early structures (e.g. the Achille Fault) are inferred from trends in the gravity data (Fig. 61b), dolerite trends (Fig. 54a), and also porphyry dyke swarms oblique to the dominant structural grain.

The dip direction of the early structures has been inferred by assuming that many of the currently mappable faults are reactivated early normal faults (although the dip direction of the Mont Blanc Fault and Gamma West Fault in Figure 61 is based on the present day structures). The naming of the main WNW-trending faults follows that of Connors et al. (2002), with an additional WNW-trending structure integrated in the early fault architecture, termed the Janus Fault (Fig. 61a), which has been overprinted by later intense deformation associated with the contractional jogs that define the Victory-Defiance Complex. This structure marks the southern extent of the Defiance Dolerite, which is a major gravity trend (Fig. 49), and a set of porphyry dykes is inferred to have intruded along this old structure.

Recently published Nd model age maps clearly define an older major regional basement boundary (aged 2.8 Ga) trending in a NNW orientation (Champion and Cassidy, 2007; Chapters 1 and 4, this volume). This trend defines the western margin of the Eastern Goldfields Superterrane (EGST), as well as the map patterns of the constituent terranes (Champion and Cassidy, 2007). The regional Boulder–Lefroy Fault is parallel to this trend and likely had its origins in the early development of the EGST. This fault is inferred to have been an early rift-related fault reactivated during D_2 inversion.

The inferred early D_{1e} architecture bears a strong resemblance to a rift system where a pre-existing NNW-trending boundary, linked to an older phase of rifting, was extended obliquely. In this interpretation the NNW-trending Boulder–Lefroy Fault marks the axis of the earlier boundary and the oblique younger extension direction was inferred to be NE–SW (Fig. 61). Analogue modeling of this type of multiphase extensional evolution has produced oblique normal fault segments, relay ramps, and breached relay ramps (figure 3 of Keep and McClay, 1997), with a marked geometrical similarity to the architecture shown in Figure 61. We infer that many of the WNW-trending faults have accommodated larger-scale oblique extension and that they were extensional faults and breached relay faults oblique to the earlier rift axis.

Such faults are not strictly transfer faults that separate steps in the rift or faults of opposite polarity, instead they will define small grabens with the accommodation space infilled by syn-rift sediments or volcanic rocks. These processes are interpreted to have occurred synchronously with rift infill in the hangingwall of the major NNW-trending faults, such as the Boulder–Lefroy, Bellisle, and Playa Faults. Major variability in the provenance of the Black Flag Group sediments is inferred to be linked to this early architecture (Squire et al., 2007; Blewett et al., 2010a; Squire et al., 2010). The early extensional architecture of the St Ives Goldfield is not directly analogous to classic

extensional models (e.g. Lister et al., 1986), which have been applied to other regions of the Yilgarn Craton (e.g. McIntyre and Martyn, 2005).

The relationships around some of the WNW-trending faults are complex. For example, the Achille Fault is interpreted to separate faults with different dips (this region is marked by the star in Fig. 61a). Significantly, this change from E- to W-dipping faults across the Achille Fault correlates with variations in the komatiite isopachs. Some NNE-trending, hard-linked transfer faults may also have developed internally within the zones of WNW-trending normal faults. The thickness change in the komatiite rocks near the Achille Fault could also have been caused by a steep-dipping, hard-linked transfer fault that was a D_{1e} precursor to the D_5 Alpha Island Fault system. The possible location of NNE-trending transfers are marked as dashed lines in Figure 61. However, the use of the isopach map of Kambalda Komatiite thickness is problematic in the Kambalda Dome region due to the amount of intense shortening and D_2 deformation documented (e.g. Stone et al., 2005). The early evolution of the northern segment of the field containing the Kambalda Dome is the least constrained.

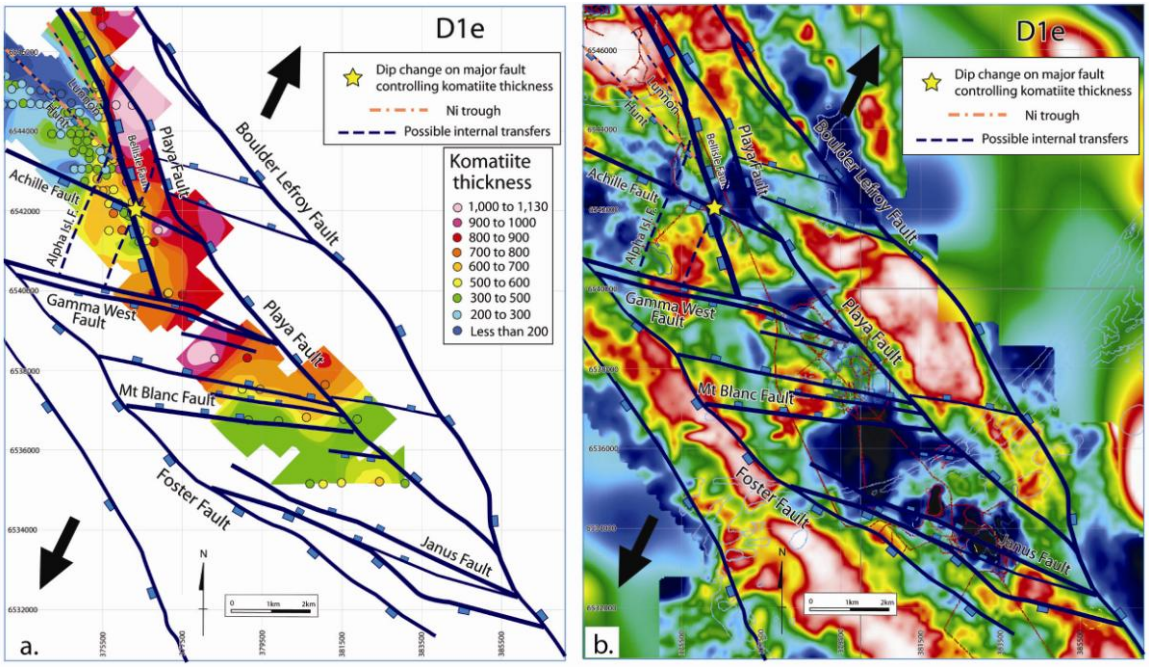

Figure 61. Inferred geometry of the early extensional fault system. This system is inferred to have extended an earlier architecture (2.9 Ga) fault architecture (Czarnota et al., 2008), with the system representing oblique extension. The Janus Fault is an additional fault to those defineed by Connors (2002) and Connors et al., (2005). This fault is over printed and obscured by later faulting events. The Ni shoots (orange dashed lines) sit in a transtensional footwall zone to a left stepping fault (Bellisle Fault): a). Early extensional architecture with isopachs of Kambalda Komatiite thickness from Connors (2002). Note the change in dip of the early faults across the Achille Fault with an associated change in komatiite thickness. The Mt Blanc Fault appears to be a key control on Komatiite and also dolerite distribution; b) Early extensional architecture with high pass filtered gravity image. Thin red lines on image represent roads and other infrastructure, white lines reflect surface topography (contours). Image from Gold Fields Pty Ltd.

The early rift architecture is also inferred to have controlled the dolerite distribution. The interaction between the faults acting as feeders for the dolerites, versus them acting as barriers to horizontal flow of magma (producing a sharp dolerite contact), is not known.

Proprietary seismic data acquired by Goldfields show that the Boulder–Lefroy fault dips to the east, with a deep sedimentary basin of Kalgoorlie Sequence rocks overlying interpreted Kambalda Sequence at depth. This would point to the Boulder–Lefroy Fault existing as a very large syn-sedimentary fault, now partially inverted, and the Kambalda anticline as a footwall anticline formed during extension and deposition of the Kalgoorlie sequence.

D_2 inversion (NE–SW compression)

The D_2 event is the first major inversion of the earlier rift architecture with reactivation of older normal faults, and also the formation of new, neoformed faults (Figs 62, 63a). The Delta Fault is an example of a fault that is inferred to have formed during D_2 shortening. The observed dextral offset in map view of the Transfer Fault across the Delta Fault (Fig. 55a) is inconsistent with the observed sinistral-reverse kinematics preserved on the Delta Fault (Fig. 56a). The offset is inferred to be related to older D_2 thrusting of the Transfer Fault of the in the hangingwall of the Delta Fault prior to the sinistral-reverse phase of movement. The offset of a steep WNW-trending plane across SW-dipping, NW-striking thrust fault will be have an apparent dextral movement in map view. A component of the development of the Kambalda Antiform also occurred during D_2 (the axis of which is marked on Fig. 63a).

Lens-like fault geometries, typical of thrust belts, developed during D_2 (Fig. 63a). The strike variations associated with these lens-like fault geometries controlled the development of later compressional and transtensional zones during later D_4 reactivation. However, one of the notable features of the structural interpretation for the Greater Revenge Area is that the critical N- and NNE-trending structures associated with the Revenge and West Revenge deposits (Figs 51, 52) appear to be bounded by WNW-trending faults (the northernmost is the Gamma Island Shear the southernmost is the Mont Blanc Fault). This suggests that these WNW-trending faults control the distribution of the N-trending fault segments.

The evolution during D_2 thrusting is inferred to have involved some initial reactivation of the D_{1e} WNW-trending faults (Fig. 62a,b). These earlier, inherited WNW-trending faults introduced pre-existing architectural complexity; however, many of these structures were not optimally oriented for slip during D_2. As a result during continued shortening, a series of newly formed (neoformed) D_2 N-trending linking faults developed that were optimally orientated for slip (Fig. 62b,c). The Repulse Shear, for example, is interpreted to be a linking thrust between two reactivated D_{1e} extensional faults (Fig. 62). These linking thrusts at a later stage became critical contractional jogs during main-stage D_4 gold. In some areas, the newly formed faults are interpreted to strongly overprint the earlier formed faults (e.g. the Janus Fault in Fig. 62).

The camp-scale geometry of WNW-trending faults controlling N-trending fault segments is inferred to be a fractal example of the regional-scale architecture. The WNW-trending faults are inferred to control not just the location of the key mafic dolerite units, but also the strike changes on regional faults, such as the Boulder–Lefroy Fault (Fig. 49). These strike changes are the key control on the location of contractional and dilational fault segments that have been linked to the location of major gold camps (e.g. Weinberg et al., 2004).

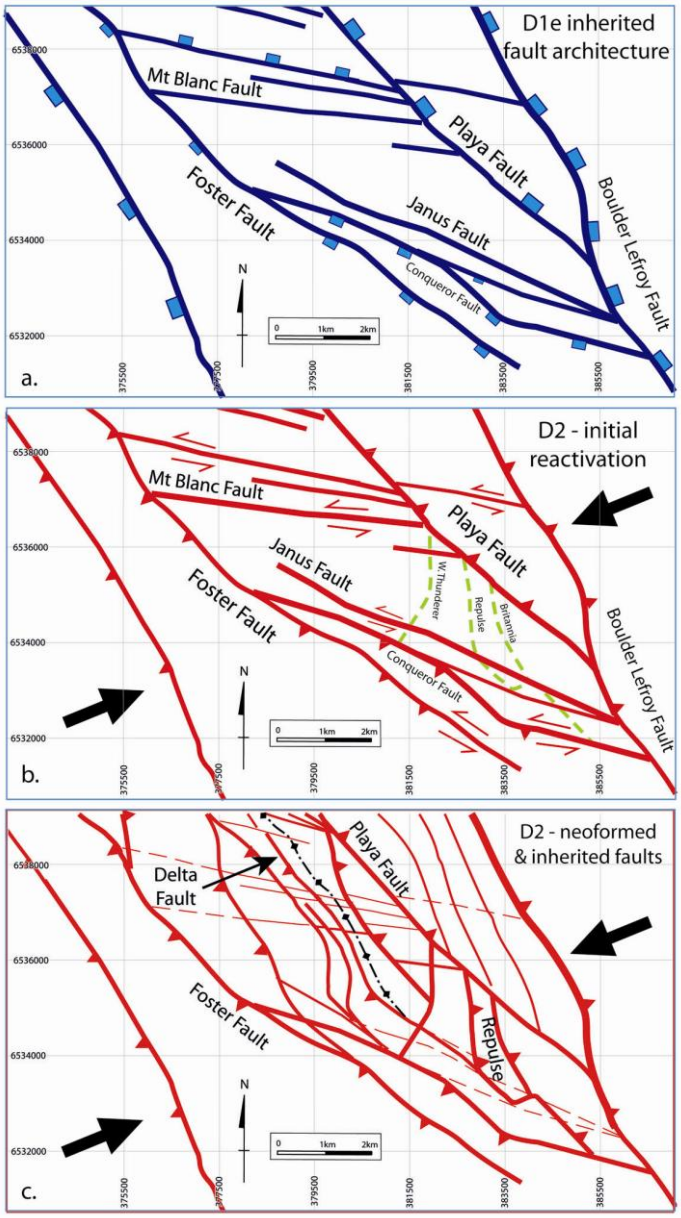

Figure 62. Interpretative model for the formation of newly formed (neoformed) and inherited faults during D_2.The Repulse Fault, which at a later stage becomes a critical contractional jog during main stage gold, initially developed as linking thrusts between two reactivated D_{1e} extensional faults. This is inferred to have created the observed geometry where the WNW-trending faults bound the N-trending fault segments. The newly formed D_2faults intensely overprint the earlier formed faults in some areas (e.g. the Janus Fault). The first phase (a) highlights the initial D_{1e} fault network, (b) shows the initial reactivation of the older D_{1e} faults during D_2, the final figure (c) highlights the formation of new faults.

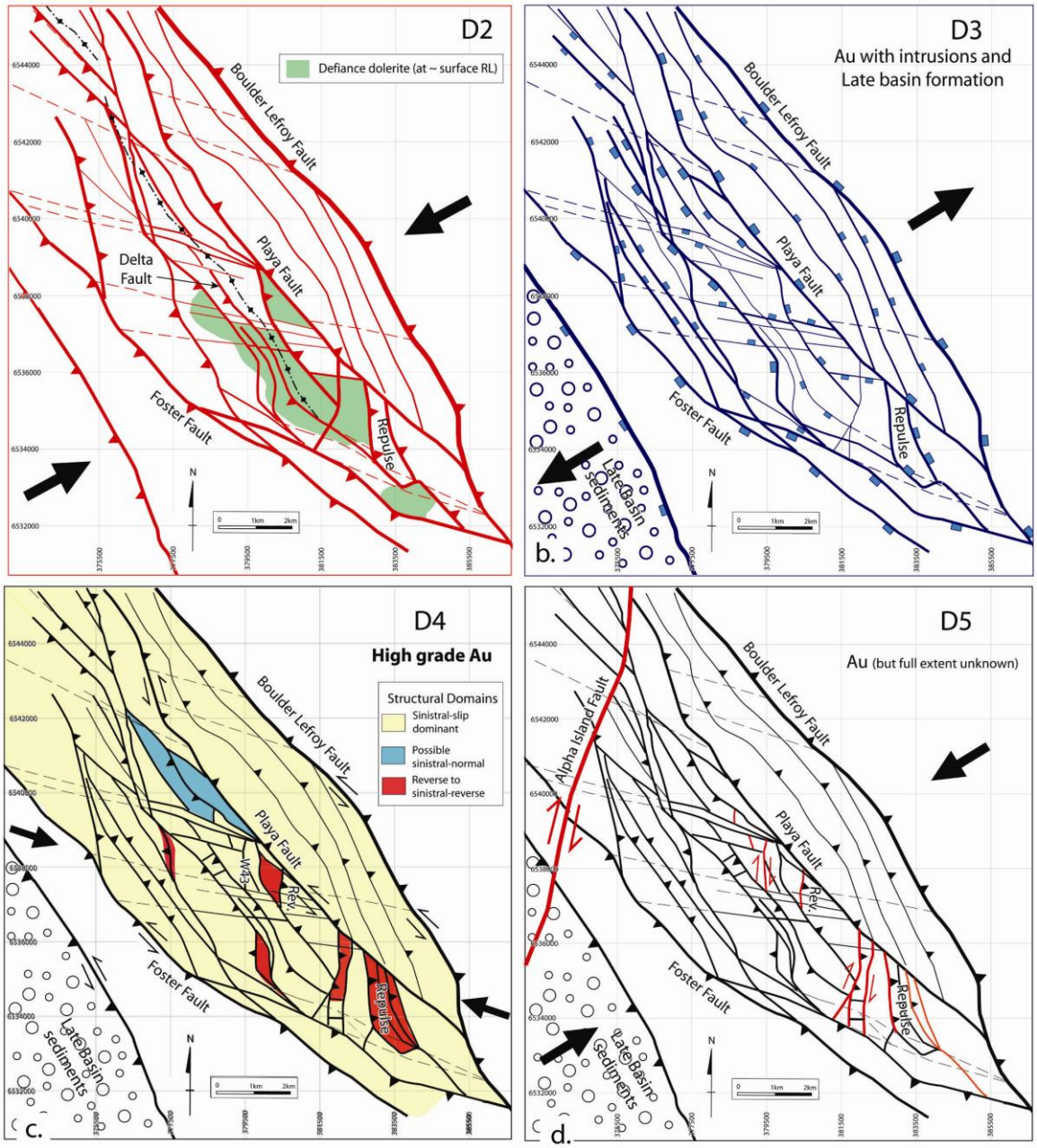

Figure 63. a) D_2 inversion of the extensional fault system. Development of the Repulse Fault occurred at this time, as did the formation of the main antiform (Kambalda Dome); b) D_3 extension. Deposition of the late basins and emplacement of related intrusions. Note the dykes near the Repulse Fault are interpreted to be utilizing an older fault trend (termed the Janus Fault in Fig. 62). Evidence for D_3 extension is preserved on the Repulse Fault (Figs 60c, 62), and also as steep-dipping normal faults in sections that control intrusive contacts and offset D_2 faults (see section lines 1-1' and 2-2' in Fig. 53); c) Main-stage gold event (D_4 in the deformation history of Blewett et al., 2010a). The W43 fault and some of the lodes within the Revenge deposit formed at this time; d) Late stage D_5 dextral reactivation. This marks the formation of the Alpha Island Fault (although this may also be a reactivated D_{1e} transfer, Fig. 62). Evidence for dextral reactivation is recorded on many N-trending structures.

D_3 Extension and late basin development (northeast–southwest extension)

The intermediate dykes that occur throughout the goldfield overprint the D_2 folds, but they are in turn overprinted by all later deformation events. The normal faults and intermediate dykes (and

associated plutons) appear to be broadly coeval. The main dyke trends, and also the early steep vein arrays on the Repulse Shear are consistent with NE–SW extension (Fig. 63b).

The D_3 extensional event is inferred to correspond to the deposition of the late basin sediments in elongate NW-trending depocentres (Nguyen, 1997; Blewett et al., 2010a). The majority of the porphyry dykes are inferred to have been emplaced during this phase, although some dykes are pre- to syn-D_2. There is also an apparent normal fault control on the shape of some of the intrusive rocks (Section line 1, Fig. 53). Some of the trends defined by gravity lows (Fig. 49) are inferred to reflect large intrusive bodies at depth that were preferentially emplaced into WNW-trending faults.

D_4 Main-stage gold mineralisation (E–W to WNW–ESE compression)

At a regional scale, previous workers have highlighted the controls that dilational and contractional jogs have had on the development of major gold systems along the NNW-trending Boulder–Lefroy Fault, which had a component of sinistral-slip during major gold mineralisation (e.g. Weinberg et al., 2004). Left-stepping strike changes have been defined as transtensional jogs, whereas right stepping strike changes have been defined as compressional jogs (Weinberg et al., 2004). Only segments of these faults are inferred to have been active during gold mineralisation, with gold deposits inferred to have formed within a seismogenic regime controlled by episodic failure of the faults (Nguyen et al., 1998; Cox and Ruming, 2004).

During main-stage gold at St Ives, defined by Blewett and Czarnota (2007) as D_4, the far field major principal stress was inferred to have been WNW–ESE (e.g. Nyugen et al., 1998; Cox and Ruming, 2004; Weinberg et al., 2005; Blewett et al., 2010b). This D_4 stress field was applied to a pre-existing D_{1e}, D_2, and D_3 architecture, resulting in a sinistral component of movement along NW- and NNW-trending faults, such as the Boulder–Lefroy Fault, Playa Fault, Bellisle, and Delta Faults. Right-stepping segments of these faults were transpressional and left-stepping segments transtensional (Fig. 63c). At this stage, new N- to NNE-trending faults also formed that crosscut older structural features (e.g. the W43 fault and some of the faults defining the Revenge lodes).

The Playa Fault is inferred to have been a major fluid conduit, and it was also a structure that produced deformation-induced permeability in its footwall and hangingwall. Fluids are also inferred to have focused along the flanks of the Kambalda Antiform and also underlying, major, dome-shaped intrusive bodies; for example under the Victory Complex (Neumayr et al., 2008).

At the local scale within the St Ives Goldfield, previous studies have highlighted the role of transpressional or contractional fault segments during the gold event (e.g. Nguyen et al., 1998). At this scale, the WNW-trending faults acted as domain boundaries to the location of the critical contractional N-trending fault segments (zones coloured red in Figure 63c). An assessment of the large-scale fault geometries (Fig. 51), highlights that the Bellisle Fault and the Gamma Island Shear have left-stepping geometries. These regions are inferred to have been transtensional zones during the syn-gold stress field (blue coloured regions in Figure 63c).

The porphyry dykes and intrusions have modified the fault architecture creating additional rheology contrasts. As a result, the D_4 deformation is not just a simple reactivation of an older fault–fracture mesh with an applied stress tensor distinct to previous deformation events. The intrusions stitched the D_2 faults in some areas, effectively removing a segment of a cohesionless fault surface from an area, with a subsequent control on how the structures where reactivated. Slip along the margins of intrusive rocks is also a key control on lode development in many areas (e.g. Mars and Santa Ana) with strike-changes of faults controlled by the intrusive contact.

D_5 late-stage dextral faulting and reactivation (northeast–southwest shortening)

During D_5, new dextral faults developed, and the major far field applied stress is inferred to have been NE–SW (Fig. 63d). These faults have been defined as D_4 faults in the terminology of Swager (1997). These N- to NE-trending dextral faults were associated with a transtensional component (NW–SE extension), with resultant development of extensive NE–SW trending vertical vein arrays in most areas that have been associated with low-grade gold in the Victory Deposit (Ruming, 2006). In the study area, the largest of the D_5 faults is the Alpha Island Fault, which has clear dextral offsets in map view (Figs 51, 52).

N–S trending fault segments were reactivated during D_5 (Fig. 63d) with associated hydrothermal alteration. The full extent of gold mineralisation associated with the D_5 event has not been ascertained; however, the 5 million ounce Mt Charlotte gold deposit to the NNW at Kalgoorlie, is inferred to be related to this event (Mueller et al., 1988), and further deposits of this type may exist within the St Ives Goldfield.

References

Archibald, NJ, Bettanay, LF, Binns, RA, Groves, DI and Gunthorpe, RJ 1978, The evolution of Archaean greenstone terrains, Eastern Goldfields Province, Western Australia: Precambrian Research, v. 6, p. 103–131.

Archibald, NJ 1985, The stratigraphy and tectonic–metamorphic history of the Kambalda ± Tramway area, WA: Western Mining Corporation, Internal Report K/2889 (unpublished).

Barley, ME and Groves, DI 1990, Deciphering the tectonic evolution of Archaean greenstone belts: the importance of contrasting histories to the distribution of mineralisation in the Yilgarn Craton, Western Australia: Precambrian Research, v. 46, p. 3–20.

Blewett, RS and Czarnota K 2007, A new integrated tectonic framework of the Eastern Goldfields Superterrane, *in* Proceedings of Geoconferences (WA) Inc. Kalgoorlie ’07 Conference, Kalgoorlie, Western Australia *edited by* FP Bierlein and CM Knox-Robinson: Geoscience Australia Record, 2007/14, p. 27–31.

Blewett, RS, Czarnota, K and Henson, PA 2010a, Structural event framework for the eastern Yilgarn Craton, Western Australia, and its implications for orogenic gold: Precambrian Research, v. 183, p. 203–229.

Blewett, RS, Miller, McLJ, Squire, R, Henson, PA and Champion, DC 2010b, Architecture and geodynamic evolution of the St Ives Goldfields, eastern Yilgarn Craton, Western Australia: Precambrian Research, v. 183, p. 275–291.

Cassidy, KF, Champion, DC, Krapež, B, Barley, ME, Brown, SJA, Blewett, RS, Groenewald, PB and Tyler, IM 2006, A revised geological framework for the Yilgarn Craton, Western Australia: Geological Survey of Western Australia, Record 2006/8, 8p.

Champion, DC and Cassidy, KF 2007, An overview of the YilgarnCraton and its evolution, *in* Proceedings of Geoconferences (WA) Inc. Kalgoorlie ’07 Conference, Kalgoorlie, Western Australia *edited by* FP Bierlein and CM Knox-Robinson: Geoscience Australia, Record 2007/14, p. 8–13.

Clark, ME, Archibald, NJ and Hodgson, CJ 1986, The structural and metamorphic setting of the Victory gold mine, Kambalda, Western Australia, *in* Gold ’86: an international symposium on the geology of gold deposits: proceedings volume *edited by* AJ Macdonald: Konsult International, Toronto, Canada, p. 243–254.

Clark, ME, Carmichael, DM, Hodgson, CJ and Fu, M 1989, Wall-rock alteration, Victory Gold Mine, Kambalda, Western Australia: Processes and P–T–X(CO2) conditions of metasomatism, *in* The geology of gold deposits: The perspective in 1988 *edited by* RR Keays,WRH Ramsay and DI Groves: Economic Geology Monthly, v. 6, p. 445–456.

Claoué-Long, JC, Compston,W and Cowden, A 1988, The age of the Kambalda greenstones resolved by ion microprobe — implications for Archaean dating methods: Earth and Planetary Science Letters, v. 89, p. 239–259.

Compston, W, Williams, IS, Campbell, IH and Gresham, JJ 1986, Zircon xenocrysts from the Kambalda volcanics: age constraints and direct evidence for older continental crust below the Kambalda–Norseman greenstones: Earth and Planetary Science Letters, v. 76, p. 299–311.

Connors, KA 2002, Lake 3D Project Results 2001–2002: Goldfields Pty Ltd, St Ives Operation, Technical Note, No. TNSIG02-002, 57p (unpublished).

Connors, KA, Stolz, EMG and Hanneson, JE 2002, Early fault architecture at St Ives: implications for Au and Ni mineralisation, *in* Applied Structural Geology for Mineral Exploration and Mining *edited by* S Vearncombe: Australian Institute of Geoscience, Bulletin, v. 36, p. 29–31.

Connors, K, Donaldson, J, Morrison, B, Davy, C and Neumayr, P 2005, The stratigraphy of the Kambalda – St Ives District: workshop notes: Goldfields Pty Ltd, St Ives Operation, Technical note No. TN SIG0329, 99p (unpublished).

Cox, SF and Ruming, K, 2004. The St Ives mesothermal gold system, Western Australia — a case of golden aftershocks?: Journal of Structural Geology, v. 26, p. 1109–1125.

Czarnota, K, Champion, DC, Cassidy, KF, Goscombe, B, Blewett, RS, Henson, PA and Groenewald, PB in press(?), Geodynamics of the Eastern Goldfields Superterrane: Precambrian Research.

Davis, BK, Blewett, RS, Squire, R and Champion, DC 2010, Architectural and geodynamic controls during Au mineralisation around the Archaean Scotia–Kanowna Dome, Kalgoorlie Terrane, Western Australia: Precambrian Research.

Dörling, SL, Dentith, MC, Groves, DI and Vearncombe, JR 1996, Mississippi Valley-type deposits of the southeast Lennard Shelf: an example of the interplay of extensional deformation, sedimentation and mineralization *in* Carbonate-Hosted Lead–Zinc Deposits *edited by* DF Sangster: Society of Economic Geology, Special Publication No. 4, p. 96–111.

Garwin, S, Hall, R and Watanabe, Y 2005, Tectonic setting, geology and gold and copper mineralization in Cenozoic magmatic arcs of Southeast Asia and the west Pacific, *in* Economic Geology 100th Anniversary Volume *edited by* J Hedenquist, R Goldfarb and J Thompson: Society of Economic Geology, Littleton, Colorado, USA, p. 891–930.

Gresham, JJ and Loftus-Hills, GD 1981, The geology of the Kambalda nickel field: Economic Geology, v. 76, p. 1373–1416.

Hammond, RL and Nisbet, BW 1992, Towards a structural and tectonic framework for the Norseman–Wiluna Greenstone belt, Western Australia, *in* The Archaean: Terrains, Processes and Metallogeny *edited by* JE Glover and SE Ho: University of Western Australia, Publication 22, p. 39–50.

Keep, M and McClay, KR 1997, Analogue modelling of multiphase rift systems: Tectonophysics, v. 273, p. 239–270.

Kositcin, N, Brown, SJA, Barley, ME, Krapež, B, Cassidy, KF and Champion, DC 2008, SHRIMP U–Pb zircon age constraints on the Late Archaean tectonostratigraphic architecture of the Eastern Goldfields Superterrane, Yilgarn Craton, Western Australia: Precambrian Research, v. 161, p. 5–33.

Krapež, B, Brown, SJA, Hand, J, Barley, ME and Cas, RAF 2000, Age constraints on recycled crustal and supracrustal sources of Archean metasedimentary sequences, Eastern Goldfields Province, Western Australia: evidence from SHRIMP zircon dating: Tectonophysics, v. 322, p. 89–133.

Krapež, B and Barley, ME 2008, Late Archaean synorogenic basins of the Eastern Goldfields Superterrane, YilgarnCraton, Western Australia. Part III: signatures of tectonic escape in an arc–continent collision zone. Precambrian Research: v. 161, p. 183–199.

Krapež, B and Hand, JL 2008, Late Archaean deep-marine volcaniclastic sedimentation in an arc-related basin: The Kalgoorlie Sequence of the Eastern Goldfields Superterrane, Yilgarn Craton, Western Australia: Precambrian Research, v. 161, p. 89–113.

Lister, GS, Etheridge, MA and Symonds, PA 1986, Detachment faulting and the formation of passive continental margins: Geology, v. 14, p. 246–250.

Love, DA, Clark, AH and Glover, JK 2004, The lithologic, stratigraphic, and structural setting of the giant Antamina copper–zinc skarn deposit, Ancash, Peru: Economic Geology, v. 99, p. 887–916.

Lund, K 2008, Geometry of the Neoproterozoic and Paleozoic rift margin of western Laurentia: implications for mineral deposit settings: Geosphere, v. 4, p. 429–444.

McIntyre, JR and Martyn, JE 2005, Early extension in the Late Archaean northeastern Eastern Goldfields Province, Yilgarn Craton, Western Australia: Australian Journal of Earth Science, v. 52, p. 975–992.

Miller, J, Blewett, R, Tunjic, J and Connors, K 2010, The role of early formed structures on the development of the world class St Ives Goldfield, Yilgarn, WA: Precambrian Research, v. 183, p. 292–315.

Mueller, AG, Harris, LB and Lungan, A 1988, Structural control of greenstone-hosted gold mineralization by transcurrent shearing — a new interpretation of the Kalgoorlie mining district, Western Australia: Ore Geology Reviews, v. 3, p. 359–387.

Neumayr, P, Walshe, J, Hagemann, S, Petersen, K, Roache, A, Frikken, P, Horn, L and Halley, S 2008, Oxidized and reduced mineral assemblages in greenstone belt rocks of the St. Ives gold camp, Western Australia: vectors to high-grade ore bodies in Archaean gold deposits?: Mineralium Deposita, v. 43, p. 363–371.

Nelson, DR 1997, Evolution of the Archaean granite–greenstone terranes of the Eastern Goldfields,Western Australia: SHRIMP U–Pb zircon constraints: Precambrian Research, v. 83, p. 57–81.

Nguyen PT 1997, Structural controls on gold mineralisation at the Revenge mine and its tectonic setting in the Lake Lefroy area, Kambalda, Western Australia: The University of Western Australia, Perth, Western Australia, PhD thesis (unpublished).

Nguyen, PT, Cox, SF, Harris, LB and Powell, CM 1998, Fault-valve behaviour in optimally oriented shear zones: An example at the Revenge gold mine, Kambalda, Western Australia: Journal of Structural Geology, v. 20, p. 1625–1640.

Prendergast, K 2007, Application of lithogeochemistry to gold exploration in the St Ives goldfield, Western Australia: Geochemistry: Exploration, Environment, Analysis, v. 7, p. 99–108.

Rasmussen, B, Mueller, AG and Fletcher, IR 2009, Zirconolite and xenotime U–Pb age constraints on the emplacement of the Golden Mile Dolerite sill and gold mineralization at the Mt Charlotte mine, Eastern Goldfields Province, Yilgarn Craton, Western Australia: Contributions to Mineralogy and Petrology, v. 157, p. 559–572.

Ruming, KJ 2006, Controls on lode gold mineralisation in the Victory Thrust Complex, St Ives Goldfield, Western Australia: The University of Newcastle, Newcastle, New South Wales, PhD thesis (unpublished).

Squire, RJ, Cas, RAF and Champion, DC 2007 The Black Flag Group: a vector to ore at St Ives, *in* Proceedings of Geoconferences (WA) Inc. Kalgoorlie '07 Conference, Kalgoorlie, Western Australia *edited by* FP Bierlein and CM Knox-Robinson: Geoscience Australia, Record 2007/14, p. 39–43.

Squire, RJ, Allen, CM, Cas, RAF, Campbell, IH, Blewett, RS and Nemchin, AA in press, Transition from greenstone volcanism to cratonisation in the eastern Yilgarn Craton, Western Australia, revealed by provenance characteristics of late Archaean sedimentary successions: Precambrian Research.

Stone,WE, Beresford, SW and Archibald, NJ 2005, Structural setting and shape analysis of nickel sulfide shoots at the Kambalda Dome, Western Australia: implications for deformation and remobilization: Economic Geology, v. 100, p. 1441–1455.

Swager, CP 1997, Tectono-stratigraphy of late Archaean greenstone terranes in the southern Eastern Goldfields, Western Australia: Precambrian Research, v. 83, p. 11– 42.

Vanderhor, F anad Groves, DI 1998, Systematic documentation of Archaean gold deposits of the Yilgarn block: Minerals and Energy Resource Institute of Western Australia, Report 193, Project M195.

Vielreicher, NM, Groves, DI, Snee, LW, Fletcher, IR and McNaughton, NJ 2010, Broad synchroneity of three gold mineralization styles in the Kalgoorlie Gold Field: SHRIMP, U–Pb, and $^{40}Ar/^{39}Ar$ geochronological evidence: Economic Geology, v. 105, p. 187–227.

Watchorn, RB 1998, Kambalda – St Ives gold deposits, *in* Geology of Australian and Papua New Guinea Ore Deposits *edited by* DA Berkman and DH Mackenzie: The Australasian Institute of Mining and Metallurgy, Melbourne, Victoria, p. 243–254.

Weinberg, RF, Moresi, L and van der Borgh, P 2003, Timing of deformation in the Norseman–Wiluna Belt, Yilgarn Craton, Western Australia: Precambrian Research, v. 120, p. 219–239.

Weinberg, RF, Hodkiewicz, PH and Groves, DI 2004, What controls gold distribution in Archean terranes?: Geology, v. 32, p. 545–548.

Weinberg, RF, Van der Borgh, P, Bateman, RJ and Groves, DI 2005, Kinematic history of the Boulder–Lefroy Shear Zone system and controls on associated gold mineralization, Yilgarn Craton, Western Australia: Economic Geology, v. 100, p. 1407–1426.

Williams, PR and Currie, KL 1993, Character and regional implications of the sheared Archaean granite–greenstone contact near Leonora, Western Australia: Precambrian Research, v. 62, p. 343–367.

Williams, PR and Whitaker, RAJ 1993, Gneiss domes and extensional deformation in the highly mineralised Archaean Eastern Goldfields Province, Western Australia: Ore Geology Reviews, v. 8, p. 141–162.

Wong, T 1986, The thermal effect of granitoid emplacement on the greenstones of the Kambalda Dome: The University of Western Australia, Perth, Western Australia, BSc (Hons) thesis, 153p (unpublished).

Chapter 6 — St Barbara Mines: the geological setting of Marvel Loch

S Shenton

St Barbara Limited

Introduction

Marvel Loch is the largest of the many shear-hosted gold deposits found within the Southern Cross greenstone belt. The Marvel Loch gold mine is located 600 m east of the Marvel Loch Township and 35 km south of Southern Cross. Prospectors Lenneburg, Williamson, and Marksman first discovered gold there in 1905.

St Barbara Ltd purchased the Yilgarn operations off Sons of Gwalia in August 2004. Currently, Marvel Loch has produced in excess of **2.5 Moz Au**.

Geological setting

The Southern Cross Province comprises several greenstone belts with one of the larger ones being the 200 km long Marvel Loch greenstone belt, running from north of Bullfinch, through Southern Cross town, Marvel Loch, Nevoria, Forrestania, and SE of Hyden (Fig. 64). Like many of the other greenstone belts, this is strongly attenuated in the NNW direction. Rock units near Marvel Loch trend NNW parallel to the greenstone belt margins, and are inferred to young away from the Ghooli granite dome. Multiple periods of folding have shortened the greenstone belt, generated district-scale folds, and accompanied faulting that has juxtaposed rock units at slightly oblique angles across the fault zones.

Marvel Loch geology

The Marvel Loch gold deposit is hosted by a steep westerly dipping package of ultramafic, mafic, and sedimentary rocks to the west, with gabbro, dolerite, and sedimentary rocks to the east (Fig. 64). In places, units are overturned and may dip steeply to the east. Rock type identification is based on textures, mineralogy, and whole rock geochemistry. In many greenstone belts, all three are well preserved and useful. However, around Marvel Loch high strain has overprinted some early textures, high grade metamorphism has developed new minerals, and alteration has modified rock chemistry. All of the stratigraphy has been overprinted by amphibolite facies metamorphism and deformed by a major shear zone (the Marvel Loch Shear Zone).

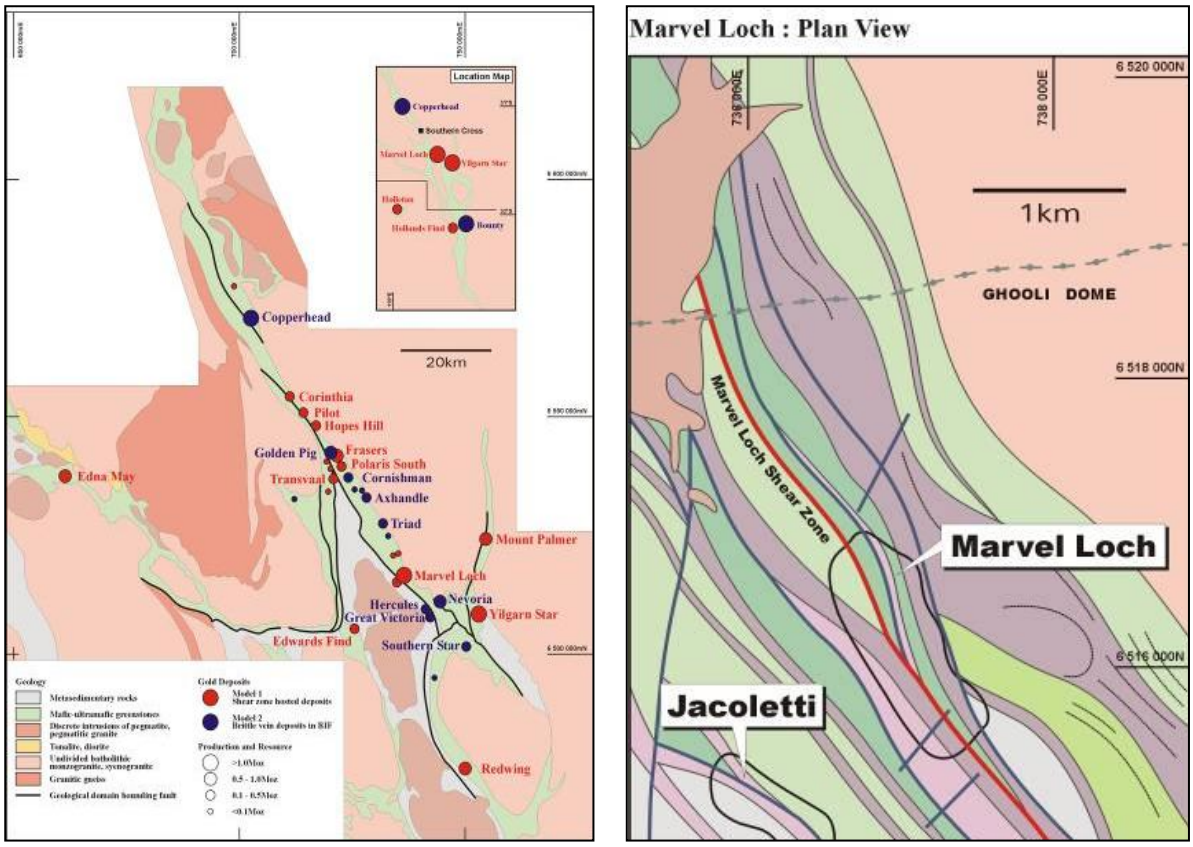

Figure 64. At left, simplified geology of the Southern Cross greenstone belt showing the distribution of gold deposits. At right, detailed geology of the Marvel loch mine area.

Gold mining is focused in ten steeply plunging ore pipes: four in the north, and three each in central and southern areas (Figs 65, 66). These pipes generally plunge 60–80^{o} south, have dimensions of tens of metres on a horizontal mine level and are continuous down plunge for over 500 m. Gold occurs in quartz veins and in altered wallrocks with sulphide minerals. The dominant sulphides are pyrrhotite, arsenopyrite, and pyrite.

The greatest challenge facing the Marvel Loch geology team today is the presence of large granitoid sills which crosscut mineralisation in all areas of the mine (Fig. 67). Their intrusion was guided by pre-existing faults, and they are themselves faulted along chlorite-bearing surfaces. At the current mining level in the south (650 m below the pit surface), a large pegmatite approximately 80–100 m thick has displaced mineralisation. This pegmatite layer has been conceptually interpreted to affect the centre and south lodes below 200 mRl and, therefore, drilling has commenced to determine the geological setting below this pegmatite.

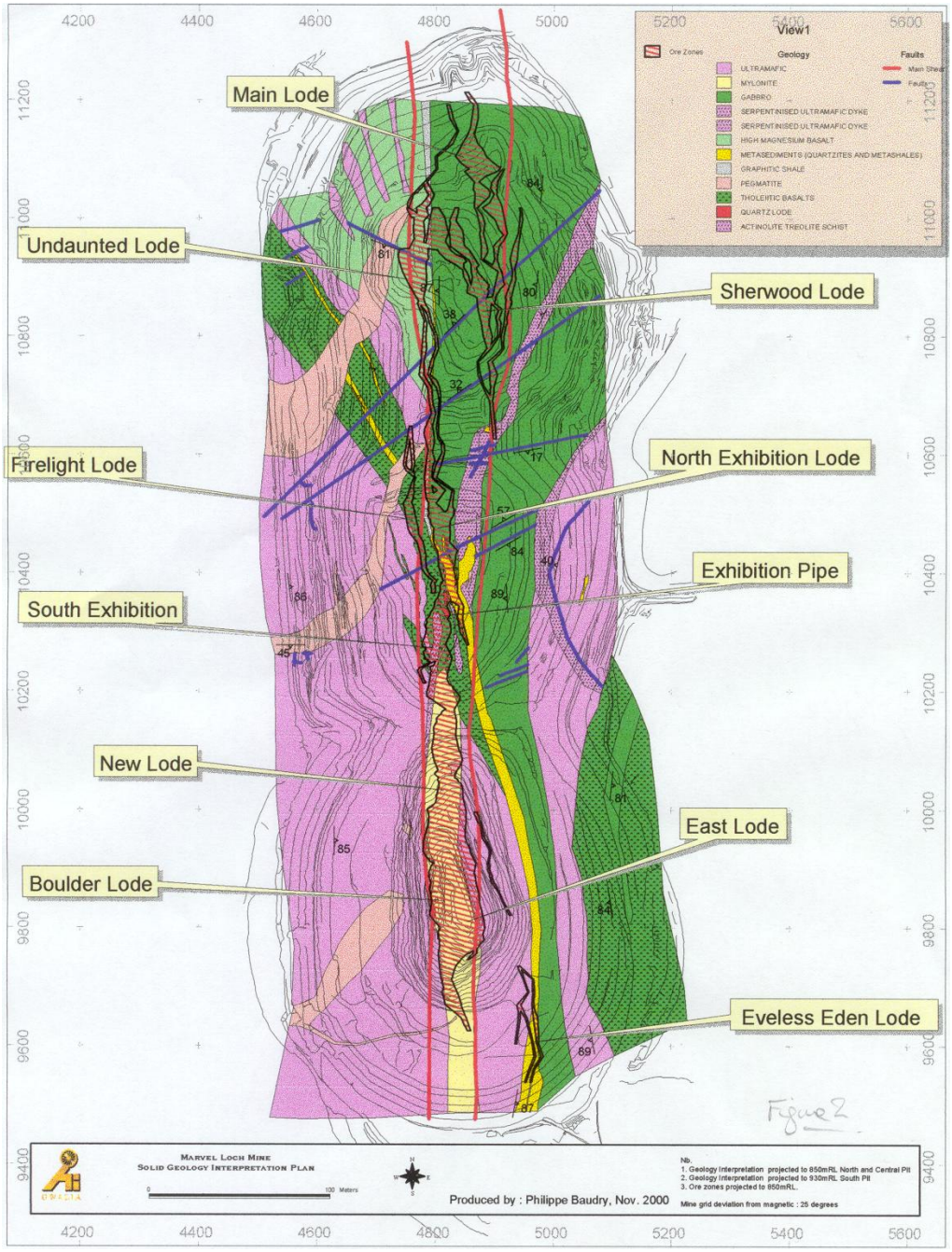

Figure 65. Plan geology of the Marvel Loch Mine showing the position and names of the main ore bodies with the pit shell shown for reference.

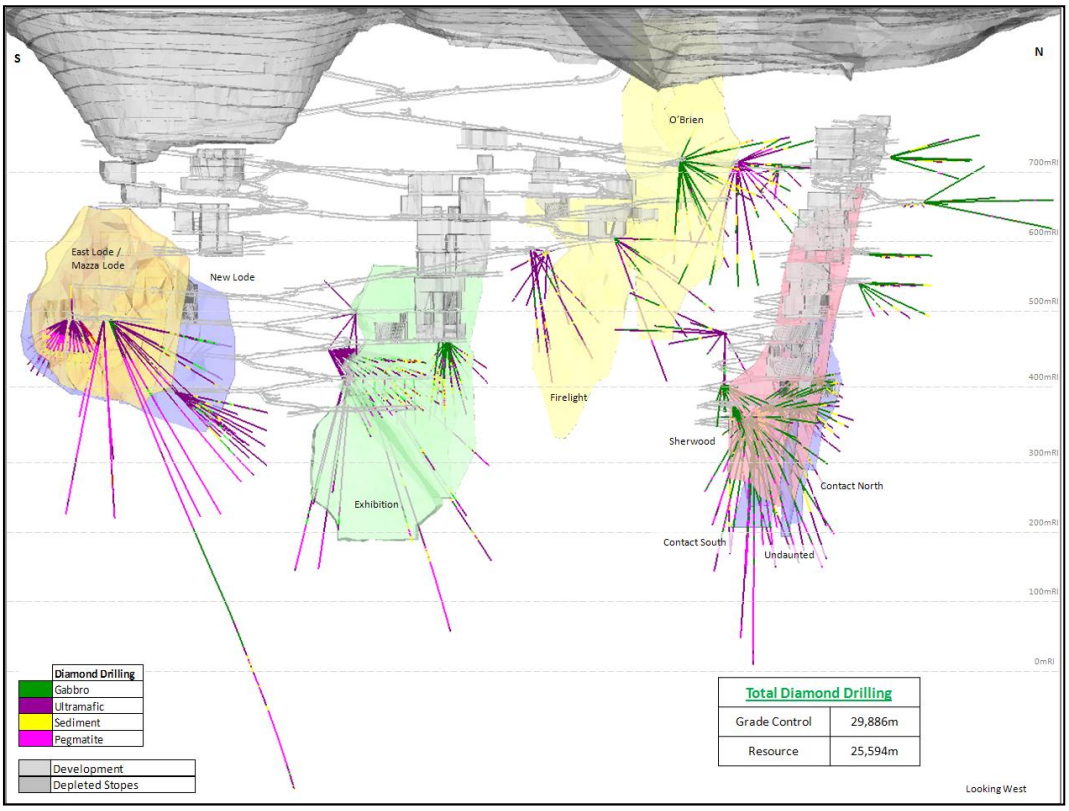

Figure 66. Long section looking west through the Marvel Loch 3D model showing the depth extent of pits, underground development, stopes, and position and shape of orebodies.

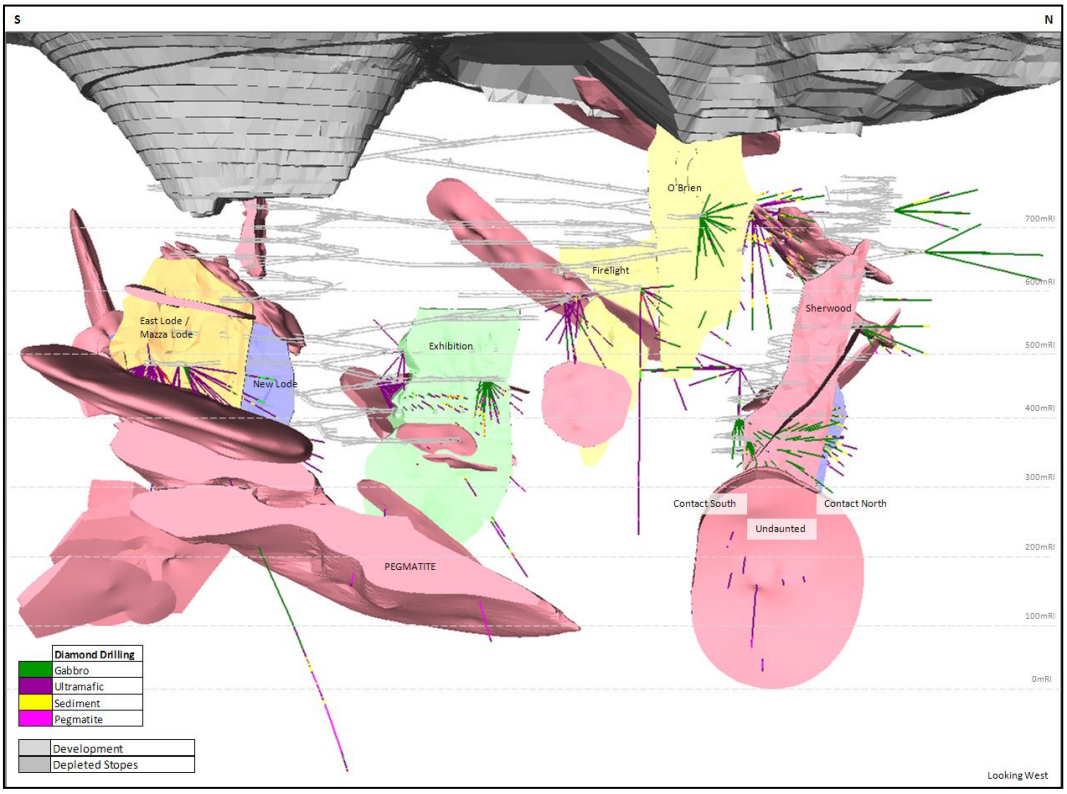

Figure 67. Same long section as for Figure 66, with the interpreted shape of post-mineralisation pegmatites shown.

Chapter 7 — The Flying Fox Ni–Cu–PGE komatiite-hosted deposit, Forrestania Greenstone Belt

J Collins, TC McCuaig

Centre for Exploration Targeting, School of Earth and Environment, The University of Western Australia

Geological setting

The Flying Fox deposit is located about 350 km east-southeast of Perth in the Forrestania greenstone belt, which is the southern extension of the Southern Cross greenstone belt, Southern Cross Domain, Youanmi Terrane in the Archean Yilgarn craton of Western Australia (Gee, 1979; Porter and McKay, 1981; Chin et al., 1984; Cassidy et al., 2006). The Forrestania belt trends approximately north–south over a length of 250 km, ranges in width from 5 to 30 km, and is flanked to the east by the Eastern Goldfield Superterrane and to the west by the South West Terrane (Gee, 1979; Cassidy et al., 2006). Six ultramafic belts are identified in the Forrestania greenstone belt (Fig. 68): the Western, Mid-Western, Takashi, Central Fold, Mid-Eastern, and Eastern, with the Flying Fox deposit located in the Western ultramafic belt (Perring et al., 1995, 1996).

The stratigraphy of the Forrestania greenstone belt consists of: 1) a lower succession of predominantly tholeiite and komatiite metavolcanic sequences intercalated with banded iron-formation (BIF), sulfidic chert layers, and localized felsic metasedimentary units; and 2) an uppermost succession of fine-grained clastic sedimentary rocks (pelitic to psammitic schists) with minor BIF horizons, located in the centre of the belt (Fig. 68). The stratigraphy has been intruded by granitic rocks which have exploited pre-existing faults, and by east–west trending dolerite dikes (Porter and McKay, 1981; Chin et al., 1984; Frost, 2003).

Lithostratigraphy and regional metamorphism

The stratigraphy at the Flying Fox deposit is interpreted to represent an east-younging succession of four distinct lithological units from east to west (Figs 69, 70): 1) quartzofeldspathic sedimentary rocks (footwall sedimentary rocks) intercalated with minor basaltic rocks, 2) a cumulate-rich compound komatiite flow sequence (terminology of Barnes, 2006b) comprising a differentiated channel facies grading upwards from olivine–tremolite rocks (ortho- and mesocumulates) to tremolite–chlorite rocks (non-cumulates), with massive sulfides located at or near the base of the package, 3) a komatiite–basalt thin flow facies sequence, where non-cumulate komatiites and high-magnesium basalts (tremolite–actinolite rocks) dominate, and 4) biotite–garnet schist (hangingwall sedimentary rocks) occupying the central portion of the Forrestania greenstone belt (Collins et al., 2010; Figure 68).

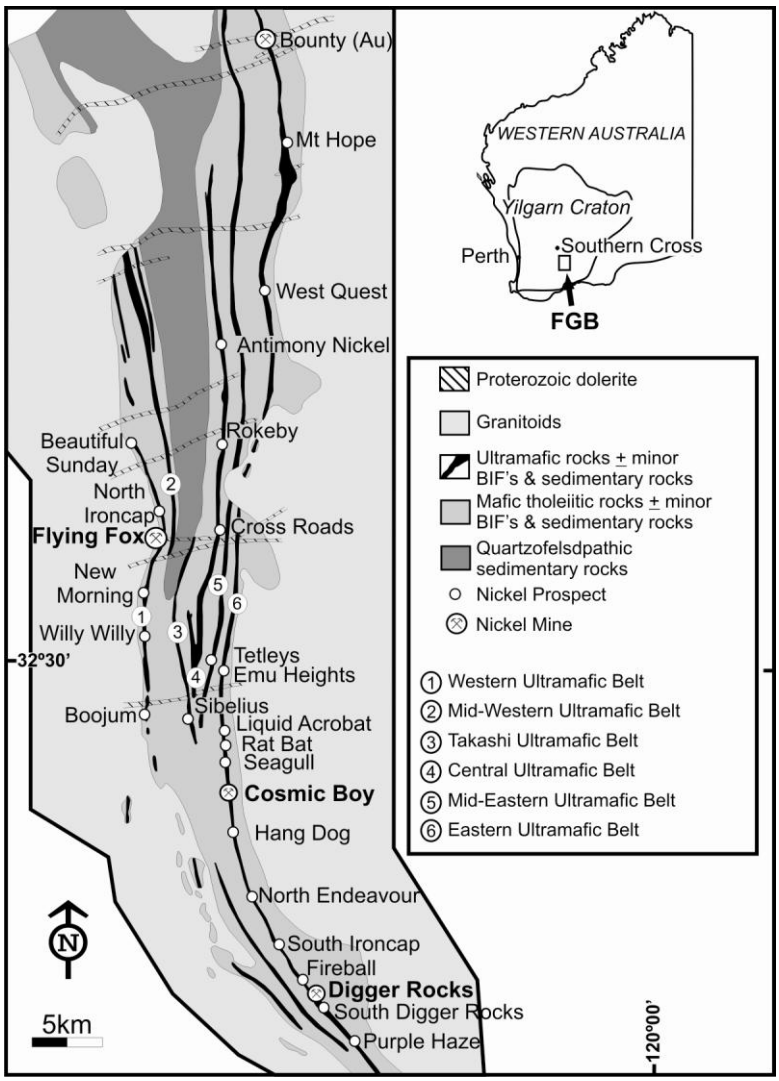

Figure 68. Simplified geological map of the Forrestania greenstone belt (FGB) in the Yilgarn craton showing the distribution of the ultramafic belts, and location of nickel prospects and mines, including the Flying Fox nickel deposit (modified after Perring et al., 1997).

The Forrestania greenstone belt has experienced upper amphibolite facies metamorphism with peak metamorphic conditions, interpreted by Porter and McKay (1981), estimated at 655° ± 30°C and 4.0 ± 1.0 kb. Regional metamorphism resulted in widespread textural destruction; however, some diagnostic textures (e.g. olivine and pyroxene spinifex textures in komatiites, olivine adcumulates, sedimentary bands in BIF) and structures (e.g. pillow rims in basalts) have been preserved in low-strain domains (Perring et al., 1997).

Mining history and production

The Flying Fox deposit was discovered in 1977 at the end of the late 1960s to early 1970s nickel boom, and Outokumpu Mining Australia Pty Ltd (OMA) subsequently mined the deposit during 1994–1997 producing c. 240 kt @ 3.2 percent Ni. Three exploration holes (c. 700 m each in length) were drilled in 1994–1995 to test for a potential fault-offset ore position (now identified as T1) located about 300–350 m east of the ore shoot. One drillhole intersected disseminated nickel

sulfides, whereas the other two drill holes intersected a barren contact. Although strong geophysical anomalies were indicated, they were not considered of sufficient interest to warrant follow-up drill testing (Frost et al., 2006). In 2002, Western Areas NL re-surveyed and re-interpreted the stratigraphy and structural overprint of the deposit ,which led to a significant new discovery, whereby the first concealed ore shoot T1 was defined in 2004. Drilling to date has successfully delineated a current mineral resource of 2 415 700 t of ore at an average grade of 4.76 percent nickel.

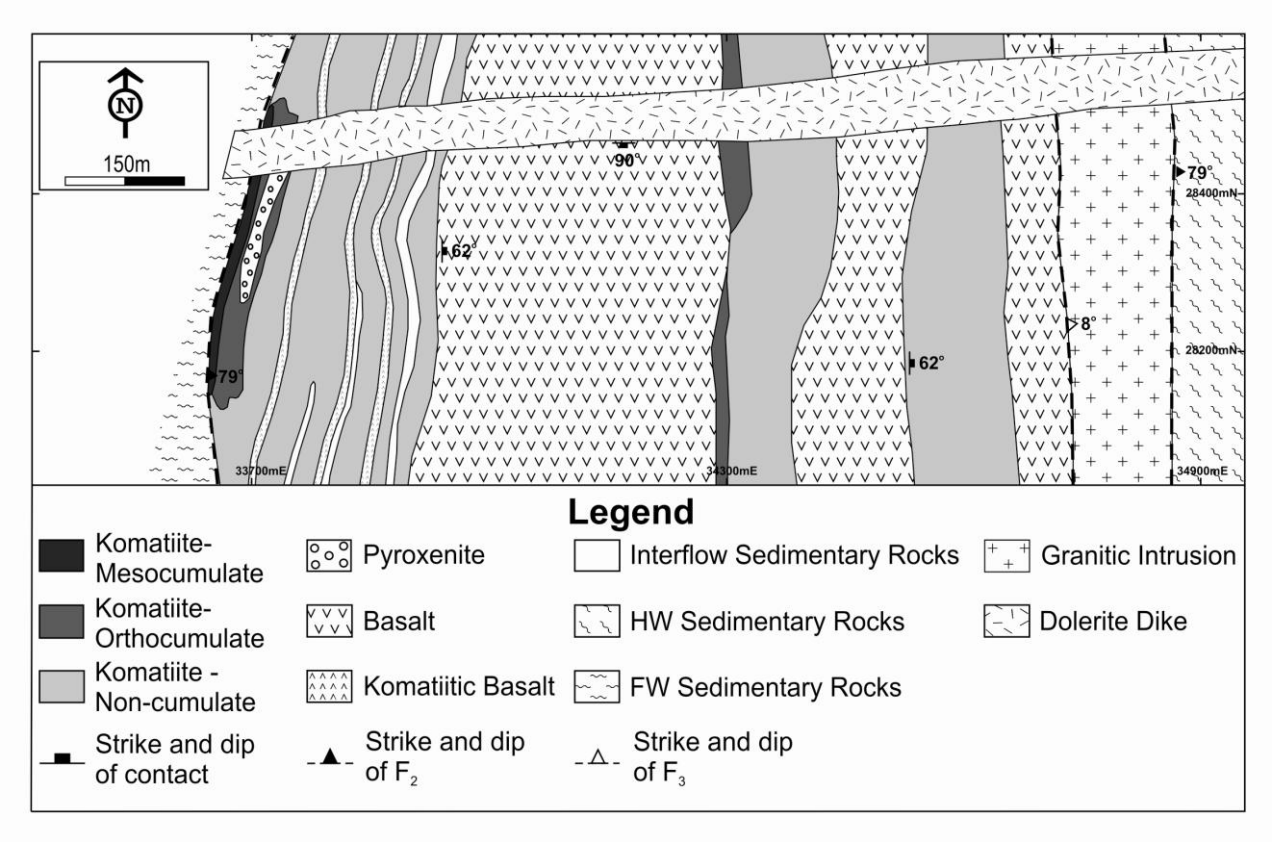

Figure 69. Geological plan map showing the distribution of rock types, nickel sulfide ore shoots, and major structures at the Flying Fox deposit. Lithological contacts and structural elements are projected from drill holes to ~1350 mRL (120 m below surface), as granitic rocks dominate from 1350 mRL to surface. Detailed geology is limited along the eastern margins as wedge drilling is concentrated at depth (modified after Perring et al., 1997; HW = Hangingwall, FW = Footwall).

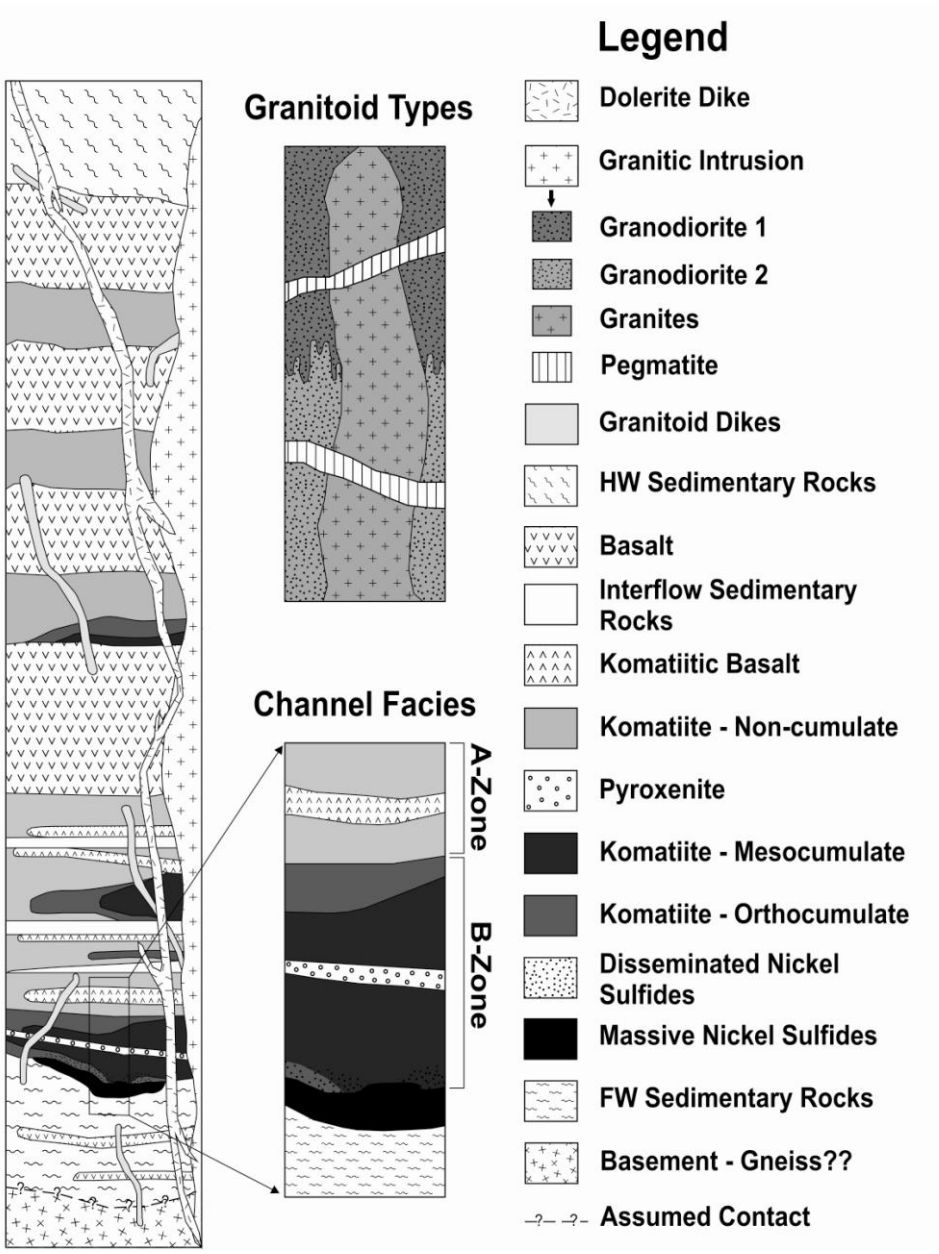

Figure 70. Lithostratigraphic profile through the Flying Fox deposit based on diamond drill hole interpretation. The basal komatiites are interpreted to be a differentiated channel flow, where A- and B-zones are identified (as defined by Pyke et al., 1973). The differentiated channel flow is directly overlain by an interflow sedimentary unit separating this zone from an overlying komatiitic-basalt sequence which is intercalated with interflow sedimentary rocks and high-magnesium basalts. The massive sulfides are concentrated along the footwall sedimentary and basal komatiite contact and are directly overlain by discontinuous zones of disseminated sulfides within the cumulate komatiitic rocks. The granitic rocks crosscut the stratigraphy and comprise at least eight types, and all stratigraphy is crosscut by the Proterozoic dolerite dike.

Deformation

The structural history of the Flying Fox deposit has been interpreted from diamond drill core and underground mapping (Collins et al., 2010), and five deformation events have been identified (Table 2; Fig. 72). The D_1 to D_3 events are interpreted to be the result of east–west compression and are coincident with upper amphibolite facies metamorphism.

During D_1 to D_2, the coaxial and non-coaxial deformation at the komatiite/sulfide and footwall sedimentary rock contact has flattened and sheared the sulfides along and off contact. During the D_3 event, the main ore body was faulted and offset up to a maximum of 350 m by flat-lying thrusts, resulting in the current location of the ore shoots (Fig. 70). The D_4 event is characterized by the emplacement of the granitic magma post-peak metamorphism during extension, which resulted in dilation along the footwall sedimentary contact creating a brittle–ductile fault and displacing the underlying stratigraphy.

The dilation of the granitic magma has created the T0 and T4 ore shoots, whereas the T5-pipe ore shoot resulted from entrainment and relocation of a portion of the T5 ore shoot by granitic magma c. 20 m to the east along a flat-lying thrust. The granitic rocks locally incorporated the sulfide ore during this event, which has created the atypical granite-hosted nickel sulfides (Fig. 70). Although the sulfides were remobilized during deformation, the massive ore is currently positioned at the base of the high-Mg komatiites (differentiated komatiites, A and B zone observed; Figs 70, 71) and is directly overlain by disseminated sulfides, which indicates that, in general, the ore shoots have been remobilized locally off their primary contact. Textures and mineralogy of alteration assemblages identified by Collins et al. (2010) indicate that fluid flow was coeval with sulfide remobilization (Table 2).

Nickel sulfide mineralisation

Nickel sulfide mineralisation at the Flying Fox deposit takes the form of a typical Type 1 sulfide-rich ore body (Lesher and Keays, 2002; Barnes, 2006) located as thin, tabular high-grade ore shoots, which, for the most part, directly underlie the lowermost komatiitic unit in the stratigraphy (Figs 69, 70). The ore is tectonically dismembered into as many as 11 discrete ore shoots that make up T0, T1/T2, T4, T5, T6/T7, and the original Flying Fox ore shoot. The ore shoots are thin (generally 2–5 m wide) and comprise varying proportions of massive, breccia, and vein/stringer sulfides. The Flying Fox deposit as a whole is a high-grade, high tonnage deposit with the majority of economic resources accounted for by massive sulfides.

Table 2. An integrated chronology of events at the Flying Fox deposit including the timing of metamorphism, magmatism, and sulfide remobilization with associated hydrothermal alteration assemblages (D_{Reg} = deformation events observed regionally, D_{FF} = deformation events observed at Flying Fox; am – amphibole, bt – biotite, cal – calcite, cb – carbonate, chl – chlorite, di – diopside, fuc – fuchsite, grt – garnet, ms – muscovite, pn – pentlandite, py – pyrite, qtz – quartz, ser – sericite, sil – sillimanite).

EVENT	DEFORMATION	METAMORPHISM	MAGMATISM	NICKEL SULFIDES	HYDROTHERMAL ALTERATION
D_{0Reg}	Ultramafic and mafic volcanism and sediment deposition			Nickel mineralisation synchronous with komatiite emplacement	Sea floor alteration of basalts and possibly komatiites resulting in dp–grt–qtz–cb veins
D_{1aReg}	E–W compression tilting the stratigraphy producing a dominant foliation (S_{1a}) dipping 62° towards 92°	Prograde metamorphism (upper amphibolite facies) and contact metamorphism (associated with the granitoid dikes)	Intrusion of granitoid dikes late D_{1a}		
D_{1bFF}	Continued E–W compression has resulted in coaxial flattening at the basalt/hangingwall sedimentary rock contact and footwall sedimentary rock and massive sulfide/komatiite contact defined by a steep foliation (S_{1b}) dipping 72° towards 92°			Sulfides revert to *Mss* and squeeze along S_{1b} fabric and off-contact	fuc in FW sedimentary rocks and sulfides, alteration haloes around stringer/vein sulfides, py–pn intergrowths, di–cb–am–qtz–grt veins in basalt and hangingwall sedimentary rocks aligned with S_{1b}
D_{2FF}	E–W extension (localized) resulting in dip-slip shearing along the coaxial flattened zones displaying normal offset	Continued prograde metamorphism		Continued remobilization during shearing	di–cb–am–qtz ± grt alteration in the basalt associated with F_3 shear
D_{3FF}	E–W compression resulted in NNE–SSW striking thrusts (F_3) that offsets the ore body by up to 250m, defined by a shallow foliation (S_3) dipping 8° towards 94°, and a crenulation cleavage			Sulfides smeared along F_3 shears, S_3 foliations and fold hinge of crenulation cleavage	
D_{4FF}	E–W extension resulting in two brittle ductile faults (F_4) at the contact between the granitic rocks and the footwall sedimentary rocks (T0 and T4) dipping 60° towards the east	Retrograde metamorphism and contact metamorphism (associated with granitic rock intrusion)	Intrusion of granitic rocks creating the two F_4 faults	Sulfides entrained in granitic rock creating breccia sulfides, smeared along F_4 fault planes, offset into the footwall sedimentary rocks, and encapsulated by granite (T5)	chl alteration of granite, qtz veining, fel phenocrysts in the granite altered to sericite, py–pn intergrowths in sulfides, bt rimming stringer sulfides, fuc in granite and sulfides
D_{5FF}	Brittle faulting observed in all rock types	Contact metamorphism (associated with dolerite dike intrusion)	Intrusion of E–W trending dolerite dike		chl–cal–ser coating F_4 faults

Layering of ore types typical of komatiite-hosted deposits (Naldrett, 1973), comprising massive sulfides overlain by matrix-textured and disseminated sulfides, is not observed at the Flying Fox deposit. However, there are thin discontinuous zones of disseminated sulfide, for example the T5 disseminated ores, directly overlying massive sulfides. The matrix-textured ores, which are observed at deposits including the Lunnon Shoot at Kambalda (Ewers et al., 1972), Alexo (Naldrett, 1973), and Kattiniq in the Raglan belt (Barnes et al., 1982; Lesher, 2007), are absent at Flying Fox, and commonly ore types occur in isolation from each other and from the komatiite host rock, especially in areas of extreme structural dislocation (Collins et al., 2010).

The T0, upper T1, T4, and upper T5 ore shoots are located on the footwall sedimentary and granitic rock contact that rolls from shallowly east dipping to a steeper 60° to the east (Fig. 71). The lower portion of T1 and T5, and T2 ore shoots are located at the base of the komatiites directly overlying the footwall sedimentary rocks and dip between 70–90° to the east (Fig. 71). Some nickel sulfide mineralisation associated with T1/T2 and T5 is located off-contact in fault splays within the footwall sedimentary rocks. The upper part of the T5 ore shoot has a pipe-like geometry, and is almost entirely enveloped by granite-pegmatite (Fig. 71). The T5 ore shoot is the largest defined of the ore shoots discovered to date and is still open at depth.

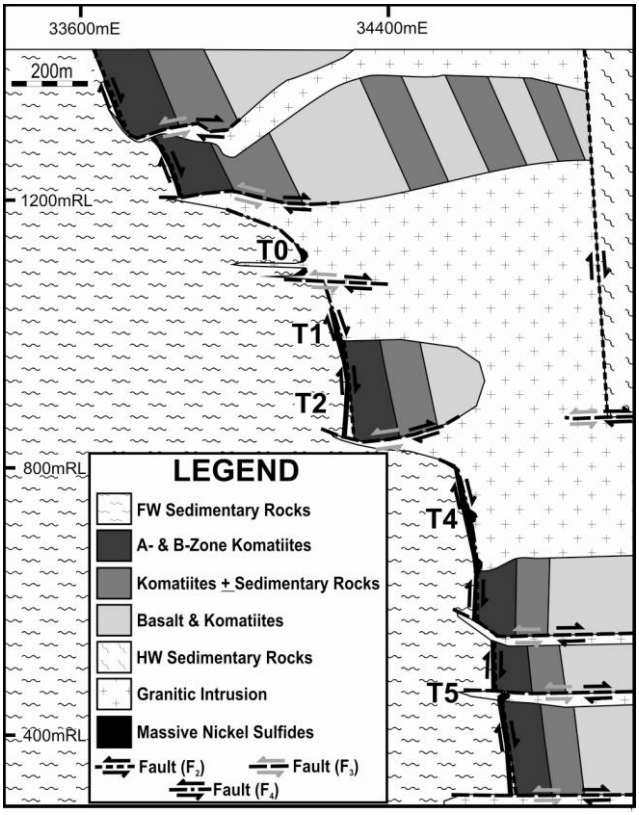

Figure 71. Simplified north-facing schematic crosssection through the Flying Fox deposit illustrating the location of T0, T1, T2, T4, and T5 ore shoots in relation to stratigraphy. Note that the massive sulfide ore shoots are dominantly located between the footwall sedimentary rock and komatiite, or footwall sedimentary rock and granite contacts, and the stratigraphy is steeper at these contacts. The flat lying faults show a dominant reverse motion, however do revert to normal motion during later extension when the granitic rocks intruded.

Figure 72. Block models showing integrated history of the Flying Fox deposit, including volcanism, deformation, and magmatism: a) D_0 – primary volcanism producing nickel sulfide mineralisation in an interpreted trough structure. Basement contact is inferred, and all stratigraphy was essentially horizontal when extruded/deposited; b) D_{1areg} – east–west compression resulted in tilting of the stratigraphy (60° towards the east). Granitoid dike intrusions syn- to post-D_{1a}; c) D_{1b} – continued east–west compression resulted in coaxial flattening along footwall sedimentary rock – komatiite and hangingwall sedimentary rock – basalt contacts which resulted in the nickel sulfides being squeezed off contact into the footwall sedimentary rocks; d) D_{2FF} – rotation in σ_1 (northwest–southeast) resulted in the coaxial flattened zones becoming shear zones with a normal sense of movement; e) D_{3FF} – rotation in σ_1 back to east–west shortening resulted in flat lying shear zones, dipping 5–10° towards the southeast, that offset the ore shoots and stratigraphy; f) D_4 – east–west compression ceased and extension occurred. Granitic magma (no less than five pulses) intruded along and exploited the D_3 shear zones, dilating at triple points creating T0 and T4 ore shoots. The T0 ore shoot was dissected by granitic magma fingering through the ore and resulted in slight rotation of the ore shoot and an apparent offset towards the west (i.e. in the direction of granitic movement). A portion of the T5 ore shoot was ripped off and entrained in the granitic magma, forming a pipe-like shoot offset up to tens of meters to the east.

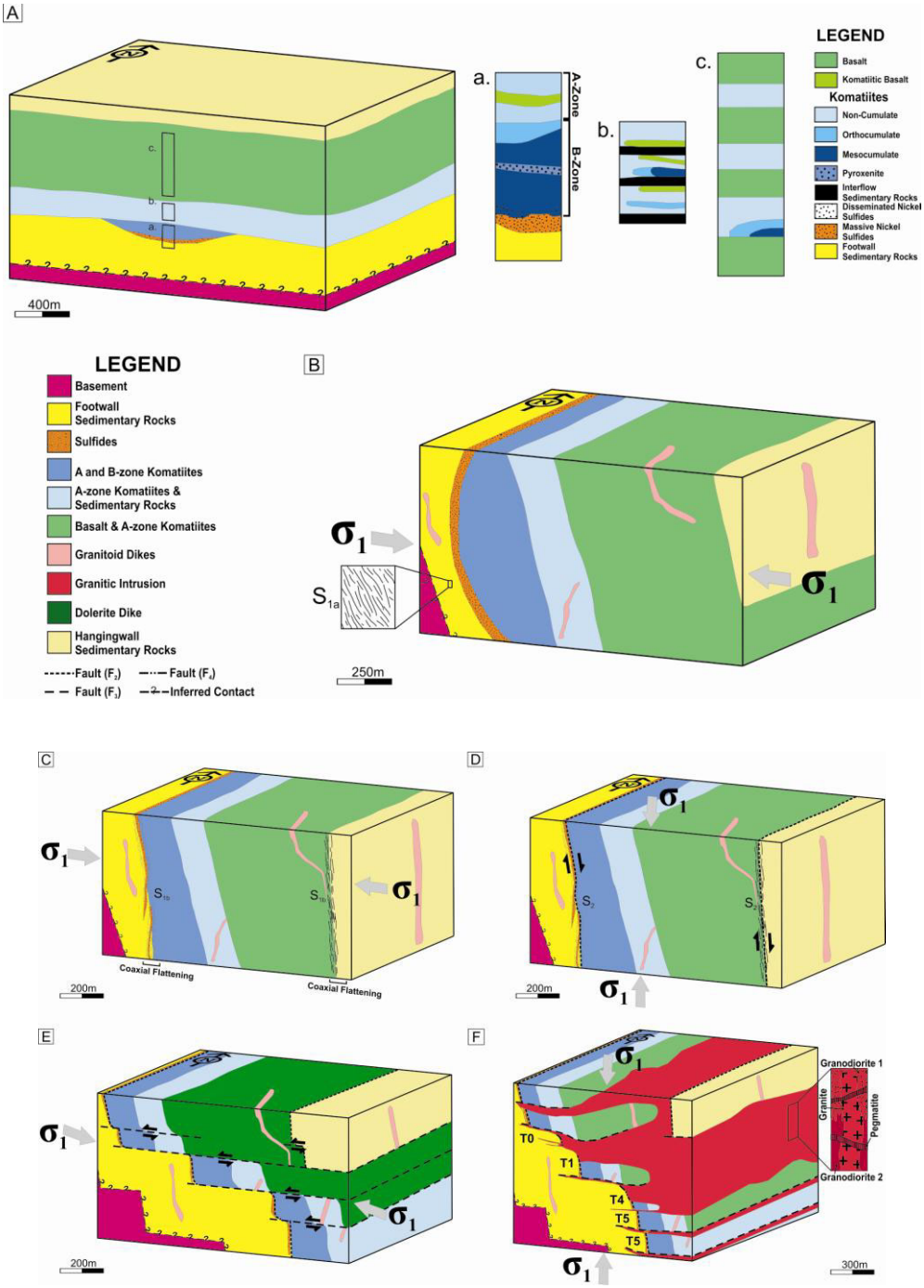

References

Barnes, SJ 2006, Komatiites: petrology, volcanology, metamorphism and geochemistry: Society of Economic Geologists, Special Publication, v. 13, p. 13–49.

Barnes, SJ, Coats, CJA and Naldrett, AJ 1982, Petrogenesis of a Proterozoic nickel-sulfide – komatiite association: the Katinniq sill, Ungava, Quebec: Economic Geology, v. 77, p. 413–429.

Cassidy, KF, Champion, DC, Krapež, B, Barley, ME, Brown, SJA, Blewett, RS, Groenewald, PB and Tyler, IM 2006, A revised geological framework for the Yilgarn Craton, Western Australia: Geological Survey of Western Australia, Record 2006/8, 8p.

Chin, RJ, Hickman, AH and Thom, R (compilers) 1984, Hyden, WA Sheet SI50-4: Geological Survey of Western Australia, 1:250 000 Geological Series Explanatory Notes, 21p.

Collins, JE, Hagemann, SH, McCuaig, TC and Frost, KM in press, Structural controls on sulfide remobilization at the Flying Fox Ni–Cu–PGE deposit, Forrestania greenstone belt, Western Australia: Economic Geology.

Ewers, WE, Hudson, DR and Davis, CES 1972, Interpretive study of a nickel–iron sulfide ore intersection, Lunnon shoot, Kambalda, Western Australia — analytical methods used in study of an ore intersection from Lunnon shoot, Kambalda: Economic Geology, v. 67, p. 1075–1092.

Frost, KM 2003, Forrestania nickel sulphide deposits, Western Australia *in* MSc Short Course — New Frontiers in Research on Magmatic NiS–PGE Mineralisation: Centre for Global Metallogeny, The University of Western Australia, Perth, Western Australia, p. 110–115.

Gee, RD 1979, Structure and tectonic style of the Western Australian Shield: Tectonophysics, v. 58, p. 327–269.

Lesher, CM 2007, Ni–Cu–(PGE) deposits in the Raglan area, Cape Smith belt, New Quebec, *in* Mineral resources of Canada: A synthesis of major deposit-types, district metallogeny, the evolution of geological provinces, and exploration methods *edited by* WD Goodfellow: Geological Survey of Canada and Mineral Deposits Division of the Geological Association of Canada, Special Publication, p. 351–386.

Lesher, CM and Keays, RR 2002, Komatiite-associated Ni–Cu–(PGE) deposits: geology, mineralogy, geochemistry and genesis, *in* The Geology, Geochemistry, Mineralogy and Mineral Beneficiation of the Platinum Group Elements *edited by* LJ Cabri: Canadian Institute of Mining, Metallurgy and Petroleum, Special Volume 54, p. 579–617.

Naldrett, AJ 1973, Nickel sulfide deposits: their classification and genesis with special emphasis on deposits of volcanic association: Transactions of the Canadian Institute of Mining and Metallurgy, v. 76, p. 183–201.

Perring, CS, Barnes, SJ and Hill, RET 1995, The physical volcanology of Archaean komatiite sequences from Forrestania, Southern Cross Province, Western Australia: Lithos, v. 34, p. 189–207.

Perring, CS, Barnes, SJ and Hill, RET 1996, Geochemistry of komatiites from Forrestania, Southern Cross Province, Western Australia: evidence for crustal contamination: Lithos, v. 37, p. 181–197.

Perring, CS, Barnes, SJ and Hill, RET 1997, The geology and volcanological setting of komatiite-hosted nickel sulphide ore shoots from Forrestania, Southern Cross greenstone belt, *in* Geology and Mineralization of the South Central Yilgarn Craton, Western Australia — A Field Guide: Kalgoorlie '97 *compiled by* WK Witt: Geological Survey of Western Australia, Record 1997/8, p. 42–63.

Porter, DJ and McKay, KG 1981, The nickel sulfide mineralization and metamorphic setting of the Forrestania Area, Western Australia: Economic Geology, v. 76, p. 1524–1549.

Pyke, DR, Naldrett, AJ and Eckstrand, OR 1973, Archean ultramafic flows in Munro Township, Ontario: Geological Society of America, Bulletin 84, p. 955–978.

RECORD 2010/26

CONTROLS ON GIANT MINERAL SYSTEMS IN THE YILGARN CRATON — A FIELD GUIDE

McCuaig et al.

This Record is published in digital format (PDF) and is available online at <http://www.dmp.wa.gov.au/GSWApublications>.

Further details of geological products produced by the Geological Survey of Western Australia can be obtained by contacting:

Information Centre
Department of Mines and Petroleum
100 Plain Street
EAST PERTH WESTERN AUSTRALIA 6004
Phone: (08) 9222 3459 Fax: (08) 9222 3444
<http://www.dmp.wa.gov.au/GSWApublications>